Brain Computer Interface for Post-Stroke Motor Rehabilitation

Mane Ravikiran Tanaji

School of Computer Science & Engineering

A thesis submitted to the Nanyang Technological University
in partial fulfillment of the requirements for the degree of
Doctor of Philosophy

2020

Statement of Originality

I hereby certify that the work embodied in this thesis is the result of original research, is free of plagiarised materials, and has not been submitted for a higher degree to any other University or Institution.

29 Dec 2020

.....

Date

.....

Mane Ravikiran Tanaji

Supervisor Declaration Statement

I have reviewed the content and presentation style of this thesis and declare it is free of plagiarism and of sufficient grammatical clarity to be examined. To the best of my knowledge, the research and writing are those of the candidate except as acknowledged in the Author Attribution Statement. I confirm that the investigations were conducted in accord with the ethics policies and integrity standards of Nanyang Technological University and that the research data are presented honestly and without prejudice.

29 Dec 2020

.....

Date

.....

Prof. Cuntai Guan

Authorship Attribution Statement

This thesis contains materials from 6 papers published and one paper submitted in the following peer-reviewed journals and papers accepted at conferences in which I am listed as an author.

Chapter 1 is partially published as a full paper, and a book chapter as:

Ravikiran Mane, Tushar Chouhan, and Cuntai Guan. BCI for Stroke Rehabilitation: Motor and Beyond. Journal of Neural Engineering. 2020. DOI: 10.1088/1741-2552/aba162

The contributions of the co-authors are as follows:

- I conducted the review of motor rehabilitation and prepared the manuscript.
- Dr. Tushar Chouhan conducted the review of cognitive and affect rehabilitation and prepared the manuscript.
- Prof. Cuntai Guan supervised the review and provided guidance, revisions and feedback on the manuscript.

Ravikiran Mane, Kai Keng Ang, and Cuntai Guan. Brain-Computer Interface for stroke rehabilitation. Springer Handbook of Neuroengineering. *(In press)*

The contributions of the co-authors are as follows:

- I conducted the review and prepared the manuscript.
- Dr. Kai Keng Ang and Prof. Cuntai Guan supervised the review and provided guidance, revisions and feedback on the manuscript

Chapter 3 and Chapter 4 are partially published as:

- Ravikiran Mane, Neethu Robinson, Vinod A. P., Seong-Whan Lee, and Cuntai Guan. Multi-view CNN with novel Variance Layer for Motor Imagery Brain-Computer Interface. Proceedings of 42nd Annual International Conference of the IEEE Engineering in Medicine and Biology Society (EMBC). 20-24 July, 2020.
- Ravikiran Mane, Effie Chew, Karen Chua, Kai Keng Ang, Vinod A.P., and Cuntai Guan. FBCNet: A Filter-Bank Convolutional Neural Network for Motor Imagery BCI in Chronic Stroke Patients. 8th International BCI Meeting. 2021. *(Accepted)*

- Ravikiran Mane, Effie Chew, Karen Chua, Kai Keng Ang, Neethu Robinson, Vinod A.P., Seong-Whan Lee, and Cuntai Guan. FBCNet: An Efficient Multi-view Convolutional Neural Network for Brain-Computer Interface. *(In preparation)*

The contributions of the co-authors are as follows:

- I developed the proposed architectures, performed the data analysis and prepared the manuscript under the guidance of Prof Cuntai Guan.
- Dr. Effie Chew, Dr. Karen Chua, Dr. Kai Keng Ang, Prof. Seong-Whan Lee, and Prof. Cuntai Guan designed the experiments for data collection.
- Dr. Neethu Robinson, Prof. Vinod A.P., Prof. Cuntai Guan provided feedback on the experiment design and the manuscript.

Chapter 5 will be submitted as:

Ravikiran Mane, Effie Chew, Karen Chua, Kai Keng Ang, Neethu Robinson, Vinod A.P., and Cuntai Guan. Deep Learning based Motor Imagery Decoding for Post-Stroke Motor Rehabilitation. *(In preparation)*

The contributions of the co-authors are as follows:

- I proposed the methodology, performed the data analysis and prepared the manuscript under the guidance of Prof Cuntai Guan.
- Dr. Effie Chew, Dr. Karen Chua, Dr. Kai Keng Ang, and Prof. Cuntai Guan designed the experiments for data collection.
- Dr. Neethu Robinson, Prof. Vinod A.P., Prof. Cuntai Guan provided feedback on the experiment design and the manuscript.

Chapter 6 is published as:

- Ravikiran Mane, Effie Chew, Kok Soon Phua, Kai Keng Ang, and Cuntai Guan. EEG Predictors for Upper Limb Motor Recovery of Stroke Patients Undergoing BCI and tDCS Rehabilitation. 7th International BCI Meeting. 21-25 May, 2018.

- Ravikiran Mane, Effie Chew, Kok Soon Phua, Kai Keng Ang, Vinod A.P., and Cuntai Guan. Quantitative EEG as Biomarkers for the Monitoring of Post-Stroke Motor Recovery in BCI and tDCS Rehabilitation. Proceedings of 40nd Annual International Conference of the IEEE Engineering in Medicine and Biology Society (EMBC). 17-21 July, 2018. **(Top-10 EMBS Student Paper Competition Finalist)**

- Ravikiran Mane, Effie Chew, Kok Soon Phua, Kai Keng Ang, Neethu Robinson, Vinod A.P., and Cuntai Guan. Prognostic and Monitory EEG-Biomarkers

for BCI Upper-Limb Stroke Rehabilitation. IEEE Transactions on Neural Systems and Rehabilitation Engineering. 27(8), 1654–1664, 2019.

The contributions of the co-authors are as follows:

- I proposed and performed the data analysis and prepared the manuscript under the guidance of Prof Cuntai Guan.
- Dr. Effie Chew, Mr. Kok Soon Phua, Dr. Kai Keng Ang, and Prof. Cuntai Guan designed the experiment for data collection.
- Dr. Neethu Robinson, Prof. A.P. Vinod, Prof. Cuntai Guan provided feedback on the experiment design and the manuscript.

29 Dec 2020

Date

Mane Ravikiran Tanaji

Acknowledgements

First and foremost, I am deeply thankful to my supervisor, Prof Guan Cuntai, for providing me with an opportunity to pursue my PhD under his guidance. His perception of application-oriented research has always inspired me to look beyond just the knowledge generation and think about the possible utility of the research for the betterment of society. He has always been approachable whenever I wanted to discuss my research ideas and has persistently pushed me to think outside the box.

Further, I am extremely grateful to my co-supervisor, Prof. Vinod Prasad, for giving me this opportunity to pursue my passion for research under his supervision. His encouragement and insightful comments have helped me a lot to grow as a researcher. He has been a source of constant motivation and immense knowledge to me.

I wish to express sincere gratitude to the School of Computer Science and Engineering, NTU for providing me with a resourceful workplace along with the financial support for my PhD study. Also, a special thanks to super co-operative Computational Intelligence Lab executive, Mr Kesavan, for his technical support.

I am also grateful to the colleagues in our research group, Dr Neethu Robinson, Dr Kavitha, and Dr Vikram for their comments and stimulating discussions. Heartfelt thanks go to my dear friends, Sukrit, Saumya, and Garima who have been there for me during all the highs and lows of the PhD. It is with them, that I have enjoyed some of the most memorable moments of this NTU life. Also, a special thanks to my lunch group friends, Subhrajit, and Abhay, for intellectual discussion on everything under the sun.

Most of all, nothing could have been possible without the unconditional support of my family. Acting as a safety net, they have provided me with the confidence

to take many critical decisions without the fear of failure. It is their upbringing, love, and motivation, that has made me who I am today.

Lastly, I thank God Almighty, for giving me much more than I deserve.

Dedicated To My Loving Family...

Abstract

Stroke is a devastating neurovascular emergency. As a result of brain damage, stroke patients generally suffer from many functional impairments and among them motor function deficits are most common and have the highest debilitating effects. Therefore, there is an everlasting need for more effective and efficient post-stroke motor rehabilitative interventions. In this quest, in the last decade, the technology of Brain Computer Interfacing (BCI) has emerged as one of the most effective tools for post-stroke motor rehabilitation. BCI systems establish a direct communication pathway between brain and external environment and empower patients for achieving functional recovery by repetitive activation of close loop motor circuits which are damaged as a result of stroke.

Therefore, considering the potential of BCI, this thesis aims to improve the existing BCI technology with the ultimate goal of achieving better motor rehabilitation outcomes.

In BCI systems, identification of users' intentions is achieved by classifying their brain activation patterns using machine learning algorithms. However, owing to the challenging nature of the brain signals, low classification accuracy remains one of the most important challenges faced by BCI. Particularly, detection of Motor Imagery (MI) from Electroencephalography (EEG) based BCI system, which is the commonly employed paradigm for motor rehabilitation, is among the most difficult tasks in the BCI domain. Therefore, this thesis first presents a novel, neurophysiologically inspired Convolutional Neural Network (CNN) named Filter-Bank Convolutional Network (FBCNet) for end-to-end MI classification from EEG data. The FBCNet is specifically designed to effectively capture the characteristic EEG activation patterns associated with MI known as Sensory-Motor Rhythms (SMR). With almost 8% higher classification accuracy over state-of-the-art methods, we show that incorporation of the neurophysiological priors in the design of deep learning architectures, as done in FBCNet, can lead to significantly more accurate BCI systems. Next, using interpretability analysis, we demonstrate that

FBCNet can achieve excellent spectro-spatial localization of discriminative SMRs but it lacks the temporal localization capabilities. Therefore, we extend the FBCNet with temporal localization capabilities. With this modification, compared to the FBCNet, the extended FBCNet further improves the MI classification accuracy by 2.5%.

Moving ahead, we analyze the classification performance of proposed and baseline deep learning architectures and traditional machine learning methods for MI detection in 25 chronic stroke patients undergoing three different BCI-based motor rehabilitation interventions for 2/4 weeks. Here, we show that in subject-specific multi-session classification settings, the proposed method of FBCNet can learn highly generalizable discriminative features which remain valid during inter-session classification. Also, from interpretability and various brain region classification analyses we demonstrate that for stroke patients, the most robust and generalizable signatures of MI are present in the motor region of the brain and deep learning architectures that learn to pay prominent attention to these features generally achieve higher inter-session classification performance.

Lastly, we analyze the EEG data generated during BCI-based motor rehabilitation from a neuroscientific perspective with an aim to gain a more detailed understanding of the process of BCI-mediated brain recovery. Specifically, we examine several EEG-derived features acquired during two different BCI-driven upper extremity rehabilitative interventions to explore the utility of EEG features for the prognostication of rehabilitative interventions. We further extend this analysis to identify and quantify the treatment-induced neurological changes in the brain activity and explore the differences in the neurological changes associated with the different rehabilitative intervention and their relationship with the treatment characterization. The results of this analysis indicate a possibility of intervention specific prognostic and monitory biomarkers. This approach can be pursued to uniquely predict the expected response of a patient to an intervention and the intervention with the highest predicted gains may then be recommended to the patient, thereby enabling a highly personalized motor rehabilitation.

Overall, the research presented in this thesis shows that EEG-based BCI systems can be used to characterize and promote recovery of stroke impaired motor functions and neurophysiologically inspired CNN architectures can significantly advance the technology of MI detection in rehabilitative BCI systems. These presented

technological advancements hold a potential to significantly improve the rehabilitation outcomes of the BCI intervention, and the quality of life of stroke survivors. Furthermore, the identification of intervention specific prognostic biomarkers can aid clinicians in suggesting the most suitable intervention for any patient. Future research can use the findings presented in this thesis to design robust and more accurate BCI systems for highly personalized and holistic post-stroke rehabilitation.

Contents

List of Figures

List of Tables

Symbols and Acronyms

Acronyms

ADL	Activities of Daily Living
ANOVA	Analysis of Variance
ARAT	Action Research Arm Test
ASR	Artefact Subspace Reconstruction
BCI	Brain Computer Interfacing
BI	Barthel Index
BMI	Brain Machine Interface
BSI	Brain Symmetry Index
CAR	Common average reference
CBF	Cerebral Blood Flow
CIMT	Constraint-Induced Movement Therapy
CNN	Convolutional Neural Network
CPNS	Common Peroneal Nerve Stimulation
CSP	Common Spacial Patterns
CST	Corticospinal Tract
DAR	Delta Alpha Ratio
DBN	Deep Belief Network
DCM	Dynamic Causal Modeling
ECoG	ElectroCorticography
EEG	Electroencephalography
ELU	Exponential Linear Unit
EMG	Electromyogram
EOG	Electrooculogram
ERD	Event Related Desynchronization
ERS	Event Related Synchronization

ESI	EEG Source Imaging
FBCNet	Filter-Bank Convolutional Network
FBCSP	Filter Bank Common Spacial Patterns
FC	Fully-Connected
FES	Functional Electrical Stimulation
FFT	Fast Fourier transform
FMA	Fugl-Mayer motor assessment
fMRI	Functional Magnetic Resonance Imaging
GRU	Gated Recurrent Unit
HK	Haptic Knob
HMM	Hidden Markov Model
ICA	Independent component analysis
ICH	Intra-Cerebral Hemorrhage
ICP	Intra-Cranial Pressure
LDA	Linear Discriminant Analysis
Leaky-ReLU	Leaky-Rectified Linear Units
LSTM	Long Short-Term Memory
MEG	Magnetoencephalography
MI	Motor Imagery
MRCP	Movement-related cortical potential
MRI	Magnetic Resonance Imaging
NIBS	Non-Invasive Brain Stimulation
NIHSS	National Institute of Health Stroke Scale
NIRS	Near-Infrared Spectroscopy
NMES	Neuro-Muscular Electrical Stimulation
nRS	modified Rankin scale
OT	Occupational Therapy
pdBSI	Pairwise Derived Brain Symmetry Index
PRI	Power Ratio Index
PT	Physiotherapy
Q-EEG	Quantitative Electroencephalography
rBSI	Revised Brain Symmetry Index
RCT	Randomized Controlled Trial
ReLU	Rectified Linear Units
RNN	Recurrent Neural Network

rsFC	Resting-State Functional Connectivity
SCB	Spatial Convolution Block
SCP	Slow Cortical Potential
SMR	Sensorimotor rhythms
SNR	Signal to Noise Ratio
SQUID	Superconducting Quantum Interference Devices
SSVEP	Steady State Evoked Potentials
SVM	Support Vector Machine
TAR	Theta Alpha Ratio
TBAR	Theta Beta Alpha Ratio
TBR	Theta Beta Ratio
tDCS	Transcranial Direct Current Stimulation
TMS	Transcranial Magnetic Stimulation
tPA	Tissue Plasminogen activator
TSNet	Temporo-Spectral Network
VR	Virtual Reality

Chapter 1

Introduction

Stroke is a highly prevalent, life-threatening neuro-vascular emergency. It is estimated that each year, there are about 16 million new stroke victims worldwide. Also, stroke ranks as the fifth largest cause of deaths in the world [2, 3]. Various degrees of cognitive, physical and affect impairments are common repercussions of stroke and most of the stroke-survivors need some form of rehabilitation [3–5]. Due to the need for inpatient care, rehabilitation, and follow-up services, the projected combined direct and indirect costs of stroke are estimated at $71-184 billion/year [3]. Therefore, considering the effects on daily activities and the high economic burden, there is a great need for novel approaches to effectively reduce the disabilities following stroke.

With close to 30% of survivors suffering from chronic motor disabilities, hemiparesis, the unilateral loss of motor control, is the most common and the most disabling condition post-stroke [2, 6]. Therefore, the majority of efforts in post-stroke rehabilitation target motor function restoration and there is a growing need for better and efficient rehabilitative interventions.

In the last decade, Brain Computer Interface (BCI) systems have emerged as one of the most promising tools for motor function restoration. BCI or Brain Machine Interface (BMI) is a system that enables a subject to interact with the environment by employing control signals generated solely by the brain activity (Figure 1.1) [7]. With the use of various neuronal signal acquisition technologies, BCI provides a real-time window in brain dynamics and offers potential to target the post-stroke

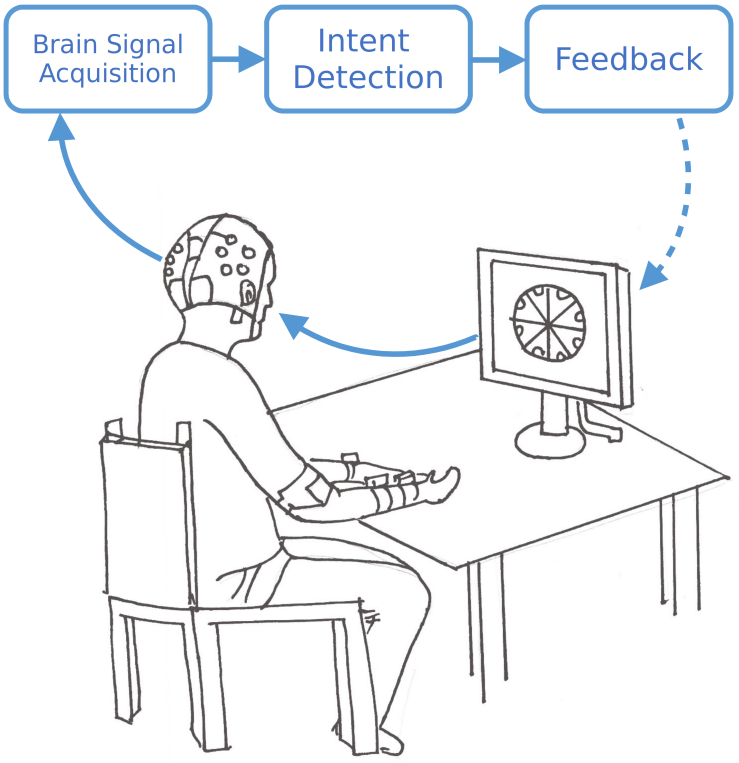

FIGURE 1.1: General Framework of Brain Computer Interfacing for post-stroke motor rehabilitation.

impairments at the source; that is at brain level [8]. In the context of motor rehabilitation, BCI systems decode the patients' intentions to move their affected limb and these decoded intentions are then used to provide a contingent sensory-motor feedback to the patient in various forms like actual movement, haptic feedback, visual feedback, etc. The extensive research in the last two decades indicates that by bridging the stroke-induced gap between motor intention and sensory feedback of motor movement, BCI-based interventions may lead to functional recovery [8, 9]. Furthermore, growing clinical evidence suggests that BCI may be one of the best interventions for post-stroke upper limb motor rehabilitation [10].

Although initial clinical results of BCI-based post-stroke rehabilitation are very encouraging, the clinical protocols and technological details of currently used BCI systems are far from perfect. The accuracy of the BCI system is one of the most important factors that influence the clinical outcomes of BCI-based post-stroke motor rehabilitation [11–16]. However, highly accurate and robust detection of users' intentions from their brain signals is still a very challenging task. Therefore, there is an urgent need for better classification algorithms, which may, in turn, improve

the overall motor function recovery in stroke patients. Furthermore, different from the technological challenges of BCI, the present clinical framework of post-stroke rehabilitation is also not very optimal for achieving the best possible recovery for all patients. The present framework mostly follows a one-fits-all approach wherein little consideration is provided to the patients' neurophysiological profile while suggesting a rehabilitative intervention [17]. This lack of personalized, neuro-imaging guided rehabilitation stems from the inadequate understating of the neuronal correlates of functional impairments and mechanisms of brain repair by rehabilitative interventions. Therefore, better knowledge of these neuronal associates of motor functions can lead to the suggestion of the most appropriate rehabilitation method for every patient resulting in improved clinical gains. Hence, by developing more accurate BCI systems and by providing insights about the brain restoration mechanisms, the methods presented in this thesis ultimately aim to enhance the protocols of post-stroke motor rehabilitation. The motivating factors that led to this area of research are explained in the next section.

1.1 Research Motivations

Owing to the huge socio-economic impact, the rehabilitation of post-stroke motor impairments has received an everlasting attention from the clinical and research community. Despite all the efforts, post-stroke motor rehabilitation remains a largely unsolved mystery mainly due to the little understanding that mankind has about the brain and its repair mechanisms. Hence, this need for better, more effective and efficient rehabilitation protocol is the ultimate challenge that motivates the work presented in this thesis.

The extensive research in the last century has resulted in multiple interventions for post-stroke motor rehabilitation. Among them, in the last decade, the technology of BCI has shown very promising potential for rehabilitation of motor impairments. In BCI systems, electroencephalography (EEG) is the most widely used signal acquisition modality and Motor-Imagery (MI) based EEG-BCI, wherein participant performs mental rehearsal of a particular motor movement, is one of the frequently investigated protocols. Therefore, owing to its high clinical relevance, EEG-BCI literature contains many reports on decoding techniques to classify various MI

classes. However, quite a lot of work is still necessary to improve the accuracy of these systems.

Noisy and high dimensional data, high inter-trial variability, and scarcity of training data are among the key challenges faced by the EEG-BCI classifiers [1]. The EEG data is generally contaminated by much stronger sources of noise resulting in high noise content and, low signal to noise ratio (SNR) [1]. Furthermore, EEG is commonly recorded using multiple electrodes and at high sampling frequencies leading to very high dimensional data. This high-dimensionality, when coupled with only 50-500 training samples per class, if not handling very carefully, results in serious overfitting of classifier models. The intrinsic nature of MI and high intra-class variability in MI signature further worsens the performance. Due to all these issues, the MI classification is considered to be among the most challenging tasks in the BCI domain [18, 19].

The classical machine learning strategies have tackled this difficult task of MI classification by paying prominent attention to the extraction of neurophysiologically sound features from EEG data. These algorithms generally employ a multistage approach wherein the EEG data is first preprocessed to reduce the noise and then neurophysiologically sound features are extracted from the data to enhance SNR and reduce dimensionality. Following this multistage approach, these methods have been observed to be effective in this scenario of limited and noisy EEG training data but they still suffer from the high susceptibility to intra-trial variance and have a high dependence on handcrafted features. To solve these issues, in recent years, the technology of deep learning, which is an extensively data-driven approach to classification, has been proposed. Deep learning based approaches eliminate the need for handcrafted feature extraction and offer end-to-end processing capability. Therefore, there is a growing interest among BCI researchers to use deep learning methods for MI decoding. In particular, architectures based on Convolutional Neural Network (CNN) have gained popularity in the BCI domain due to their ability of effectively learning the local connectivity patterns from the given data [20–23]. Although observed to be effective, deep learning based methods suffer severely due to the lack of sufficient training data and presence of high dimensional features. Therefore, with all these challenges, there is a need for an end-to-end MI decoding algorithm which can classify various MI classes with high accuracy while being less susceptible to small, noisy and high-dimensional data.

Furthermore, although stroke patients are among the most-important target population, exploration of advanced techniques for MI classification is still largely limited to the data from healthy population. Alteration of brain dynamics, changes in EEG brain rhythms and modifications in motor function control are some of the known effects following stroke [24, 25]. Furthermore, it has been documented that close to 13% stroke patients cannot control the MI-BCI using classical machine learning techniques [15]. Therefore, it is necessary to investigate how advanced MI classification techniques perform in stroke population and if they can extend the technology of MI-BCI to more patients by achieving better classification accuracy. Moreover, the use of advanced classification techniques in patient population also greatly necessitates interpretability of the model decisions. In stroke patients, since the aim is to restore the brain activation to a healthy state, it is important to evaluate the information encoded by the classification algorithm. Therefore ease of decision explanation is another important parameter when it comes to patients' data.

Different from the advancements in the rehabilitation technology, fundamental mechanisms of post-stroke neuronal repair are also not very well understood. The basic underlying principle behind stroke rehabilitative utility of all the interventions is brain's ability of adaptation and associative learning termed as brain plasticity [26]. This ability of brain allows the functional and structural reorganization of the neuronal population to restore or substitute for the functional capabilities of the damaged brain area [27]. Although the general idea of brain plasticity is at the root of all the rehabilitative interventions, the mechanism in which each treatment targets the brain dynamics is distinct, resulting in a very heterogeneous treatment-induced motor function improvements [28]. Presently, reasoning based speculative information is available on the mechanisms of treatment-induced neuronal recovery but there is no consensus about the exact neurodynamics caused by the interventions and is still an open research question.

With the availability of various rehabilitative interventions, the patient's response to a particular intervention also depends on the patient's clinical profile adding another level of variability in the clinical outcomes. Stroke is a very heterogeneous disease. The type, size and location of stroke injury differs greatly across patients, which results in substantial variability between patients and their response to therapy [29]. This heterogeneity in patients' clinical profile along with

the not-so-well-known neurodynamics elicited by different rehabilitative interventions makes the task of patient stratification very difficult but necessary. Assigning a patient to a particular intervention becomes a task of matching two not-so-well defined systems with almost no information about their interactions along with the aim of maximizing clinical motor recovery.

With a spectrum of the available rehabilitative interventions to choose from and considering the heterogeneity in the outcomes, the prognostication of the treatment-induced motor recovery becomes an essential aspect of stroke care and planning. The aim of the prognostication is to allow clinical teams, patients, and families to optimize rehabilitation plans with realistic goals and optimum allocation of time and resources[30]. As outcome prediction is an integral part of any disease management and treatment planning, many studies in stroke also have been conducted to understand the effects of various demographic, clinical, radiological factors to predict important stroke outcomes like the degree of disability and death. Many factors, such as stroke severity[31–33], stroke lesion volume [33, 34], age[31–33, 35], and comorbidities[31–33, 35, 36] have been observed to provide some information on the motor status at the end of spontaneous recovery period, but they have been found to be of very little use for the prognostication of treatment-induced motor recovery, particularly in chronic stage[28, 30, 37].

As the post-stroke motor impairments are the effects of damaged neuronal population in the brain, in the recent years, multitude of neuroimaging studies have explored the relationship between neuroimaging features and motor impairments at various stages of stroke recovery [24, 38, 39]. All these studies in the stroke rehabilitation attempt to answer three basic questions. 1. What is this patient's potential for recovery?, 2. What is the best rehabilitation strategy for this person, given her/his clinical and neurological profile?, and 3. How exactly the rehabilitation treatment affects brain dynamics to reduce functional impairments? [17, 40]. The inherent variability in the healthy human brain combined with the heterogeneity in stroke has made it hard to answer these questions. Despite these challenges, various modalities like, Magnetic Resonance Imaging (MRI) [24, 41], functional MRI (fMRI) [37, 42, 43], Near-Infrared Spectroscopy (NIRS) [44, 45], Transcranial Magnetic Stimulation (TMS) [30, 46], Magnetoencephalography (MEG) [47], and EEG [48–51] have been used to effectively understand the neurodynamics of stroke. Presently, many studies have explored the hemodynamic brain activations during

stroke with fMRI because of the high spatial resolution provided by this modality. However, limited reports present the modifications in electrical brain activations using EEG during stroke rehabilitation.

A high temporal resolution, non-invasive and fast acquisition capabilities, easy setup, bedside availability, and low-cost have rendered EEG to be a very attractive modality in stroke progression monitoring [52]. Various studies have explored the utility of spectrum of EEG features like band power spectra, entropy, synchrony, connectivity calculated from different brain areas to encapsulate the brain dynamics in various stages of stroke progression from few minutes (acute state) to few years (chronic state) after the stroke onset. Among these features, Quantitative EEG (QEEG) features like band-power spectra, brain asymmetry, entropy which are simple to calculate and more interpretable have been investigated considerably in the acute, sub-acute prognosis and clinical management [50–57]. However, very few studies have explored the utility of these indices in the chronic state rehabilitation [49]. Therefore, exploration of EEG based prognostic and monitory biomarkers may provide fresh insights into the mechanisms of recovery following BCI-based post-stroke motor rehabilitation.

1.2 Research Objectives

The main objective of this thesis is to improve the clinical outcomes of BCI-based post-stroke motor rehabilitation. This thesis aims to achieve this objective by addressing two key challenges in this field. The usability of the BCI system, as well as the clinical outcomes resulting from its rehabilitative use depends on the accuracy of the used decoding algorithm. Therefore, this thesis first aims to develop more accurate classification algorithms for MI decoding. Second, the response of every patient to the BCI-based rehabilitation is unique and there is a very high-variability in patients clinical outcomes. Therefore, by analyzing the EEG and clinical data collected during a BCI based rehabilitation trial, this thesis also aims to identify the prognostic and monitory biomarkers of neuronal and functional recovery following post-stroke motor rehabilitation. The major specific research objectives are listed below.

1. Development of novel deep learning based methods for robust and accurate classification of MI from EEG data for use in post-stroke motor rehabilitation.
    - Developing new deep learning architectures for effective decoding of MI signals in an EEG-based BCI.
    - Validating the above methods using experiments to decode different types of MI in healthy subjects and stroke patients.
    - Analyzing the suitability of these methods to classify multi-session EEG data in post-stroke motor rehabilitation trial.
    - Investigating the features encoded by the classification algorithms to ensure neurophysiologically relevant feature learning by the data-driven algorithms.
2. Identification of EEG based biomarkers for prognostication and monitoring of BCI-based motor rehabilitation to achieve better clinical outcomes by highly personalized rehabilitation.
    - Investigating the possibility of intervention specific prognostic biomarkers to uniquely predict patients' response to the available rehabilitative intervention and ultimately prescribe the intervention with best possible gain to every patient leading to a personalized rehabilitation plan.
    - Exploring the neurological changes observed during rehabilitative interventions and their relationship with the clinical motor and behavioural recovery to provide a better and causal understanding of post-stroke recovery and neuronal repair.
    - Quantifying the differences in neurological changes associated with different rehabilitative interventions to understand the exact mechanisms of neuronal repair stimulated by the given intervention and to use this information for optimizing the rehabilitative interventions.

The above-mentioned challenges and the research objectives will be addressed in this thesis. The specific contributions made in this direction are detailed in the next section.

1.3 Contributions of the Thesis

The main contributions of this thesis, directly related to the above-mentioned research objectives, can be summarized as follows:

This thesis presents novel, neurophysiologically inspired, CNN architectures for MI classification. Being based on the deep learning framework, these architectures offer all the advantages of deep learning, mainly, the end-to-end classification capability and the high model capacity. Additionally, these architectures mitigate the shortcomings of deep learning methods, mainly, the high dependence on training sample size, and the high susceptibility to overfitting while handling noisy and high dimensional data, by encoding the neurophysiological priors of MI in their design. The specific contributions are listed below.

- First, a compact and neurophysiologically inspired CNN architecture named Filter-Bank Convolutional Network (FBCNet) is proposed for MI classification.
- In FBCNet, a novel Variance layer is proposed for effective extraction of EEG temporal information and parameter reduction. This proposed layer is based on the neurophysiological signatures of MI and hence is the key contributor in the better classification accuracies offered by FBCNet.
- The classification performance of FBCNet is evaluated using multiple publicly available MI datasets from healthy subjects to compare and robustly quantify the accuracy improvements offered by FBCNet over state-of-the-art classical machine learning algorithms and deep learning architectures.
- The analysis is further extended to present one of the first reports on the comparison between classical machine learning algorithms and deep learning architectures for MI decoding in 71 chronic-stroke patients. Furthermore, it is demonstrated that for stroke patients, classical machine learning approaches may outperform the general-purpose deep learning architectures and careful fusion of deep learning methods and neurophysiological knowledge of MI, as done in FBCNet, can achieve the best classification accuracies for both healthy subjects and stroke patients.

- Additionally, using three different explainable AI techniques, the better classification accuracy achieved by FBCNet is reasoned. Also, the difference between the EEG data from healthy and stroke patients is discussed in the context of MI classification.

- Next, the FBCNet architecture is further extended for better extraction of the high level temporal information.

- The classification superiority of extended FBCNet is demonstrated using multiple datasets with data from healthy as well as stroke patients.

- Furthermore, the utility of existing and proposed classification algorithms is investigated to improve the MI-decoding accuracy during two BCI-based post-stroke upper-extremity motor rehabilitation trials. The multi-session data from 25 stroke patients who underwent 2/4 weeks of rehabilitation is analyzed to assess the stability and robustness of the classification algorithms in classifying inter-session MI data from stroke patients.

- Also, model interpretability analysis is employed to analyze the information learned by deep learning algorithms. This analysis provides insights about how the overlap between model leanings and neurophysiological signatures of MI results in much more robust and generalizable classification models.

Following the analysis of stroke rehabilitation from a classification perspective, the relationship between EEG data collected during two different BCI-based motor rehabilitative intervention is explored to understand the mechanisms of neuronal recovery facilitated by these interventions. Specifically, the EEG-based prognostic and monitory biomarkers of functional recovery following stroke are explored to uniquely characterize individual rehabilitative interventions. The specific contributions are listed below.

- The prognostic capabilities of EEG based features, specifically, Quantitative EEG (QEEG) features, are investigated to predict the functional motor recovery following BCI and transcranial Direct Current Stimulation (tDCS) coupled BCI rehabilitative interventions.

- Inter-intervention differences between prognostic capabilities of various QEEG features are investigated to analyze the possibility of intervention-specific

prognostic biomarkers. In this analysis, it is hypothesised that these biomarkers can encapsulate the interactions between the intervention and the patient, and can uniquely predict the clinical efficacy of the given intervention.

- Next, to uniquely characterize the neuronal recovery stimulated by different interventions, the possibility of intervention-specific monitory biomarkers is investigated. Following the identification of these biomarkers, the change in them can be used to monitor the evolution of neuronal recovery providing a finer scale to monitor patients' progress.

- Based on findings of the above-mentioned analyses, an idea of highly personalized rehabilitation is presented to maximize the clinical gains of any post-stroke rehabilitation program.

1.4 Organization of the Thesis

The above contributions to the aforementioned research challenges are presented in this thesis across various chapters which are summarized as follows.

Chapter 2 presents a brief overview of stroke, post-stroke impairments, various methods of post-stroke motor rehabilitation and the role of BCI technology in stroke rehabilitation. Moreover, various methods of MI decoding that are used in BCI based post-stroke rehabilitation are reviewed and the limitations of the existing methods are highlighted. Also, a review of relevant studies in the literature related to stroke progression, management, monitoring, and prognostication is presented.

Chapter 3 presents the first contribution of this thesis, the neurophysiologically inspired CNN architecture named FBCNet, for classification of EEG-MI data. All the analyses related to FBCNet including the classification performance and interpretability analysis is presented in this chapter. In Chapter 4, the limitation of FBCNet in temporal localization of discriminative features is identified. Following this, the FBCNet architecture is further extended to incorporate explicit temporal localization. The impact of this modification on classification accuracy and model learning are analyzed in this chapter.

Following this, chapter 5 analyzes the effectiveness of the proposed, as well as, existing state-of-the-art methods for MI decoding in post-stroke motor rehabilitation

trials. This chapter focuses on investigating the capabilities of various algorithms to effectively tackle inter-session variability in the EEG data collected during multi-session rehabilitation trials. Using interpretability analysis, this chapter further presents a novel relationship between pre-intervention EEG data, rehabilitation session classification accuracy, and clinical gain following rehabilitative intervention. These findings provide a way for patient stratification in BCI based rehabilitation trials.

Next, building upon the premise of the previous chapter, chapter 6 presents the neurophysiological analysis of the EEG data acquired during post-stroke upper extremity motor rehabilitation trial using two different BCI interventions with an aim to identify the intervention specific prognostic and monitory biomarkers of stroke recovery.

Finally, chapter 7 concludes this thesis and discusses its clinical and technological significance. It also presents a few possible future directions.

1.5 List of Publications

The contents of this thesis are the contributions made by the author and are reported in the following publications:

Journal articles

1. **Ravikiran Mane**, Tushar Chouhan, and Cuntai Guan. BCI for Stroke Rehabilitation: Motor and Beyond. Journal of Neural Engineering. 2020. DOI: 10.1088/1741-2552/aba162

2. **Ravikiran Mane**, Effie Chew, Kok Soon Phua, Kai Keng Ang, Neethu Robinson, Vinod A.P., and Cuntai Guan. Prognostic and Monitory EEG-Biomarkers for BCI Upper-Limb Stroke Rehabilitation. IEEE Transactions on Neural Systems and Rehabilitation Engineering. 27(8), 1654–1664, 2019.

3. **Ravikiran Mane**, Effie Chew, Karen Chua, Kai Keng Ang, Neethu Robinson, Vinod A.P., Seong-Whan Lee, and Cuntai Guan. FBCNet: An Efficient

Multi-view Convolutional Neural Network for Brain-Computer Interface. *(In preparation)*

4. **Ravikiran Mane**, Effie Chew, Karen Chua, Kai Keng Ang, Neethu Robinson, Vinod A.P., and Cuntai Guan. Deep Learning based Motor Imagery Decoding for Post-Stroke Motor Rehabilitation. *(In preparation)*

Book Chapters

5. **Ravikiran Mane**, Kai Keng Ang, and Cuntai Guan. Brain-Computer Interface for stroke rehabilitation. Springer Handbook of Neuroengineering. *(Under revision)*

Conference proceedings

6. **Ravikiran Mane**, Effie Chew, Karen Chua, Kai Keng Ang, Vinod A.P., and Cuntai Guan. FBCNet: A Filter-Bank Convolutional Neural Network for Motor Imagery BCI in Chronic Stroke Patients. 8th International BCI Meeting. 2021. *(Accepted)*

7. **Ravikiran Mane**, Neethu Robinson, Vinod A. P., Seong-Whan Lee, and Cuntai Guan. Multi-view CNN with novel Variance Layer for Motor Imagery Brain-Computer Interface. Proceedings of 42nd Annual International Conference of the IEEE Engineering in Medicine and Biology Society (EMBC). 20-24 July, 2020.

8. **Ravikiran Mane**, Effie Chew, Kok Soon Phua, Kai Keng Ang, Vinod A.P., and Cuntai Guan. Quantitative EEG as Biomarkers for the Monitoring of Post-Stroke Motor Recovery in BCI and tDCS Rehabilitation. Proceedings of 40nd Annual International Conference of the IEEE Engineering in Medicine and Biology Society (EMBC). 17-21 July, 2018. **(Top-10 EMBS Student Paper Competition Finalist)**

9. **Ravikiran Mane**, Effie Chew, Kok Soon Phua, Kai Keng Ang, and Cuntai Guan. EEG Predictors for Upper Limb Motor Recovery of Stroke Patients Undergoing BCI and tDCS Rehabilitation. 7th International BCI Meeting. 21-25 May, 2018.

Chapter 2

BCI for Stroke Rehabilitation: Literature Review

Stroke is a fatal neuro-vascular emergency with very high prevalence globally. It is one of the leading reasons for acquired adult disabilities [6]. Number of stroke incidents have been projected to be rising steadily with an increasingly ageing population. Also, improvements in healthcare technology have resulted in a decrease in stroke fatalities leading to a large and increasing number of people living with permanent post-stroke impairments. It is estimated that close to 1% of the world population is living with after-effects of cerebrovascular incidents with close to 30% of them suffering from chronic motor disabilities [58]. Hemiparesis is the most common and the most disabling condition post-stroke. Therefore, the majority of efforts in post-stroke rehabilitation target upper limb motor function restoration and there is an everlasting need for better rehabilitative interventions.

A Brain Computer Interface (BCI), is a system that enables humans to interact with their surroundings via employing control signals generated solely by brain activity, without the intervention of peripheral nerves and muscles [7, 59]. With the use of various brain signal acquisition technologies, BCI provides a real-time

The contents of this chapter have been partially published as a full paper, and a book chapter under review as:

1. Ravikiran Mane, et al., BCI for Stroke Rehabilitation: Motor and Beyond. Journal of Neural Engineering. 2020.
2. Ravikiran Mane, et al., Brain-Computer Interface for stroke rehabilitation. Springer Handbook of Neuroengineering. *(Under revision)*

window in brain dynamics and offers a potential to target post-stroke impairments at the source [8]. The extensive research in the last two decades has indicated the vast potential of BCI technology particularly in post-stroke motor rehabilitation [10].

This chapter provides an overview of BCI technology for post-stroke motor rehabilitation. First, a short description of post-stroke brain dynamics is provided. Next, the technological aspects of the BCI system are discussed with a focus on non-invasive methodologies. Particularly, the technological challenges in the use of EEG-based BCI systems for motor rehabilitation are presented. Following this, the rationale behind the use of BCI technology for brain restoration is discussed. Studies presenting the clinical use of BCI technology for motor rehabilitation are reviewed with a focus on critical analysis of system implementation, clinical efficacy, and associated mechanisms of functional recovery. Finally, the literature on personalized stroke rehabilitation by prognostication of stroke recovery is presented.

2.1 Stroke

Stroke is caused by the cessation of blood flow to the parts of the brain and is mainly classified into two groups: ischemic stroke and hemorrhagic stroke. Ischemic stroke results from the formation of a blood clot in arterial systems of the brain, blocking the blood supply to certain brain areas. It is the most prevailing type of stroke and it attributes to almost 80% of the total stroke incidents. Lack of blood flow and oxygen to the brain cells caused by ischemic stroke initiates an ischemic cascade resulting in the immediate dysfunction of the affected neuronal population with the possibility of irreversible damage and death of the affected cells [60]. On the other hand, the hemorrhagic stroke is caused by the rupture of aneurysm or leaking of weak brain vessels. Depending on the location of the bleeding, hemorrhagic stroke can lead to many different complications. The Intra-Cerebral Hemorrhage (ICH), that is the bleeding inside the brain matter, has threefold effects; the clotting of leaking blood results in the formation of hematoma and the expanding hematoma increases Intra-Cranial Pressure (ICP) damaging the brain tissue by compression. The arterial blood also expresses direct toxic effects on the brain tissue resulting in inflammation and contributes to secondary injury [61]. Furthermore, disrupted

vascular supply causes hypoxia (lack of blood flow) downstream of the punctured artery. The second type of hemorrhagic stroke, the extra-cerebral hemorrhage, refers to bleeding within the skull but outside of the brain tissue and it threatens the brain functions by increased intracranial pressure. Although the extra-cerebral hemorrhage is much less severe than the intra-cerebral bleeding, it is much more prevalent.

In the ischemic stroke, brain cells get damaged by hypo-perfusion. Cerebrovascular tissue undergoing ischemia has two layers: (a) inner core of severe ischemia with blood flow below 10-25%, displaying necrosis of both neuronal as well as supporting glial elements; and (b) outer layer of less severe ischemia (penumbra), supplied by collaterals, and contains cells which can be retrieved by timely therapeutic intervention. Although the inner core suffers sudden death after stroke, the primary goal in the critical care of the ischemic stroke is to save the cells in the ischemic penumbra by dissolving or removing the blood clot and restoring the blood flow.

In ICH, the rupturing of a blood vessel leads to mechanical tissue disruption (secondary to the jet of blood) and hematoma formation, followed by secondary injury processes, including disruption of the blood-brain barrier, expansion of perihematomal edema, inflammation, neuronal cell death, seizures, pressure on brainstem, and chemical or cellular barriers to repair [61]. Also, expanding hematoma and secondary inflammation results in the increased ICP which threatens ischemic insult by reduced perfusion rates caused by increased ICP. Considering these effects, as opposed to the ischemic stroke, the critical care of the hemorrhagic stroke aims to control the bleeding by clot formation and to stabilize the patient.

In ischemic as well as hemorrhagic stroke, despite receiving a timely acute intervention, the majority of the stroke survivors often suffer from some form of neuronal damage. This damage results in either acute or chronic functional disabilities.

2.1.1 Post-Stroke Deficits

Stroke, being a neurological event, is clinically presented with variable degrees of motor, sensory, cognitive, and speech impairments. In case of a focal stroke, partial or complete loss of contralesional motor functions is the most common clinical symptom. The acute stroke symptoms vary largely based on the location of the

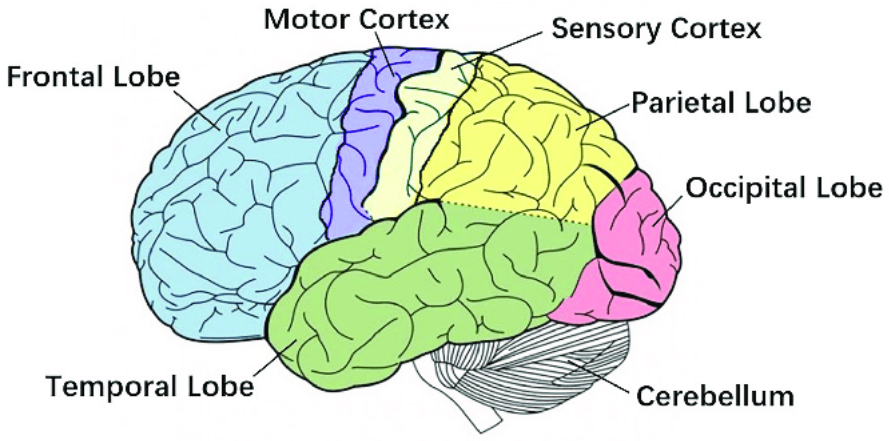

FIGURE 2.1: Anatomical organization of the brain (as presented in [62]): Anatomically, the brain cortex is primarily divided into four regions or lobes; the Frontal lobe, the Occipital lobe, the Temporal lobe, and the Parietal lobe. Although most brain functions rely on multiple regions working in conjunction, these lobes are known to specialize in particular tasks. The Frontal lobe is known to be associated with the higher cognitive functions like attention, planning and decision making. The Parietal lobe, along with the motor and sensory cortex, is responsible for control and integration of the motor and sensory information. The Temporal lobe is in-charge of language, speech and memory associated functions. The processing of visual information primarily happens in the Occipital lobe. Owing to this anatomical and functional segregation, a stroke in a particular area of the brain severely affects the functions controlled by that region.

lesion. Motor deficits like upper body paralysis, one-sided facial droop, muscle weakness, gait disturbance, altered movement coordination, and hemiplegia [63]; cognitive deficits related to attention, orientation, memory and thinking, dementia [64–66], visuospatial and spacial neglect [67, 68], aphasia [69], dysarthia[70], loss of sensation [71] and dysphagia [72] are commonly observed following stroke. Depending on the severity of the stroke, in 40% of the patients, these symptoms resolve in the acute stage. However, in the remaining cases, a certain degree of sensory and motor deficits are most prevailing. As motor impairments prominently affect the activities of daily living and are most disabling, majority of the post-stroke research is focused on the motor impairments and restoration of motor functions.

2.1.2 Typical Recovery of Post-Stroke Deficits

The loss of neural tissue associated with stroke induces profound neurophysiological changes throughout the brain which elicits a wide range of behavioral impairments.

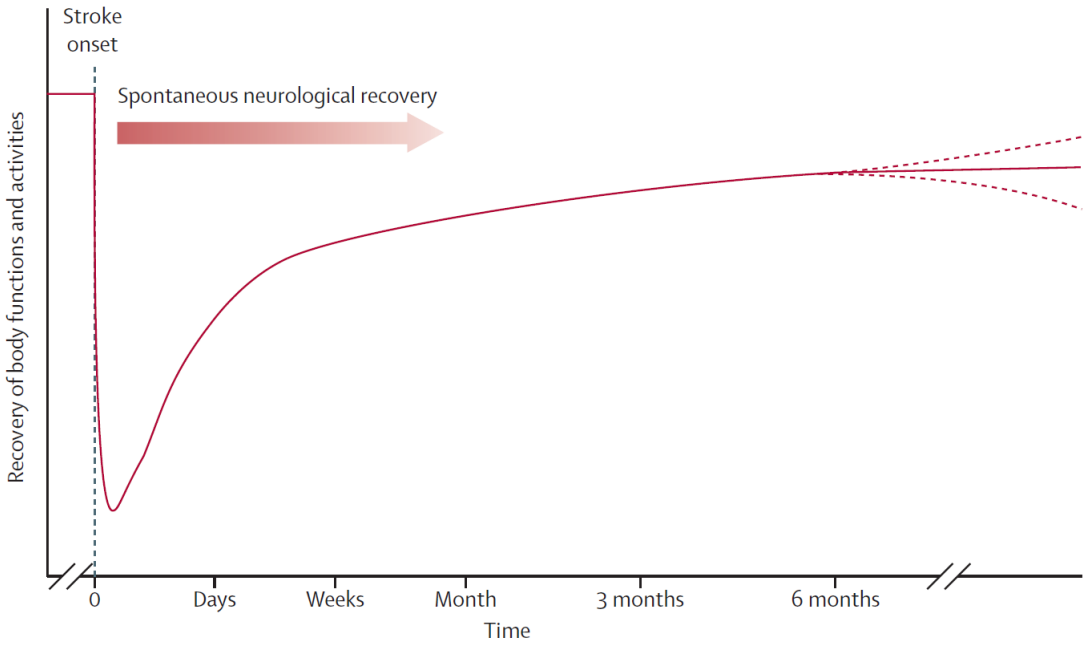

FIGURE 2.2: Hypothetical pattern of recovery after stroke (adapted from Langhorne et al. [80]).

Such impairments are not solely a manifestation of the damaged brain region but are also an expression of the ability of the rest of the brain to maintain normal function. In a quest of regaining functional control, as a natural response to the stroke, a cascade of various system, molecular and cellular level events, that facilitates neuronal protection is triggered [40, 73]. As a clinical manifestation of these events, patients experience improvements in body functions and activity. This reduction in impairments is solely determined by time and is termed as spontaneous recovery [63]. The time window, as well as the rate of spontaneous recovery, widely varies in different patients. Majority of the motor improvements happen within three months post-stroke [63, 74, 75]. Spontaneous recovery, although very important, is often incomplete and vast heterogeneity across subjects is observed in the final persistent impairments [9]. It has been observed that the rate of spontaneous recovery and final degree of impairments is loosely dependent on multiple individual and neuroanatomical factors like previous medical morbidities, genetics [76, 77], age[78], initial severity of the deficits, lesion location, and area spared by injury [46, 79]. However, this complex process of recovery is still not understood in depth.

All the observed neuro-anatomical changes triggered by the stroke, which are driven by the discrete pathophysiological events, can be systematically organized into

three recovery epochs. The initial few hours after stroke onset, which presents an opportunity to salvage the threatened neuronal tissue via neuroprotection or reperfusion, constitutes the first epoch and is termed as the acute state. The time generally after 24 hours of stroke onset to a few weeks, constitutes the second epoch, which is the sub-acute state. In the sub-acute state, the mechanisms of neuronal repair are initiated and maximum spontaneous as well therapy-induced brain recovery is observed. This state generally lasts up to 3-6 months after the stroke and at the end of this stage, all the stroke-induced endogenous repair events slow down with patient attaining relatively stable condition. The third epoch, starting after 6 months post-stroke, denotes the chronic phase. In the chronic phase, the modifications in brain functions are relatively difficult but still possible.

As the post-stroke impairments are the clinical manifestation of the underlying neuro-dynamics, they also follow the above-mentioned epochs of recovery. The acute state represents the time of maximum impairments and life-critical support system is necessary during this time. Although very heterogeneous, with the neuronal recovery at its peak, in the sub-acute state, the most dramatic reduction in impairments happens in the first 30 days after the stroke. This significant improvement continues even up to 90 days after stroke in patients with more severe deficits [80, 81]. Also, the sub-acute state is the most promising window for therapy-induced recovery. At the end of the sub-acute stage, almost 60% of patients recover completely and regain functional independence but remaining patients suffer some level of motor and/or cognitive impairments with relatively reduced odds of complete recovery. In the chronic state, with the spontaneous recovery slowed down, the therapeutic approaches aim to maintain and improve the patient's physical condition. This process of recovery and control regain is summarized using a representative hypothetical pattern of recovery in Figure 2.2.

Since very little spontaneous recovery is observed in chronic state, the population of patients with chronic impairments have the maximum need for novel rehabilitative interventions. These interventions can attempt to reduce functional impairments and improve the patient's quality of life. Also, as impairments of motor functions are most commonly diagnosed in stroke patients and as motor rehabilitation is the topic of this thesis, hereafter, this thesis focuses primarily on the post-stroke motor deficits and their rehabilitation.

2.1.3 Post-Stroke Motor Rehabilitative Interventions

The spontaneous recovery after stroke is often incomplete and a multitude of rehabilitative interventions have been proposed and are in use for promoting upper and lower limb motor recovery after stroke. These therapies aim to maximize the motor recovery by supplementing the spontaneous recovery in the acute and sub-acute state, and enhancing and maintaining the motor functions in the chronic state. Using the observations from spontaneous recovery, various rehabilitative interventions including Occupational Therapy (OT), Physiotherapy (PT), task-oriented repetitive training using robotic devices, mental practice of movements using Motor Imagery (MI) BCI, Functional Electrical Stimulation (FES), Non-Invasive Brain Stimulation (NIBS), as well as therapies based on pharmacological, biological, and stem-cell principles are being investigated for the upper extremity motor rehabilitation [82]. Although the exact mechanism of how these interventions promote motor recovery is not well known, all these treatments are based on different rationale about why and how they should promote motor recovery.

Physiotherapy and occupational therapy are the two most common motor rehabilitative intervention and are used as a control intervention while accessing the efficacy of many novel interventions. Physiotherapy aims to reduce motor impairments by repetitive task practice. Specific physiotherapy oriented interventions, including various task-oriented exercises, Constraint-Induced Movement Therapy (CIMT), mirror therapy, bilateral arm training, have been observed to be clinically effective [83]. The general principle behind all these therapies based on task repetition is that, the performance of repetitive tasks should result in the strengthening of the task engaged synapses and improved motor performance should be observed by the strengthening of remaining neuronal pathways [84]. Occupational therapy, used in conjunction with the physiotherapy, aims to reduce the degree of functional disability by effective use of remaining motor capacity.

The repetitive task training using different robotic devices is based on the similar principles of physiotherapy and have been observed to be comparable or superior to the traditional physiotherapy approaches in upper limb rehabilitation [85, 86]. Robotic rehabilitation allows high-repetition, high-intensity, consistent, precise, programmable training along with the ability of continuous measurement of various performance indicators. Due to these advantages, many different robotic systems are being developed, particularly for the purpose of stroke rehabilitation

[17]. Furthermore, robotics is being used as adjuvant therapy in many randomized control trials [87–89].

In the domain of repetitive task rehabilitation, CIMT is a relatively different therapy. CIMT involves restricting the use of unaffected upper extremity forcing an individual to use the affected hand to perform task-based activities. The CIMT is primarily devised as a counter to the compensatory behavior of 'learned no-use'. Learned no-use is a phenomenon that is thought to be related to the loss of lesioned but surviving neuronal pathways caused by no use of the affected hand. Based on this approach, CIMT has been clinically proven to be effective in sub-acute as well as chronic state [90, 91].

NIBS is another class of rehabilitative interventions which attempts to change the brain activations by application of weak electric or magnetic fields to the brain [39]. Among the plethora of techniques explored in NIBS, transcranial Direct Current Stimulation (tDCS) and Transcranial Magnetic Stimulation (TMS) are the two most common techniques. In tDCS, a weak (1-2 mA) direct current is delivered to the specific brain areas, whereas the TMS stimulates the brain by application of rapidly changing focal magnetic field which in turn induces electrical currents in the brain. The aim of the NIBS is to modify the cortical excitability and neuroplasticity to bring out clinical gains [92]. Depending on the polarity of the stimulation, NIBS has been demonstrated to successfully up-regulate or down-regulate the cortical activations in healthy subjects as well as in stroke patients [93, 94]. Despite being able to successfully modulate the cortical activity and proven to be safe, the clinical utility of NIBS is not very clear. A systematic meta-analysis [95] has reported the clinical superiority of NIBS, but recent guidelines established by European Chapter of the International Federation of Clinical Neurophysiology observed no evidence of the utility of standalone NIBS for upper extremity motor rehabilitation. Hence more study is necessary in this domain [96]. Along with the utilization as a standalone intervention, NIBS is also being used as an adjuvant intervention along with other therapies like virtual reality training [97, 98], OT [99], CIMT [100], robot-assisted training [101]. In this setting, NIBS is applied to increase the cortical excitability and neuroplasticity and while the brain is in this excited state, the primary therapies try to stimulate the appropriate neuronal pathways expecting increased brain activation and better reception and retention of the therapeutic effects.

Lastly, based on the phenomena of MI, the mental practice of movements using BCI is a relatively new intervention in the field of post-stroke motor rehabilitation. By restoration of normal neuronal motor circuits, BCI-based interventions have shown very promising results for motor function restoration. Being the topic of this thesis, BCI-based motor rehabilitation is discussed in detail in Section 2.3.

2.1.4 Stroke Assessment Scales

With the advancements and availability of novel rehabilitation technologies, it is important to judge the clinical utility of these interventions. In order to facilitate comparisons between various interventions and patient groups, robust measures of quantification of post-stroke clinical status are necessary [102]. Defining these scales of assessments in stroke setting is a challenging task because numerical quantification of the terms 'disability' and 'impairments' is not very straightforward. The designed clinical assessments are expected to be exhaustive as well as easy to perform. As both of these goals can not be achieved simultaneously and as there are distinct requirements of assessment in different stages of stroke, quite a few clinical stroke assessment scales have been designed to quantify the mortality, impairments, and disability post-stroke. Some of the most frequently used scales are discussed here.

The National Institute of Health Stroke Scale (NIHSS) is one of the most widely used scales in acute stroke setting and is considered to be a routine clinical practice. It is a 15-item, comprehensive, non-linear scale and incorporates the assessment of consciousness, motor functions, sensory loss, language, speech, neglect, coordination, visual fields, and extraocular movements[103] ranging from 0 (no impairment) to 42 (maximum). Being relevant, comprehensive, reliable and easy to perform, NIHSS is widely used in stroke research as well and many studies have been using NIHSS at admission, at discharge and/or 30 days post-stroke as a clinical endpoint.

NIHSS provides the measurement of overall clinical status of the patient and it is not focused on the assessment of sensorimotor functions. In particular, to assess the sensorimotor-impairments post-stroke, Fugl-Mayer motor assessment (FMA) [104] scale is being predominantly used in motor rehabilitation trials in recent years. FMA is an ordinal scale with 3 points assigned to each item and assesses five domains of sensory-motor impairments, viz, 1. Upper and lower limb motor

functions, 2. Sensory functions, 3. Balance, 4. Range of motion of joints, and 5. Joint pain. The FMA scale ranges from 0 (maximum impairment) to 226 (no impairments) points and this test takes approximately 40 minutes to complete. As FMA also encompasses multiple domains, various rehabilitation studies have been observed to conduct partial FMA test assessing only the domain relevant to the rehabilitation target. Despite the complexity, FMA has been observed to be comprehensive, highly consistent, reliable, and accurate [105, 106] and hence it is being widely used in the research settings.

Although FMA is a reliable scale for the quantification of sensorimotor impairments, it does not reflect the disabilities caused by those impairments. For this purpose, Barthel Index [107] (BI) and modified Rankin scale [108] (mRS) are being extensively used. BI, which can be considered as a 'basic' evaluation of Activities of Daily Living (ADL), assesses the individual's ability to perform 10 functional tasks scoring each on the rating of 0-10 with 10 indicating full independence. The BI score > 80 is generally related to the functional independence and subjects with BI< 40 are considered to be very dependent. The mRS which is primarily used to assess 'global disability' with a focus on mobility is an ordinal hierarchical scale which ranges from 0-6. mRS focuses on the disabilities originating from the loss of walking functions with 0 indicating no symptoms, 3 indicating moderate disability and 6 being death. Owing to very easy to conduct procedures and high significance to the patients, mRS and BI are often administered in the clinical settings.

Apart from the NIHSS, FMA, BI and mRS, many other measures of recovery are being used in the clinical and research settings. Scales including but not limited to Motor Status Score (MSS) [109], Medical Research Council (MRC) scale for muscle strength, Wolf Motor Function Test (WMFT), Motor Activity Log (MAL), Stroke Impact Scale (SIS), Functional Independence Measure (FIM), Motricity Index, Modified Ashworth Scale (MAS), Action Research Arm Test (ARAT), Nine Hole Peg Test (NHPT), Glasgow Coma Scale are also in use and an extensive list is available at [110].

This section presented an overview of stroke, post-stroke brain dynamics, stroke-induced impairments, and rehabilitative interventions for post-stroke motor rehabilitation. With this brief clinical background, in the next section, we discuss the technological aspects of BCI with a focus on post-stroke motor rehabilitation.

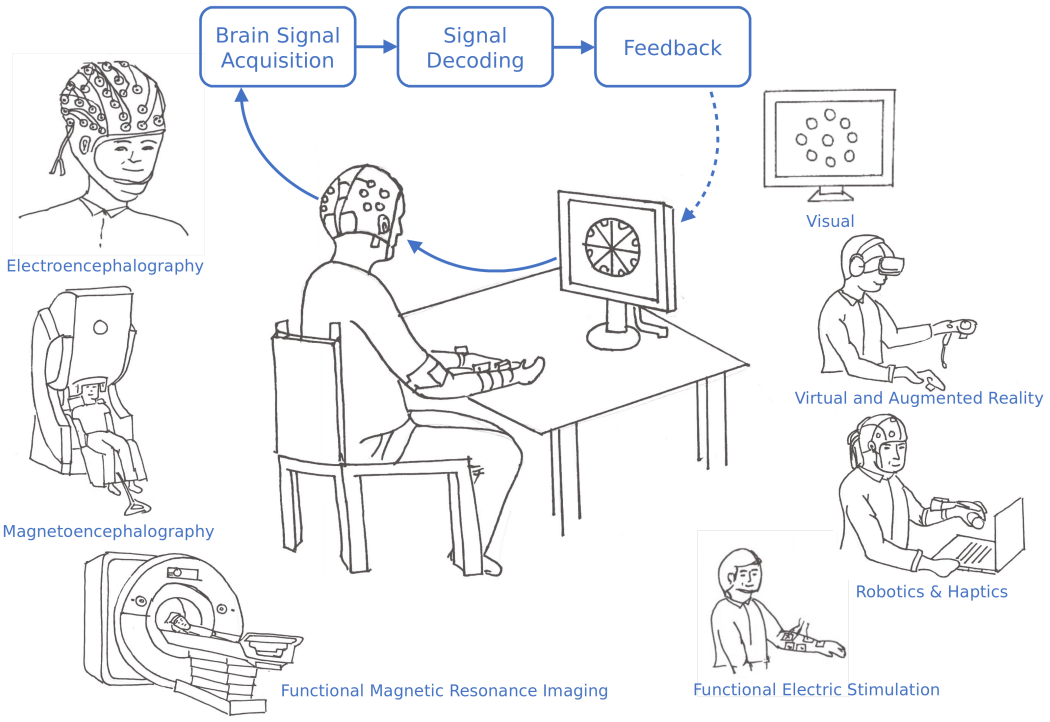

FIGURE 2.3: Overview of the BCI system.

2.2 Technology of BCI

BCI, from a technological point of view, can be conceptualized as a system to transform real-time neurophysiological signals into computer commands. BCI tries to identify specific and distinguishable brain activation patterns associated with an external or internal stimulus (e.g. imagined or actual hand movement, performing mathematical calculation etc...) which is then coupled with a predefined visual or somatosensory feedback to the user. Therefore, any BCI system is necessarily composed of three functional components, viz., brain signal acquisition device, signal decoding algorithm, and feedback device. This functional view of the BCI system is depicted in Figure 2.3 and this section will provide a technological overview of the various components of the same.

2.2.1 Brain Signal Acquisition

Acquisition of brain signals, using various signal acquisition modalities, is the foremost step in the BCI. The real-time brain dynamics can be captured by many

different modalities with their associated advantages and limitation. Also, different devices capture different kinds of neuronal information. Depending on the location of sensors, brain signal acquisition devices can be primarily classified into two categories, invasive and non-invasive. Invasive devices tap the brain signals from cortical regions by placing the electrodes deep inside the brain and hence termed as "Invasive", whereas, the non-invasive devices record the neural activity from outside of the brain, either by placing electrodes on the scalp or by using imaging technologies.

Invasive brain signal acquisition: The invasive systems involve surgical implantation of electrodes or electrode array directly on or in the brain. Being directly implanted in the brain, the invasive approach of signal recording offers very high spatial and temporal resolution resulting in high information transfer rates. However, they also come with several associated challenges, particularly related to high risk of infection and biocompatibility [111]. Hence, due to multiple clinical risks such as requirements of surgical implantation, periodic replacement of sensors, and repeated surgeries, invasive recording practices are not commonly used in humans. In humans, invasive recordings are used as a last resort in patients suffering from severe neurological disorders with no other means for communication and control. Microelectrode array recordings and ElectroCorticography (ECoG) are the two most prominent invasive recording technologies.

- **Microelectrode array recording:** Microelectrode array recording involves implanting an array of many microelectrodes deep inside the brain cortex. Since these electrodes are implanted inside the cortex, they offer excellent signal quality. However, they have the highest clinical risk. BrainGate is one successful example of BCI using Microelectrode array recording in humans [112].
- **ElectroCorticography:** ECoG is a semi-invasive approach and it involves brain recording by placing electrode array over cortex without breaking the blood-brain barrier (BBB). The ECoG electrodes are placed just under the cranium and they capture the electrophysiological signals from the cortex. This positioning of ECoG electrodes allows for very good spatial and temporal resolution while avoiding the problems of biocompatibility which are associated with the micro-electrode arrays. The need for surgical implantation is the only limitation of the ECoG recording.

Non-invasive brain signal acquisition: The clinical risks associated with invasive recordings have led to the invention of non-invasive recording techniques. Non-invasive recording methods employ over-the scalp measurement of brain activity. Although non-invasive methods generally suffer from poor signal quality due to the lack of direct access to the cortex, these methods offer minuscule clinical risk. Therefore, most of the BCI systems are based on non-invasive recording methods. Some of the most widely used non-invasive recording protocols are depicted in Figure 2.3 and are explained below.

- **Functional Magnetic Resonance Imaging (fMRI):** fMRI provides information about the metabolism of the brain by measuring the haemodynamic activations using Blood Oxygen Level Dependent (BOLD). Conceptually, fMRI captures the change in the oxygen concentrations in different parts of the brain. Since the more active neurons in the brain consume more amount of oxygen, the changes in the oxygen levels captured by the fMRI signals provide precise spatial localization of neuronal phenomena. Due to this advantage of very high spatial resolution, despite having poor temporal resolution and being costly, fMRI is used in BCI systems which require precise spatial information.

- **Near-Infrared Spectroscopy (NIRS):** Similar to fMRI, NIRS also measures the haemodynamic brain activations. Different from fMRI, NIRS uses optodes to emit and detect optical waves in the near-infrared wavelength to capture the change in the oxygenation levels of the brain. Compared to fMRI, NIRS offers relatively poor spatial resolution and it can only record the cortical activity. However, NIRS's low cost and portable nature makes it a very viable alternative to fMRI in BCI applications.

- **Magnetoencephelography (MEG):** Different from the previously mentioned methods, MEG measures the electrophysiological activations in the brain. The MEG provides information about electrical currents in the brain by measuring the magnetic field produced by them using an array of Superconducting Quantum Interference Devices (SQUID). MEG is very promising neuroimaging modality because of its very high temporal resolution as well as high spatial resolution. However, very high cost and non-portable nature have limited its applications to research settings.

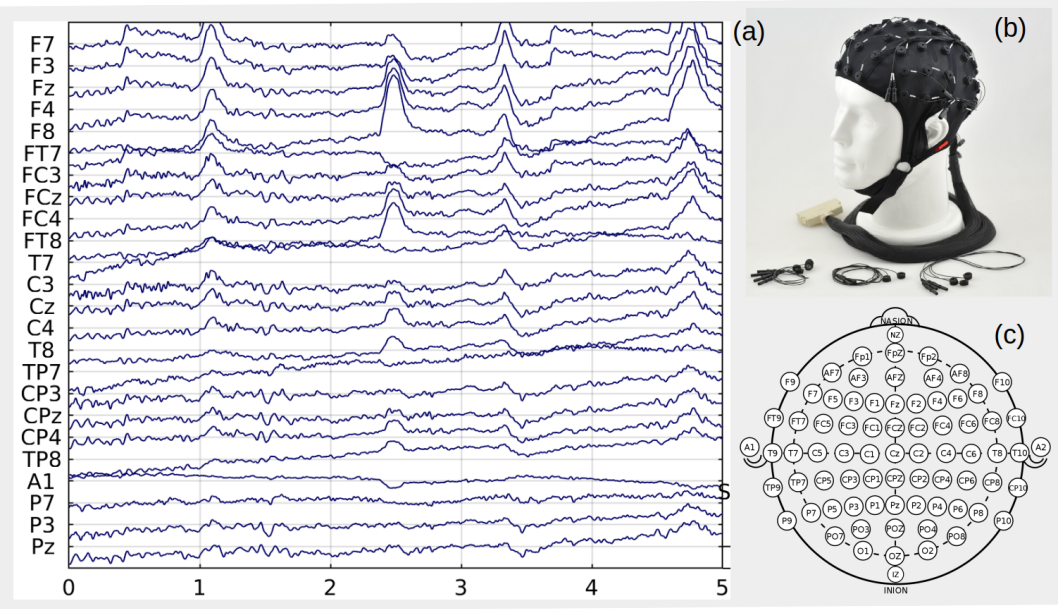

FIGURE 2.4: The EEG acquisition system and typical EEG signals. Typically, EEG signals are captured by placing multiple electrodes on the scalp (part-b), which are arranged in an international 10-20 system (part-c). The typical EEG waveform from multiple electrodes is presented in part-a.

- **Electroencephalography (EEG):** EEG is one of the most widely used and oldest brain signal acquisition methods. EEG measures the electrophysiological activity from the cortex by measuring the electrical potentials at different brain locations using multiple electrodes placed on the scalp (Figure 2.4). Among all other techniques, EEG is the most cost-effective and portable modality. Also, it offers the best temporal resolution which makes it the most suitable modality for use in BCI systems. As a tradeoff, EEG suffers from poor spatial resolution. Also, being a non-invasive modality, the EEG is generally contaminated with a high degree of noise and has a poor signal to noise ratio.

Despite its limitations, compared to other non-invasive methods, due to low cost, easy to use portable setup, good temporal resolution, and acceptable spatial resolution, EEG has become the gold standard in BCI systems. Therefore, the rest of the thesis is focused on EEG based BCI systems.

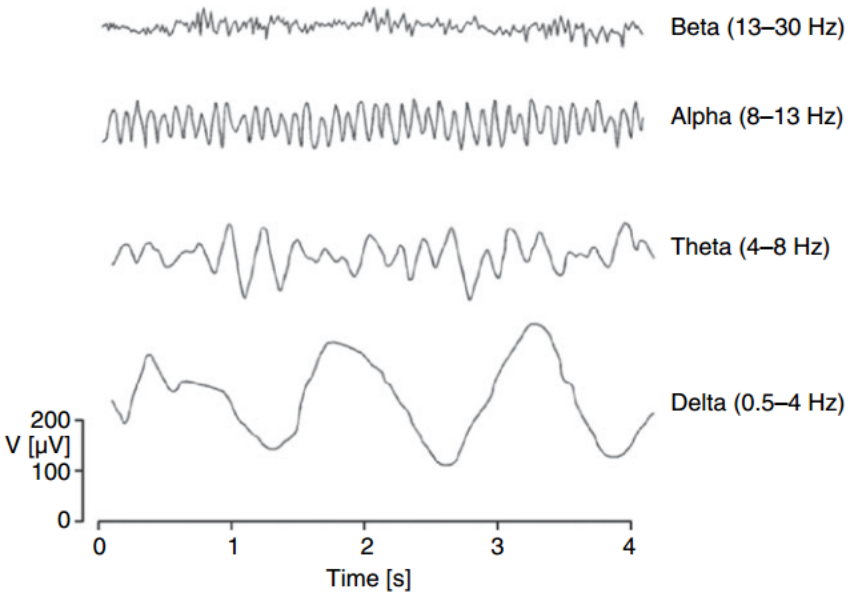

FIGURE 2.5: Examples of EEG rhythms and their frequency range. (Adapted from [1])

2.2.2 User Intent Detection

Following the signal acquisition, the interpretation of these signals by identification of various discriminative brain patterns is the next step in the BCI cycle. The effectiveness of this detection process primarily depends on two factors. First and foremost, the control strategy implemented in the BCI system determines the amount of intrinsic discriminative information present in the brain signals. Second, the efficiency of the implemented decoding algorithm dictates how much of that discriminative information can be extracted by the classifier to discern different brain activity with high accuracy. Since the control strategy and decoding algorithms determine the accuracy and the usefulness of any BCI system, this section will present some of the commonly used EEG-BCI strategies and challenges associated with them in detail.

2.2.2.1 Control strategies

The control strategy is a characteristic and distinguishable pattern of brain activation, which is caused by a mental process or state and can be uniquely identified from recorded data. As an example, decreases in EEG power at contralateral motor area following imagination of unilateral hand movement is a well-documented

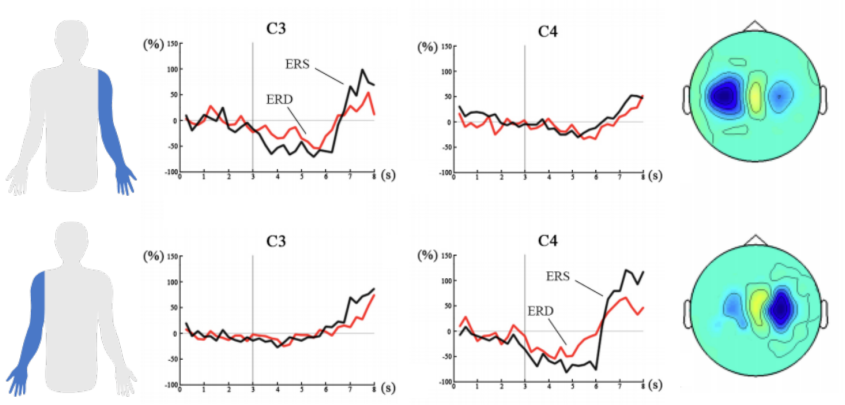

FIGURE 2.6: Example of EEG sensorymotor rhythms (Adapted from [115]). The top and the bottom row correspond to the average power in the motor region channels during a motor movement of the right and left hand respectively. Motor Execution (ME) (red line) or Motor Imagery (MI) (blue line) of various limbs results in the observation of Event-Related Desynchronization (ERD) and Event-Related Synchronization (ERS) in the EEG signals from the contralateral motor regions of the brain. As can be seen from the top row, the average power in the 8-12 Hz band drops following the ME or MI constituting ERD. Following the ERD, the power rapidly increases resulting in ERS. As shown in the topo-plot, the ERD and ERS are localized in the motor regions of the brain.

control strategy [7]. In BCI literature, there are few widely used control strategies and activation patterns associated with them can be broadly classified into *spontaneous responses* and *evoked responses*.

Spontaneous responses are the brain activation patterns that are intrinsically generated by the underlying neuronal process and no external stimulus is required to observe them. *Slow Cortical Potentials (SCP)*, which can be categorized as a spontaneous response, were one of the first control strategies used to drive BCI systems [113]. SCP are slow changes in the cortical EEG amplitude which can be observed anywhere on the scalp lasting from 300ms to several seconds. The fact that humans can learn to voluntarily regulate these potentials based on feedback has led to the use of SCP for designing BCI [114]. However, extensive training is required for successful modulation of SCP. The system using SCP as a control signal provides feedback to the user based on the observed SCP amplitude and then user controls this amplitude to select on-screen options or to move a cursor [114].

Sensorimotor Rhythms (SMR) is another spontaneous response which can be characterized by modulation of EEG power in mu (8-12Hz) and beta (12-30 Hz) bands

at the primary and supplementary motor cortex (see Figure 2.6). SMRs show a decrease in amplitude during actual movement, preparation of movement or movement imagination and this decrease is termed as Event-Related Desynchronization (ERD). Also following movement or movement imagination, power in mu and beta bands increases at the contralateral region constituting Event-Related Synchronization (ERS). Due to its intuitiveness and high similarity with the actual motor control, SMR is the most widely used control strategy in motor rehabilitative BCI systems. In SMR-BCI, the user is asked to perform an actual movement or motor imagery (MI) of different limbs (left hand, right hand, both hand etc..) and the characteristic pattern associated with each of these actions is used to provide a distinct feedback [47, 88, 116–119]. Being a spontaneous response, MI is one of the most difficult to classify activation patterns. Therefore, considering its clinical application and decoding difficulty, many advanced decoding algorithms have been proposed for MI classification from EEG data.

Movement-related cortical potential (MRCP) is a low-frequency (0-5Hz) negative shift in EEG signal and it occurs about 2s before a voluntary movement. Being a spontaneous response, MRCP is thought to reflect processes involved in movement planning and movement preparation and is observed over the primary motor cortex, sensorimotor cortex, and supplementary motor areas. MRCP has been mostly explored as a mental switch and its detection is used as a trigger for associated feedback [120–122].

Apart from the above-mentioned strategies, Error potential [123] and Readiness potential [124] are some other spontaneous responses used in BCI systems.

Evoked responses are activation patterns that are generated in the brain as a response to external stimulus. P300 and Steady-State Evoked Potentials (SSEP) are the two most commonly used evoked responses in EEG-BCI field. The P300 is an abrupt positive deflection in brain activity that is observed approximately 300 ms after the user is presented with a rare stimulus. This shift is generally observed in parietal lobe and magnitude of positive deflection is proportional to the rarity of the stimulus and the attention paid by the user. Visual P300 has been used in many assistive BCI systems for communication using a speller application [125, 126]. In most common P300 spellers, alphabets are arranged in a grid pattern and individual row or column is flashed in random order. Patients are instructed to concentrate on a letter they want to spell and P300 can be observed when

the row and column corresponding to the desired letter is flashed, identifying the character. These BCIs need very small training and offer high information transfer rates. SSEP is another family of evoked responses, which are observed when users are subjected to external stimulus (visual, auditory, or somatosensory) that is modulated in a constant known periodic pattern. This modulation pattern can be traced in EEG activations. Selective attention by the user on a particular pattern results in modulation of power or phase of EEG signals at certain brain areas and this phenomenon provides a suitable task for BCI [127–130].

Generally, the BCI systems that are based on the evoked responses tend to be more accurate and offer higher information transfer rates than their spontaneous response based counterparts. However, the need for external stimulus and lack of natural origin in brain systems limits the application of evoked response based BCI for rehabilitation purpose. Therefore, despite being difficult to decode, most of the BCI systems used in clinical applications are based on the spontaneous responses.

2.2.2.2 Challenges in EEG Decoding

The control strategy used in the BCI system generally dictates the amount of discriminative information present in the brain activations. However, because these brain activations are captured by the signal acquisition modalities and are then transferred to the classification algorithm, the signal acquisition systems also add another set of challenges in decoding of user's intentions. In this regards, the EEG data presents quite a few challenges to classification algorithms. Classification algorithms need to give special considerations and address these challenges to achieve good decoding performance. Some of the most important challenges associated with the EEG data are as follows:

- **High Noise and low SNR:** The EEG data is recorded by placing electrodes over the scalp and cortical brain signals travel through the cranium before reaching EEG electrodes. This results in significantly altered signal characteristics and reduced information content [1]. Also, the amplitude of the brain potentials at the EEG sensor is particularly small which leads to high contamination of EEG signals by much stronger sources of noise like eye blinks, muscle movements and power-line interference [1]. Therefore, EEG signals contain a high amount of noise and low Signal to Noise Ratio (SNR).

Due to this characteristically low SNR, it becomes essential to either treat the EEG data through relevant preprocessing techniques or to design classifiers that can learn generalizable patterns even in the presence of high noise.

- **Curse of Dimensionality:** The EEG data is generally recorded using multiple electrodes at high frequency. This results in very high dimensional feature vectors. As an example, a single EEG trial recorded from 32 electrodes over 2s period, in its raw form, can typically have a 64K dimensional feature vector. Such high dimensional feature vector typically necessitates a large amount of training data to avoid overfitting of the classifier models.

- **Small Sample Size:** The collection of labelled EEG data is a costly and time-consuming task. For example, in a typical MI-BCI paradigm, nearly two hours are necessary to collect mere 100 training samples. Furthermore, collection of EEG data is mentally taxing and high levels of fatigue are very common during BCI trials. These factors pose practical limitations on the collection of large EEG datasets. Therefore, most of the BCI datasets contain only 50-500 training samples per class, per subject that can be used for training of the classification models. This small number of training of samples when coupled with high-dimensional features, leads to overfitting of classifier models. Therefore, EEG-BCI calls for classifiers that can be trained even in the absence of sufficiently large training data.

- **Non-stationarity and High Intra-class Variability:** The EEG data is highly non-stationary in nature. It implies that different trials of EEG data from same class show very high variations in their spatial and temporal profile. This non-stationary nature of the EEG leads to high intra-class variability in the BCI trials.

- **Inter-session, and Inter-subject Variability:** The non-stationary nature of the EEG data also leads to significant variations in the characteristic brain patterns across sessions for the same subject and across subjects. The inter-session variability significantly limits the use of classifier models trained with one session data across multiple sessions. Also, due to high inter-subject variability, the classifier model needs to be trained separately for each subject.

All the above-mentioned characteristics of EEG make the task of brain state decoding from the EEG data very challenging. Therefore, by differently addressing

these challenges, multiple methods have been proposed for effective classification of EEG signals. These methods can be primarily grouped into two categories, viz., 1. Traditional machine learning strategies, and 2. Deep learning methods.

2.2.2.3 Traditional Approach of EEG Classification

The traditional machine learning strategies are the BCI decoding algorithms, that have tackled the task of MI classification, by paying prominent attention to the extraction of neurophysiologically sound features from EEG data. These algorithms, to beat the challenges associated with the EEG data, generally rely on effective extraction of small set of neurophysiologically relevant features. Although difficult, the extraction of a few relevant features leads to enhanced SNR and reduced feature dimensionality. This ultimately enables efficient training of classifier models even in the absence of large training samples while avoiding the problem of model overfitting.

To effectively extract the important and generalizable features from the EEG data and to achieve good classification performance, the traditional machine learning strategies generally take a multistage approach, wherein the EEG is processed through the stages of preprocessing, feature extraction, and classification.

Preprocessing

Preprocessing is performed to enhance the quality of raw EEG data before extraction of relevant features from it. In EEG-BCI systems, spectral filtering, spatial filtering and selective artefact removal are the three most commonly employed preprocessing steps. Spectral filtering generally involves high pass filtering for removal of DC drift and detrending (cut off frequency, f_c : 0.1 - 0.5 Hz) , low-pass filtering to remove high-frequency noise (f_c: 40 - 100 Hz), and notch filtering for removal of power line interference (f_c : 50 Hz or 60Hz). Spatial filtering is typically performed to reduce noise that is common to many electrodes or to enhance local activity at a particular electrode. Common Average Referencing (CAR), bipolar referencing, and laplacian filtering are some of the most commonly used spatial filtering approaches in EEG based BCI [131].

Advanced signal processing techniques are used for selective isolation and removal of activity generated by confounding sources outside the brain. Electrooculogram

(EOG) - electrical signals generated by eye movements and Electromyogram (EMG) - signals generated by muscle movements are two main sources of such a structured noise in EEG data. Independent Component Analysis (ICA) [132] is one of the most popular methods for selective isolation of both EOG and EMG. ICA treats multi-channel EEG data as an unmixing problem and tries to decompose it into statistically independent sources. Following ICA decomposition, sources that carry the signature of EOG and EMG activity are removed and the data is reconstructed using remaining sources. Infomax-ICA [133], fast-ICA [132] and AMICA [134] are some of the most widely used implementations of ICA in EEG-BCI field. In addition, many advanced tools like MARA [134], SASICA [135], ADJUST [136], have been developed for automatic identification of artefactual ICA components.

Artefact subspace reconstruction (ASR) is another promising tool for short-time high-amplitude artefacts correction in continuous EEG data [137]. Other than above-mentioned mainstream approaches, many more preprocessing techniques have been explored by the EEG-BCI researches and interested readers can refer to [138] for an extensive review of artefact removal technology. Also, few BCI research groups have proposed end-to-end EEG preprocessing pipelines like PREP [138], ADJUST [136] and HAPPE [139]. [139] provides an overview of the effects of various preprocessing steps on processed EEG data in-terms of retained signal and removed noise.

Overall, the prepossessing algorithms aim to clean the EEG data by removing noise and retaining signals of interest.

Feature extraction

Feature extraction attempts to extract neurophysiologically relevant and distinguishable information from preprocessed data. Generally, the control strategy used in BCI system strongly influences the selection of relevant features. EEG based BCIs most commonly extract temporal, spectral, and spectro-temporal features. Temporal features try to encode the typical time course of neurological signal and are generally time-locked with the associated activity. As an example, in P300 BCI, the appearance of peak positive amplitude in EEG data indicates the user's choice to select a particular letter. Spectral features are extracted when relevant information is encoded in power or phase of EEG signal. SMR-BCI as well as SSEP-BCI generally use spectral features [47, 116–118]. Spectro-temporal features

are extracted using methods like wavelet decomposition and they simultaneously capture the temporal and spectral dynamics. These features have been observed to be useful owing to the non-stationary nature of neurophysiological signals.

EEG Source Imaging (ESI) is another method that is used to transform the recorded sensor space EEG data into a source space, identifying various cortical sources underlying the observed data. The spectral or temporal features are then extracted from this source space data providing better features and high interpretability of the observed phenomena. [140] provides an excellent review on the use of ESI in the BCI field.

In recent years, data-driven feature extraction methods are also becoming popular. These methods try to identify discriminating patterns using a supervised approach. **Common Spacial Patterns** (CSP) is one such widely used method which tries to spatially filter the EEG data for extracting the most class discriminative features [141]. In CSP, a spatial filtering matrix W is calculated from the two class data, such that the resultant projected data will have a maximum variance for one class while minimizing variance from other class. To calculate the projection matrix W, the CSP algorithm minimizes the objective function in (2.1).

$$J(W) = \frac{WX_1X_1^TW^T}{WX_2X_2^TW^T} = \frac{WC_1W^T}{WC_2W^T} \tag{2.1}$$

where X_1 and X_2 are matrices of EEG signals recorded corresponding to classes 1 and 2 respectively, C_1 and C_2 are the covariance matrices corresponding to classes 1 and 2 respectively.

Following the calculation of W, the EEG data is projected to a discriminative subspace and the log-variance based features are extracted as following:

$$S = W^TX \tag{2.2}$$

$$Features = log(var(S(t))) \tag{2.3}$$

The CSP has many advantages and it has been used for a variety of BCI applications owing to its simplicity and computational efficiency. However, it also suffers from some drawbacks. CSP is sensitive to noise and non-stationarities in EEG data. Moreover, when the size of the training data available is small, CSP is also

prone to overfitting. Considering these limitations, many modifications to CSP have been proposed. In particular, a modification of CSP, named **Filter Bank CSP** (FBCSP) [142] is one of the most successful feature extraction algorithms and has been widely used in SMR-BCI studies [15, 88, 119, 143, 144]. FBCSP first decomposes the EEG into multiple narrow-band signals, achieving EEG spectral localization. The narrow-band EEG is then spatially filtered using CSP algorithm and then features extracted from all the bands are concatenated to form the feature vector.

Overall, feature extraction algorithms, along with preprocessing step, extract the relevant features from EEG data while discarding the noise, reducing the dimensionality and improving the signal-to-noise ratio.

Classification

Classification is the final stage in the signal processing pipeline of the traditional machine learning strategies and aims to predict the outcome expected by users from the extracted feature vector. The data in BCI application is generally characterized by huge number of features and very less training trials. Also, neuroimaging data from the different recording sessions and different users possesses inherent fluctuations in features associated with the same mental process. This inter-session and inter-subject variability in features complicates the design of classifier. Moreover, closed-loop BCI system is a bidirectional adaptive system where user's brain also undergoes modifications over sessions to learn the task at hand and hence classifier needs to adapt to these dynamic changes as well. Owing to the above characteristics, along with noisy features, classifiers in the BCI field tend to overfit on training data and perform poorly on testing data [145]. Hence, the above points need to be considered while designing any BCI classifier and recent advances in this field have tried to address these issues.

Classifiers used in BCI domain can be broadly clustered into generative or discriminative categories. To classify a feature vector, generative classifiers compute the likelihood of all classes and choose the most likely. Bayes' quadratic [146] and Hidden Markov Model (HMM) [147] are the two most prominent generative classifiers in BCI. These classifiers are also adaptive in nature and allow modifications in the learned model based on changing signal characteristics [148]. Discriminative classifiers only learn the discriminating features between classes to directly

classify the feature vectors [149, 150]. In BCI field, linear discriminative classifiers like Support Vector Machine (SVM)[151–154], Linear Discriminant Analysis (LDA) [118, 146, 155, 156] and their variants are among the most widely used classifiers. They have been preferred in real-time BCI applications due to their low computational complexity and low variance [145]. In recent years, transfer learning approaches are being explored to deal with the problem of small training sets and to tackle the inter-session and inter-subject variability [18]. To address the issue of large feature vector, tensor representation of features has been proposed [157]. Overall many classifiers have been explored for application in BCI domain and an extensive review of them can be found in [18, 145].

In conclusion, following the three-staged approach, the traditional classifiers have effectively tackled the task of EEG decoding. However, their high dependence on handcrafted features, low model capacity, and far from perfect classification performance leave a lot to be desired.

2.2.2.4 End-to-end Classification with Deep Learning

As it can be observed from the last section, although, the traditional machine learning approaches have been quite successful in the BCI domain, their classification accuracy highly depends on the identification of relevant neurophysiological phenomena, a task which is not trivial. Therefore, different from this approach of handcrafted feature extraction, there has always been an interest in developing an end-to-end classification system which can learn the discriminative information just from the raw brain signals, without the necessity of human expert knowledge. To address this requirement, in recent years, deep learning, which is an extensively data-driven approach to classification has shown very promising results.

Deep learning, a field of machine learning, represents the class of computational models that encode complex mappings from the data to the classification label using a series of nested simple mappings. In the simplest form, deep learning models include multiple stacked layers of artificial components called “neurons” that linearly weigh the features at their input and apply a non-linear transformation on the resultant product before passing it to the next layer. The most important feature of these models is that the parameters of all these linear transformations are learned in an end-to-end manner, directly from the training data, by optimizing the

cost function associated with correct predictions. This capability of complete optimization of the model only based on the data and its associated label while having a capacity to model highly complex mappings has made deep learning methods extremely popular in many fields of machine learning. Particularly, deep learning architectures have been very successful in processing complex data such as text and images and have achieved the best results on many open benchmark tasks.

At their core, deep learning architectures are primarily composed of many layers of different functional units. Among them, fully-connected, convolutional, and recurrent layers are most commonly used.

Fully-Connected (FC) layers are composed of the most basic unit of the neural network, which is a perceptron ,or a neuron. Each neuron in every FC layer receives the output of all the neurons from the preceding layer, resulting in a web where all the neurons in any layer are connected to all the neurons from the preceding layer, hence the name fully-connected layer. Even before the envisioning of deep learning, the FC layers have been used as a neural network based classifiers in the BCI systems [158]. In such systems, FC layers are used to learn the approximate non-linear functional mapping between the extracted BCI features and classification labels. Even with the advances in deep learning, almost all the deep learning architectures contain at least a few FC layers.

Following the perceptron, inspired by the visual system and the neurocognition model, Convolutional Neural Network (CNN) is the next most important type of layer in the deep learning models [159]. Different from the FC layer, convolutional layers, restrict the connections between neurons from different layers. In CNN layer, neurons in a given layer are only connected to a subset of neurons from the preceding layer. This structure of restricted connections, which is similar to the convolution operation in the signal processing domain, encourages the model to learn invariant representations of the data. This property of invariant representations stems from another fundamental characteristic of convolution operation, that it shares weights among different sections of the input. This weight sharing reduces the amount of computation significantly, and also, the shared weights can be interpreted as local feature extractors. Furthermore, CNN layer, when used in combination with a pooling layer, results in a network whose activations are invariant to slight translations in the input features. The property of translation

invariance along with effective learning of local pattern has made CNN very effective for processing of structured data like images.

Both FC and CNN layers are feed-forward neural networks, networks whose flow of data is only in one direction. However, in some machine learning tasks, like machine translation, video processing, time-series prediction, etc.., the temporal dependency between the data-points is important information. To process such sequential data, Recurrent Neural Networks (RNNs) have been proposed [160]. RNN is a generalization of feedforward neural network that has internal memory. Recurrent layer, in its most basic form, by incorporation of memory elements, receives the preceding layer's current output and its own output from the previous time-step. So, by using the current and the past network state, the RNN can effectively learn sequential information in any signal. Furthermore, advanced versions of RNN, that address the RNN's problem of vanishing gradients, named Long Short-Term Memory (LSTM) [161] and Gated Recurrent Unit (GRU) [162] are being more widely used instead of regular RNN.

Using the CNN, RNN and FC as primary building blocks, many more advanced deep learning networks have been proposed in the literature.

Following the success of deep learning in other fields, many researchers have explored its applicability for EEG classification. Overall, till 2019, more than 150 papers have published the research on the use of deep learning for applications in EEG-BCI [19]. In particular, architectures based on CNN have gained popularity in the BCI field due to their ability of effectively learning the local connectivity patterns from the given data [19–23]. Furthermore, BCI researchers are also investigating the use of RNNs for extracting the temporal information from the EEG signals [163]. Among these works, some of the notable works for end-to-end MI classification from the EEG signals are presented next.

A paper by An et al. [164], is one of the first works that presented the use of deep learning for MI classification. In this work, the Fast Fourier transform (FFT) based features are manually extracted from the multi-channel EEG data and the extracted features are classified with the help of deep learning architecture using Deep Belief Network (DBN). Although this paper demonstrated that deep learning can be successfully used in MI domain, it merely used the deep learning network as classifier and feature extraction was still manually performed.

Sakhavi et al. [165] presented one of the first works which employed deep learning for extraction of relevant feature from the EEG data and its classification. In this work, authors proposed a multi-layer CNN architecture for extraction of dynamic energy features which are then classified using an FC layer classifier. Using a deep learning based feature extraction, this architecture achieved state-of-the-art classification performance at the time of its publication. However, this architecture still needed extensive preprocessing of the EEG data.

In an influential paper, Schirrmeister et al. [20] presented two CNN based deep learning architectures named Deep ConvNet and Shallow ConvNet for end-to-end classification of EEG-MI data. Both of these architectures implement stacked CNN layers for extraction of spatial and temporal discriminative information from the EEG data. Operating on minimally processed data, the Deep ConvNet architecture significantly improved the accuracy of four class MI classification.

Following the Deep ConvNet architecture, based on the recently proposed depth-wise CNN, Lawhern et al. proposed a compact general-purpose deep learning architecture [22]. With the extensive experiments, this paper, for the first time, demonstrated that single deep learning architecture can successfully learn to classify EEG data from multiple BCI paradigms.

Different from the CNN based architectures, Zhang et al. presented a convolutional recurrent attention model (CRAM) that utilizes a convolutional neural network to encode the high-level representation of EEG signals and a recurrent attention mechanism to explore the temporal dynamics of the EEG signals as well as to focus on the most discriminative temporal periods [163]. Based on the CNN-RNN cascade, this network has achieved state-of-the-art classification performance in subject-independent classification tasks.

In conclusion, deep learning models have outperformed state-of-the-art classical machine learning techniques. However, the achieved improvements in subject-specific classification settings are still marginal [20–23]. Unlike other domains, this lack of substantial improvements by deep learning can be traced back to the nature of BCI datasets. Scarcity of training data along with the high feature dimensionality results in heavy overfitting of deep learning models and this creates unique challenges for adaptation of deep learning methods in the BCI field [19].

Table 2.1: Prominent EEG motor imagery classification algorithms.

Method/Architecture	Design	Advantages	Limitations
Deep Classifier [164]	Classification of EEG power in 8-12 Hz band using Deep Belief Networks (DBN). Ada-boost using the classifiers trained from different channels.	The first use of DBN for EEG classification.	Manual feature extraction in a form of signal power.
C2CM [21]	Extraction of envelop energy features followed by a CNN based temporal feature learning and classification using a fully connected layer.	Extraction of temporal information using CNN filters resulting in reduced dependence on manual feature extraction.	The spatial filters were extracted using traditional machine learning method of FBCSP.
Deep ConvNet [20]	Five layered CNN architecture with the first layer for spatial feature learning and the next four layers for temporal feature learning.	A fully data-driven model with end to end training capabilities.	High number of trainable parameters and high model complexity.
Shallow ConvNet [20]	A two-layered CNN architecture with the first layer for spatial feature learning and the next layer for temporal feature learning.	A very compact architecture.	Low model complexity limits the possibility of performance boost if more training data becomes available.
EEGNet [22]	A 3 layered CNN architecture with the first layer for temporal feature learning followed by a depthwise and a pointwise convolution for learning temporally localized spatial information.	Extremely general purpose and compact architecture with good classification performance across multiple BCI tasks.	-
CRAM [163]	A CNN-LSTM model which uses CNN layers to encode the high-level representation of EEG signals and an LSTM attention mechanism to explore the temporal dynamics and to focus on the most discriminative temporal periods.	Among first models to incorporate LSTM self-attention for EEG classification. With this design, the model achieved significantly better classification accuracies in subject-Independent BCI setting.	The increased model complexity with the inclusion of LSTM module may lead to worse performance in subject-specific BCI studies.
MI-EEGNet [166]	A Mobilenet inspired CNN architecture which uses differently sized CNN kernels for multi-scale feature extraction.	The use of differently sized CNN kernel allows parallel multiscale extraction of EEG features leading to better classification accuracy.	-
RFNet [167]	Extraction of Riemannian geometry-based feature for spatial feature learning followed by an LSTM-attention module for temporal feature learning.	One of the first architecture to combine Riemannian geometry-based features with deep learning methods resulting in superior classification performance.	-

Therefore, further improvements in deep learning architecture are necessary to achieve better classification performance in the BCI domain.

2.2.3 Feedback

Following the classification of brain signals, afferent visual, auditory, somatosensory or haptic feedback is the last step in closed-loop BCI systems and it provides the user with perceivable output associated with predicted intention. Feedback modalities used by BCI system range from simple 1D cursor control [168] to extremely complex 3D control of a robotic exoskeleton [169] and this selection of feedback is primarily dependent on the objective on BCI and the employed control strategy. Some BCI systems implement the feedback to replace or augment the existing functional capabilities of the user. As an example, P300-BCI spellers provide visual feedback and display the predicted letter selected by the user. In completely locked-in patients, this system provides an alternative method for communication. Hence, in these BCIs, accuracy, information transfer rate (ITR) and intuitiveness of the BCI feedback is very important as it greatly determines the usability of these systems. In BCI systems used to restore the normal functions, the correct feedback acts as a reward to the user for producing appropriate brain activation. Hence, in these systems, accurate and time-locked feedback is of paramount importance. This contingent feedback is thought to restore damaged brain by positively reinforcing associated brain activity.

BCI systems used in communication domain commonly provide text [170], graphical [168] and auditory [171] feedback. In the control domain, BCI systems have been used to control robotic exoskeleton [169] as well as wheelchair [172] to augment upper and lower limb functions respectively. With technological improvements, the BCI-control of lower limb assistive robots is also being explored [173]. BCI systems which are focused on the restoration of upper and lower limb motor functions generally employ a combination of visual [174, 175], robotic [12, 47, 88, 119, 176, 177], FES [116, 121, 178–181], Neuro-Muscular Electrical Stimulation (NMES) [182] and Virtual Reality (VR) [183] as a feedback paradigm.

2.3 BCI-based Post-Stroke Motor Rehabilitation

Following the establishment of the technological framework of BCI systems, many researchers have explored its utility for the rehabilitation of patients suffering from various functional impairments. Particularly, the use of BCI for restoration of motor impairments following stroke has seen tremendous interest from the research community. In the view of clinical applications, there are two main strategies followed for use of BCI in stroke patients. The first approach, named *Assistive BCI*, aims to bypass the neuronal pathways and uses BCI system as an alternative path for communication and/or for continuous control of the external devices like robotic orthosis [184]. These devices improve the quality of life by acting as a substitute for the lost neuronal control. The second category, named *Rehabilitative BCI*, is targeted to regain the functional capabilities by restoration of damaged neuronal pathways using principles of neuroplasticity [185]. Since restoration of motor functions is the objective of this thesis, this section will discuss the clinical use of rehabilitative BCI systems for post-stroke motor rehabilitation.

2.3.1 Principles of Neuronal Recovery by BCI

Neuroplasticity is the brain's ability to undergo substantial structural and functional reorganization throughout human life and it forms the scientific basis of all the rehabilitative efforts of brain restoration [17, 40]. In fact, numerous neuroimaging studies have confirmed that the cognitive and the motor function improvements following post-stroke rehabilitation are associated with structural modification and functional recovery in the brain [9, 40]. Hence, it is postulated that the effectiveness of any post-stroke rehabilitative intervention will be dependent on its ability to promote restorative neuroplasticity [9].

The stimulation of neuroplasticity from BCI intervention can be conceptualized primarily into four mechanisms; viz, 1. Neurofeedback training, 2. Operant conditioning by reinforcement, 3. Reinforcement of neuronal circuits by repetitive engagement, and 4. Hebbian learning.

Neurofeedback training refers to the volitional/conscious modulation of brain activations by the user [185]. Reduced cortical activity and slowing of brain rhythms in the insulted hemisphere are some of the well-known deficits following stroke and

are poised to be associated with motor and cognitive impairments [24, 38]. Neurofeedback training targets these abnormal activations with the philosophy that restoration of brain activations to 'more normal' state will result in functional recovery [8]. To achieve this goal, the patients are provided with a continuous visualization of the brain activity from certain regions and are asked to volitionally up or down regulate this activity. As an example, in multiple motor rehabilitation studies, patients are asked to up-regulate the cortical activity in the mu and beta bands from the lesioned primary or supplementary motor areas to achieve improvements in upper limb motor functions [47, 180, 181, 186]. It has been shown that repetitive neurofeedback training results in a long-term and sustained change in the targeted activation patterns and this change is associated with a reduction in functional impairments [47, 180, 181, 186, 187].

Operant conditioning by reinforcement is one of the classical mechanisms of human learning wherein modification in the strength of a behaviour is achieved by rewarding the desired actions and punishing the undesired ones [188]. In the context of BCI, the operant conditioning is achieved by rewarding the patient in a form of visual or sensory feedback upon successful elicitation of the targeted action and providing negative or no feedback on insufficient activations. Most of the BCI systems designed for motor rehabilitation follow this mechanism wherein the successful elicitation of the attempted/imagined limb movement by the patient is rewarded by actual movement of the stroke-affected limb using a robot or electrical stimulation whereas an unsuccessful attempt does not produce any movement [177, 178, 189–191]. This kind of intrinsic, contingent and scheduled reward of success is expected to drive neuroplastic changes in the same way as the human brain learns to interact with a novel stimulus. Also, repetitive success is sought to drive motivation which in-turn may enhance the rehabilitative efficacy of the BCI intervention [8].

The effectiveness of the neurofeedback training and operant conditioning highly depends on the identification of the best cortical activation target to train, which is not a trivial task. Hence, to altogether circumvent this problem, rather than training on a particular rhythm, some BCI systems focus on natural tasks as a whole. As an example, some of the BCI systems for motor rehabilitation train the patients to perform motor movement/imagination [13, 88, 119, 144, 154, 179].

The training is achieved by first recording the whole brain activation pattern associated with the specified tasks and then strengthening it by repetitive training wherein identification of this pattern is provided with a rewarding feedback. The fact that multiple brain systems are involved in the execution of most of the cognitive, and motor tasks and simultaneous activation, and successful coordination between these systems is necessary for functional improvement forms the basis for this mechanism. Damage to the white matter systems like corpus callosum and corticospinal tract following stroke hampers this essential coordination and results in functional impairments [24, 38, 42, 192]. Hence, the BCI-based, task-focused training that results in repetitive recruitment of the normal motor or cognitive circuits, may strengthen the stroke affected neuronal connectivity leading to functional improvements.

'Neurons that fire together wire together', which is the principle of Hebbian plasticity, is thought to be one of the important neuronal repair mechanism stimulated by the BCI systems, particularly in the motor rehabilitation settings. Motor impairments following stroke create a gap between motor intention and execution wherein patients' intention to move doesn't produce any actual movement which results in the lack of sensory feedback to the brain [8, 193]. Some of the BCI systems aim to bridge this gap and close the natural motor loop by providing immediate sensory feedback using robotic or haptic devices that is contingent with users' movement intention [13, 88, 119, 144, 154, 177, 179, 194, 195]. Here, it is hypothesized that re-establishing the contingency between cortical activity related to the attempted or imagined movement and the proprioceptive feedback (actual movement) may strengthen the sensory-motor loop and stimulate the neuroplasticity that leads to motor recovery. This simultaneous activation of the outputs and inputs to the motor cortex which triggers the Hebbian plasticity has been thought of as a mechanism behind the neuroplasticity following these rehabilitative interventions [17, 40, 194].

Lastly, the above-mentioned mechanisms are complementary to each other and hence, depending upon the selection of neuronal rehabilitation target and the design of the feedback modality, any rehabilitative BCI system may stimulate the brain recovery by any or all of the mentioned mechanisms.

2.3.2 Efficacy and Effectiveness of BCI for Post-Stroke Motor Rehabilitation

Motor rehabilitation is by far the most researched application of BCI in the stroke domain. In fact, restoration of upper extremity motor impairments in severely impaired stroke patients served as initial motivation for the exploration of BCI technology in the post-stroke rehabilitation field. Patients with severe impairments do not possess the minimum movement capabilities that are necessary to be eligible for the conventional rehabilitation paradigms like OT, or PT, or CIMT and this necessitates the search for a novel rehabilitative intervention. The findings that even the imagination of motor movements, known as MI, results in the recruitment of the same neuronal circuit as the one associated with the actual movement indicated the potential of BCI for rehabilitation. This observation prompted the exploration of whether the severely affected stroke patients, who present with complete loss of motor control, can perform MI and generate the cortical activations associated with the MI. An initial study comprising eight chronic stroke patients with severe upper limb hemiplegia indicated that most of the patients could indeed successfully modulate the sensory-motor rhythms and control an MEG based BCI system [47]. Although this study did not report any functional improvement, it paved the way for further exploration of the rehabilitative potential of BCI technology. The first report on clinical improvements was published by Ang et al. [87] wherein eight chronic stroke patients had participated in a BCI mediated upper limb rehabilitation. The BCI system was based on the MI protocol and successful detection of MI from real-time EEG signals was rewarded with the centre-out movement of the impaired hand using the MIT-Manus robot. Following 12 rehabilitation sessions over four weeks, a significant improvement in motor function of 4.9 points was observed on an FMA. Another longitudinal case study that comprised 60 BCI rehabilitation sessions spread over a period of eight months indicated that clinical improvements following rehabilitation are associated with the increased corticospinal tract integrity and enhanced cortical activations in the sensory-motor area [176].

Following the initial clinical results, with support from neuroimaging studies, in the last decade, extensive research has been conducted, exploring the application of BCI for post-stroke motor rehabilitation. Multiple controlled trials have been conducted and they have indicated that, while being available to much diverse

spectrum of patients, BCI systems can achieve clinical gains which are at par with conventional rehabilitation techniques like occupational therapy, robotics, and functional electric stimulation for upper limb motor restoration following stroke [12, 14, 45, 88, 144, 175, 177, 179–181, 196]. Also, a 2018 meta-analysis of these studies observed that BCI intervention is associated with Standardised Mean Difference (SMD) of 0.79 on upper extremity FMA scale which is comparable with other widely used therapies like CIMT (SMD = 0.81), mirror therapy (SMD = 0.61), and robotics (SMD = 0.35) [10].

Collectively, from all these studies, it can be observed that BCI has been quite effective for restoration of post-stroke motor functions. However, there are still many open research questions, investigation of which, can drastically improve the effectiveness of the BCI intervention.

Since reinforcement learning and Hebbian plasticity are thought to be important mechanisms of BCI operation, the role and design of feedback which acts as a reward, is very crucial. Studies have explored the clinical efficacy of numerous feedback modalities like visual [45, 175, 196], robotic[88, 144, 197–199], FES [14, 179, 180], NMES [154], and more recently, VR [200, 201] with the main aim to provide perceptual and sensory feedback and all these modalities have been observed to elicit motor recovery when used in conjunction with the BCI control. However, how the selection of these modalities and the design of the feedback paradigm affect clinical outcomes is still elusive. For example, in a controlled study [182], the authors reported that sensory feedback of movement may be the crucial element of the BCI based rehabilitation and visual feedback alone is not sufficient to evoke functional gains. This observation becomes counter-intuitive in light of the clinical gains following multiple studies using neurofeedback based BCIs [174, 175, 186]. These results may be caused by the type of interface used for visual feedback and hence the effect of the presentation technique used for visual feedback needs to be investigated [202]. Moreover, immersive feedback provided by the VR systems may help in enhancing the effect of visual feedback [200, 201]. Furthermore, contingent sensory feedback using robotics, FES or NMES is thought to promote the neuronal repair by stimulating the Hebbian plasticity. However, it is necessary to explore if a similar clinical recovery can be achieved without afferent sensory feedback. If equivalent gains can be achieved by using only a visual or VR feedback then it can lead to a much more portable, simpler and affordable

rehabilitation system that can be used at home which is one of the ultimate goals for the BCI technology.

Contingent and concomitant activation of the cortical areas is essential for the stimulation of Hebbian plasticity. Hence, timing and latency of feedback become important parameters in the BCI studies that provide sensory feedback. It is postulated that following motor intention, the afferent sensory feedback generated by actual movement is responsible for disinhibition of motor cortex and hence the timing of this disinhibition may be an important factor in determining the effectiveness of motor learning [203]. One initial lower limb rehabilitation study also highlights this point where it is observed that only the group that received a Common Peroneal Nerve Stimulation (CPNS) timed to reach the brain at the peak negative phase of the MRCP resulted in functional improvements [121]. Also, one recent upper limb rehabilitation study examined the effect of different feedback intervals in a robotic rehabilitation study [203]. Although significant functional improvements were observed, conclusive remarks on optimal timing and latency of feedback could not be extracted. Hence, more studies are necessary to identify the optimal feedback duration and standardization of the same in future BCI systems is essential.

The widespread inclusion of BCI systems in the regular rehabilitation practice necessitates knowledge about how the duration, intensity and frequency of BCI rehabilitation affect the clinical outcome. One initial study indicates that the total number of sessions and BCI intensity (BCI trials/session) and not the frequency of sessions impacts the final clinical outcomes and neurological improvements [204]. However, another study reported that clinical gains on the Action Research Arm Test (ARAT) scale were not dependent on the BCI usage time [11]. Considering the clinical relevance, lack of studies, and contradicting evidence, investigation in this direction is required.

A few BCI-based upper limb rehabilitation studies have explored the addition of NIBS as adjuvant therapy. NIBS, which can be provided as a TMS or tDCS, is generally administered just prior to a BCI rehabilitation session to modify the cortical activation state [96, 205]. In stroke patients, generally, excitatory NIBS stimulation is applied over the ipsilesional motor cortex (M1) and inhibitory NIBS stimulation is applied over contralesional M1 with an aim to target the reduced ipsilesional M1 activations and increased inter-hemispheric inhibition [39]. The

facilitatory state of the brain following NIBS has been thought to have a priming effect that may enhance the effectiveness of the succeeding BCI therapy [96]. Hence, in recent years a few studies have combined the NIBS with BCI based rehabilitation [119, 143, 183, 206], but the additive clinical benefits of NIBS are not clear. Two controlled studies that have used tDCS for brain priming have reported similar clinical outcomes in control and experimental groups [119, 206]. However, despite similar clinical gains, neuroimaging studies indicate that the brain recovery mechanisms stimulated by BCI and BCI+tDCS intervention might be very distinct [192]. These findings indicate a potential for sequential training using BCI and BCI+NIBS interventions with a possibility of additive clinical gains.

Also, before proceeding with the inhibitory stimulation of the contralesional hemisphere using NIBS, thorough understanding of the role of the contralesional hemisphere in the post-stroke condition is necessary. It is a general consensus that the contralesional hemisphere shows increased activation following stroke [39]. It is postulated that this increased activation results in an enhanced inhibitory drive on the lesioned hemispheres [39]. Contrarily, a few studies suggest that the increased activation in the contralesional hemisphere is the brain's attempt to compensate for the lost ipsilesional functions [40]. BCI rehabilitation trials have been conducted on the basis of both positive [11, 207] and negative [119, 183] role of the contralesional hemisphere and all these studies have shown clinical improvements. Hence, more knowledge about the role of the contralateral hemisphere is necessary and this may lead to some major modifications in the existing BCI protocol [39].

Lastly, upper limb rehabilitation studies indicate that the motor function improvements following BCI rehabilitation may be associated with the accuracy of the BCI system. Many studies have observed a significant correlation between the BCI accuracy and clinical gains [11–16]. Moreover, most of the controlled trials wherein the control group received random feedback, which is essentially a chance level accurate system, have reported far less functional improvements compared to the experimental group [14, 175, 177, 180]. The reason for this association between BCI accuracy and improvement is not clearly understood. One hypothesis is that the higher BCI accuracy may elevate the level of confidence and motivation in patients which may better promote reward-based plasticity. Moreover, higher BCI accuracy may also impart greater patient engagement whereas irrelevant feedback

from a less accurate BCI system may result in frustration and hence can negatively affect the rehabilitation [175]. Also, greater engagement may be associated with a higher level of patient attention and this may be one of the reasons behind the success of BCI rehabilitation. These findings indicate that more accurate BCI systems might be more effective in promoting motor function recovery.

The collective evidence from all clinical trials indicate that BCI based rehabilitation is feasible and effective for post-stroke motor function restoration and there is much more room for improving the clinical outcomes of the BCI interventions [10].

2.4 Personalized Stroke Rehabilitation

The previous section presented that BCI is one of the best rehabilitative interventions available for patients with severe post-stroke motor impairments. However, as mentioned in Section 2.1.3, other than BCI, a plethora of other rehabilitative interventions are available for post-stroke motor recovery. This availability of multiple interventions along with the highly diverse response of patients to any particular interventions indicates a possibility of personalized rehabilitation. The far-reaching objective of personalized rehabilitation is to create a tailored rehabilitation plan for every patient, such that, by combination of multiple rehabilitative interventions, each patient will be able to achieve maximum possible functional recovery.

Although personalized rehabilitation seems like an ideal scenario, its materialization is a very difficult task. Specifically, in stroke patients, there is high heterogeneity in the damage to the neuronal tissue caused by the stroke and the exact relation between neuronal damage and observed functional impairments is not very well known. To further complicate the matters, very little understating of exact mechanisms of neuronal recovery stimulated by different rehabilitative interventions is available. Therefore, to achieve this holy grail of personalized rehabilitation, multiple studies have been conducted. All these studies, that explore the prognostication and characterization of post-stroke recovery, have sought answers to some of the following questions.

1. What are the neurological or physiological features that can characterize the observed motor impairments in acute, sub-acute and chronic states of stroke?

2. Is it possible to predict the extent of motor impairments at the end of spontaneous recovery? What are the features that provide this prognostic information?

3. Are there any neuro-physiological features that can help in identifying the patient's overall potential of recovery?

4. How to predict the patient's response to a particular intervention? and is it possible to identify the intervention which is most suitable and beneficial to a particular patient?

5. Can the rehabilitative intervention-induced brain dynamics be quantified and can the subject independent, treatment specific mechanisms of recovery be determined?

The answers to these questions can be a way to the demystification of personalized rehabilitation, but they are far from trivial. In this quest, a multitude of neuroimaging studies have explored a wide range of brain signal acquisition modalities and spectrum of features derived from them to find their relationship with neuronal recovery. All these studies can be logically grouped in the three broad categories, viz., Neuronal characterization of motor impairments, Prognostication of spontaneous motor recovery, and Prognostication and characterization of intervention induced recovery. This section provides a brief overview of these efforts with a focus on the possibility of personalized stroke rehabilitation.

2.4.1 Neuronal Characterization of Motor Impairments

Characterizing a brain activity that is specifically related to present motor functions, and brain abnormalities that are indicative of the degree of impairments in a particular patient are quite necessary and difficult tasks. Neurological understanding of motor impairments helps to pin-point the exact cause of observed motor deficits and provides a target for therapeutic interventions. This knowledge is important for the improvement of the existing or formulation of new rehabilitative therapies. Although very useful, obtaining this knowledge has been proved to be a challenging task because of the large inter-subject heterogeneity in the properties of individual stroke. This task is further complicated by the many-to-one

relationship between the brain state and the motor impairments, as various brain abnormalities have been observed to manifest into a similar degree of clinical impairments. Furthermore, the brain dynamics in the acute, sub-acute and chronic states post-stroke is very different which makes the neuronal correlates of motor impairments sensitive to time post-stroke as well. Despite these challenges, various neuroimaging studies have provided some knowledge about brain dynamics related to the observed clinical impairments.

In the acute stage of stroke, particularly EEG and fMRI studies have been used to locate and quantify the regions of brain abnormalities whose rectification has, in turn, manifested as improvement in motor status. In particular, continuous bedside EEG monitoring has revealed an evolution of stroke and the effects of interventions. Many EEG studies have reported local abnormalities in EEG amplitudes in various frequency bands to be related to the degree of hypoperfusion of the underlying cortical tissue quantified using cerebral blood flow (CBF)[208–212]. Loss of fast β (12-30 Hz) rhythms, as well as a reduction in the amplitude of somato-sensory evoked potentials, have been observed to be related to 50% reduction in the CBF. Further loss of fast frequencies, as well as, slowing down of first theta (4-8 Hz), and then delta (1-4 Hz) rhythms, is associated with the areas in the ischemic penumbra. An ischemic core has been reported to be expressed by focal suppression of all frequencies as well as a loss of presynaptic evoked responses [213]. Consistent with CBF relationship, the amount of localized reduction in the power of high-frequency oscillations has been found to be proportional to the size and proximity of infarct, one day post-stroke, characterizing the core and penumbra [214]. To further strengthen these understandings, one study reported prompt resolution of local delta abnormalities within 20 minutes after the administration of Tissue Plasminogen Activator (tPA) [54], which was followed by the motor function improvements. This study highlighted the sensitivity of EEG in the characterization of acute state brain abnormalities.

In the sub-acute stage and chronic stage, although very important, little attention has been given to the brain state characterization with most of the studies being focused on the prognostication. In a study conducted with 13 sub-acute patients, Finnigan et al. reported a significant correlation of NIHSS with global relative alpha power and Delta Alpha Ratio (DAR) at 48-hours post-stroke [55]. Furthermore, available literature suggests the effectiveness of DAR, and Power Ratio Index

(PRI), which is the ratio of power in fast v/s slow oscillations, in the sub-acute state motor status characterization [51, 54, 215]. The general trend of reduction in the power of high-frequency oscillations and increase in the low-frequency oscillations has been observed to be related to the poor clinical motor status in the sub-acute stages as well [52]. A number of MRI studies have reported the extent of damage to the Corticospinal Tract (CST) to be an independent predictor of motor impairments in the sub-acute as well as chronic state [46]. Furthermore, the Resting-State Functional Connectivity (rsFC) findings from the early and late sub-acute stage suggest that degree of motor impairments is correlated with decreased rsFC [216]. Quantified using laterality index from the primary motor cortex (M1), fMRI studies have also suggested that greater motor impairments are associated with less lateralized patterns of activation, which indicates that dominance of contralesional hemisphere over ipsilesional hemisphere is harmful to motor recovery [217].

In summary, reduced power in high-frequency oscillations, reduced ipsilesional activations, increased contralesional activations and reduced functional connectivity have been observed to be associated with the post-stroke poor motor status.

2.4.2 Prognostication of Spontaneous Motor Recovery

Prognostication of clinical status and motor impairments at the end of the acute and sub-acute stage is one of the most studied topics in the field of post-stroke rehabilitation. As in case of any life-threatening disease, in stroke as well, many demographic as well as neuroimaging features have been studied to predict the mortality and impairments. In stroke, as most of the deaths happen in first 30 days post-stroke, and as spontaneous motor recovery slows down around 3 to 6 months post-stroke, prediction of clinical status at 30-days, and/or 3,6 months post-stroke has been studied most extensively. This understanding of future clinical outcomes is important as it helps the clinicians, patients, and relatives to set realistic expectations and achievable therapy gains in the sub-acute state. Also, this knowledge allows efficient allocation of rehabilitation resources. Furthermore, the studies reporting neuroimaging predictor of clinical outcomes also aim to understand the neurological rationale behind the prognostic utility of any feature to

advance the knowledge of spontaneous recovery. Most importantly, as various rehabilitative interventions are inspired by the observations of spontaneous recovery, this knowledge of clinical predictors of spontaneous recovery also serves as a guideline in the exploration of predictors of treatment-induced clinical recovery. With very high clinical relevance, many EEG, MRI, fMRI and TMS based studies have been conducted particularly in the acute and sub-acute stages.

Similar to brain state characterization, various EEG spectral power features based studies have been observed to be effective in acute and sub-acute stage prognostication as well. In a study comprising 11 patients, global acute delta change index, calculated from the EEG data acquired in less than 18 hours post-stroke, was observed to be predictive of NIHSS outcomes 30 days post-stroke [53]. The amount and rate of decrease in the delta power in the acute state were significantly correlated with the better NIHSS score indicating an association between the faster resolution of delta abnormalities and better motor outcomes [53]. In another study which used EEG spectral power captured within 72 hours from the stroke onset, it was reported that the alpha and theta absolute energies were best and significant predictors of short term motor disabilities measured using modified Rankin scale, whereas, long term disabilities were better predicted using delta absolute energy[215]. Acute high global delta-alpha ratio and low relative alpha power were observed to be significant predictors of better NIHSS 30 days post-stroke [55]. A study conducted using MEG scan (2-10 days post-stroke) observed that significantly high absolute alpha power in the lesioned hemisphere and low delta power in the contralesional hemisphere were predictors of better recovery measured using NIHSS, 9 months post-stroke [218]. This study particularly highlighted the role of contralesional hemispheric activity in stroke rehabilitation. The inter-hemispheric interactions and their relationship with functional recovery were further studied using Brain Symmetry Index (BSI) which quantifies the interhemispheric imbalance in cortical activations. In multiple studies, the high value of acute state BSI was observed to be a predictor of death and disabilities 7 days post-stroke (NHISS), and 6 months post-stroke (modified Rankin scale) [57, 219, 220]. These observations, supported by other neuroimaging modalities, established a consensus that greater activation of contralesional hemisphere induces inhibitory drive on the ipsilesional hemisphere resulting in bad prognosis [221]. Furthermore, a study conducted using high-density EEG acquired within 3 weeks post-stroke, observed that high beta coherence between ipsilesional M1 and remaining cortex was related to the better

motor functions at the end of 3 months post-stroke [222]. As a general agreement, reduction in the high-frequency spectral power and increase in the acute brain asymmetry have been observed to be predictors of bad motor outcomes.

The studies using MRI to assess the structural integrity post-stroke suggest that the location of acute infarct and ischemic penumbra and not the volume are indicators of sub-acute motor outcomes measured using NHISS [223]. The extent of CST white matter integrity in the acute state, quantified as fractional anisotropy measure of ipsilesional and contralesional CST, has been observed to be a strong predictor of 12-months post-stroke motor impairments on Fugl-Mayer motor assessment scale [224]. Furthermore, the extent of CST damage, quantified as CST lesion load, has also been observed to be a good predictor of motor outcomes 3 months post-stroke[225]. TMS, another test used to qualitatively assess the extent of CST integrity, have been reported to be a very robust predictor of sub-acute motor recovery. A recent meta-analysis comprising 14 studies and 480 patients in total reported that the presence of acute state motor evoked potentials (within 7 days post-stoke) in TMS test is indicative of very good upper limb motor functions[226]. Although the presence of MEP was observed to be related to better outcomes, absence of MEP is not altogether indicative of poor outcomes. Considering this drawback, Stinear et al. [227] reported a multi-modality sequential algorithm which was observed to be quite successful in predicting motor outcomes at 3 months post-stroke. This approach highlighted the use of complementary information provided by different neuroimaging modalities. Along with the EEG, resting state or task state functional MRI is also being widely used to quantify the spatially precise cortical activations and their relationships. Multiple studies have reported better clinical outcomes to be associated with "more normal" task state and resting-state cortical activation patterns, quantified as greater activation of ipsilesional M1 and promoter cortex [228–234].

As a conclusive remark, presence of power and coherence in the high-frequency brain oscillations, greater ipsilesional activations and higher cortical excitability, improved inter-hemispheric imbalance, lesser damage to descending ipsilesional white matter pathways, presence of MEP, and more normal brain activation patterns in the acute stage are predictors of better clinical motor outcomes in the sub-acute state and indicate the possibility of good spontaneous recovery by restorative mechanisms.

2.4.3 Prognostication and Characterization of Intervention Induced Recovery

With some level of understanding of neurodynamics involved in the spontaneous recovery, several studies have also been conducted to comprehend the brain dynamics involved in the rehabilitative intervention-induced motor recovery. The neuroimaging studies in the field of rehabilitation therapy primarily seek knowledge about two kinds of brain features, 1. Pre-intervention features which can predict the intervention-induced motor gains and are indicative of the patient's possibility to respond to that particular therapy (prognostication), and 2. Features encapsulating the neuronal recovery that will presumably manifest as motor improvements (monitoring). The prognosticative features are particularly important in the domain of patient stratification and personalized rehabilitation, as the expected motor recovery predicted using these features can be used as a guideline while suggesting any therapy to the patient and it will also be helpful in setting realistic rehabilitation goals. The monitory features, on the other hand, aim to understand how exactly the particular therapy brought about the observed motor improvements and what are the neurodynamics that resulted in this recovery. This knowledge enhances the understanding of the exact neuronal mechanism of recovery as well as it provides the targets for the development of new rehabilitative interventions. As only the mechanisms of treatment-induced motor recovery are of interest and outcomes observed in the acute state might be because of the combined effects of treatment and contentious recovery, only the studies in the chronic state will be considered. Also, as the rationale behind the rehabilitative utility of interventions is quite unique, we will study the neuroimaging results from each intervention separately with the primary focus on the PT, robotic, and BCI-robotic interventions.

Most of the neuroimaging studies investigating the post-stroke therapy-induced motor recovery are related to the treatment gains induced by classical occupational and physiotherapy. In a chronic state EEG study comprising of 53 patients who underwent 24 sessions of PT, Chen et al. analyzed the predictive capabilities of EEG network connectivity parameters calculated based on Dynamic Causal Modeling (DCM) and observed that the connectivity patterns in the beta plus gamma or theta band provided very high accuracy in classification of predicted motor recovery as favorable or poor [48]. In an another EEG network connectivity study, Philips et

al. investigated the use of generalized measures of association and graph analysis for the prognostication and monitoring of 12 weeks intensive therapeutic UE intervention in 30 chronic stroke subjects. They found the high value of local efficiency pre-treatment to be a significant predictor of treatment gains, whereas the decrease in the beta band intra-density of the unaffected hemisphere was correlated with the treatment-induced recovery [36]. These results are contradictory to the existing literature where an increase in the intra-density is associated with more normal brain activation. In an influential longitudinal study, Wu et al. investigated the brain connectivity patterns using dense EEG array (256 electrodes) in 12 hemiparetic stroke patients across 28 days of extensive arm therapy. It was observed that high pre-intervention beta coherence between ipsilesional M1 and ipsilesional parietal operculum was a predictor of low treatment-induced gains. Also, the treatment gains were observed to be correlated with change in the beta coherence between ipsilesional M1-PM positively and with change in the beta coherence between ipsilesional M1 - parietal cortical regions negatively. This association highlighted the importance of connectivity and information sharing between ipsilesional M1 and rest of the brain and provided evidence about its relationship with the observed motor gains [235]. Furthermore, Platz, et al. reported the prognostic abilities of alpha and beta ERD observed during movement execution [236].

Many fMRI and TMS studies have also explored brain modulations related to monitoring and prognostication of treatment-induced motor gains with the primary focus on the cortical activations, resting-state functional connectivity, and cortical map reorganization [46, 237–240]. Two large meta-analysis studies reviewed the fMRI based monitory biomarkers and observed that treatment-induced recovery was associated with an increase in the activation within the ipsilesional M1, dorsal premotor cortex, and supplementary motor area, and change of laterality index from negative to positive [34, 43]. Moreover, in a study comprising of 21 chronic patients, Stinear et al. reported that the presence of MEP is a predictor of treatment-induced gains as well as the increased FA asymmetry and motor cortex damage predicted lower functional recovery following 30 days of training [46]. This study highlighted the similarities between acute and chronic state recovery.

Some studies related to prognostication and monitoring of robotic UE rehabilitation have also been reported in the literature. In a recent EEG study, Trujillo et al. assessed the prognostic capabilities of QEEG features in 12 sessions of chronic state

rehabilitation. Pre-intervention resting-state DAR and PRI were observed to be negatively correlated to the treatment-induced motor gains indicating a lower value of low frequency oscillations at the baseline to be predictive of higher clinical gains which is analogous to the acute state recovery. More interestingly, this study did not observe any treatment-induced changes in the EEG [49]. Another study, which conducted 30 days of UE robotic rehabilitation in one patient, reported treatment-induced reduction in the delta and increase in alpha rhythms [241]. In Caimmi et al. [242], authors reported the changes in the ERD/ERS patterns in the healthy subjects along with the robotic rehabilitation of one stroke patient. In an fMRI and TMS study, conducted with 20 chronic stroke patients undergoing 8 weeks robotic rehabilitation, it was observed that lower baseline value of MEP on TMS and lower M1 laterality index (indicating greater activations of contralesional M1) were significantly correlated with higher UE motor improvements. These results are quite surprising and directly contradicted the results from [46]. Furthermore, another study which did a combined analysis of the changes in the fMRI over a 12 weeks rehabilitation using robotics alone and BCI-robotics systems reported that increase in the functional connectivity of the supplementary motor area, and the ipsilesional, as well as contralesional M1, were associated with better treatment gains [42]. This study reported the positive role of contralesional M1 in the post-stroke motor recovery.

In the BCI based rehabilitation, although quite a few clinical studies have been conducted, very few of them have reported the prognostication or monitoring of BCI mediated motor recovery. Among these studies, in a 12-week BCI-robotic intervention, conducted with 11 subjects, the motor improvement was observed to be negatively correlated with the BSI calculated from the EEG task state data of all the rehabilitation sessions [144]. Although this can't be considered either prognostic or monitory features, this study indicated the utility of EEG in BCI mediated recovery. Another similar study, conducted with 10 sessions of BCI-robotics, reported that the number of sessions with coherence index > 0.5, calculated using EEG data, correlated with FMA scores. In [175], Pichiorri et al. observed the effects of BCI neurofeedback in the 1-month of UE motor rehabilitation and reported that the BCI training resulted in the stronger task state desynchronization of alpha and beta bands and the treatment motor gains were correlated with the changes in the resting state ipsilesional intrahemispheric connectivity. This study again highlighted the role of ipsilesional intra-hemispheric information transfer and

its relationship with motor recovery. The only fMRI study conduced during 10 sessions of BCI-Robotics intervention, reported an increased CBF to the ipsilesional M1 and re-balancing of inter-hemispheric CBF asymmetry to be associated with better motor recovery [192].

Therefore, from the literature, it can be observed that neuroimaging modalities hold a promise for effective characterization and prognostication of neuronal recovery following stroke. However, much more research, particularly related to BCI-based rehabilitation, is still needed to achieve the goal of personalized post-stroke motor rehabilitation.

2.5 Summary

This chapter provided an overview of BCI technology for post-stroke motor rehabilitation. First, a concise description of post-stroke brain dynamics was provided to explain the stroke and after-effects of stroke. This was followed by a brief description of various post-stroke motor rehabilitative interventions. Next, the technological aspects of the BCI system were discussed with a focus on non-invasive methodologies. Existing methods used to implement a typical BCI system, including signal acquisition, signal classification, and feedback were detailed. Particularly, the technological challenges associated with the building of robust and highly accurate EEG classification system were discussed. Following the technological details, the clinical use of BCI systems for post-stroke motor rehabilitation was reviewed. The limitations of present BCI rehabilitation systems, including the low accuracy, and the lack of standardized protocols were highlighted. Lastly, for achieving maximum clinical recovery, a possibility of personalized rehabilitation was discussed. In this regard, the review of literature on prognostic and monitory biomarkers of post-stroke rehabilitation was presented and the lack of information about the exact mechanisms of neuronal recovery was highlighted.

Overall, with the clinical and technological background presented in this chapter, the remainder of the thesis will focus on enhancing the clinical outcomes of BCI-based motor rehabilitation by improving the BCI-decoding accuracy and exploring the possibility of highly personalized rehabilitation.

Chapter 3

FBCNet: A Novel CNN Architecture for MI Decoding

3.1 Introduction

As presented in the previous chapter, the BCI systems employed for post-stroke motor rehabilitation are most commonly based on the EEG-MI paradigm. Although this paradigm is most relevant and intuitive for motor rehabilitation, the detection of MI from the EEG data is among the most challenging tasks in the BCI field. Therefore, owing to its high clinical relevance and challenging nature EEG-BCI literature contains many reports on decoding techniques to classify various MI classes with high accuracy. As reviewed in Section 2.2.2, classical machine learning techniques like linear and non-linear classifiers, nearest-neighbour classifiers as well

The work presented in this chapter has been partially published as:

1. Ravikiran Mane, et al., Multi-view CNN with novel Variance Layer for Motor Imagery Brain-Computer Interface. Proceedings of 42nd Annual International Conference of the IEEE Engineering in Medicine and Biology Society (EMBC). 20-24 July, 2020.
2. Ravikiran Mane, et al., FBCNet: A Filter-Bank Convolutional Neural Network for Motor Imagery BCI in Chronic Stroke Patients. 8th International BCI Meeting. 2021. *(Accepted)*
3. Ravikiran Mane, et al., FBCNet: An Efficient Multi-view Convolutional Neural Network for Brain-Computer Interface. *(In preparation)*

as more data-driven techniques like neural networks and deep learning have been explored for this task of MI classification [20–23, 142].

A part of difficulty in EEG-MI classification stems from the characteristics of EEG data. Noisy and high dimensional data, and scarcity of training samples are among the key challenges that are inherent to the EEG data and EEG-BCI classifiers need to address these challenges to achieve good accuracy [1]. Particularly, the contamination weak brain signals by high amplitude sources of noise like muscle and eye movements leads to very low signal to noise ratio.

A part of difficulty in EEG-MI classification stems from the characteristics of EEG data. Noisy and high dimensional data, and scarcity of training samples are among the key challenges that are inherent to the EEG data. Also, the contamination EEG by high amplitude sources of noise, like muscle and eye movements, along with the very weak brain signals, leads to very low signal to noise ratio. Hence, EEG-BCI classifiers need to address these challenges to achieve good accuracy [1]. Furthermore, the intrinsic nature of MI and high intra-class variability in MI trials add another layer of difficulty in MI classification. Due to all these issues, the MI classification with high accuracy is still an open research question [18, 19].

As mentioned in Section 2.2.2, the traditional machine learning strategies have tackled this difficult task of MI classification by paying prominent attention to the extraction of neuro-physiologically sound features from the EEG data. These algorithms generally employ a multistage approach wherein the EEG data is first preprocessed to reduce the noise and then neurophysiologically sound features are extracted from the data to enhance SNR and reduce dimensionality. Neuroscientific studies have documented that MI elicits characteristic EEG activation patterns known as sensory-motor rhythms (SMR). SMRs are generally observed at the contralateral and ipsilateral sensory-motor regions in the form of a time-locked, event-related desynchronization/ synchronization (ERD/ERS) [243]. It is also known that different classes of MI differ in the spectro-spatial distribution of SMRs [243]. In fact, one of the most successful algorithms for MI classification named CSP and its extension known as FBCSP [142] extract exactly this discriminative information to learn a more generalizable classifier model leading to high classification accuracy. An efficient and effective embodiment of neurophysiological priors in the classifier design can be considered as a reason behind the success of FBCSP algorithm. Hence, FBCSP and many other traditional machine learning

techniques have been observed to be effective in this scenario of limited and noisy EEG training data but they still suffer from the high susceptibility to intra-trial variance and have a high dependence on handcrafted features.

Deep learning, which is an extensively data-driven approach to classification, has also shown very promising results in many domains and there has been a growing interest among BCI researchers to use deep learning methods for MI decoding. In particular, architectures based on convolutional neural networks have gained popularity in the BCI domain due to their ability of effectively learning the local connectivity patterns from the given data [20–23]. Although these architectures have been observed to outperform the state-of-the-art traditional machine learning techniques, achieved improvements in subject-specific classification settings are still marginal [20–23]. Unlike other domains, this lack of substantial improvements by deep learning can be traced back to the nature of BCI datasets. Scarcity of training data along with the high feature dimensionality results in the heavy overfitting of deep learning models and creates unique challenges for adaptation of deep learning methods in the BCI field [19]. Encoding the neurophysiological priors in the classifier architecture can be a solution to this problem of overfitting.

Furthermore, although stroke patients are among the most-important target population, exploration of deep learning techniques for MI classification is still largely limited to the data from healthy people. Alteration of brain dynamics, changes in EEG brain rhythms and modifications in motor function control are some of the known effects following stroke [24, 25]. Furthermore, it has been documented that close to 13% of the stroke patients cannot control the MI-BCI using traditional machine learning techniques [15]. Therefore, it is necessary to investigate how deep learning architectures perform in stroke population and if they can extend the technology of MI-BCI to more patients by achieving better classification accuracy. One initial report indicates that deep learning architectures may actually perform worse than classical machine learning techniques, but this result needs further verification with the data from large stroke population [244].

Lastly, the use of deep learning in patient population also greatly necessitates interpretability of the classification decisions. In stroke patients, since the aim is to restore the brain activation to a healthy state, it is important to evaluate the information encoded by the neural network. Therefore, ease of decision explanation is another important parameter when it comes to patients' data.

To address the above challenges, this chapter presents a Filter-Bank Convolutional Network (FBCNet), which is a novel end-to-end CNN architecture for subject-specific MI classification. FBCNet architecture takes a hybrid approach; it leverages the recent advances in deep learning technologies and mitigates their shortcomings by encoding the neurophysiological priors of MI in the architecture design. Highly motivated by the FBCSP algorithm, FBCNet encodes spectro-spatial discriminative information with the help of spectral filtering of the EEG and CNN based spatial filtering. Next, a novel Variance layer is proposed for effective extraction of distinct MI signatures encoded by the temporal fluctuations, and dimensionality reduction. Use of this layer results in extremely compact architecture. The FBCNet consists of only two trainable layers and hence offers a direct interpretation of learned features. While being simple and interpretable, FBCNet also offers significantly higher classification results. In this chapter, the classification superiority of FBCNet, over other deep learning architectures and FBCSP, is investigated with the help of two publicly available MI datasets. The analysis is further extended to two MI datasets covering in total 71 chronic stroke patient. In addition, using three different explainable AI techniques, the better classification accuracy achieved by FBCNet is reasoned. Also, a discussion on the difference between the data from healthy and stroke patients in the context of MI classification is provided. Following are the main contributions of this chapter:

- A compact and neurophysiologically inspired CNN architecture named FBCNet is proposed for MI classification.
- In FBCNet, a novel Variance layer for effective extraction of EEG temporal information and parameter reduction is presented.
- One of the first reports on the comparison between classical machine learning algorithms and deep learning architectures for MI decoding in a large population of chronic-stroke patients is presented.
- It is shown that for stroke patients, classical machine learning approaches may outperform the general purpose deep learning architectures and careful fusion of deep learning methods and neurophysiological knowledge of MI, as done in FBCNet, can achieve the best classification accuracies for both the healthy subjects and the stroke patients.

The PyTorch implementation of the FBCNet is made available at `https://github.com/ravikiran-mane/FBCNet`.

3.2 Related Works

Many traditional machine learning techniques have been proposed for EEG-MI classification and an extensive summary of them can be found in [18]. Among them, as presented in Section 2.2.2, FBCSP is one of the most successful algorithms [142]. Decomposition of EEG into multiple narrow-band signals is the first step in the FBCSP algorithm and it achieves spectral localization of the EEG data. Next, these narrow-band EEG signals are spatially filtered using a CSP algorithm which extracts discriminative spatial patterns such that the filtered output will have a maximized class discriminative variance. Finally, from these spectro-spatially localized features, the most informative features are selected using Mutual Information based Best Individual Features with Parzen Window (MIBIFPW) algorithm [245] and the selected features are classified with Support Vector Machine (SVM) algorithm. FBCSP is a notable traditional machine learning algorithm in MI classification, and has inspired the design of FBCNet architecture and hence, the FBCNet results are compared with FBCSP.

Along with traditional machine learning techniques, in recent years, many deep learning architectures have also been proposed for the use in EEG-BCI domain [20–23, 246]. In [20], Schirrmeister et. al. proposed two CNN based architectures named Deep ConvNet and Shallow ConvNet. Being inspired by FBCSP, both of these architectures also contain temporal and spatial filtering using convolutional layers. Although proven to be effective, unlike FBCSP, these networks lack the explicit multi-band spectral filtering of the input EEG data. Building upon Deep ConvNet, Robinson et al. showed that the multi-view representation of EEG using a filter bank is indeed highly effective by achieving higher classification accuracy over broad-band Deep ConvNet [246]. EEGNet, proposed by Lawhern et al., is another CNN architecture that is also inspired from FBCSP, and similar to Deep ConvNet, implements a temporal convolution layer which is followed by a spatial convolution layer [22]. By implementing the depth-wise spatial convolution, EEGNet is constructed to learn separate spatial filters for each of the temporally filtered signals. Representing yet more similarity with the FBCSP, EEGNet also achieved

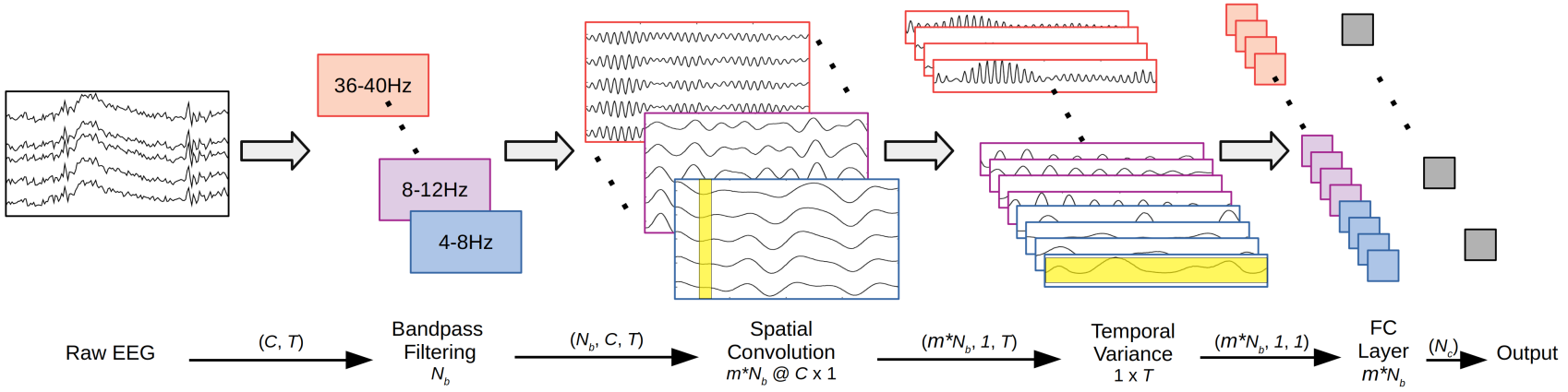

FIGURE 3.1: FBCNet architecture.

TABLE 3.1: FBCNet architecture

Block	Layer	# Kernels	Kernel Size	# Parameters	Output	Options
Spectral Filtering	Input				$(1, C, T)$	
	Filter-Bank				(N_b, C, T)	
Spatial Convolution	Depthwise Conv2D	$m * N_b$	$(C, 1)$	$m * N_b{}^*C + m * N_b$	$(m * N_b, 1, T)$	depth = m, max L2 weightnorm = 2
	BatchNorm			$2^*m * N_b$	$(m * N_b, 1, T)$	
	Activation - ELU				$(m * N_b, 1, T)$	ELU, ReLU, Leaky-ReLU
Temporal Feature Extraction	Variance Layer		$(1, T)$		$(m * N_b, 1, 1)$	Variance, Average, Max, Log-Variance, Standard Deviation
Classifier	Flatten				$m * N_b$	
	Fully connected Layer	$m * N_b$		$m * N_b * N_c + N_c$	N_c	max L2 weightnorm = 0.5
	Log-Softmax				N_c	

C: number of EEG channels, T: number of time points, N_b: number of frequency bands, m: number of convolution filters per frequency band, N_c: number of output classes

higher classification accuracies than both Deep and Shallow Convnets. However, both Deep ConvNet and EEGNet lack the explicit multi-view EEG representation and task tailored temporal feature extraction. Therefore, this work tries to address these limitations by incorporating the above-mentioned missing components. The classification performance of the proposed method are compared with Deep ConvNet and EEGNet.

3.3 Methodology

3.3.1 Proposed Architecture : Filter-bank Convolutional Net

FBCNet is designed with the aim of effectively extracting the spectro-spatial discriminative information which is the signature of MI while avoiding the problem of overfitting in the presence of small datasets. In its core, FBCNet architecture is composed of the following four stages:

1. Multi-view data representation: The multi-view representation of the EEG data is obtained by spectrally filtering the raw EEG with multiple narrow-band filters.
2. Spatial transformation learning: The spatial discriminative patterns for every view are then learned using a Depthwise Convolution layer.
3. Temporal feature extraction: Following spatial transformation, a novel Variance layer is used to effectively extract the temporal information.
4. Classification: A fully connected (FC) layer finally classifies features from Variance layer into given classes.

The multi-view EEG representation followed by the spatial filtering allows extraction of spectro-spatial discriminative features and Variance layer provides a compact representation of the temporal information. With this brief design philosophy, this sub-section provides details of the FBCNet architecture which is presented in Figure 3.1 and summarized in Table 3.1.

Spectral Localization by Multi-view Data Representation

Let us denote a single-trial raw EEG data as $x \in \mathbb{R}^{C \times T}$ and its corresponding label as $y \in \{0, 1, ..., N_c\}$, where C represents number of EEG channels, T represents time points and N_c is total number of distinct classes.

It is known that MI related information in EEG data is spectrally localized with most information being present in the mu (8-12 Hz), and low and high beta (12-20, 22-32 Hz) bands [243]. Therefore, to localize this discriminative information, in its first stage, FBCNet creates a multi-view representation of the broad-band EEG data wherein each view represents a narrow-band localized EEG. The multi-view representation, $x_{FB} \in \mathbb{R}^{N_b \times C \times T}$, is generated by spectrally filtering the raw EEG x with a filter bank $F = \{f_i\}_{i=1}^{N_b}$ consisting of N_b number of narrow-band temporal filters. Following the filtering operation, the time-series along the third dimension of x_{FB} becomes spectrally localized. Therefore,

$$x_{FB} = F \otimes x \quad \in \mathbb{R}^{N_b \times C \times T} \tag{3.1}$$

Where, $\otimes$ indicates bandpass filtering operation.

The filter bank F can consist of any number of filters with varying cut-off frequencies. In this particular work, the filter bank is constructed using $N_b = 9$ filters with non-overlapping frequency bands, each of 4Hz bandwidth, spanning from 4 to 40 Hz (4-8, 8-12, ..., 36-40 Hz). The filtering is done using the Chebyshev Type II filter with transition bandwidth of 2Hz and stopband ripple of 30dB. This selection of filter bank was motivated by the traditional division of EEG in neurologically significant spectral bands that was proposed in the FBCSP algorithm and it has been shown to achieve good classification accuracies across multiple works [142, 245, 247].

Spatial Localization by CNN

Following the deterministic spectral localization, spatial localization of EEG discriminative features is achieved by a Spatial Convolution Block (SCB) comprising of a Convolution layer, a Batch Normalization layer [248] and an Exponential Linear Unit (ELU) nonlinearity. FBCNet uses a Depthwise Convolution layer [249] of kernel size = $(C, 1)$ for learning spatially discriminative patterns. Also, the use

of Depthwise Convolutions results in each of these filters being associated with EEG from only one frequency band, and the depth parameter m controls the number of spatial filters per frequency band. Also, the Convolution kernel, that is sized to span across all the channels, effectively acts as a spatial filter. The use of Depthwise Convolution and kernel of size $(C, 1)$ is motivated by the FBCSP algorithm which also learns spatially discriminative filters for every narrow-band filtered EEG. Following the CNN layer, Batch-normalization is applied along the feature map dimension before applying the ELU nonlinearity. Each convolutional kernel is also regularized by using a maximum norm constraint of 2 on its weights; $||w||^2 < 2$ (weight-normalization). Effectively, SCB outputs $m \times N_b$ time-series, $x_{SCB} \in \mathbb{R}^{(m \times N_b) \times 1 \times T}$, which are spectro-spatially localized. In the default FBCNet structure, the value of m is set to be equal to the number of CSP filters extracted in the FBCSP algorithm ($m = 16$ for BCIC-IV-2A Data and $m = 4$ for all other datasets, see section 3.3.3 for more details). The effect of different values of m on model performance is also evaluated in the ablation analysis.

Temporal Feature Extraction by a Variance Layer

The raw EEG data generally contains large number of features along the time dimension and these features present the most amount of intra-class variance and high noise content. Therefore, to avoid overfitting of classification models, it is necessary to reduce the time dimensional features by effective extraction of the most relevant temporal information. Max or Average Pooling strategies are most commonly employed techniques for this purpose of reduction in feature dimensions [20, 22, 246]. However, these generic strategies do not provide the most optimal solution for EEG temporal information extraction. The Max Pooling strategy only considers the point of maximum activation and ignores other data points in the pooling region. This results in a loss of most of the information and more focus on a single point which may also be a high amplitude noise. In comparison, Average Pooling is a better suited strategy. Figure 3.2 demonstrates the pooling strategies using a small segment of EEG data. It can be observed from Figure 3.2 (a), the time average of EEG trial, as indicated by dashed lines, possesses relatively less discriminative information as compared to the actual EEG data. Furthermore, for the bandpass filtered EEG, the effectiveness of Average Pooling further reduces

because filtered data has zero temporal mean across the entire time window for all classes.

Therefore, for effective extraction of temporally discriminative information, this work propose a novel Variance layer which characterizes a time series by computing its variance. So, in the forward pass, for any time varying signal, $x(t)$, the output of the Variance layer, is given by,

$$v = Var(x(t)) = \frac{1}{T}\sum_{t=1}^{T}(x_t - \mu)^2 \tag{3.2}$$

where, T is total number of time-points and μ is the mean of $x(t)$.

From the time-series perspective, the variance of time-series filtered in a given frequency band corresponds to the signal power in that band. So, in the forward direction, Variance layer extracts the band power of input time-series. This feature is more suitable for EEG classification since band power modulations, in a form of ERD/ERS, are known to encode neurophysiological information associated with different MI classes. Moreover, as it can be observed from the Figure 3.2 (a), the temporal variance and not the mean of EEG trials have the most class-discriminative power. Therefore, the Variance layer can extract neurophysiologically relevant features, which also have better class-discriminative capabilities.

The effect of variance layer is yet more significant for the EEG data during the learning phase (backpropagation) of the neural network using gradient descent optimization. In the backpropagation phase, the learnable parameters of the network are updated based on the gradient of the loss function. So, for any network, if $L_v = \frac{\partial L}{\partial v}$ is the incoming loss at the variance layer then the backpropagated loss from this layer with respect to the input $x(t)$, L_{x_t}, is given by,

$$\begin{aligned} L_{x_t} &= \frac{\partial L}{\partial x_t} = \frac{\partial L}{\partial v}\cdot\frac{\partial v}{\partial x_t} = L_v\frac{2}{T}(x_t - \mu) \\ \therefore\quad L_{x_t} &\propto (x_t - \mu) \end{aligned} \tag{3.3}$$

As it can be observed from (3.3), the outgoing loss from the Variance layer is proportional to the deviation of x_t from the mean of the signal. Therefore, the Variance layer provides more importance to the signal points which are away from the mean

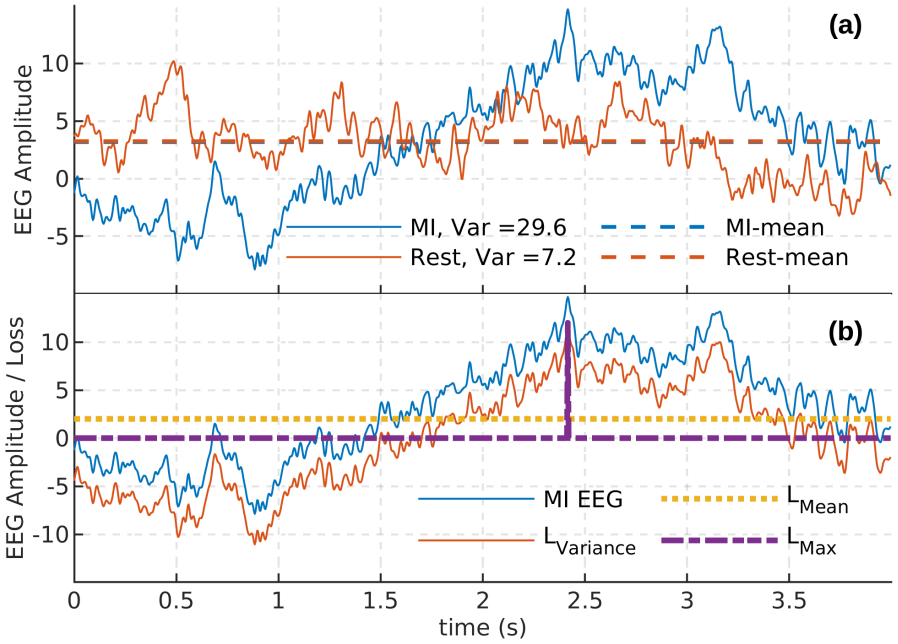

FIGURE 3.2: The suitability of Variance layer for EEG motor imagery classification. Part (a) is a class averaged EEG activity at the right motor cortex area (C4 channel) during MI of left hand and rest state. Here, a typical ERD pattern which is a dip in EEG amplitude between 0-1.5s, can be seen when the subject is performing the MI, whereas, no such pattern exists during the resting state. Also, it can be observed that these two classes have almost similar mean but they can be easily classified using their variance (see caption). Part (b) shows the loss redistribution by various feature reduction strategies. It can be seen that the loss redistribution by Variance layer provides more weightage to the ERD and ERS regions in the MI waveform.

by assigning a higher proportion of the incoming gradient to these points. This also aligns with the characteristics of EEG wherein the deviation from the mean in a form of ERD or ERS is a distinct signature of MI. Moreover, the backpropagation rules for Average Pooling and Max Pooling are not adequately suited for EEG data. As given by (3.4), the Max Pooling follows a winner-takes-all approach wherein entire incoming loss is assigned to a single element and the weight updates of the subsequent layer only depend on this single element. This is inadequate for encoding the time-varying pattern of ERD and ERS. On the other hand, the Average Pooling layer distributes the incoming loss equally among all the data points ((3.5)) and by giving equal importance, it fails to provide an additional weightage

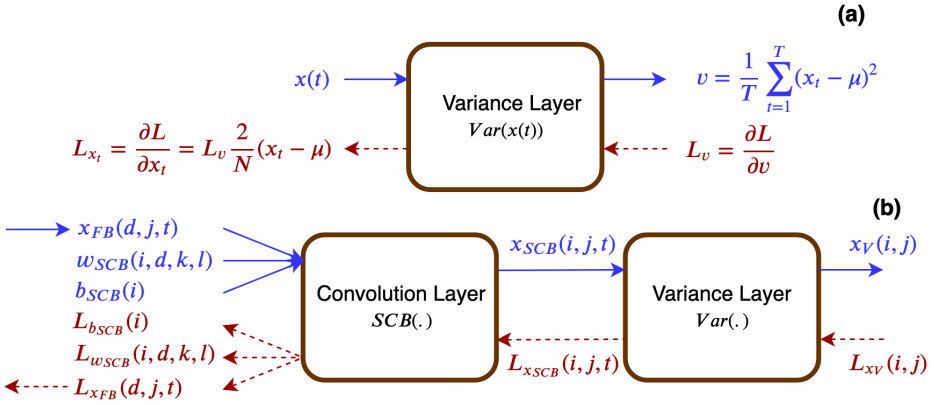

FIGURE 3.3: The role of Variance Layer. Part (a) presents the forward and backward pass operations by the proposed Variance layer. In the forward pass, this layer computes the variance of the input time series. whereas, in the backward pass it redistributes the incoming loss proportional to the deviation of input time-series from its mean. Part (b) presents how the redistribution of loss by Variance layer affects the downstream learning of convolution layer in FBCNet.

to the more relevant parts of the EEG time-series (Figure 3.2 (b)).

$$L_{x_t}^{max} = \frac{\partial L}{\partial x_t} = \begin{cases} L_{max} & for\ \ t^* = argmax_t(x(t)) \\ 0 & \text{otherwise} \end{cases} \tag{3.4}$$

$$L_{x_t}^{avg} = \frac{\partial L}{\partial x_t} = \frac{\partial L}{\partial \mu} \cdot \frac{\partial \mu}{\partial x_t} = L_\mu \frac{1}{T} \tag{3.5}$$

Considering the suitability of the proposed Variance layer for EEG data, it is used in FBCNet for effective temporal feature extraction. The output of SCB is passed to a Variance layer and it computes the temporal variance of the individual time-series as given by (3.6) in the forward pass.

$$x_{V_{i,j}} = \frac{1}{T}\sum_{t=1}^{T}(x_{SCB_{i,j,t}} - \mu_{i,j})^2 \in \mathbb{R}^{(m \times N_b) \times 1} \tag{3.6}$$

where, $\mu_{i,j}$ is the temporal mean of $x_{SCB_{i,j,t}}$.

As it can be observed, the application of Variance layer across the entire time-duration reduces the number of features from $(m \times N_b \times T)$ to $(m \times N_b)$, resulting in high degree of feature reduction.

The overall role of Variance layer is summarized in Figure 3.3. By computing the backpropagation of loss at the intermediate layers, it can be observed that,

TABLE 3.2: Description of evaluation datasets

Dataset	BCIC-IV-2A Data	Korea Uni. Data	Stroke Data: A	Stroke Data: B
Subject Type	Healthy Subjects	Healthy Subjects	Stroke Patients	Stroke Patients
# of Subjects	9	54	37	34
# of Sessions	2	2	1	1
# of Trials	288	200	160	160
# of Classes	4	2	2	2
# of Channels	22	20	27	27
# Time-points	1000	1000	1000	1000
Analysis	CV, HO	CV, HO	CV	CV

CV: 10-fold Cross Validation on session 1 data, HO: Hold Out - training with session 1 data and test with session 2 data.

in the presence of Variance layer, the downstream convolutional filters are trained to maximize the class-discriminative variance. This computation is elaborated in Section A.1.

Classification

Finally, $(m \times N_b)$ features extracted by the Variance layer are given to a FC layer with linear activation. The output of the FC is then passed through the softmax layer to get the output probabilities of each class. The FC layer weights are also regularized using a maximum norm constraint of 0.5; $||w||^2 < 0.5$ (Weight-normalization).

3.3.2 Evaluation Datasets

In the BCI domain, extreme inter-subject variability is observed in classification performance of different algorithms. Therefore, for robust comparison of the performance, the FBCNet is tested using the following four diverse EEG-MI datasets:

1. *BCIC-IV-2A Data*: A 4 class MI data from BCI Competition IV Dataset 2A [250].
2. *Korea Uni. Data*: A 2 class MI data from Korea University EEG dataset [251].
3. *Stroke Data: A*: A 2 class MI vs rest dataset [119].

4. *Stroke Data: B*: A 2 class MI vs rest dataset [88].

Among these datasets, the BCIC-IV-2A Data [250] and the Korea Uni. Data [251] contain the EEG data collected from healthy people. Moreover, these two datasets are publicly available and many state-of-the-art classification algorithms have used these datasets as a benchmark. Since applications to post-stroke motor rehabilitation is a focus of this thesis, two big datasets, Stroke Data: A and Stroke Data: B, containing the MI data from chronic-stroke patients, are included in the analysis. The Stroke Data: A is collected as a part of a clinical trial that investigated the combined effect of BCI-mediated rehabilitation and transcranial Direct Current Stimulation (tDCS) in chronic stroke patients [119]. The Stroke Data: B is collected as a part of another clinical trial investigating the efficacy of BCI-mediated upper extremity motor rehabilitation in chronic stroke patients [88]. Altogether, the proposed architecture is evaluated on MI-EEG data from 63 healthy people and 71 stroke patients. All the analysis in this work is performed on a 0-4 seconds post-cue data.

The most important dataset characteristics are summarized in Table 3.2 and more detailed data description is provided in Section A.2.

3.3.3 Experiments

To evaluate the performance of FBCNet, the following two experiments were conducted:

1. **Cross Validation Analysis (CV)**

   Subject-specific classification accuracy in 10-fold CV setting is a primary performance metric of this study. In a 10-fold CV, 9 folds were used for training and 1 fold was used for testing. The folds were constructed by sequential, class-balanced allocation of trials and this allocation was maintained constant for the entire analysis. The sequential allocation of trials was performed to ensure that the results can be reproduced by other researchers in the future. The complete data from Stroke Data: A and Stroke Data: B datasets, and session 1 data from BCIC-IV-2A and Korea Uni. datasets was used in the CV analysis. The inter-session data was not used in the CV analysis to avoid the

confounding influence of inter-session variability, which is a known problem in the BCI domain.

2. **Hold Out Analysis (HO)**

   To understand the effect of inter-session variability on the classification performance, a subject-specific, inter-session, HO analysis was conducted for the BCIC-IV-2A Data and Korea Uni. Data. In HO analysis, the complete data from session 1 for the given subject was used for the training purpose and the resulting model was tested on the session 2 data. This analysis provides information about algorithms' capabilities in extracting highly generalizable discriminative features which remain valid during inter-session classification.

In this manner, the performance of FBCNet was compared with one traditional machine learning algorithm of FBCSP-SVM [142], and two state-of-the-art CNN architectures, namely, Deep ConvNet [20], and EEGNet-8,2 [22]. All the methods were used in the most optimal settings as recommended by the respective authors. The detailed settings for each of these algorithms are provided in Section A.3.

3.3.4 Training Procedure

A same training procedure was followed for training FBCNet, Deep ConvNet, and EEGNet-8,2. Architectures were trained using Adam optimizer at default settings (learning rate = 0.001, betas = $0.9, 0.999$) [252]. The log-cross-entropy loss was used for gradient updates. As proposed in [20], a two-stage training strategy was used. In this strategy, the training data was further divided into the training set and the validation set. In the first stage, the model was trained using only the training set with the early stopping criteria whereby the validation set accuracy was monitored and training was stopped if there was no increase in the validation set accuracy for consecutive 200 epochs. After reaching the stopping criteria, network parameters with best validation set accuracy were restored [20]. Starting from this model, the training procedure was continued in the second stage wherein the model was trained with the complete training data (train + validation set). The second stage training was stopped when the validation set loss reduced below the stage 1 training set loss. Lastly, to avoid the case of infinite training in the situation of non-convergence, the maximum number of training epochs were limited to 1500

and 600 for training stage 1 and 2 respectively. In the CV analysis, the data from 1 fold among the 9 training folds was separated as a validation set. In the HO analysis, 20% of the training data was set aside as a validation set. In both the CV and HO analysis the test fold/set was not used in any training step.

3.3.5 Ablation Analysis

The FBCNet architecture consists of multiple components and hyperparameters and to understand their effect on the classification accuracy the following ablation analysis was performed.

Contribution of temporal Variance layer:

A novel Variance layer for extraction of temporal information is one of the most important contributions of this work. Therefore, the contribution of temporal Variance layer was assessed by replacing it with commonly used pooling strategies of Average and Max Pooling. This arrangement results in the same number of features at the FC layer and offers a direct way to compare the Variance layer with conventional strategies of feature reduction. Moreover, a variant of variance, the log-variance, is used by the FBCSP as a temporal feature extractor. Therefore, to assess if this can further improve the performance, the use of a Standard Deviation Layer ($\sqrt{Var}$) and a Log-Variance Layer ($Log(Var)$) instead of Variance layer was investigated.

Effect of number of convolutional filters:

The number of convolutional filters per frequency band, m, in the SCB, is the very important hyperparameter in FBCNet architecture. In its default settings, the value of m was kept to be equal to the number of CSP filters in the FBCSP algorithm for fairness in comparison ($m = 16$ for BCIC-IV-2A Data and $m = 4$ for all other datasets). To further analyze the sensitivity of FBCNet to the value of m, the classification accuracies at 5 different values of m with $m = 2, 4, 8, 16, 32$ were investigated.

Choice of non-linear activation:

In the SCB of FBCNet, an ELU non-linearity has been used. This choice of ELU non-linearity, as opposed to the popularly used Rectified Linear Units (ReLU), is based on the nature of the EEG data which is generally centered around zero with almost equal amount of positive and negative data points. The use of ReLU non-linearity, which is linear for positive inputs and which zeros down the negative inputs, for zero-centered data will lead to zero contribution in the output by many EEG data points. Therefore, FBCNet has used the ELU non-linearity, which outputs a non-zero value for both positive and negative inputs and its gradient is also non-zero for all positive and negative data-points. In this analysis, this choice of ELU non-linearity, was verified by investigating the classification performance in the presence of 3 different non-linear activation functions, viz. ELU, ReLU, and Leaky-ReLU.

Effect of Batch-normalization and Weight-normalization:

Batch-normalization [248] and Weight-normalization [253] are among the recent strategies that have been proposed for effective training of neural network architectures. Batch-normalization is used to standardize the intermediate outputs of the network to zero mean and unit variance for a batch of training examples. Therefore, as proposed by [248], the Batch-normalization was applied on the output of convolutional layers before the nonlinearity. FBCNet also implements a weight-normalization [253] strategy which regularizes the network weights and improves the conditions of optimization problem on the Convolution and FC layer weights. To assess if these strategies actually improve the performance and training conditions in FBCNet, the classification accuracies were computed in the absence of one and both of these factors.

3.3.6 Interpretability and Visualizations

The adaption of deep learning in the medical domain necessitates some form of explanation for models' decisions. When used in the rehabilitation settings, it is imperative that the neural network learns the neurophysiological signatures of the particular activity. Therefore, it is crucial to investigate and understand the exact

knowledge encoded by any neural network to ensure that the performance of the model is being driven by relevant features as opposed to noise or artefacts in the data. Therefore, to understand the knowledge extracted by FBCNet and to explain the better classification performance, the following three analyses were performed:

Visualization of convolutional kernel weights

In this approach, the convolutional kernel weights from the trained model were directly visualized and interpreted. Generally speaking, the direct interpretation of convolutional kernel weights is very difficult due to the cross-filter-map connectivity between any two layers. However, the shallow nature of FBCNet with only one convolution layer altogether eliminates the cross-filter-map connectivity and hence this direct interpretation becomes possible. Moreover, the Depthwise convolution layer implementation of FBCNet, wherein every convolution filter receives only one view of narrow-band filtered EEG results in the spatial filter being specific to a particular frequency band. Therefore, analysis of convolutional kernel weights directly provides the information about the spectro-spatially discriminative patterns learned by the FBCNet. The results of this analysis are presented for one representative subject. Lastly, despite the high information content, the convolutional kernel weights cannot be used for quantitative comparison across different subjects and this drawback has motivated the use of the next visualization technique.

Visualization of input feature relevance

This approach focuses on calculating the relevance of every input feature on the resulting classification decision for each trial. This family of analysis is based on the principles of gradient backpropagation, wherein for every trial, the gradient of the output with respect to the input is calculated. This value of gradient indicates how sensitive the output is to a change in a particular feature. A large positive or negative gradient value implies that a small perturbation in the value of a given feature will lead to a large change in the output. Therefore, this gradient of input with respect to the output, is referred to as a feature relevance score. Many advanced methods have been proposed in the literature to solve the problems associated with the above discussed vanilla gradient backpropagation approach. Therefore, for achieving the most accurate results, this analysis calculates the single-trial EEG

feature relevance score using a DeepLIFT method with the Rescale rule [254, 255]. In this analysis, from the training data, an average of all the trials belonging to one class was used as a reference to the DeepLIFT algorithm. With this reference, the single-trial relevance for every trial from other class was computed. Then the subject level relevance of input signals was calculated by averaging the normalized absolute per-trial relevance over all the trials. The extracted relevance were then used to infer the importance given by the trained model to a particular set of EEG channels and frequency bands.

Since DeepLIFT produces relevance in the input space, which is same for all subjects in the dataset, it enables a quantitative analysis of models trained using different subject's data. Therefore, using DeepLIFT, a dataset-level relevance analysis is also performed. In particular, the trained FBCNet models from the subjects with classification accuracy $> 70\%$ from the Korea Uni. Data which contains the data from healthy subjects were analyzed. Moreover, for the purpose of relevance analysis, because both Stroke Data: A and Stroke Data: B share the same recording protocol, these datasets were combined to form a single dataset containing the data of stroke patients. The trained FBCNet models were analyzed for stroke patients with classification accuracy $> 70\%$. The relevance scores from subjects with classification accuracy $> 70\%$ are presented because they represent robustly trained models which have encoded the information that generalizes well on the test data. Moreover, a small percentage of subjects are known to be BCI-illiterate, that is, these subjects cannot generate class discriminative MI-EEG patterns and this is another reason for exclusion of subjects with accuracy $<70\%$ from the interpretability analysis [251].

Visualization of Extracted features by t-SNE

This approach is used to understand the reason behind the difference in classification accuracies achieved by the different architectures for a given subject. To qualitatively compare across architectures, a 2-dimensional projection of the features at the last fully connected layer of FBCNet, EEGNet-8,2 and Deep ConvNet were computed using a t-SNE algorithm for all the trials during their test fold[256]. t-SNE is an unsupervised visualization algorithm which projects higher dimensional data in low dimensions for the purpose of visualization and interpretation. Therefore, a clearly identifiable and separable cluster of trials from different

TABLE 3.3: Number of trainable parameters for all CNN-based models

Dataset	Deep ConvNet	EEGNet-8,2	FBCNet
BCIC-IV-2A Data	282,879	4,028	4,180
Korea Uni. Data	278,827	3,002	902
Stroke Data: A	283,577	3,114	1,154
Stroke Data: B	283,577	3,114	1,154

classes at the fully connected layer indicates the capability of the architecture in extracting highly discriminative features in the previous layers. Moreover, analysis of the test data also conveys whether the discriminative features extracted from the training data are sufficiently generalizable on the unseen test data. Lastly, the t-SNE projections of the raw EEG data were inspected to assess if any direct class-discriminative information is present in the raw EEG itself.

3.3.7 Statistical Analysis

The statistical significance of differences in classification accuracy achieved by different algorithms is assessed using a Wilcoxon signed-rank test for BCIC-IV-2A Data which has small sample size, and paired t-test for the remaining three datasets. To avoid the false discoveries in a multiple comparison situation, the p-value was corrected with Bonferroni correction for multiple comparisons.

3.4 Results

3.4.1 Validation of Baseline Implementations

Result I: Baseline methods achieved the same accuracy as previously reported in the literature

As a first step of the analysis, the implementations of FBCSP-SVM, Deep ConvNet, and EEGNet were validated by comparing the achieved classification accuracies with the previously reported results. In the literature, the classification performance of FBCSP-SVM algorithm has been evaluated on 0.5-2.5s epoched BCIC-IV-2A data in HO manner [165]. Using these same settings, our implementation of FBCSP-SVM reached a 4-class classification accuracy of 68.47% which

TABLE 3.4: Average subject-specific classification accuracy

Dataset	Test Configuration	FBCSP-SVM	Deep ConvNet	EEGNet-8,2	FBCNet
BCIC-IV-2A Data	CV	**75.89**	72.20	73.13	75.27
Korea Uni. Data	CV	64.61**	68.33*	70.89	**73.36**
Stroke Data: A	CV	71.37**	68.81**	69.15**	**75.49**
Stroke Data: B	CV	74.14**	71.11**	73.47	**77.38**
BCIC-IV-2A Data	HO	68.06	72.22	73.15	**74.11**
Korea Uni. Data	HO	60.36*	60.77*	63.63	**65.75**

The best performing method for each analysis is highlighted in boldface. The *, and ** represent that the classification performance of FBCNet is significantly better than the given baseline method with *: $p_{corrected} < 0.05$, and **:$p_{corrected} < 0.001$.

was not different from the previous report (acc. = 67.01%, $p > 0.05$) [165]. Similarly, the EEGNet-8,2, and Deep ConvNet implementations were validated by comparing the CV classification accuracy for BCIC-IV-2A, session 1 data with the results reported in [22] (data epoched at 0.5-2.5s from the cue presentation). Our implementation of Deep ConvNet, and EEGNet-8,2 resulted in accuracy of 68.67% and 72.77% respectively and it was not different from the previously reported classification performance of 70% for both architectures (exact numerical values were not available) [22]. Apart from this baseline comparison, all the later analyses were conducted using the complete 0-4s EEG time segment for all datasets.

3.4.2 Classification using FBCNet

Result II: FBCNet achieved significantly better classification accuracies compared to baseline methods

Figure 3.5 and Table 3.4 present complete classification results for all datasets using all the methods. From Table 3.4, it can be observed that FBCNet achieved the best classification performance across all datasets in both CV and HO settings. Also, in most cases, the improvement in accuracy achieved by FBCNet over baseline methods was statistically significant (Table 3.4). The BCIC-IV-2A Data in CV setting was the only exception wherein FBCSP-SVM achieved better accuracy than FBCNet (75.89% vs 75.27%) but this difference was not statistically significant ($p > 0.05$). More detailed classification results are presented in Section A.4.

Result III: FBCNet matched the performance of best performing baseline method for most subjects

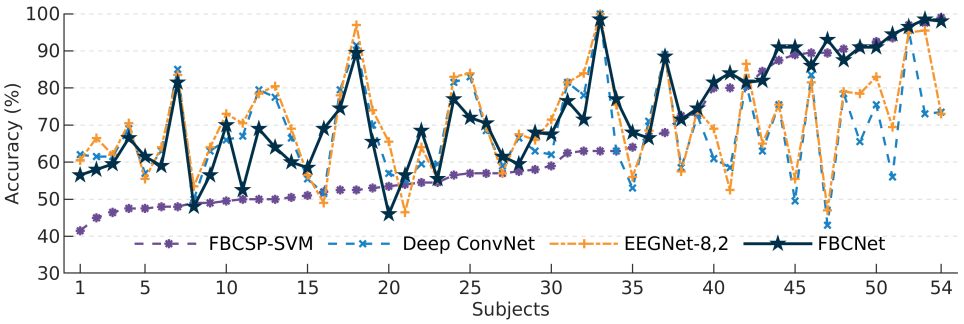

FIGURE 3.4: Classification accuracy for each subject from Korea Uni. Data in 10-fold cross-validation settings (sorted by FBCSP-SVM acc.). It can be observed that deep learning architectures (Deep ConvNet, EEGNet-8,2) performed far better than FBCSP-SVM, the classical approach, for subjects with FBCSP-SVM accuracy <70%. On the other end of the spectrum, the performance of deep learning architectures was far worse than that of FBCSP-SVM in subjects with FBCSP-SVM accuracy >70%. Here, in contrast, FBCNet matched the performance of the best performing method for most of the subjects resulting in the best subject averaged classification accuracy. A similar trend was observed in other datasets as well.

TABLE 3.5: Average classification accuracies for 25% subjects with highest cross validation accuracy in each dataset.

Dataset	FBCSP-SVM	Deep ConvNet	EEGNet-8,2	FBCNet
Korea Uni. Data	90.11	84.79	87.43	**92.46**
Stroke Data: A	90.46	83.71	84.96	**93.05**
Stroke Data: B	89.53	82.05	84.21	**92.81**

TABLE 3.6: Average classification accuracies for 25% subjects with lowest cross validation accuracy in each dataset.

Dataset	FBCSP-SVM	Deep ConvNet	EEGNet-8,2	FBCNet
Korea Uni. Data	48.00	54.50	54.61	**56.25**
Stroke Data: A	53.23	53.74	52.28	**55.31**
Stroke Data: B	53.55	61.88	**65.00**	57.74

Following the analysis of classification accuracies averaged over all subjects, the performance of all algorithms for every subject was investigated. As an example, Figure 3.4 presents the 10-fold CV accuracies for all subjects in Korea Uni. Data. Here, a significant difference was observed in the classification accuracies achieved by different algorithms for each subject. In particular, both baseline deep leaning methods, Deep ConvNet, and EEGNet-8,2, resulted in similar accuracies, which were significantly different from the accuracies achieved by classical machine learning approach of FBCSP-SVM (paired t-test, $p_{\text{KoreaUni.Data}} = 0.017$). Moreover, it

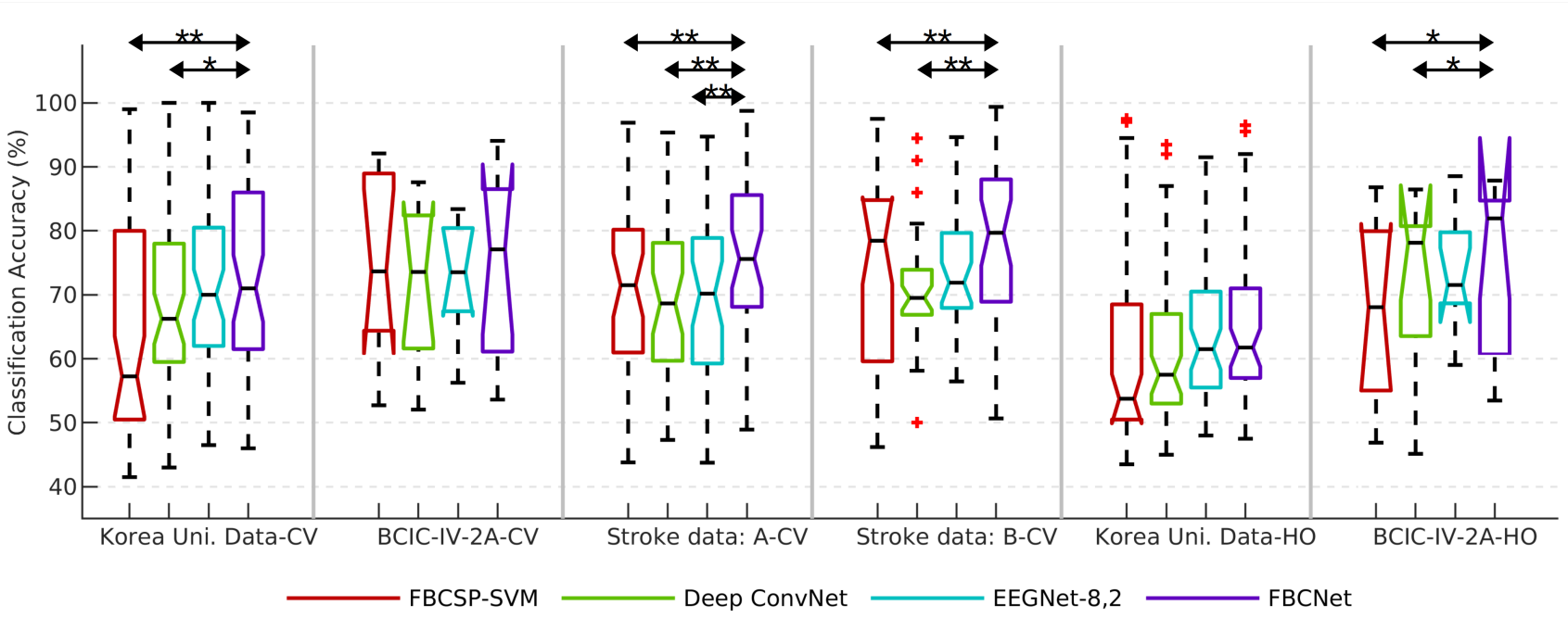

FIGURE 3.5: Subject-specific classification accuracies for all datasets. Here the box represents first and third quartile and a horizontal line in the middle denotes the median classification accuracy. It can be observed that across all datasets FBCNet achieves the best median classification accuracy. Also, as represented by *, and **, the higher accuracy by FBCNet was statistically significant in most cases (*: $p_{corrected} < 0.05$, **:$p_{corrected} < 0.001$).

was observed that deep learning architectures performed far better than the classical approach, for subjects with FBCSP-SVM accuracy <70%. Conversely, the performance of deep learning architectures was worse than that of FBCSP-SVM in subjects with FBCSP-SVM accuracy >70%. In contrast to all baselines, as can be observed from Figure 3.4, FBCNet matched the performance of the best performing method for most subjects resulting in the best average classification accuracy. A similar but statistically insignificant trend was observed in other datasets as well.

To quantitatively investigate this pattern, the average classification accuracy for 25% subjects with the highest and the lowest CV accuracy in each dataset was analyzed (Table 3.5, and Table 3.6). Here, it was observed that the average classification accuracies of top 25% subjects for FBCSP-SVM were significantly higher than that of Deep ConvNet, and EEGNet-8,2 (t-test, all $p < 0.05$ except $p_{FBCSP-EEGNet}$ for Korea Uni. Data) and the accuracies for FBCNet were even higher than that of FBCSP-SVM (statistically not significant). For bottom 25% subjects, FBCSP-SVM was observed to perform worse than deep learning algorithms and this difference was statistically significant in Korea Uni. Data and Stroke Data: B (all $p < 0.01$). The bottom 25% classification accuracy for FBCNet was in between FBCSP-SVM and EEGNet-8,2, with it being significantly better than FBCSP-SVM for Korea Uni. Data and only significantly worse than EEGNet-8,2 for Stroke Data: B.

Result IV: Highest number of subjects achieved >70% accuracy with FBCNet

In the BCI field, a system with > 70% 2-class classification accuracy is generally considered to be usable by healthy subjects and stroke patients [257]. Therefore, the number of subjects for whom classification algorithm managed to achieve at least 70% CV accuracy were analyzed and the results are presented in Table 3.7. Among baseline methods, EEGNet-8,2 resulted in the most number of subjects being able to achieve >70% accuracy for Korea Uni. Data. Whereas, for both stroke datasets, FBCSP-SVM resulted in the most number of subjects with >70% accuracy. Better than all baseline methods, for all datasets, FBCNet was able to achieve >70% accuracy for most number of subjects. Compared to the best baseline method (FBCSP-SVM), FBCNet resulted in 19% more stroke patients (Stroke Data:A+B) with >70% accuracy.

TABLE 3.7: Number of subjects with CV classification accuracy > 70%.

Dataset	Total Subjects	FBCSP-SVM	Deep ConvNet	EEGNet-8,2	FBCNet
Korea Uni. Data	54	17	21	27	**28**
Stroke Data: A	37	20	18	19	**26**
Stroke Data: B	34	23	16	22	**25**
Stroke Data (A+B)	71	43	34	41	**51**

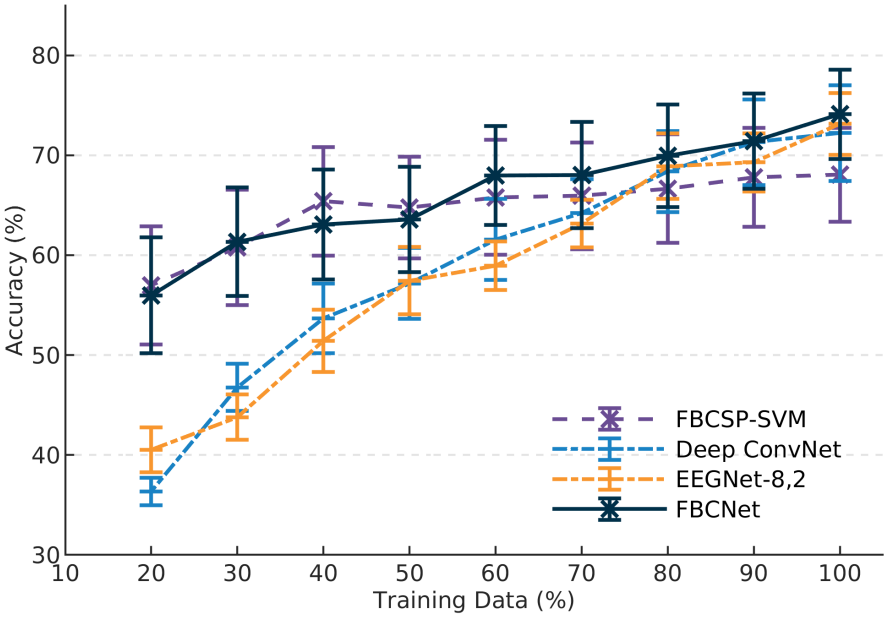

FIGURE 3.6: The sensitivity of classification algorithms to small training sets. Here the effect of a small number of training samples on the test accuracy is evaluated using the BCIC-IV-2A Data for various algorithms. A fraction of the training data (x-axis) is used to train a model which is then tested on data from an independent test session. It can be observed that the baseline deep learning architectures (Deep ConvNet and EEGNet-8,2) are highly sensitive to the small training sets whereas the classical approach of FBCSP-SVM is relatively less susceptible. The proposed method (FBCNet) matches the accuracy achieved by deep learning methods in the presence of ample training data while retaining relatively better performance even when the training set is small. The error bars represent a standard mean error.

Result V: FBCNet was least affected by datasets with fewer training samples

The sensitivity of classification algorithm to fewer training samples was evaluated using the separate test session data from BCIC-IV-2A Data in hold out analysis.

Here, all the algorithms were trained using various fractions of the training dataset ranging from 20% to 100% in steps of 10%. Trained models were then tested on a separate session 2 data and the test accuracy was analyzed as a function of training data percentage. Results of this analysis are presented in Figure 3.6. Here, both baseline deep learning architectures were observed to be highly sensitive to small training sets with an accuracy drop of almost 35% when the number of training trials were reduced to 20%. Contrarily, FBCSP-SVM was least affected by a reduction in the training set. In fact, the drop in accuracy using FBCSP-SVM only became statistically significant when the portion of training samples was reduced to 30%. Furthermore, compared to both Deep ConvNet and EEGNet-8,2, better classification accuracies achieved by FBCSP-SVM were statistically significant when training data was reduced below 50%. However, the maximum accuracy achieved by FBCSP-SVM, when using the complete training data was much lower compared to these baseline deep learning methods (Table 3.4). Different from FBCSP-SVM, at 100% of the training data, the best accuracy was achieved by FBCNet. Moreover, the accuracy curve of FBCNet closely followed the characteristics of FBCSP-SVM with a similar sensitivity to the reduced training set as that of FBCSP-SVM. Also, at 20% of the training data, the drop in FBCNet accuracy was only half of the accuracy drop using Deep ConvNet and EEGNet-8,2.

3.4.3 Ablation Results

Result VI: Temporal feature extraction using Variance layer resulted in significantly better classification accuracies

To analyze the contribution of the novel Variance layer in the improved results achieved by FBCNet, the effect of different temporal feature extraction layers on the classification accuracies was investigated and Figure 3.7 presents these results. Among all the temporal feature extraction layers, FBCNet with Variance layer achieved the highest classification accuracies in all analysis. Log-Variance and Standard Deviation layers were observed to be the next best-performing feature extractors. However, compared to Variance layer, the accuracy drop by these layers were statistically significant in most cases (all $p < 0.05$ except for Log-Variance in Stroke Data: A, Stroke Data: B, and BCIC-IV-2A Data-HO analysis). Feature extraction using Average and Max layer resulted in consistently worse accuracies

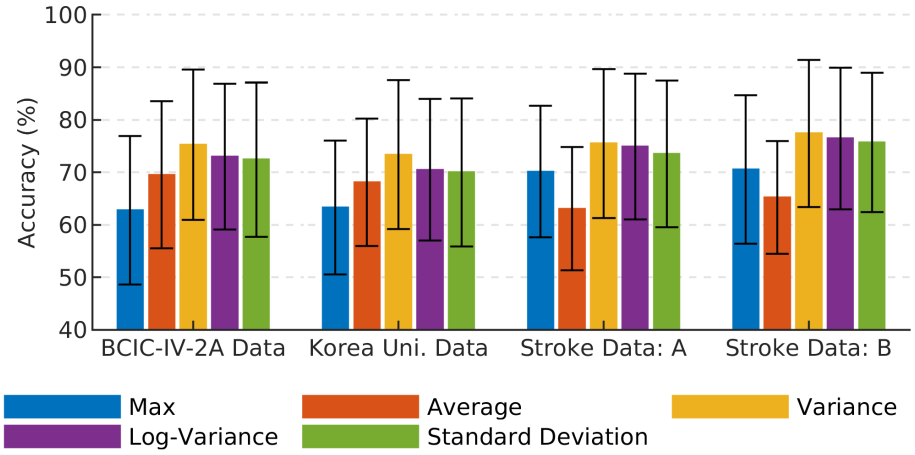

FIGURE 3.7: FBCNet cross validation classification accuracies with different temporal feature extraction layers (mean±std). Temporal feature extraction using Variance layer resulted in best classification accuracies across all datasets. Log-Variance and Standard Deviation layer, which are modified versions of Variance layer, resulted in better actuaries than Average, and Max layer, but in most cases, they were significantly worse than the Variance layer.

across all datasets. When compared with the Variance layer, there were 5%-15% drop in classification accuracies while using Average or Max layer and these differences were highly significant (all $p < 0.005$). Lastly, Max layer was the worst-performing layer in two datasets collected from healthy participants (BCIC-IV-2A Data and Korea Uni. Data) whereas the Average layer produced worst results in two datasets collected from stroke patients (Stroke Data: A and B), and the difference in accuracy between the Max and the Average layer was significant for most datasets (all $p < 0.05$ except $p_{\text{KoreaUni.Data}-\text{HO}} = 0.052$). More detailed results of this analysis are presented in Table A.7.

Result VII: Increasing the number of spatial filters in FBCNet architecture resulted in marginally improved classification results

The average classification accuracy achieved by FBCNet with different number of spatial filters is presented in Figure 3.8. In this analysis, the number of spatial filters, m, in FBCNet was varied and its effect on the classification accuracy was investigated. A positive trend was observed between the number of spatial filters and the resulting classification accuracy with m=32 resulting in the best classification accuracies across most datasets. Although the classification accuracy was observed to increase with more number of spatial filterers, this accuracy improvement was only marginal and not statistically significant in most cases. Changing

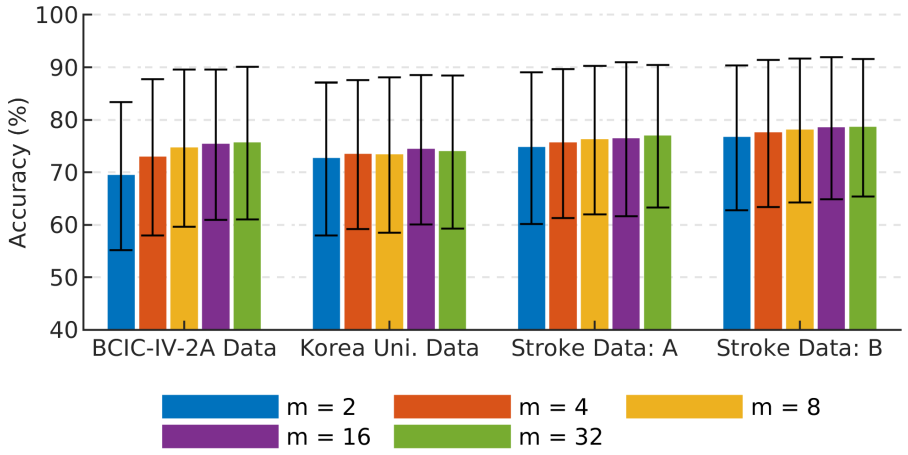

FIGURE 3.8: FBCNet cross validation classification accuracies with different number of spatial filters per frequency band (m) (mean±std). The classification accuracy marginally improved with increase in m. However, this improvement was not significant in most cases.

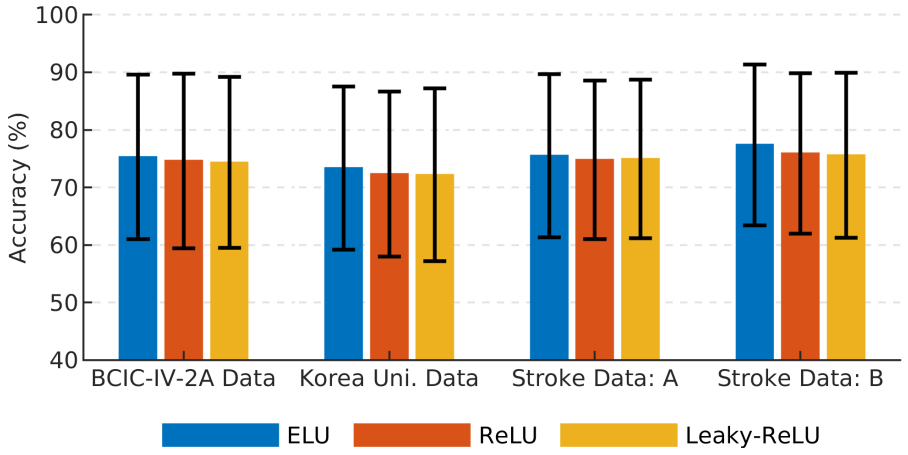

FIGURE 3.9: FBCNet cross validation classification accuracies with different non-linear activation functions. Use of Exponential Linear Units (ELU) achieved best classification accuracy across all tasks. (bars and error-bars indicate mean ± std of accuracy, ELU: Exponential Linear Units, ReLU: Rectified Linear Units).

the value of m from the default setting ($m = 16$ for BCIC-IV-2A Data and $m = 4$ for all other datasets) resulted in a significant gain only in Korea Uni. Data-CV analysis ($p = 0.009$). Also, the complexity of FBCNet was linearly proportional to m, therefore, increase in m resulted in FBCNet with more learnable parameters and longer training times. More detailed results of this analysis are presented in Table A.8.

Result VIII: ELU activation produced best classification accuracies

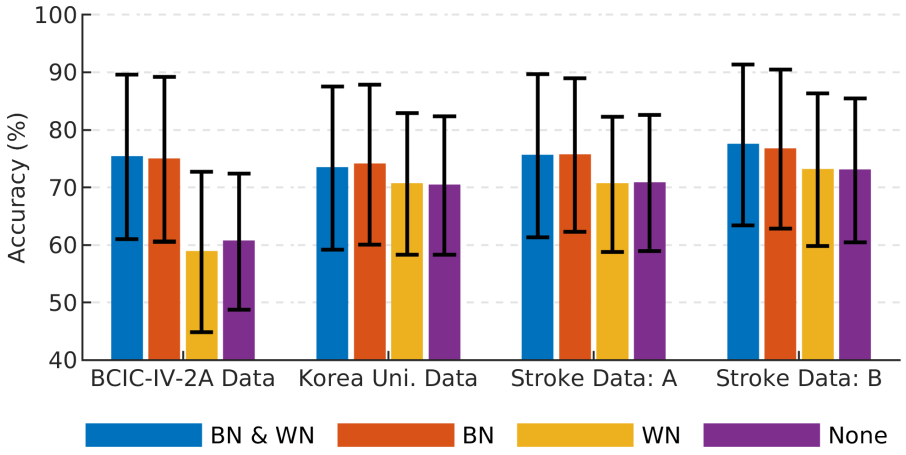

FIGURE 3.10: FBCNet cross validation classification accuracies with and without batch-normalization and weight-normalization. Presence of Batch-normalization significantly improved the classification accuracy, whereas weight-normalization did not had any effect on the accuracy. (bars and error-bars indicate mean ± std of accuracy).

The classification accuracies in the presence of ELU, ReLU or Leaky-ReLU activation functions are presented in Figure 3.9. In this analysis, the use of ELU non-linearity resulted in the best classification accuracy across all classification tasks. Furthermore, the improvement in the accuracy by ELU over ReLU and Leaky-ReLU was statistically significant for most analyses (all $p < 0.01$, except BCIC-IV-2A Data-CV and Stroke Data: A). Also, the classification accuracies did not differ significantly between ReLU and Leaky-ReLU activation functions (all $p > 0.05$).

Result IX: Batch-normalization and not Weight-normalization significantly impacted the classification performance

The results for ablation analysis of Batch-normalization and Weight-normalization are presented in Figure 3.10. In this analysis, the presence of Batch-normalization significantly improved the classification accuracy across all datasets (all $p < 0.005$). On the other hand, the classification accuracies were largely unaffected by the presence or absence of Weight-normalization (all $p > 0.05$ except for BCIC-IV-2A Data-HO analysis).

3.4.4 Interpretation of FBCNet Learning

Result X: Subject specific features learned by FBCNet were neurophysiologically sound

Figure 3.11 presents the results of interpretability analysis for a representative subject from the Korea Uni. dataset. For this subject, from the input relevance analysis, 12-16Hz and 24-28Hz were observed to be the two most relevant frequency bands and they together constituted to 50% of the total input relevance. Also, as presented in Figure 3.11 (b), the channel relevance patterns for these frequency bands were highly focused on the motor area of the brain. Following this high relevance, the FBCNet learned convolution filter weights associated with these two frequency bands were visualized (Figure 3.11 (a)). Here, the trained FBCNet model was observed to have assigned high filter weights to the EEG channels at motor areas of the brain (C1, C3, C2, C4). Next, to understand the generalizability of these discriminative features learned by FBCNet on the unseen test data, the input of the final fully connected layer in 2 dimensions for the test data was visualized using t-SNE and these visualizations are presented in Figure 3.11 (c). First, it was obseved that no clear class discriminative information can be identified from the raw EEG data (Figure 3.11 (c-1)). Next, the visualization of test features at the last layers of EEGNet-8,2, and Deep ConvNet demonstrated two slightly separable clusters for the 2 data classes, indicating the presence of some discriminative information (Figure 3.11 (c-2) and (c-3)). Lastly, two much more disjoint class-discriminative clusters were observed for the features at the last layer of FBCNet (Figure 3.11 (d-4)). Consequently, for this subject, the classification accuracies using Deep ConvNet, EEGNet-8,2, and FBCNet were 65.5%, 78.5%, and 91.0% respectively.

Result XI: Greater inter-subject variability in the relevance patterns was observed for stroke patients

To understand general trends in the relevance patterns across subjects and to explore if the data from stroke patients is any different from healthy subjects, a group level relevance analysis was performed and its results are presented in Figure 3.12. For reasons explained in section 3.3.6, this analysis was performed on subgroup of subjects with test classification accuracy >70%.

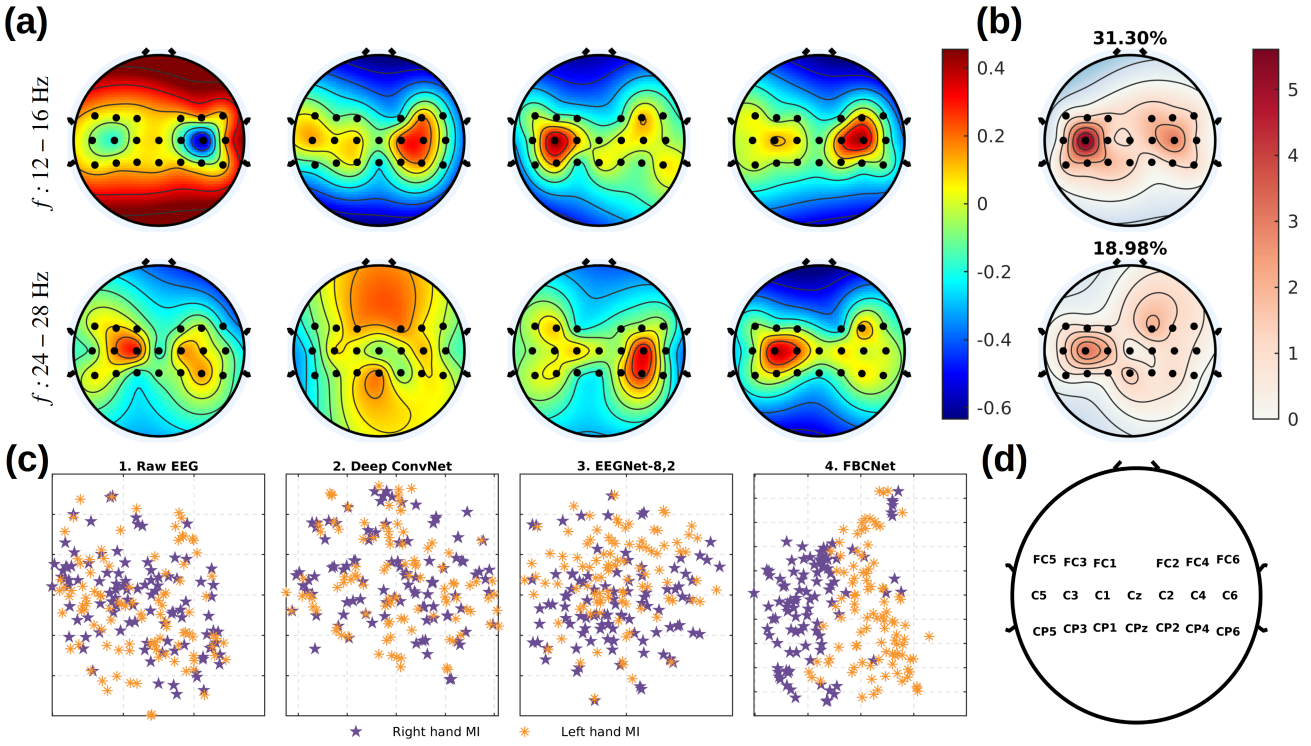

FIGURE 3.11: Representative subject level visualizations of FBCNet learning for one subject from Korea Uni dataset. Part (a) presents 8 spatial convolution kernels (4 per frequency band) learned by FBCNet for the EEG data filtered between 12-16 Hz and 24-28Hz for this subject. All these spatial filters have higher weights for the electrodes in the motor region (C1, C3, C2, C4 - the electrode names are presented in part (d)). Part (b) presents the electrode relevance for the same two frequency bands. With 31.30% of the total input relevance, data in the 12-16Hz, was observed to be the most important feature for FBCNet classification. Also, in this band, the most relevance was concentrated at the left and the right motor area (C3, and C4). Part (c) presents the visualization of EEG features in 2 dimensions using t-SNE for the same subject. Part c-1 is the visualization of the raw EEG data. Part c-2, c-3, and c-4 present the visualization of EEG features at the input of the final fully connected layer in trained Deep ConvNet, EEGNet-8,2, and FBCNet respectively for the test data. Due to the clear superiority of FBCNet in the extraction of highly generalizable features, FBCNet achieved 91.0% classification accuracy for this subject, whereas Deep ConvNet and EEGNet-8,2 resulted in 65.5% and 78.5% respectively.

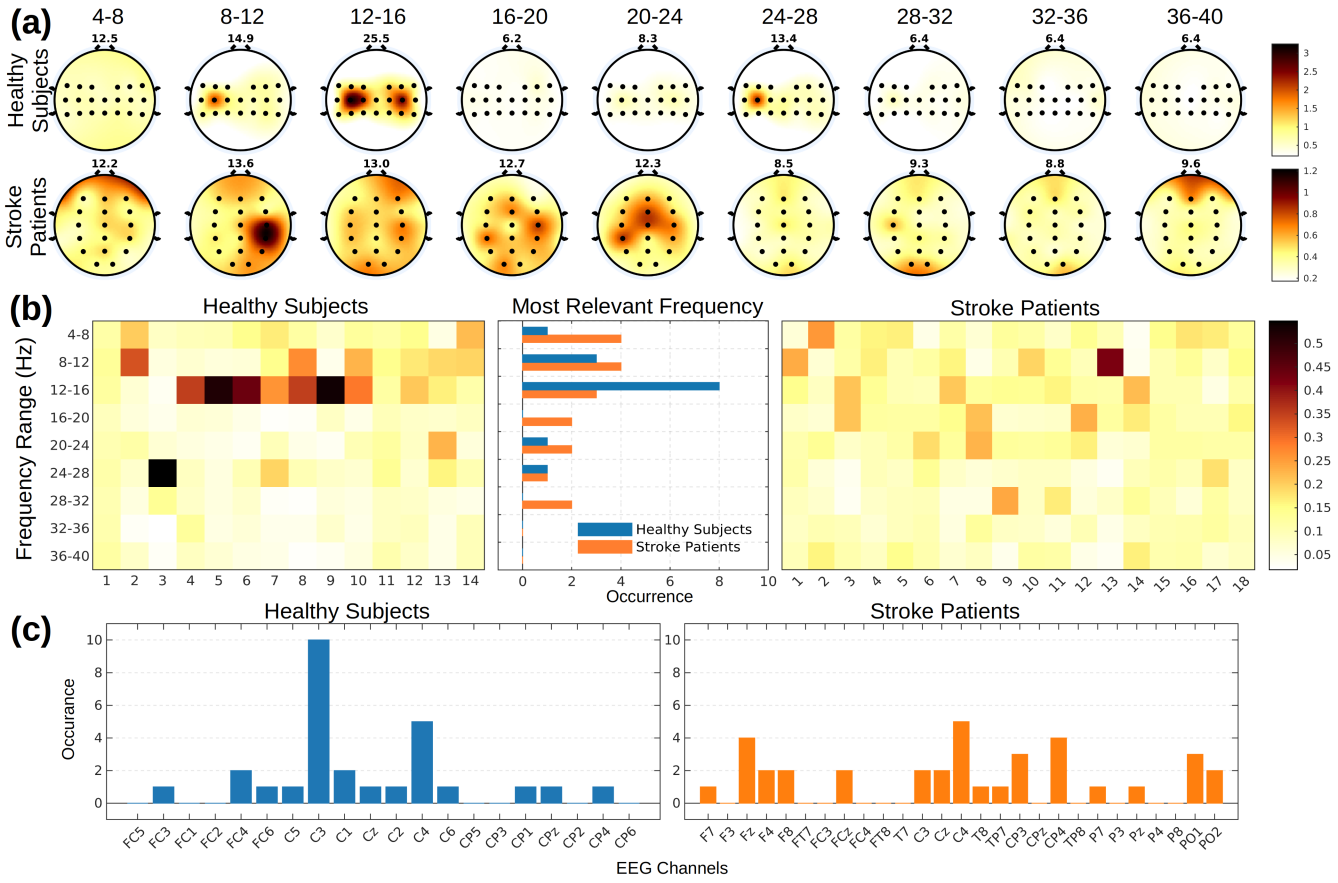

FIGURE 3.12: Group level relevance analysis for healthy subjects and stroke patients. Part (a) presents the subject-averaged channel-frequency input relevance patterns for healthy subjects and stroke patients. The number in the title is the percentage relevance for the given frequency band. Investigating more on the subject-averaged relevance, Part (b) presents the heatmap of frequency band relevance for each subject. Also, the histogram in the centre presents a normalized count of subjects for whom the given frequency band has the highest relevance. Next, part (c) presents the normalized histogram of subjects for whom the given EEG channel is among the 2 most relevant channels. See Section 11 for more details.

As a first step, the subject-averaged relevance patterns were inspected (Figure 3.12 (a)) at all frequency bands and EEG channels for stroke patients' and healthy subjects' data. For healthy subjects, the 12-16Hz and 8-12Hz were observed to be the two most relevant frequency bands and they constituted to 40% of the total input relevance across all subjects in the subgroup. Also, the channel relevance in these two frequency bands were most concentrated at the left and the right motor areas of the brain (C3, C4). Contrarily, the averaged relevance patterns for stroke patients were observed to be highly diffused and all the frequency bands in the 4-24Hz range resulted in similar input relevance. Moreover, the channel relevance patterns in these frequency bands were also much more diffused and many channels received similar total relevance scores. Yet, the C4, CP4, and P4 channels in the 8-12Hz range, and C3, C4, and CP4 channels in the 12-16Hz range were observed to have slightly higher relevance than other channels.

Next, the channel-frequency band relevance patterns were visually inspected for each healthy and stroke subject. Here it was observed that for most healthy subjects, the 8-12 Hz frequency band was highly relevant whereas the most relevant frequency range largely differed across stroke patients. To concisely visualize this difference, the heat-map of filter band relevance for healthy and stroke subjects was plotted and it is presented in Figure 3.12 (b). As can be seen from the heatmap, as well as the normalized histogram, the 12-16Hz was observed to be the frequency band with the highest relevance in half of the healthy subjects. Also, the difference between the relevance of the first and the second most relevant frequency band was very high for healthy subjects (average difference = 12.49% of the total relevance). Contrarily, for stroke patients, no single highly relevant frequency band could be identified and most relevant frequency band was highly subject-specific. Moreover, for each stroke patient, the input relevance was distributed across multiple frequency bands and the difference in the relevance of the first and the second most relevant frequency band was quite low (average difference = 5.24% of the total relevance). Furthermore, this difference was significantly different from healthy subjects' data (independent samples t-test, $p < 0.005$).

Next, the group level channel relevance patterns for stroke patients and healthy subjects were analyzed. Here the 2 most relevant EEG channels were investigated for each subject and resultant histograms for healthy subjects and stroke patients are presented in Figure 3.12 (c). Here, the C3 or C4 channels were observed to be

among the 2 most relevant channels for most (93%) healthy subjects. Also, the two most informative channels constituted to 18.93% of the total relevance for healthy subjects. Contrarily, a high inter-subject variability was observed in the 2 most relevant channels for stroke patients (Figure 3.12 (c)). Furthermore, the average relevance of the 2 most relevant channels in stroke patients was only 13.81%.

3.5 Discussion

This chapter proposed the FBCNet model which is a novel, neurophysiologically inspired, end-to-end CNN architecture for MI classification that can learn generalizable discriminative features in the presence of limited data and produce better classification accuracies. The performance of FBCNet was evaluated against the state-of-the-art classical machine learning and deep learning approaches using EEG-MI data from a large corpus of healthy subjects (n = 54 + 9 = 63) and chronic stroke patients (n = 37 + 34 = 71). To the best of our knowledge, this is the first work that compares the performance of deep learning approaches with classical machine learning methods for such a large population of healthy and stroke subjects. Besides the differences in the classification accuracies, using interpretability analysis, this work also presented some of the key differences in stroke patients' and healthy subjects' data from the perspective of MI classification. Next, it was showed that use of a hybrid approach, as done in FBCNet, which leverages the complex feature learning capabilities of deep learning methods and mitigates their sensitivity to small datasets by incorporating the neurophysiological priors for MI classification in the architecture design may lead to significant improvements in MI-BCI classification accuracies. It can be contemplated that, the three-stage approach of the spectral, spatial and temporal localization of EEG features in FBCNet has resulted in an architecture which is constrained enough that it effectively focuses on neurophysiological signatures of MI even in the absence of large training datasets while being flexible enough to efficiently handle the intra-class variability in EEG trials. Therefore striking a balance between model complexity (more trainable parameters to extract deeper encoded generalizable patterns) and constraints (neurophysiologically reasonable patterns) can be the way to successfully adapt deep learning methods into the BCI domain.

3.5.1 Performance of Classical Machine Learning Approach and State-of-the-Art Deep Learning Architectures

This chapter first investigated how one of the most successful classical MI classification method of FBCSP fares against recent deep learning architectures. The experimental results showed that, there was no statistically significant difference between the subject-averaged classification accuracy achieved by FBCSP-SVM and Deep ConvNet, EEGNet-8,2 for all but one analysis and these results are in line with the previous literature [20, 22, 244]. However, although statistically insignificant, FBCSP-SVM was observed to be the best performing baseline method for both stroke subjects' datasets (Table 3.4). Contrarily a reversed trend was observed for the healthy subjects' data from Korea Uni. dataset. This difference in best performing baseline methods can be thought to be associated with the different amount of training data present across these datasets. Both stroke datasets have 20% less training trials as compared to the Korea Uni. dataset (160 vs 200 trials/subject) and this less amount of training data may have affected the performance of deep learning architectures on a larger scale as compared to its impact on the FBCSP. To further test this theory, that baseline deep learning architectures are more sensitive to the amount of training data, the performance of these methods was evaluated on the BCIC-IV-2A hold out set with a variable amount of training data (Figure 3.6). In this analysis as well, it was observed that, compared to FBCSP-SVM, the accuracy of baseline deep learning architectures dropped significantly when trained with reduced amount of data. This indicates that in the absence of adequate training data, general purpose deep learning architectures may result in worse classification accuracies compared to more task tailored approaches like FBCSP-SVM.

Furthermore, although the difference in the amount of training data can account for dataset-level differences in classification accuracies of the baseline architectures, it cannot explain the large differences in the classification performance of these algorithms for individual subjects. As can be seen in Figure 3.4, for most subjects, the classification accuracy differed significantly between FBCSP-SVM and baseline deep learning methods. Here, a general pattern was observed that FBCSP-SVM resulted in extreme (very high or very low) classification accuracies for most of the subjects and contrarily, average classification accuracies were achieved by most subjects using Deep ConvNet and EEGNet-8,2. Inter-subject variability in the EEG

data distributions can be one possible explanation for these observed differences. It is probable that neurophysiologically constrained model of FBCSP-SVM is inadequate for subjects with high intra-class variability and non-standard MI-EEG patterns and more complex deep learning models may achieve relatively better accuracy for these subjects by learning some of those complex patterns. However, this additional flexibility in the deep learning architectures may also be detrimental to their performance in subjects with better class discriminative features. In this case, particularly with the limited and noisy training data, deep learning architectures may end-up learning non-generalizable patterns leading to poor test set performance. This indicates that striking a balance between model complexity and constraints may benefit all BCI users.

3.5.2 Classification Performance of FBCNet

The FBCNet was aimed to strike the balance between model capacity and complexity by incorporation of neurophysiological knowledge within the deep learning framework. So, it can be contemplated that striking this balance may have resulted in a model that has optimal learning capacity while being less susceptible to relatively small and noisy EEG data. The results using FBCNet strongly support this hypothesis wherein the FBCNet has resulted in the best classification accuracy across all datasets and this improvement in accuracy by FBCNet over baseline methods is statistically significant for most datasets (Table 3.4). Furthermore, in the analysis of individual subject classification accuracies, the FBCNet was observed to closely match the performance of the best performing classification algorithm for every subject in the datasets (Figure 3.4). Due to this, similar to FBCSP-SVM, the average classification accuracy of 25% best performing subjects by FBCNet was even better than that of FBCSP-SVM (Table 3.5). Also, the average accuracy of FBCNet for worst performing 25% subjects was in-between the FBCSP-SVM and baseline deep learning methods (Table 3.6) and this consequently resulted in most number of subjects being able to control the BCI with >70% classification accuracy using FBCNet (Table 3.7). Furthermore, the FBCNet was observed to be much less susceptible than baseline deep learning architectures to small training sets (Figure 3.6), indicating that the neurophysiologically constrained architecture of FBCNet can more effectively learn the generalizable class-discriminative patterns and avoid overfitting in cases of limited training data.

Moreover, unlike FBCSP, in the presence of more training data, the FBCNet accuracies improved continuously indicating that FBCNet can also effectively utilize a higher amount of training data when it is available. All these results indicate that the incorporation of neurophysiological knowledge within the deep learning framework, as done in FBCNet, may lead to better MI classification accuracies.

3.5.3 Role of Variance Layer

The Variance layer for temporal feature extraction is another important contribution of the FBCNet architecture. The use of variance operation along the temporal dimension was motivated by the fact that variance of a filtered signal represents the spectral power in the time-series and spatio-temporal differences in EEG spectral power are known class-discriminative features of MI. Therefore, it was hypothesized that variance may be a more suitable operation for temporal consolidation of EEG signals and this hypothesis was confirmed by experimental results. In the ablation analysis of temporal feature extraction layer, FBCNet with Variance layer resulted in significantly better performance than Average and Max layer which are two most widely used feature reduction strategies in the deep learning field (Figure 3.7). Hence Variance layer might be better suited for temporal feature consolidation in deep learning networks designed for MI classification.

3.5.4 Effect of Hyperparameter Selection

In the ablation analysis, the effect of other FBCNet design choices and hyperparameter values was also invested. The number of spatial filters per frequency band (m) is one of the most important hyperparameters in the FBCNet architecture. For this hyperparameter, a positive trend was observed between m and classification accuracy (Figure 3.8) and FBCNet with $m = 32$ resulted in the best performance which was marginally better than the default FBCNet setting. However, because the complexity of FBCNet is linearly proportional to the value of m, it was decided not to change the m value. Still, on unknown datasets, it is recommended to test the classification accuracies with different values of m. Next, the ELU non-linear activation function resulted in the best classification accuracies across all datasets (Fig. 3.9). This is in-line with the EEG literature [20, 22] and better performance

with ELU can be attributed to smooth activation function of ELU for negative inputs. Also, the performance of FBCNet was greatly affected by the absence of batch-normalization whereas there was no effect of weight-normalization on the classification accuracies.

3.5.5 Interpretability Analysis

Interpretability of the knowledge learned by the neural network architecture is a necessity when used in the clinical settings. Since FBCNet only contains 2 trainable layers and uses Depthwise Convolutions, the class discriminative features learned by FBCNet were extremely easy to analyze. The CNN kernel weights in the spatial convolution block of FBCNet represent the spectrally localized spatial transformation filters and they provide the information of how much weight is given to every EEG channel in extracted features. Also, the weights of the fully connected layer can be directly compared to analyze the importance given to any particular filter in a given frequency band in the classification decision. Given this ease of analysis, the CNN kernel weights were visualized. In this analysis, for most subjects from the Korea Uni. Dataset, high CNN weights were assigned to the EEG channels in the motor region of the brain (C3 and C4) in the 8-16Hz and 24-32Hz frequency range (Figure 3.11). This indicates that FBCNet successfully focused on the neurophysiologically sound features because spectro-spatially discriminative patterns at the primary motor cortex in the alpha (8-12Hz) and high beta bands (23-30Hz) of EEG are well-known signatures of left vs right-hand MI [243]. Moreover, it was observed that by encapsulating the true signatures of MI, these features also generalized well on the unseen test data (Figure 3.11 (c)) which in-turn explained the higher classification accuracies achieved by FBCNet.

Following the individual subject interpretability analysis, the possible difference in the class discriminative patterns between healthy subjects and stroke patients were investigated using input feature relevance analysis by DeepLIFT (Figure 3.12). In this analysis, relevance patterns were observed to be consistent across multiple subjects with highest relevance in the 8-16Hz and 24-32Hz frequency range at the motor region of the brain (C3, C4 channels) for healthy subjects' data. These relevance patterns are in-line with the neurophysiological signatures of MI [243]. However, for stroke patients, these patterns showed large inter-subject variability

and they were also much more spatially and spectrally diffused for individual patients. These spectro-spatially spread relevance patterns in stroke patients may indicate that the damage in the brain caused by stroke may have resulted in compensatory recruitment of non-motor areas by the brain [40]. However, to further investigate this phenomena, more data with distinct MI tasks from stroke patients is needed. Yet, the large inter-subject differences between the stroke patients' relevance pattern can be attributed to stroke-induced subject-specific modification in the brain and therefore, the compensatory recruitment of non-motor areas is a plausible explanation for the spectro-spatially spread relevance patterns in stroke patients.

3.6 Summary

In this chapter, a neurophysiologically motivated end-to-end CNN architecture named FBCNet was proposed for subject-specific MI classification that can learn generalizable discriminative features in the presence of limited data and produce better classification accuracies. This architecture proposed a hybrid approach for the task of MI classification in which the complex feature learning capabilities of deep learning methods were leveraged and their sensitivity to small datasets was mitigated by incorporating the neurophysiological priors of MI in the architecture design. This proposed approach achieved significantly better classification accuracies across 4 motor imagery datasets among which two were collected from chronic stroke patients. Moreover, with interpretability analysis, it was demonstrated that improved performance by FBCNet was driven by the effective learning of neurophysiologically relevant EEG feature. Furthermore, it was showed that there are differences in the MI data between healthy subjects and stroke patients and FBCNet can perform well on both healthy and patient data. Overall, the results indicate that inclusion of neurophysiological priors while designing deep learning architectures, as done in this work, will result in an architecture that is constrained enough that it can effectively focus on neurophysiological signatures even in the absence of large training datasets while being complex enough to effectively utilize a higher amount of training data when it is available and such an approach may lead to better classification results in the field of MI-BCI.

Chapter 4

FBCNet with High Level Temporal Information

4.1 Introduction

The previous chapter presented the FBCNet architecture for MI classification from the EEG data. More significantly, in FBCNet, a novel Variance layer was proposed for the effective extraction and consolidation of the discriminative temporal information from the EEG data. From the mathematical formulation, owing to its gradient function and its effect on the downstream learning, it was observed that the Variance layer might be the best suitable layer for the EEG temporal information extraction. This hypothesis was also confirmed by the superior classification results achieved by the FBCNet with the Variance layer. One important property of the proposed Variance layer was that it compressed the entire input time series into a single feature, achieving extremely compact temporal feature extraction. Although this approach proved to be effective to combat the problem of model overfitting, it left a room for further improvement. In the literature, the

The work presented in this chapter has been partially published as:

1. Ravikiran Mane, et al., FBCNet: An Efficient Multi-view Convolutional Neural Network for Brain-Computer Interface. *(In preparation)*

MI is known to be associated with the time domain fluctuation in the EEG in a form of ERD and ERS patterns [243]. This knowledge highlights the importance of temporal feature extraction for MI decoding. Also, ERD and ERS patterns are known to be in the order of few hundred milliseconds [243]. This understanding that, within the EEG trial, the ERD/ERS patterns, which are the signatures of the MI, are more concentrated in smaller time windows, motivates further extraction of higher level temporal information from the smaller EEG segments. Particularly, with higher temporal representation capacity, the extraction of more temporal information from the spectro-spatially localized EEG data, may result in improved classification accuracies.

Considering this importance of the time domain information in EEG-MI classification, many deep learning architectures have been proposed which include special layers for extraction of temporal information. In this domain, the CNN-RNN cascade based architectures are most widely explored [163, 258–261]. In these architectures, the initial part of the network is constructed using the convolutional layers which extract the higher level spatial features from the EEG data. These features are then passed to the vanilla RNN, or more popularly, the LSTM layers, for extraction of temporal information and time domain dependence. In this manner, CNN-RNN cascade networks have shown promising results in EEG classification, but the classification improvement by these networks has also been limited by the lack of sufficient training data [163]. High model complexity can be considered to be one of the crucial drawbacks of these architectures and more compact architectures like FBCNet, when coupled with the LSTM may improve the MI detection accuracies.

Hence, considering the importance of high level temporal information, this chapter extends the previously presented FBCNet architecture, proposing a FBCNet with High Level Temporal Information (FBCNet with HLTI) architecture. In FBCNet with HLTI architecture, the temporal feature extraction capabilities of FBCNet are improved by extracting the Variance features from multiple small time windows along the temporal dimension. This approach results in the extraction of one Variance feature for every time window and assignment of different weights to each of these features leads to the effective modulation of the high level EEG temporal importance. Next, in FBCNet+LSTM architecture, the FBCNet with HLTI is further extended with the LSTM layer for effective extraction of temporal dependence

between the EEG time windows. With this motivation, as done in Chapter 3, the classification performance of FBCNet with HLTI and FBCNet+LSTM is evaluated with the help of two publicly available datasets and two datasets from the stroke patients. Furthermore, to understand the effect of temporally windowed feature extraction on the network learning, an interpretability analysis has been conducted. The results indicate that moderate extraction of High Level Temporal Information can significantly increase the classification accuracies for less accurate subjects while maintaining the accuracies for highly accurate subjects.

4.2 Methodology

4.2.1 FBCNet with High Level Temporal Information

The FBCNet with High Level Temporal Information (FBCNet with HLTI) is designed to extend the temporal feature extraction capabilities of FBCNet. Therefore, it retains the four-stage design of the FBCNet and modifies the temporal Variance layer with a windowed Variance layer. So, at its core, as visualized in Figure 4.1, the FBCNet with HLTI contains the following four components:

1. Multi-view data representation: The multi-view representation of the EEG data which is obtained by spectrally filtering the raw EEG with multiple narrow-band filters.
2. Spatial transformation learning: As done in FBCNet, the spatial discriminative patterns for every view are then learned using a Depthwise Convolution layer.
3. High level temporal feature extraction: Different from the FBCNet, a windowed Variance layer is used to effectively extract a high level time domain discriminative information.
4. Classification: Finally, the features from all time-series and windows are classified using an FC layer into given classes.

With this brief design philosophy, the distinguishing aspects of FBCNet with HLTI are mentioned in this subsection.

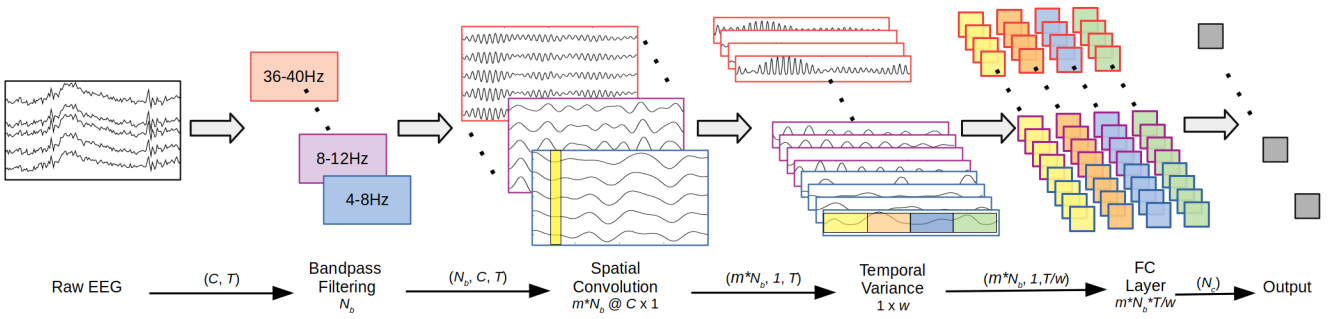

FIGURE 4.1: The architecture of FBCNet with High Level Temporal Information. (C: number of EEG channels, T: number of time points, N_b: number of frequency bands, m: number of convolution filters per frequency band, N_c: number of output classes, w: size of the temporal window).

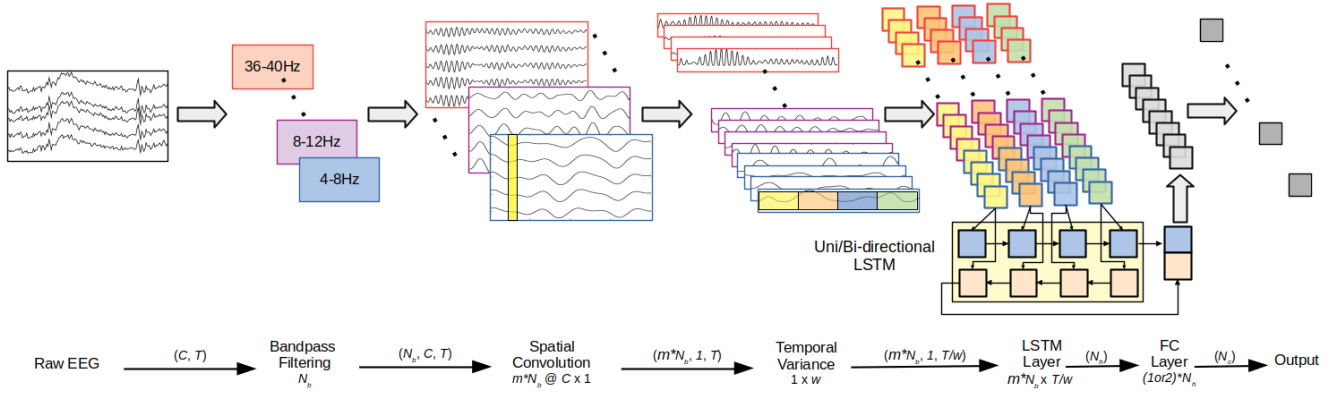

FIGURE 4.2: The FBCNet+LSTM architecture. (C: number of EEG channels, T: number of time points, N_b: number of frequency bands, m: number of convolution filters per frequency band, N_c: number of output classes, w: size of the temporal window, N_h: number of LSTM hidden units).

Spectro-spatial Localization by Multi-view Data Representation and CNN

The FBCNet with HLTI inherits the spectro-spatial localization architecture of the FBCNet. Therefore, considering that the single-trial raw EEG data is represented as $x \in \mathbb{R}^{C \times T}$ and its corresponding label as $y \in \{0, 1, .., N_c\}$, where C represents number of EEG channels, T represents time points and N_c is the total number of distinct classes, the FBCNet with HLTI architecture generates the spectrally filtered multi-view representation of the data, x_{FB}, as:

$$x_{FB} = F \otimes x \quad \in \mathbb{R}^{N_b \times C \times T} \tag{4.1}$$

Where, $\otimes$ indicates bandpass filtering operation and $F = \{f_i\}_{i=1}^{N_b}$ denotes a filter bank consisting of N_b number of narrow-band temporal filters. As done in FBCNet, in the FBCNet with HLTI architecture, the filter bank is constructed using $N_b = 9$ filters with non-overlapping frequency bands, each of 4Hz bandwidth, spanning from 4 to 40 Hz (4-8, 8-12, ..., 36-40 Hz).

Similar to the FBCNet, following the spectral localization, a Spatial Convolution Block (SCB), comprising of a Depthwise Convolution layer, a Batch Normalization layer [248] and an Exponential Linear Unit (ELU) nonlinearity is used to learn the spatial localization of the filtered EEG data. For SCB to effectively act as a spatial filter, the kernel size of the Depthwise Convolution layer in SCB is set to $(C, 1)$. Furthermore, the depth parameter m controls the number of spatial filters per frequency band learned by SCB and it decides the capacity of the network in the extraction of spatially discriminative information. Following the results from the FBCNet's ablation analysis, in the default FBCNet with HLTI structure, the value of m is set to be 32. Also, the effect of different values of m on FBCNet with HLTI's classification performance is evaluated in this study's ablation analysis. In this manner, SCB outputs $m \times N_b$ time-series, $x_{SCB} \in \mathbb{R}^{(m \times N_b) \times 1 \times T}$, which are spectro-spatially localized.

High Level Temporal Feature Extraction by a windowed Variance Layer

The temporal information extraction capability of the FBCNet with HLTI stems from the use of windowed Variance layer. In the vanilla FBCNet architecture, the Variance layer computes the variance of the entire time-series and output is given as:

$$x_{FBCNet_{V_{i,j}}} = \frac{1}{T}\sum_{t=0}^{T}(x_{SCB_{i,j,t}} - \mu_{i,j})^2 \in \mathbb{R}^{(m\times N_b)\times 1} \tag{4.2}$$

where, $\mu_{i,j}$ is the temporal mean of $x_{SCB_{i,j,t}}$.

Different from the vanilla FBCNet, the windowed Variance layer in FBCNet with HLTI architecture extracts the variance from smaller time windows. As opposed to a single output feature per time-series in FBCNet, the windowed Variance layer outputs T/N_s feature for every time series. Here, N_s represents the number of samples in the window of size w and $N_s = w \times sampling\ frequency$. So, the output of the windowed Variance layer is given by:

$$x_{FBCNet\ with\ TL_{V_{i,j,k}}} = \frac{1}{N_s}\sum_{t=k\times N_s}^{(k+1)\times N_s - 1}(x_{SCB_{i,j,t}} - \mu_{i,j,k})^2 \in \mathbb{R}^{(m\times N_b)\times 1\times (T/N_s)} \tag{4.3}$$

where, $\mu_{i,j,k}$ is the temporal mean of $x_{SCB_{i,j,t}}$ from the k^{th} window.

Here, the window size parameter, w, controls the number of temporal features extracted from each time series. In this particular analysis, since the ERD and ERS events are known to be of the order of 500ms, the default value of w is set to be equal to 0.5s [243]. Also, the effect of different values of w on FBCNet with HLTI's classification performance is evaluated in this study's ablation analysis. In this manner, the windowed Variance layer outputs $m \times N_b$ features per time window for T/N_s time windows.

Classification

Finally, in FBCNet with HLTI, the Variance features from all the time windows are concatenated and are given to an FC layer with linear activation. In this manner, the FC layer receives $(m \times N_b \times (T/N_s))$ features for every trial. The output of

the FC is then passed through the softmax layer to get the output probabilities of each class. As done in FBCNet, the FC layer weights are also regularized using a maximum norm constraint of 0.5; $||w||^2 < 0.5$ (Weight-normalization).

4.2.2 FBCNet+LSTM

The FBCNet with HLTI presented in the previous sections has higher temporal feature extraction capability, but it still lacks the ability to extract the temporal dependence between the features from the different time windows. To extract this time domain relationship, the FBCNet with HLTI architecture is extended to include an LSTM block formulating the FBCNet+LSTM architecture. This architecture is presented in Figure 4.2.

The FBNet+LSTM architectures comprise of the same layers as that of the FBCNet with HLTI with the addition of LSTM block and modifications in the classification layer. Therefore, only these differences are detailed in this section.

Extraction of temporal dependence using LSTM

To incorporate the feature of temporal dependence learning, the FBCNet with HLTI architecture is updated to include an LSTM block. Here, the output of the windowed Variance layer, which is $m \times N_b$ features per time window for T/N_s time windows, is passed to an LSTM block in a sequential manner. In the LSTM block, in its default form, the number of LSTM layers is kept to be one and a bidirectional LSTM is used considering the presence of bidirectional interactions between EEG time-series. Along with these settings, the suitability of unidirectional LSTM and an LSTM block with two layers is also investigated in the ablation analysis. Furthermore, the number of hidden units, N_h is another hyperparameter in the LSTM design. In its default settings, to keep the model complexity low, the N_h is set to 16 for all the 2-class datasets. For the BCIC-IV-2A Data, considering its 4 class nature, the N_h is set to 32. The effect of different values of N_h is also tested in the ablation analysis. Furthermore, to avoid overfitting, a Dropout layer is also included in the LSTM architecture and the dropout probability is set to be 0.25. In this manner, the output of the last node from the forward directional LSTM

and the first node from the reverse directional LSTM is appended as an output of the LSTM block. In effect, the LSTM block outputs $2 \times N_h$ features.

Classification

Lastly, the $2 \times N_h$ features extracted by the LSTM block are passed to an FC layer with linear activation. Following the FC layer, a softmax layer is used to to get the output probabilities of each class. Also, similar to the FBCNet with HLTI, the FC layer weights are regularized using a maximum norm constraint of 0.5; $||w||^2 < 0.5$.

4.2.3 Datasets, Experiments and Training Procedure

Similar to the FBCNet analyses, the performance of FBCNet with HLTI and FBCNet+LSTM is analyzed using four diverse MI datasets:

1. *BCIC-IV-2A Data*: A 4 class MI data from BCI Competition IV Dataset 2A [250].
2. *Korea Uni. Data*: A 2 class MI data from Korea University EEG dataset [251].
3. *Stroke Data: A*: A 2 class MI vs rest dataset [119].
4. *Stroke Data: B*: A 2 class MI vs rest dataset [88].

The most important dataset characteristics are summarized in Section 3.3.2 and Table 3.2, and more detailed data description is provided in Section A.2.

Also, similar to the FBCNet analysis, the above datasets were analyzed in the 10-fold cross validation (CV) and hold out settings (HO). The details of these analysis settings are presented in detail in the Section 3.3.3.

Furthermore, the FBCNet, FBCNet with HLTI and FBCNet+LSTM architectures were trained using the same training strategy. As detailed in the Section 3.3.4, the two-stage training was conducted using an Adam optimizer at default settings (learning rate = 0.001, betas = $0.9, 0.999$) [252].

4.2.4 Ablation Analysis

Both, the FBCNet with HLTI and FBCNet+LSTM architectures have multiple hyperparameters and to understand their effect on the classification accuracy, the following ablation analysis was performed.

Role of m and w in FBCNet with HLTI architecture

In the FBCNet with HLTI architecture, the number of spatial filters per frequency band (m) and the size of the temporal window in the variance layer (w) are the two most important hyperparameters. The value of m determines the spatial learning capacity of the network, whereas the window size w determines the network's temporal learning capacity. Furthermore, these two factors together determine the number of trainable parameters in the network and the network's overall complexity. Therefore, in the ablation analysis, the effect of these two hyperparameters on FBCNet with HLTI's classification accuracy was examined with 5 different values of m (m = 2, 4, 8, 16, 32) and 5 different values of w (w = 4s, 2s, 1s, 0.5s, 0.1s).

The classification accuracy of FBCNet+LSTM architecture will also depend on the value of m and w. However, considering the long training times and infeasible number of experiments, in FBCNet+LSTM experiments, the m and w were not changed from their default values (m = 32, w = 0.5s).

Role of number and type of LSTM layer, and number of LSTM hidden nodes in the FBCNet+LSTM architecture

In the FBCNet+LSTM, the number and the type of LSTM layer, and the number of LSTM hidden nodes are the three most important hyperparameters and it is important to analyze the effect of these parameters on the classification accuracy. However, considering the long training duration of the LSTM networks, this ablation analysis was done in two parts. In the first part, an HO analysis was conducted on the BCIC-IV-2A data and Korea Uni. Data, and the effect of all the three hyperparameters was analyzed. All the combinations of uni/bi-directional LSTM layer, one/two stacked LSTM layers, and 16/32/64 hidden nodes were investigated. Based on the results of this analysis, the best combination of the number and the

type of LSTM layer was identified. In stage two, using the previously identified combination of the number and the type of LSTM layer, an ablation analysis for the number of LSTM hidden nodes was conducted on all the datasets.

4.2.5 Interpretability and Visualizations

Along with the classification performance, to understand whether the incorporation of temporal localization in the FBCNet architecture results in the modifications in the temporal relevance patterns, a comparative interpretability analysis was conducted. As done in the previous chapter, the input feature relevance was computed and visualized using a DeepLift algorithm [254, 255]. In this analysis, the subject level and dataset level relevance patterns were computed and compared between the vanilla FBCNet and FBCNet with HLTI. The subject-level analysis was focused on the subjects who showed a significant difference between classification accuracies for FBCNet and FBCNet with HLTI. In the dataset level analysis, the relevance patterns, using FBCNet and FBCNet with HLTI, from all the subjects, were averaged and compared. More details of the relevance calculations are presented in Section 3.3.6.

4.2.6 Statistical Analysis

As done in the Chapter 3, the statistical significance of differences in classification accuracy achieved by different algorithms was assessed using a paired t-test for all datasets except BCIC-IV-2A Data. For BCIC-IV-2A Data, owing to its small sample size, the differences in classification accuracy was statistically tested using the Wilcoxon signed-rank test. To avoid the false discoveries in a multiple comparison situation, the p-value was corrected with Bonferroni correction for multiple comparisons.

TABLE 4.1: Average subject-specific classification accuracy

Dataset	Analysis	FBCSP-SVM	Deep ConvNet	EEGNet-8,2	FBCNet	FBCNet with HLTI	FBCNet+ LSTM
BCIC-IV-2A Data	CV	75.89	72.20	73.13	75.54	**77.89**	67.24
Korea Uni. Data	CV	64.61**	68.33*	70.89	73.84	73.69	**74.07**
Stroke Data: A	CV	71.37**	68.81**	69.15**	76.86	**77.99**	76.30
Stroke Data: B	CV	74.14**	71.11**	73.47	78.47*	**81.47**	79.09
BCIC-IV-2A Data	HO	68.06	72.22	73.15	71.87	**74.31**	65.40
Korea Uni. Data	HO	60.36**	60.77**	63.63	66.31	68.62	**69.19**

The best performing method for each analysis is highlighted in boldface. The *, and ** represent that the classification performance of FBCNet with HLTI is significantly better than the given baseline method with *: $p_{corrected} < 0.05$, and **:$p_{corrected} < 0.001$.

4.3 Results

4.3.1 Classification Performance of FBCNet with HLTI

Result I: FBCNet with HLTI achieved significantly higher classification accuracies than the vanilla FBCNet

The complete classification results using FBCNet with HLTI are presented in Table 4.1. From the table, it can be observed that the FBCNet with HLTI, in its default form of FBCNet-32-0.5s (FBCNet-*m*-*w*), when compared with FBCNet and other baseline architectures, achieved the best classification accuracies across all the datasets in both CV and HO settings. The Stroke Data: B resulted in the highest classification improvement of 3% using FBCNet with HLTI over FBCNet and this improvement was statistically significant after the correction for multiple comparisons. The least improvement was observed in the Korea Uni. Data. For the other datasets, the FBCNet with HLTI increased the classification accuracies by almost 2% over FBCNet. When compared to the baseline methods of FBCSP, Deep ConvNet and EEGNet, in all analyses, the FBCNet with HLTI achieved almost 6% higher classification accuracies and this difference was statistically significant in most cases. More detailed classification results, with the statistical analysis, are presented in Table B.1.

Result II: FBCNet with High Level Temporal Information resulted in improved classification accuracy for less accurate subjects

Following the analysis of subject averaged classification accuracies, the performance of FBCNet with HLTI for each subject was investigated. In this analysis, the aim

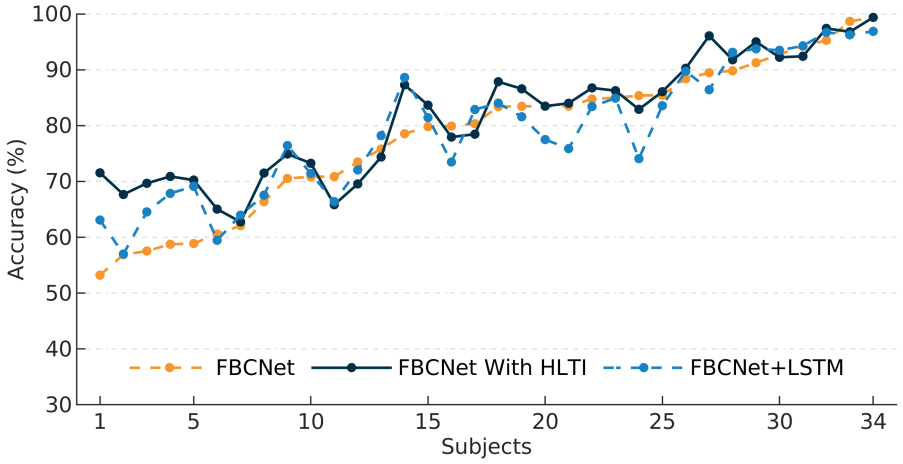

FIGURE 4.3: Classification accuracy for each subject from Stroke Data: B in 10-fold cross-validation settings (sorted by FBCNet acc.). It can be observed that, both, FBCNet with, and without temporal localization, resulted in identical classification accuracy for most of the highly accurate subjects. However, the incorporation of temporal localization significantly improved the classification accuracies in subjects with poor FBCNet performance. Also, the classification performance of FBCNet+LSTM was in between that of the FBCNet and FBCNet with HLTI. A similar trend was observed in other datasets as well.

was to identify the subjects who benefited from the use of additional temporal information in FBCNet with HLTI. So, the CV classification accuracies for all subjects from the Stroke Data: B datasets were analyzed and the results are presented in Figure 4.3. From the figure, it can be observed that both, the FBCNet and FBCNet with HLTI resulted in very similar accuracies for most subjects who were already achieving high classification accuracies using FBCNet. The drastic difference in the classification accuracies between these two algorithms was observed in subjects who had very poor accuracy using FBCNet. For these subjects, almost 10% improvement in classification accuracies was observed with the use of FBCNet with HLTI.

To quantitatively investigate this pattern, the average classification accuracy for 25% subjects with the lowest CV accuracy using FBCNet was analyzed. In this analysis, the bottom 25% subjects in the Stroke Data: B datasets resulted in average classification accuracy of 61.56% with FBCNet whereas, FBCNet with HLTI and FBCNet+LSTM achieved an average accuracy of 68.46% and 65.03% respectively. Furthermore, this 7% difference between the classification accuracy of FBCNet and FBCNet with HLTI, when tested with independent sample t-test, was

TABLE 4.2: Best FBCNet with HLTI configurations for all analyses.

Dataset	Analysis	FBCNet	FBCNet with HLTI : Best m, w	Best Configuration (FBCNet-m-w)
BCIC-IV-2A Data	CV	75.54	**77.89**	FBCNet-32-0.5s
Korea Uni. Data	CV	74.28	**74.40**	FBCNet-16-0.5s
Stroke Data: A	CV	76.29	**78.14**	FBCNet-16-0.5s
Stroke Data: B	CV	78.47	**81.47**	FBCNet-32-0.5s
BCIC-IV-2A Data	HO	71.87	**74.31**	FBCNet-32-0.5s
Korea Uni. Data	HO	66.31	**69.62**	FBCNet-32-0.1s

statistically significant ($p < 0.005$). Also, a similar, but statistically insignificant trend was observed in Stroke Data: A.

Result III: Temporal window of 0.5s seconds along with m = 32 resulted in best classification accuracies for most datasets

To understand the impact of the number of filters per frequency band (m) and the size of the temporal window (w) on the classification accuracies, an ablation analysis was conducted and results of this analysis for one representative dataset are presented in Figure 4.4. In this analysis, it was observed that the classification accuracy initially improved with an increase in m and then declined for higher values of m, for most datasets. A similar trend was observed for the temporal window size. For all datasets, the classification accuracies improved when window size was reduced from 4s to 0.5s. Also, for all datasets, except Korea Uni. Data, the classification performance degraded for the temporal window size smaller than 0.5s. In this manner, as presented in Table 4.2, the temporal window of 0.5 seconds along with m = 32 resulted in the highest dataset level classification accuracy in most datasets. More detailed ablation analysis results for the remaining datasets are presented in Section B.2.

4.3.2 Classification Performance of FBCNet+LSTM

Result IV: FBCNet+LSTM achieved marginally higher classification accuracies than the FBCNet with HLTI architecture in one dataset

The classification accuracies achieved by FBCNet+LSTM architecture for all the analyses are presented in Table B.1. The FBCNet+LSTM classification accuracies

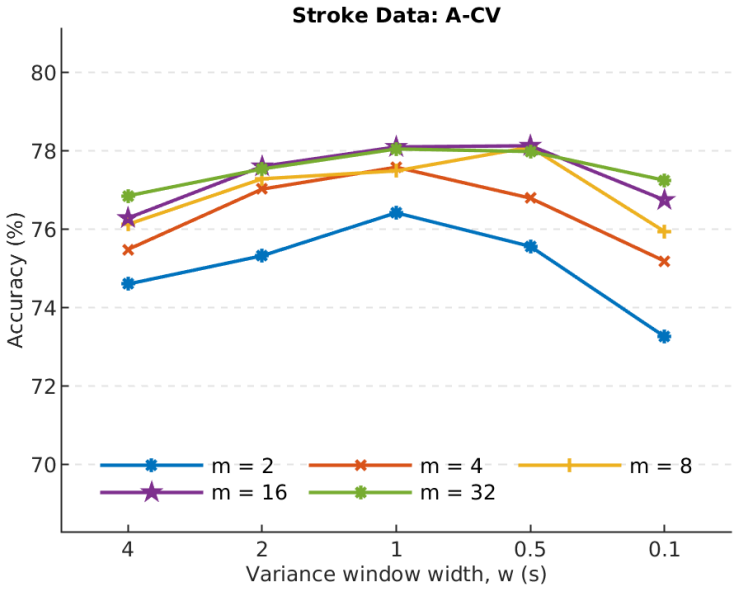

FIGURE 4.4: FBCNet with HLTI's cross validation classification accuracies with different number of spatial filters per frequency band (m) and different temporal window sizes (w) for Stroke Data: A dataset. The classification accuracy marginally improved with increase in m. Also, varying the temporal window size from 4 to 0.5 seconds resulted in the increased accuracy. However, the accuracy degraded for too small window size of 0.1 seconds. A similar trend was observed in other datasets as well.

were observed to be higher than that of vanilla FBCNet, and lower than the FBCNet with HLTI for the two stroke datasets. However, this difference in accuracies was not statistically significant (all $p > 0.05$). For the Korea Uni. Dataset, the FBCNet+LSTM architecture marginally outperformed the FBCNet with HLTI architecture and achieved the best subject averaged classification accuracies in both, the CV and the HO analysis. Contrarily, the classification accuracy using FBCNet+LSTM was significantly lower than that of FBCNet and FBNet with TL for the BCIC-IV-2A Data. More detailed classification results, with the statistical analysis, are presented in Table B.1.

Result V: Single layer, bidirectional LSTM resulted in higher classification accuracies than two layered, unidirectional counterparts

The LSTM networks, due to their sequential nature, need longer training time and are harder to train. Therefore, before analyzing all the datasets, a preliminary ablation analysis, using BCIC-IV-2A and Korea Uni. Data was performed to initially check the performance of uni vs bi-directional and one vs two layered LSTM

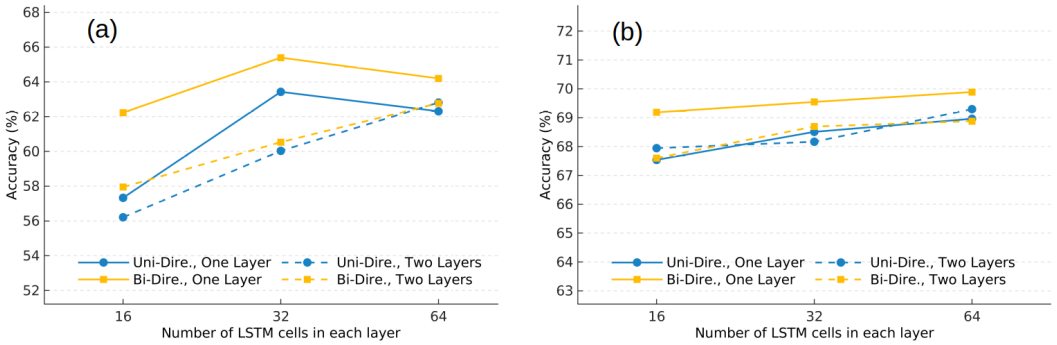

FIGURE 4.5: Effect of number of LSTM cells per layer, number of layers, and Uni/Bi-Directional configuration on HO classification accuracies of FBCNet+LSTM for (a) BCIC-IV-2A Data, and (b) Korea Uni. Data. For both the datasets, the single layer, bidirectional LSTM configuration always resulted in higher classification accuracies. The best number of LSTM cells per layer was observed to be highly analysis specific.

TABLE 4.3: Effect of number of LSTM hidden nodes (N_h) on FBCNet+LSTM classification accuracies

Dataset	Analysis	$N_h = 16$	$N_h = 32$	$N_h = 64$
BCIC-IV-2A Data	CV	64.87	**67.24**	68.22
Korea Uni. Data	CV	**74.07**	73.22	72.68
Stroke Data: A	CV	**76.30**	76.23	75.67
Stroke Data: B	CV	79.09	**79.17**	78.80
BCIC-IV-2A Data	HO	62.23	**65.39**	64.20
Korea Uni. Data	HO	69.19	69.55	**69.89**

The best performing method for each analysis is highlighted in boldface.

configurations. Figure 4.5 presents the results of this analysis. From the results, it was observed that the bidirectional LSTM always outperformed its unidirectional counterpart. Also, for both the datasets, the classification accuracies with one LSTM layer were always better than that of the two layered LSTM configuration. Contrary to these consistent results, the number of LSTM hidden nodes achieving the best classification accuracy were different for both the datasets.

Following these preliminary results, the effect of number of LSTM hidden nodes on the FBCNet+LSTM's classification performance for all datasets was analyzed and these results are present in Table 4.3. In this analysis, a single layer, bidirectional LSTM configuration of FBCNet+LSTM was used with a different number of LSTM hidden nodes. The results indicated that the best number of LSTM hidden nodes were variable across the datasets, but the difference in their classification accuracies was not significant for any of the analysis.

4.3.3 Interpretability Analysis

Since the FBCNet with HLTI architecture resulted in significantly higher classification accuracies, its trained models were analyzed with DeepLift algorithm to understand the reasons behind this improved classification performance.

Result VI: Significant accuracy improvements by FBCNet with HLTI were associated with improved temporal and spatial relevance patterns

The results of the interpretability analysis for a representative subject from Stroke Data: B, whose classification accuracy showed significant improvement when using the FBCNet with HLTI architecture, are presented in Figure 4.6. For this subject, first, the input time relevance patterns for vanilla FBCNet and FBCNet with HLTI were analyzed to explore whether the use of an architecture designed for extraction of high level temporal information, can lead to the modification in the temporal input relevance patterns. The results of this analysis are presented in Figure 4.6 (a). It can be observed from the figure that despite the use of Variance layer, the vanilla FBCNet learned to provide almost equal importance to all the time points in the entire EEG segment. Contrarily, the FBCNet with HLTI resulted in more than 50% higher relevance in the 0.5s to 1s EEG time segment. Furthermore, in the 1.5s to 4s time window, the relevance of FBCNet with HLTI was close to 10% lower than that of FBCNet.

Along with the modifications in the temporal relevance patterns, by updating the downstream convolutional kernel weights, FBCNet with HLTI also resulted in the modified spectro-spatial relevance patterns and these results for the same subject are presented in Figure 4.6 (b). It was observed that the spectro-spatial relevance patterns of the trained FBCNet model were more focused on the lower frequency bands with 4-8 Hz frequency band achieving the highest relevance. Also, in this band, the higher relevance was given to the channels in the frontal and occipital regions of the brain. Contrarily, the use of FBCNet with HLTI resulted in significantly higher relevance in the 8-12 Hz and 20-24 Hz frequency bands. Moreover, the relevance in these bands was more concentrated in the central-motor and occipital regions of the brain. With these modifications in the input relevance patterns, for this subject, the use of FBCNet with HLTI improved the classification accuracy to 69.67% over the vanilla FBCNet's 57.54%.

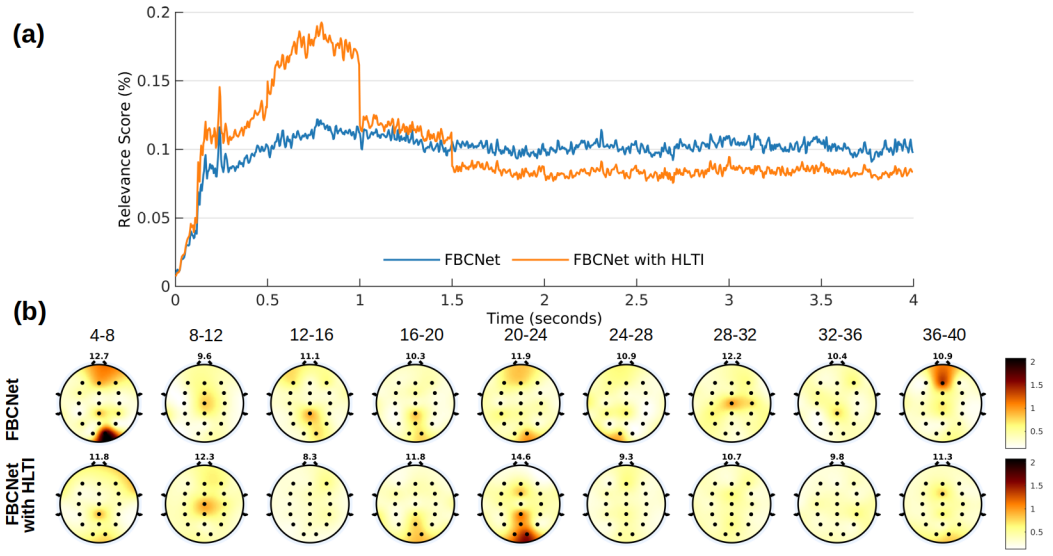

FIGURE 4.6: Representative subject level relevance analysis of FBCNet and FBCNet with HLTI for one subject from Stroke Data: B dataset which showed significant improvement in classification accuracy using FBCNet with HLTI. Part (a) presents a subject level input-time relevance when analyzed with vanilla FBCNet and FBCNet with HLTI. It can be observed that the FBCNet with HLTI modified the temporal relevance patterns to provide much higher importance to the 0.5-1s EEG-time segment. Contrarily, FBCNet assigned almost the same relevance to all the time-points. Part (b) presents the channel-frequency input relevance patterns for the same subjects when analyzed with vanilla FBCNet and FBCNet with HLTI. The number in the title is the percentage relevance for the given frequency band. Here, it can be observed that the use of FBCNet with HLTI resulted in significantly increased relevance in the 8-12 Hz and 20-24 Hz frequency bands. Also, the relevance in these bands was more concentrated in the central-motor and occipital regions of the brain. Owing to these more neurophysiologically sound learnings, the use of FBCNet with HLTI improved the classification accuracy for this subject to 69.67% over the vanilla FBCNet's 57.54%.

Result VII: At dataset level, the relevance patterns of FBCNet with HLTI were more neurophysiologically sound

Following the single-subject analysis, to understand the effects of FBCNet with HLTI which were common across all the subjects, a dataset level relevance analysis was performed and the results of this analysis are presented in Figure 4.7. First, the modifications in the temporal relevance patterns were investigated and when averaged across all subjects, no significant change in the temporal relevance patterns was observed by the use of FBCNet with HLTI over vanilla FBCNet. Next, the changes in spectro-spatial relevance patterns were investigated. In this analysis,

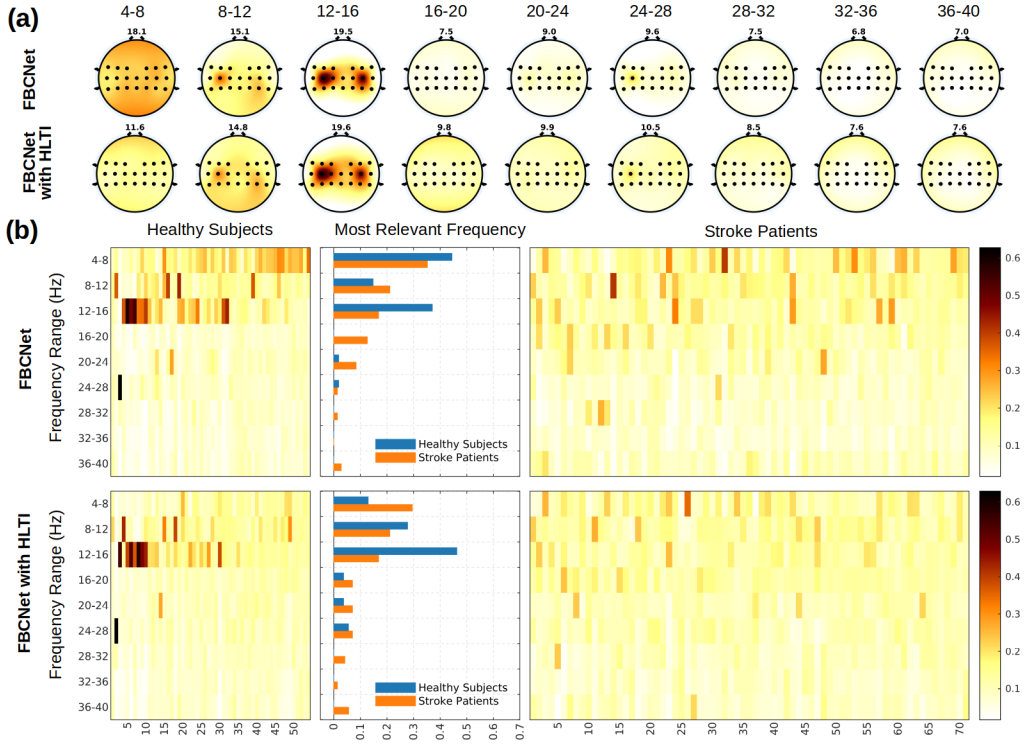

FIGURE 4.7: Group level relevance analysis for healthy subjects and stroke patients with vanilla FBCNet and FBCNet with HLTI. Part (a) presents the subject-averaged channel-frequency input relevance patterns for healthy subjects when analyzed with vanilla FBCNet and FBCNet with HLTI. The number in the title is the percentage relevance for the given frequency band. Here, it can be observed that the use of FBCNet with HLTI resulted in significantly reduced relevance in the 4-8 Hz frequency band and the relevance of the higher frequency bands was increased. Investigating more on the subject-averaged relevance, Part (b) presents the heatmap of frequency band relevance for each subject. Also, the histogram in the centre presents a normalized count of subjects for whom the given frequency band has the highest relevance. Here, by comparing the two histograms, it can be observed that, with FBCNet with HLTI, the 12-16 Hz was the highest relevant band for the most number of the healthy subjects, whereas, with FBCNet, the 4-8Hz band was the most relevant one. In the adjacent heatmap, a similar pattern of relevance shift to the higher frequency bands can be observed for stroke patients as well.

for healthy subjects, as presented in Figure 4.7 (a), a very high difference in the 4-8 Hz frequency band relevance was observed. Here, the use of FBCNet with HLTI resulted in a significant reduction in the 4-8 Hz relevance and the relevance in the higher frequency bands was marginally increased. Furthermore, as presented in the Figure 4.7 (b), this shift in the spectral relevance patterns was common to many healthy subjects and stroke patients. Due to this, as presented by the histogram in Figure 4.7 (b), the distribution of the most relevant frequency bands also changed

significantly with the use of FBCNet with HLTI.

4.4 Discussion

Extending the previously presented FBCNet architecture, this chapter proposed FBCNet with HLTI and FBCNet+LSTM architectures to incorporate the high level temporal information in the FBCNet architecture. In this work, it was hypothesized that the temporal representation capacity of the FBCNet can be further expanded and it may lead to improved classification performance, particularly in subjects who lack significant spectro-spatial discriminative information and achieve poor classification accuracies with FBCNet. To expand the temporal representation capacity, two approaches were investigated. The first approach was to use a windowed Variance layer and this resulted in a formulation of FBCNet with HLTI architecture. The second approach extended the FBCNet with HLTI architecture to include an LSTM block for extraction of temporal dependence between the features from the different windows and produced the FBCNet+LSTM architecture. To validate the above hypothesis, the classification performance of the vanilla FBCNet, and the proposed FBCNet with HLTI, and the FBCNet+LSTM architectures was evaluated using four EEG-MI datasets. The classification results indicated that the extraction of high level temporal information, in moderate quantity, as done in FBCNet with HLTI, can lead to improved classification performance, particularly in subjects with low classification accuracies, while avoiding the performance degradation due to model overfitting in highly accurate subjects. Along with the difference in the classification accuracies, this hypothesis was further tested with the use of interpretability analysis. Overall, results indicate that moderate incorporation of temporal information in the classification decisions can lead to improved EEG-MI classification accuracies.

4.4.1 Classification Performance of FBCNet with HLTI and FBCNet+LSTM

The FBCNet with HLTI, and the FBCNet+LSTM were designed to incorporate a higher amount of temporal information in the FBCNet architecture. Here, it was contemplated that, although the time dimension of the EEG generally includes

a higher amount of noise and results in model overfitting, the incorporation of a moderate amount of temporal feature extraction in the architecture design might improve the classification performance while avoiding the model overfitting to the noise. This hypothesis was strongly supported by the observed classification results (Table 4.1). First, the FBCNet with HLTI architecture, when compared to the FBCNet, resulted in best classification accuracies across all datasets and all analysis. At the minimum, these results confirmed that the incorporation of additional temporal information was not detrimental to the model training and it was not leading to the model overfitting. Moreover, in one dataset, this incorporation of temporal information achieved 3% average classification improvement over the FBCNet architecture and this difference was also statistically significant. In the remaining datasets as well, the FBCNet with HLTI achieved marginally improved classification accuracies over the vanilla FBCNet. This indicated that, depending on the additional information that can be extracted from the temporal domain, the incorporation of temporally localized feature extraction can lead to marginal to significant gains in classification accuracy.

The above hypothesis was further supported by the analysis of individual subject classification accuracies (Figure 4.3). This analysis revealed that FBCNet with and without HLTI resulted in very similar classification accuracies for the most high accuracy subjects. The significant difference in the classification accuracies was only observed in the subjects with poor FBCNet classification accuracies. For some of these subjects, who may have additional discriminative information present in the time-domain, the use of FBCNet with HLTI significantly improved the classification accuracies. For these subjects, the additional temporal information extracted by FBCNet with HLTI may have resulted in the improved classification accuracies.

The importance of the appropriate amount of temporal feature extraction was further explored in the FBCNet with HLTI's ablation analysis. At its default settings, motivated from the neurophysiological knowledge, the FBCNet with HLTI used the temporal window size (w) of 0.5s. Along with this setting of $w = 0.5$, the effect of less and more amount of temporal representation using $w = 4$s, 2s, 1s, and 0.1s was explored. Here, as hypothesized, the classification accuracies improved with more temporal feature extraction from $w = 4$s to 0.5s, they peaked at $w = 0.5$s, and then declined for $w = 0.1$s, for most datasets. Korea Uni. Data was the only exception to this pattern and it achieved the best classification accuracy of

the temporal window size of 0.1s, indicating a slightly higher information content in the temporal domain.

Lastly, despite having a dedicated LSTM block for extraction of temporal feature dependence, the performance of FBCNet+LSTM was observed to be better than the vanilla FBCNet, but worse than that of FBCNet with HLTI (Table 4.1). Also, along with the subject averaged classification accuracies, the same pattern was observed in the individual subject classification accuracies as well (Figure 4.3). One possible explanation for these poor results with FBCNet+LSTM can be that the additional model complexity may have resulted in the overfitting of FBCNet+LSTM models in the presence of limited training data and availability of more data may lead to better performance with the FBCNet+LSTM. This hypothesis was also partially supported by the observed results. The FBCNet+LSTM outperformed the FBCNet with HLTI architecture only for the Korea Uni. Data and incidentally that dataset contained the maximum number of training trials per class among all the datasets under consideration (Table 3.2). So, there is a possibility that with the availability of more data, the extraction of temporal feature dependence using the LSTM block, as done in FBCNet+LSTM, may outperform the vanilla approach of feature concatenation.

4.4.2 Interpretability Analysis

Following the classification results, the interpretability analysis of the trained FBCNet with HLTI model was performed to understand the effect of incorporation of the additional temporal information. In this analysis, for subjects who showed considerable improvements in the classification accuracies using FBCNet with HLTI, significant modifications in temporal relevance patterns were observed (Figure 4.6). Here, compared to the vanilla FBCNet, the FBCNet with HLTI was observed to exhibit temporal localization capabilities and for a representative subject, a much higher temporal relevance in the 0.5 - 1s time window was observed. This high relevance in 0.5 - 1s time window is also neurophysiologically significant wherein the most information about the MI is known to be present the 0.5 - 2.5s post-cue time window [243]. Although this drastic change in the temporal relevance patters was observed in some subjects, it was not common across all subjects. The most common effect of FBCNet with HLTI architecture was observed in the spectral

domain (Figure 4.7). Here, as opposed to most subjects having high relevance in the 4-8 Hz frequency band using FBCNet, in FBCNet with HLTI architecture, the most number of subjects exhibited highest relevance in the 8 - 16 Hz frequency bands. This high relevance in the 8 - 16 bands also overlaps with the characteristic mu and beta frequency bands which have been neurophysiologically documented to encode the MI associated ERD and ERS patterns [243]. Therefore, from these results, it can be said that the incorporation of additional temporal information in FBCNet with HLTI resulted in the extraction of more neurophysiologically sound features which ultimately improved the classification accuracies.

4.5 Summary

This chapter proposed two extensions of previously presented FBCNet architecture for the incorporation of additional EEG time domain information. For this purpose, first, an architecture of FBCNet with High Level Temporal Information (FBCNet with HLTI) was presented. The FBCNet with HLTI architecture extended the temporal feature extraction capabilities of FBCNet with the use of a windowed Variance layer. Furthermore, to encapsulate the temporal dependence between the features from different time windows, the FBCNet with HLTI was expanded with an LSTM block to construct FBCNet+LSTM architecture. The classification performance of both of these architectures was evaluated using four diverse MI datasets. By achieving the best classification accuracies in most datasets, the FBCNet with HLTI architecture was observed to be able to successfully extract an additional temporal information while avoiding model overfitting. The FBCNet+LSTM resulted in best classification accuracies in one dataset and the results indicated that the FBCNet+LSTM may achieve better classification accuracies with a higher amount of training data. Overall the results presented in this work indicate that constrained extraction of EEG time domain information, as done in FBCNet with HLTI, may lead to improved classification accuracies in the EEG-BCI domain.

Chapter 5

Deep Learning based MI Decoding for Post-Stroke Motor Rehabilitation

5.1 Introduction

The previous chapter presented two extensions of the FBCNet architecture for effective extraction of high level temporal information for MI classification from the EEG data. The classification results of these architectures indicated that extraction of high level temporal information can result in improved BCI classification accuracy. Although the work presented in the previous two chapters had explored the performance of the proposed algorithms on stroke patients' data, the analysis was limited to a single session EEG data. The practical use of BCI systems for post stroke motor rehabilitation is generally far different from the single session classification scenario. Most commonly employed BCI based motor rehabilitative clinical trials include a calibration session and multiple rehabilitation sessions. These trials

The work presented in this chapter will be submitted as:

1. Ravikiran Mane, et al., Deep Learning based Motor Imagery Decoding for Post-Stroke Motor Rehabilitation. *(In preparation)*

generally collect a labelled multi-class MI data in the calibration session for each stroke patient. This calibration session data is then used to train a subject-specific MI feature extraction and classification model which is later employed during the rehabilitation sessions for online detection of the MI and to provide appropriate feedback to the user. In this manner, in stroke rehabilitation trials, a model trained on the calibration session data is used to classify data from multiple rehabilitation sessions which are spread across multiple weeks. Such inter-session classification presents unique challenges to the MI decoding algorithms.

High inter-session variability in the EEG activation patterns associated with any particular mental process is a well-known challenge in the EEG-BCI field. Although the reasons for this variability are not well documented, various time-varying affect and cognitive factors, such as fatigue, memory load, attention, reaction time have been postulated to modulate instantaneous brain activity leading to inconsistent EEG activation patterns across sessions [262]. Furthermore, along with the above mentioned intrinsic sources of variability, the variation in external conditions like, differences in electrode impedance, position of EEG electrodes, and ambient noise levels, also affect the quality of EEG recordings across different sessions. Owing to these phenomenon, the classification models trained on a specific session data, commonly suffer performance drop when tested on the data from different recording sessions. Therefore, the application of BCI rehabilitation systems in such multi-session classification settings necessitates the classification algorithm to learn highly generalizable patterns of MI for achieving high and consistent classification accuracies across multiple sessions. Consequently, most of the BCI-based post stroke motor rehabilitation trials in the literature have used traditional machine learning methods for MI detection [88, 119, 144]. The traditional machine learning methods are known to have high bias and low variance compared to their deep learning counterparts, which may lead to a model with better generalization capabilities and higher classification accuracies in the multi-session settings [18]. However, as seen in the previous chapters, recent advances in the deep learning technology have lead to significant improvements in the BCI classification accuracies, particularly in healthy subjects. These observations necessitate an investigation in the classification performance of traditional machine learning and deep learning methods for multi-session MI decoding in post-stroke motor rehabilitation trials and to best of our knowledge, no such work has been presented in the literature.

Along with the inter-session variability, high inter-subject heterogeneity in the BCI classification accuracies is another factor that needs to be considered while designing a BCI-based motor rehabilitative intervention. It is known that around 15-30% users cannot produce a task-specific signature of MI that is robust enough to control a BCI system [15, 251, 262]. The underlying reasons behind this BCI illiteracy are not well-understood; however, diverse psychological and neurophysiological factors, like resting-state SMR amplitude [263, 264], psychometric parameters [265], mood and motivation [266], long-range EEG temporal correlations [267], and grey matter volume of the supplementary motor area, supplementary somatosensory area, and dorsal premotor cortex [268], have been reported to be associated with, and predictive of, the subject-specific BCI classification performance [262]. Considering this difficulty, before the admission in the BCI rehabilitative intervention, it becomes necessary to identify if a particular stroke patient will be able to control the BCI system with sufficient accuracy. To solve this issue, some rehabilitation studies have included a separate BCI screening session [88, 119, 144]. In this session, the patients are subjected to the data collection protocol of the calibration session and this session's cross validation classification accuracy is used as an indicator of the BCI illiteracy. Although this method has been observed to be effective, it still lacks the information about the multi-session classification performance in the rehabilitation settings [88, 119, 144]. Therefore, investigation about the better predictors of multi-session classification accuracies in the post-stroke rehabilitation settings is necessary.

Lastly, there are two typical types of BCI systems that are observed in the stroke rehabilitation context. The first type of systems are based on the principles of neurofeedback and these systems use the amplitude of SMR based features from the motor areas to provide visual feedback or directly control an external orthosis [47, 180, 181, 186, 187]. These neurofeedback training based systems aim to target the stroke induced abnormal brain activations with the philosophy that restoration of brain activations to 'more normal' state will result in functional recovery [8]. However, precise identification of the 'abnormal brain states', particularly, in a chronic state, is still a very challenging task. Therefore, the second type of systems, which are based on the principles of Hebbian learning, circumvent this challenge altogether and aim to achieve improved motor functions by repetitive and concomitant activation of motor and sensory-motor circuits. In these systems, the MI is identified from the whole brain activations using machine learning techniques

and successfully detection of MI is rewarded with positive feedback [88, 119, 144]. Such systems have been observed to improve clinical motor functions [88, 119, 144]. Still, in these systems, understating of the features learned by machine learning techniques for MI detection and rehabilitation is a crucial factor, which is more often than not, overlooked.

Considering the above-mentioned knowledge gaps, this work presents an extensive retrospective analysis of the EEG data from 25 stroke patients undergoing three different BCI-mediated upper extremity motor rehabilitation interventions from the MI classification perspective. First, experiments are conducted to analyze the classification performance of the traditional machine learning algorithms, baseline deep learning architectures, and the previously proposed architecture of FBCNet (Chapter 4), in decoding multi-session EEG data. This is followed by an interpretability analysis of the classification models trained using the calibration data to understand the spectro-spatial discriminative features learned by the FBCNet. Next, the interpretability analysis is extended to identify the predictors of rehabilitation session accuracies from the calibration session data. Lastly, with interpretability and selective channel analysis, three categories of stroke patients are presented and the relationship between these categories and observed clinical improvements is discussed. The results of this study indicate that the previously proposed architecture of FBCNet can achieve the best classification accuracies in the decoding of multi-session EEG data from stroke patients. Also, from the interpretability analysis, it was observed that, if the MI associated information in the calibration session is localized in the motor areas of the brain, then it leads to higher classification accuracies during rehabilitation sessions and better clinical improvements.

5.2 Methods

5.2.1 Datasets

In this work, the EEG data collected during two BCI-based post-stroke upper extremity motor rehabilitation trials is retrospectively analyzed. The first clinical trial, which has been referred as Stroke Data: A in the previous chapters, was conducted to investigate the combined effect of BCI-mediated rehabilitation and

transcranial Direct Current Stimulation (tDCS) in chronic stroke patients [119]. The second clinical trial, which has been referred as Stroke Data: B in the previous chapters, was conducted to investigate the efficacy of BCI-mediated upper extremity motor rehabilitation in comparison to the physiotherapy and robotic rehabilitation [88]. Since along with the classification performance, this chapter also explores a relationship between EEG features and post-intervention clinical gains, this section provides detailed information about these two clinical trials.

5.2.1.1 Ethics Statement

The experimental procedures involving human subjects described in this study were approved by the Domain Specific Review Board of the National Healthcare Group, Singapore and were in accordance with the Code of Ethics of the World Medical Association. Both the Stroke Data: A, and the Stroke Data: B clinical trials, were registered in the ClinicalTrials.gov with Clinical Trial Registration Unique Identifier NCT01287975 and NCT01897025 respectively.

5.2.1.2 Patients

The Stroke Data: A clinical trial was designed as a two-armed randomized controlled trial. In this trial, the patients aged between 21 and 70 years who had their first-ever stroke at least 9 months prior to study enrollment and were experiencing moderate to severe unilateral impairment of UE motor functions, were deemed to be eligible to participate. The pre-intervention degree of impairments was assessed with UE motor part of FMA [104] and patients with FMA between 11 to 45 were considered for the study. Patients with moderate to severe motor impairments were targeted in this study since they have fewer other therapeutic options owing to their greater difficulty in movement execution. In this trial, the subject exclusion criteria were presence of epilepsy, cognitive impairment, neglect, other psychiatric or neurological diseases, spasticity score > 2 on the Modified Ashworth Scale in the elbow or shoulder, severe arm pain, grip strength < 10 kg as measured by a dynamometer, contraindications to tDCS or TMS like pacemakers, cranial implants, intrathecal pumps, ventricular shunts, or participation in other trials targeting stroke motor recovery. With this study design, 42 patients who showed interest in the study were assessed with the above inclusion criteria and

out of them, 5 were excluded. As the intervention involved control of robotic actuator using MI-BCI and because not all the stroke patients can elicit MI associated brain patterns, the remaining 37 patients were screened for their ability to control the MI-BCI. The data collected from these 37 patients during the screening session was the same data that was used in the previous chapters to explore the classification performance of various MI decoding algorithms in stroke patients. Following the screening session, 11 subjects were excluded because of not meeting the MI-BCI performance criteria (2-class classification accuracy $> 57.5\%$) and another 7 subjects declined to participate in the study. The remaining 19 eligible patients participated in the intervention and were randomly assigned to either receive only a BCI-based rehabilitation (refereed as Group-I intervention hereafter, n = 9) or BCI-based rehabilitation coupled with the transcranial Direct Current Stimulation (refereed as Group-II intervention hereafter, n = 10).

The Stroke Data: B clinical trial was designed as a three-armed randomized controlled trial. In this trial, the patients aged between 21 and 80 years who had their first-ever stroke at least 4 months prior to study enrollment and were experiencing moderate to severe unilateral impairment of UE motor functions (pre-intervention FMA between 10 to 50 points), were deemed to be eligible to participate. Subjects were excluded if they had medical instability such as unresolved sepsis, postural hypotension, end-stage renal failure terminal illness, severe aphasia, inattention, hemispatial neglect, severe visual impairment, epilepsy, severe depression, psychiatric disorder, recurrent stroke, skull defects compromising EEG cap fit, severe spasticity (MAS >2 in any shoulder, elbow or wrist/finger muscles), severe pain assessed by visual analogue scale (VAS) >4/10, fixed joint contractures, skin conditions such as infections or eczema which could be worsened by robotic exoskeletal or EEG cap contacts. With this study design, 1007 patients were assessed with the above inclusion criteria and out of them, 34 met the criteria. These 34 patients were further screened for their ability to control the MI-BCI and 5 of them were excluded for not meeting the MI-BCI performance criteria (2-class classification accuracy $> 57.5\%$). 7 more patients declined to participate in the study and the remaining 22 patients were randomly assigned to BCI-based rehabilitation (refereed as Group-III intervention hereafter, n = 6), robotic rehabilitation (n = 8), and rehabilitation with physiotherapy + occupational therapy (n = 7). In this clinical trial, the EEG data was only collected from the patients enrolled in the BCI-based

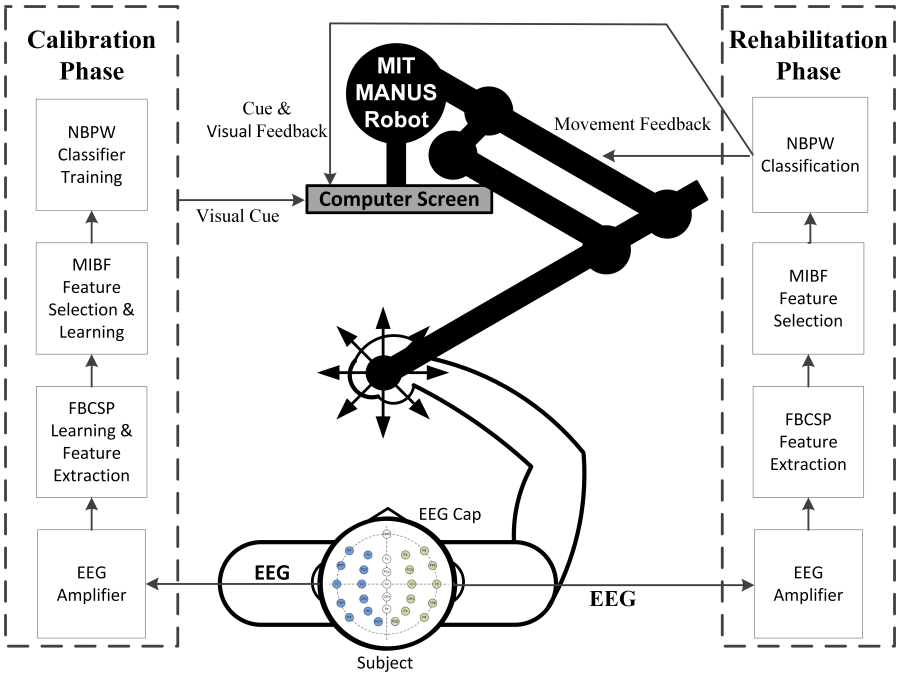

FIGURE 5.1: Architecture of brain computer interface (BCI) system for upper extremity rehabilitation. Abbreviations: FBCSP, filter bank common spatial pattern; MIBF, mutual information-based best feature; NBPW: Naive Bayesian Parzen Window.

rehabilitation and therefore only these patients from this clinical trial are analyzed in this work.

5.2.1.3 BCI Rehabilitation Protocols

In both, the Stroke Data: A and Stroke Data: B clinical trials, all the 25 stroke patients were randomly assigned to one of the BCI-based rehabilitative interventions (Group-I to Group-III). In both the clinical trials, the common BCI intervention involved BCI triggered robotic movement of the patients' stroke-affected hand upon the detection of MI. In a trial based setting, patients performed MI of the affected hand movement; which was identified online from the EEG data using FBCSP algorithm and successful detection of MI was rewarded by immediate passive movement of the affected hand. In Stroke Data: A trial, patients were asked to perform MI of center out reaching movement using the affected hand and the robotic feedback, which involved the actual center-out movement of the affected hand, was provided using an MIT-MANUS robot. Different from Stroke Data: A trial, the patients in the Stroke Data: B trial were asked to perform MI of the open-close action using

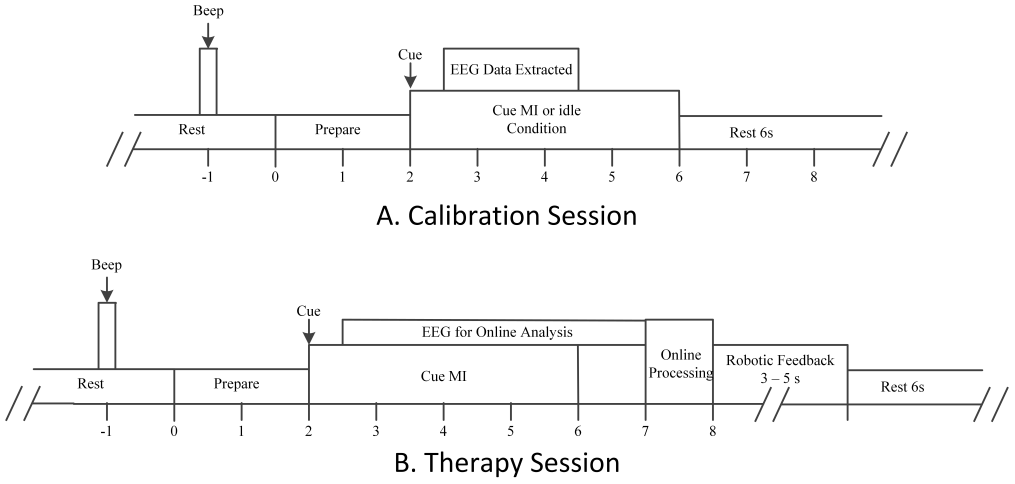

FIGURE 5.2: Timeline of BCI intervention for upper extremity rehabilitation. (A) Single-trial timeline of motor imagery (MI) of stroke-affected hand or rest state for the calibration session before the commencement of therapy. (B) Single-trial timeline of MI of stroke-affected hand and robotic feedback in therapy session.

the affected hand and the robotic feedback, which involved actual open-close action of the affected hand, was provided using Haptic Knob (HK) robot. In both the trials, as the BCI intervention involved detection of MI from the rest condition, patients in both the groups first participated in one calibration session. In the calibration session, EEG data from 160 trials (80 trials of MI of the affected hand, 80 trials of rest state) was collected to generate a subject-specific FBCSP model for the classification between MI and rest state. The calibration session did not include any robotic feedback but the patients' hands were strapped to the robotic device to maintain maximum similarity between the calibration and therapy sessions. This trial protocol in the calibration session, which was same in both the clinical trials, is presented in Figure 5.2 (a). In this work, the above-mentioned data collected during the calibration session is referred as calibration data.

Following the calibration session, patients in all the groups participated in multiple BCI-based rehabilitation sessions. Each rehabilitation session involved one evaluation run and four therapy runs. The evaluation run was composed of 40 trials that randomly consisted of 20 trials of eyes open rest state and 20 trials of MI of stroke-affected hand. Very similar to the calibration session, every run started with preparation cue which was followed by the MI or rest clue. Based on the instructions in the cue, patients either performed MI of the affected hand or remained in a rest state for the next 4 seconds. The EEG data collected during

FIGURE 5.3: BCI rehabilitation systems used in Stroke Data: A (part (a)) and Stroke Data: B clinical trials (part (b)).

0.5 to 4.5 seconds from the instruction cue was processed online, and unlike the calibration session, robotic feedback was provided upon the successful detection of MI. The robotic movement was followed by 6 seconds of inter-trial rest period. The purpose of the evaluation run in every rehabilitation session was to validate the correctness of the previously trained FBCSP model. The four therapy runs in each rehabilitation sessions consisted of the MI of the stroke-affected hand. In these therapy runs, to maximize the rehabilitation efficacy, all the trials were designed to be of MI class and there were no resting state trials in the therapy runs. The trial protocol during the therapy runs was the same as that of evaluation run with an exception of zero rest state cues. This protocol is presented in Figure 5.2 (b). In this work, since the classification performance is of interest and as the actual therapy run contained a single class data, only the 2-class EEG data (20 trials each of MI and rest) collected during the evaluation run of every rehabilitation session was analyzed and it is referred as the rehabilitation data.

Following the above-mentioned format of the rehabilitation session, the patients in intervention Group-I and Group-II received the robotic Feedback with the MIT-MANUS robot, whereas, the HK robot was used to provide feedback to Group-III patients. Also, along with the BCI therapy provided to the Group-I patients, the patients in Group-II received 20 minutes of 1 mA bi-hemispheric tDCS (the anode over the ipsilesional M1 and the cathode over the contralesional M1) before the start of every rehabilitation session. The location of the M1s were approximately determined as the positions of the C3 and C4 electrodes in the international 10-20

EEG montage. The bi-hemispheric tDCS was applied with an aim to decrease contralesional cortical excitability and to increase the ipsilesional cortical excitability. To ensure the randomized blinding in Stroke Data: A clinical trial, the Group-I patients also received a similar, but sham-tDCS where the current was applied only for the first 30s. In this manner, the Group-I and Group-II patients participated in 10 rehabilitation sessions over a period of 2 weeks, whereas the Group-III patients received the rehabilitation for 18 sessions spreaded over a period of 6 weeks. The representative rehabilitation protocol for Stroke Data: A clinical trial is presented in Figure 5.1. The Stroke Data: B clinical trial also followed the exact same rehabilitation protocol with a difference of robotic feedback being provided using an HK robot instead of the MIT-MANUS robot. The actual set-up used in these two rehabilitation trials is presented in Figure 5.3.

5.2.1.4 Clinical Evaluations

In both the Stroke Data: A and Stroke Data: B clinical trials, the clinical assessment of motor functions of the affected hand was performed using the motor part of the UE Fugl-Meyer Assessment (FMA) (range 0-66) before and after the intervention (FMA_{pre}, FMA_{post}). In Group-I and Group-II interventions, the post-intervention assessment was conducted 2 weeks after the end of the intervention, whereas, in group-III, it was conducted 6 weeks after the end of the intervention. The treatment gain, ΔFMA was calculated as the difference between pre-intervention and post-intervention FMA scores (FMA_{pre} - FMA_{post}).

5.2.1.5 EEG Data acquisition

During both the clinical trials, the brain activity was continuously captured using the Neuroscan Nuamps EEG amplifier with 27 unipolar channels positioned according to the international 10/20 system at a sampling frequency of 250Hz. All the channels were referenced to the ear electrode and the electrode impedances were kept well below 5kΩ. The EEG data was captured in the voltage range of $\pm 130mV$ and the acquisition hardware bandpass filtered the data from 0.05 to 40Hz.

5.2.2 Classification Algorithms, Experiments and Training Procedure

In this work, as done in Chapter 3, the classification performance of the FBCSP [142], which is one of the most successful traditional machine learning algorithms, was compared with the more recent deep learning architectures of Deep ConvNet [20] and EEGNet [22], and the previously proposed architecture of FBCNet with HLTI. As previously done, all three baseline methods of FBCSP, Deep ConvNet, and EEGNet were used in the best-recommended settings by the respective authors and their detailed configuration is described in Section A.3. For the FBCNet with HLTI architecture, considering the results presented in the previous chapter, and to maintain the minimum model complexity, the $m = 4$ and $w = 1$s flavor was used in this analysis. Hereafter, for naming simplicity, this architecture is referred to as FBCNet.

In this work, all three deep learning architectures were trained using the same training strategy. As detailed in the Section 3.3.4, the two-stage training was conducted using an Adam optimizer at default settings (learning rate = 0.001, betas = $0.9, 0.999$) [252]. The training procedure for FBCNet is detailed in Section A.3.

In this manner, with the above mentioned four classification algorithms, the following classification analyses were performed:

Hold Out Analysis: An inter-session classification of rehabilitation data

In the BCI-mediated rehabilitation trials, the classification models are trained using the data collected during the calibration session and these models are then used in the rehabilitation session for real-time MI decoding. This protocol was exactly matched in the Hold Out (HO) analysis and the HO classification accuracy averaged across all the rehabilitation sessions was the primary performance matrix in this work. In this HO analysis, the calibration session data for each subject was used for training the classification models, and the trained models were then tested on the evaluation run of all the rehabilitation sessions. Similar to the training procedure mentioned in Section 3.3.4, the training data was further divided as the training set (80%) and the validation set (20%) and the training was conducted in two stages. The results of this analysis provide information about the classification algorithms'

capabilities in extracting highly generalizable discriminative features which remain valid during multi-session classification.

Cross Validation Analysis: 10 fold CV classification of the calibration and rehabilitation data

Along with the HO analysis, to further gauge the class discriminative information present in any particular session's EEG data, a 10 fold Cross Validation (CV) analysis was conducted. In this analysis, the CV classification performance of all the algorithms was analyzed using the calibration as well as rehabilitation session data. The significance of CV analysis is that it isolates the effect of the intersession-variability present in the HO analysis and provides an indicative upper bound on the maximum class discriminative information that is present in any session's EEG data. Furthermore, the difference in the HO and CV analysis indicates the extent of difference in the data distribution between the calibration session and any particular rehabilitation session.

Selected Channel HO Analysis: An inter-session classification of rehabilitation data with selective channels from different brain regions

This analysis is an extension of the HO analysis, wherein, instead of using all channel EEG data, a HO analysis was conducted using the EEG data from only selected channels which are located in a particular brain region. This analysis was motivated by the results of the interpretability analysis (Figure 5.6) and was conducted to explore the extent of generalizable class discriminative information that is present in a particular area of the brain. For this analysis, based on the interpretability results, the 27 EEG channels were divided into three regions, the motor-temporal region (channels T7, C3, CZ, C4, T8, TP7, CP3, CPz, CP4, TP8), the frontal region (channels F7, F3, Fz, F4, F8, FT7, FC3, FCz, FC4, FT8) and the occipital-parietal region (channels P7, P3, Pz, P4, P8, PO1, PO2). This analysis was conducted only with FBCNet architecture.

5.2.3 Interpretability Analysis

The use of deep learning for rehabilitation purpose greatly necessitates the interpretability of the classification decisions. In stroke patients, since the aim is to restore the brain activation to a healthy state, it is important to evaluate the information learned by the neural network from the calibration session. Therefore, as done in the previous chapters (Section 3.3.6), the input feature relevance patterns were computed and visualized using a DeepLift algorithm [254, 255]. This analysis was focused on the FBCNet models which were trained using the calibration session data in the HO analysis. Moreover, for further exploration of the relationship between model relevance from different brain regions and the HO classification accuracy, the EEG channel relevance was grouped into the motor, the frontal, and the occipital regions (same division as done in the selected channel HO analysis). From these regions, based on the observed channel relevance patterns, the relevance score from the top 2 highly relevant channels from each region was summed to calculate the representative relevance from each of these regions. This selection of only top 2 channel relevance was motivated by the observation that in most of the subjects the most amount of relevance was concentrated at one or two EEG channels (see Figure 5.6), and the averaged relevance across all the channels did not correctly represent this highly concentrated relevance pattern.

5.2.4 Relationship between Interpretability, Classification Accuracy and Clinical Improvements

Following the relevance analysis, a possibility of relevance based predictors of the rehabilitation session classification accuracy was explored. In this analysis, the relevance patterns learned by the FBCNet model from the calibration session data were investigated, to check if they provide any information regarding the online classification accuracies in the rehabilitation sessions using the same model. For this purpose, based on the results of the visual inspection, a correlation analysis, using the Pearson's correlation formula, was conducted between the average rehabilitation session classification accuracy and the total relevance from the top 2 channels from the motor, frontal, and occipital regions of the brain.

Along with the relationship between the relevance and the classification accuracies, the relationship between the classification accuracies and the observed clinical improvements was also investigated. In this analysis, the aim was to gain insights into the process of clinical recovery. Therefore, to investigate if there is any relation between the regions of the brain that encode the MI associated information and the clinical recovery, the subjects were grouped based on the regions of the brain that achieved maximum classification accuracy in the selected channel HO analysis. Following this grouping, average FMA improvement for each group was tested using single factor Analysis of Variance (ANOVA) to check for any statistically significant differences.

5.2.5 Statistical Analysis

As done in the Chapter 3, the statistical significance of differences in the classification accuracy achieved by different algorithms, was assessed using a paired t-test. To avoid the false discoveries in a multiple comparison situation, the p-value was corrected with Bonferroni correction for multiple comparisons. Whether the clinical improvements follow a normal distribution was tested using Shapiro Wilk test. For normally distributed data, the between-group differences were tested with one-way ANOVA. Whenever the assumptions of normal distribution were violated, the between-group differences were tested with the Kruskal-Wallis Test and Friedman's Test.

5.3 Results

5.3.1 Clinical Improvements

Result I: All the three BCI rehabilitative interventions resulted in improved motor function, but the individual subject improvements were highly heterogeneous

The clinical improvements achieved by all the stroke patients following the BCI-based rehabilitation are presented in Table 5.1. At the end of the Stroke Data: A clinical trial, following 2 weeks of rehabilitation, the subjects from Group-I achieved

TABLE 5.1: Clinical improvements following three different BCI motor rehabilitative interventions

Group-I		Group-II		Group-III	
Subject	ΔFMA	Subject	ΔFMA	Subject	ΔFMA
I-1	12	II-1	0	III-1	7
I-2	3	II-2	13	III-2	3
I-3	16	II-3	4	III-3	10
I-4	3	II-4	5	III-4	10
I-5	−1	II-5	7	III-5	11
I-6	9	II-6	0	III-6	8
I-7	0	II-7	7		
I-8	4	II-8	4		
I-9	3	II-9	10		
		II-10	0		
Average	5.44±5.68		5.00±4.27		8.17±2.92

ΔFMA is the improvement in the patients' Fugl-Meyer Assessment score at the end of the BCI intervention.

an average clinical improvement of 5.44 FMA points ($p = 0.02$) and the average improvement in Group-II subjects was 5.00 FMA points ($p = 0.006$). Following 6 weeks of rehabilitation, the patients in Group-III achieved an average improvement of 8.17 FMA points ($p = 0.001$). The average improvement in all 25 patients from the three groups was 5.92 FMA points ($p < 0.001$). In this manner, the combined as well as the individual group FMA improvements were statistically significant Also, with a standard deviation of 4.63 FMA points, the individual subject clinical improvements were observed to be highly heterogeneous. Furthermore, there was no significant effect of intervention group on the observed clinical gains (single-factor ANOVA, $F = 0.944$, $p = 0.404$).

5.3.2 Classification Results

Result II: FBCNet achieved significantly better classification accuracies compared to baseline methods in all analyses

The classification accuracies achieved by all the four classification algorithms in the HO and CV analyses are presented in Table 5.2, and 5.3. In both the HO and the CV analysis, the proposed method of FBCNet achieved the best classification accuracies across all the groups. In the HO analysis, the classification accuracy of FBCNet was higher than the best performing baseline methods by 4%, 5%, and

TABLE 5.2: Average rehabilitation session classification accuracies in an HO settings

Methods	Group-I	Group-II	Group-III
FBCSP	53.46**	59.17**	66.41*
Deep ConvNet	56.81*	62.34**	52.61**
EEGNet	57.69*	60.99**	56.95**
FBCNet	**62.03**	**69.39**	**69.86**

The best performing method for each analysis is highlighted in boldface. The *, and ** represent that the classification performance of FBCNet is significantly better than the given baseline method with *: $p_{corrected} < 0.05$, and **:$p_{corrected} < 0.0001$.
The classification accuracies presented for Group-I and Group-II are average of 10 rehabilitation sessions, whereas, Group-III classification accuracies are average of 18 rehabilitation sessions.

TABLE 5.3: Average 10-fold cross validation classification accuracies

Methods	Group-I		Group-II		Group-III	
	Calib.	Rehab.	Calib.	Rehab.	Calib.	Rehab.
FBCSP	72.83	67.12**	82.50	77.98**	81.21	72.17**
Deep ConvNet	71.59	65.93**	79.47	70.09**	70.59	62.91**
EEGNet	69.54	66.69**	79.62	72.99**	71.13	65.75**
FBCNet	**77.48**	**73.91**	**87.43**	**85.12**	**86.70**	**76.75**

The best performing method for each analysis is highlighted in boldface. The *, and ** represent that the classification performance of FBCNet is significantly better than the given baseline method with *: $p_{corrected} < 0.05$, and **:$p_{corrected} < 0.0001$.
Despite very high differences in the values, the calibration session accuracy differences did not reach statistical significance due to very low sample size.
The classification accuracies presented for Group-I and Group-II are average of 10 rehabilitation sessions, whereas, Group-III classification accuracies are average of 18 rehabilitation sessions.

3% in Group-I to Group-III respectively and this difference in classification accuracies was statistically significant (all $p_{corrected} < 0.05$). Also, in HO analysis all the three baseline methods performed very similarly and the difference in classification accuracies achieved by them was not statistically significant. In the 10-fold CV analysis, the FBCNet achieved 7%, 7%, and 4% higher average classification accuracies than the best performing baseline methods in the three groups and these differences were highly statistically significant (all $p_{corrected} < 0.001$). Similar, but statistically insignificant improvements with FBCNet were observed in the calibration session CV analysis as well. Also, different from the HO analysis results, in CV analysis, following FBCNet, the FBCSP algorithm was observed to the second best performing classification method in all the CV analyses.

Along with the average classification accuracies, the classification performance of

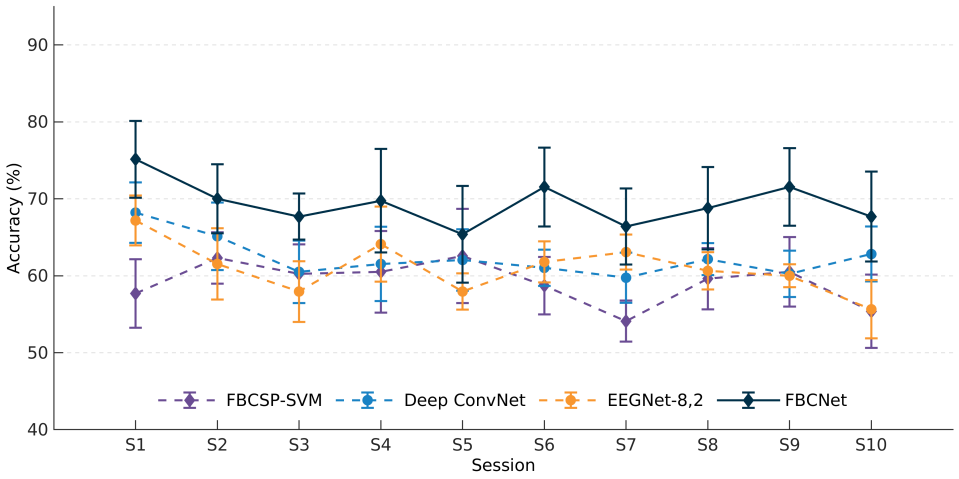

FIGURE 5.4: Classification accuracy during each rehabilitation session for Group-II intervention in hold out settings. It can be observed that all the baseline classification methods performed very similarly across all the sessions and the session-wise classification accuracies with FBCNet were observed to be consistently higher than all these baseline methods. Also, this difference in classification accuracies was highly statistically significant. The error bars represent a standard mean error.

these algorithms for individual rehabilitation session was also explored and these classification results for Group-II patients' HO and CV analysis are presented in Figure 5.4 and 5.5. From these figures, it can be observed that the classification accuracy of FBCNet was consistently superior to all the baseline methods in all the rehabilitation sessions. The same case was observed in other groups' data as well and more detailed classification results for Group-I and Group-III are presented in Section C.1.

Result III: The rehabilitation session HO accuracies were significantly less than the CV accuracies

Following the separate analysis of CV and HO accuracies, the CV and HO accuracies for each rehabilitation were compared. In this analysis, with at least 6% difference, it was observed that, for all the patient groups the HO classification accuracies were significantly less than that of the CV accuracies (FBCNet, all $p < 0.001$).

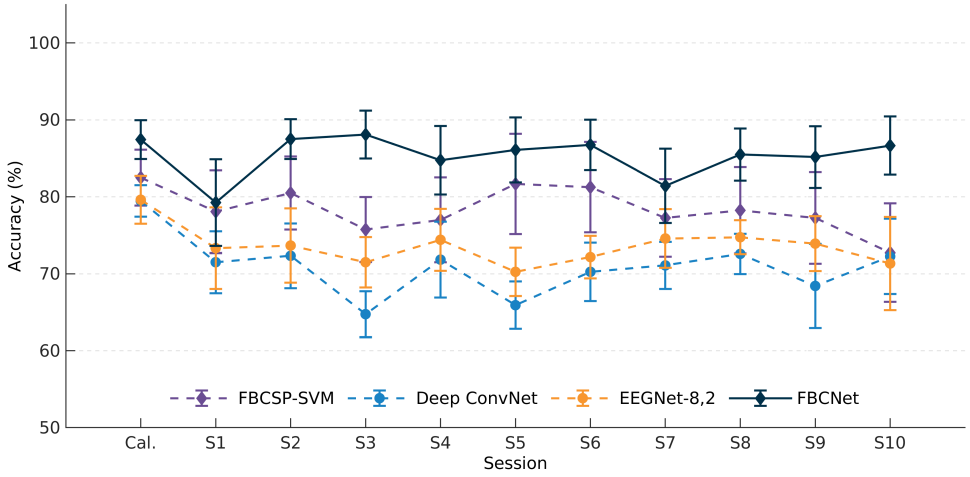

FIGURE 5.5: Classification accuracy during each rehabilitation session for Group-II intervention in 10-fold cross-validation settings. It can be observed that the baseline deep learning architectures (Deep ConvNet, EEGNet-8,2) performed far worse than FBCSP-SVM, the classical approach, during all the rehabilitation sessions. In contrast, the session-wise classification accuracies with FBCNet were observed to be consistently higher than all the baseline methods and this difference in classification accuracies was highly statistically significant. The error bars represent a standard mean error.

5.3.3 Interpretability Results

Result IV: Subject specific features learned by FBCNet from the calibration session data were neurophysiologically sound

Following the classification analysis, the relevance patterns of the FBCNet models trained using the calibration session data for the HO analysis were investigated to understand the learned class discriminative information that will be used for MI detection and rehabilitation. The results of this analysis, which are the spectro-spatial input relevance patterns, for three representative subjects from the Group-III intervention are presented in Figure 5.6. This analysis of the subject-specific relevance patterns indicated that for some patients, like subject III-6 presented in the top row of the Figure 5.6, the spectro-spatial relevance patterns were highly concentrated in the motor region of the brain in the 8 - 16 Hz frequency band. Also, as a result of this neurophysiologically sound feature learning, the HO classification accuracies for these subjects were observed to be quite high. Contrarily, in few other patients, as presented in the last row of the Figure 5.6, high relevance in the frontal region, in the low-frequency band, was observed and the HO classification

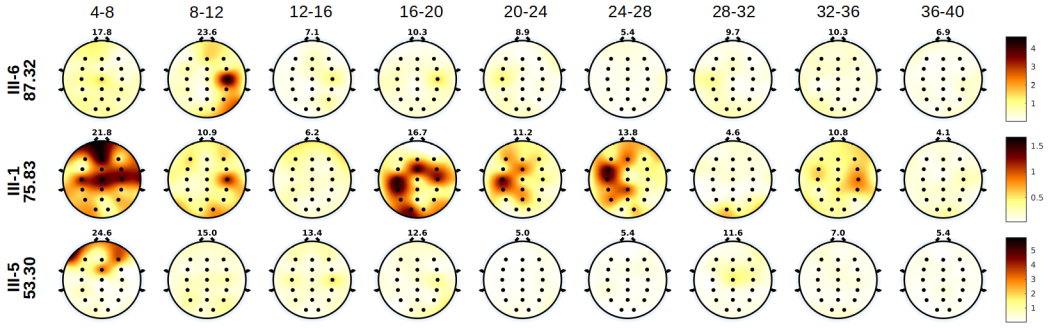

FIGURE 5.6: Representative subject level visualizations of relevance patterns learned by the FBCNet model using the calibration session data in HO analysis for three subjects from the Group-III intervention. From the figure, it can be identified that, for subject III-6 (the first row), a maximum of 23.6% input relevance was concentrated in the 8-12 Hz frequency band, and in this band, the most amount of relevance was assigned to the C4 electrode in the motor region. This relevance pattern, which highly coincides with the neurophysiological signature of MI, resulted in this subject achieving 87.32% average classification accuracy across all the rehabilitation sessions in the HO analysis. Contrarily, for subject III-5 (the last row), the most relevance was attributed to the 4-8 Hz band in the frontal region of the brain. This relevance pattern, which is not a known MI signature, resulted in subject III-5 achieving chance level classification accuracy in the rehabilitation sessions. For subject III-1 (the middle row), the relevance pattern was observed to be concentrated in the motor and the frontal areas of the brain. Consequently, this subject achieved an average classification accuracy of 75.83%.

accuracies for these patients were quite low. Also, in the remaining patients, the spectro-spatial relevance patterns were observed to be concentrated in the motor and frontal region in varying degrees (Figure 5.6, middle row).

5.3.4 Relationship between Interpretability and Classification Results

Result V: Subjects with significantly higher calibration session relevance in the motor region achieved much higher rehabilitation session accuracies.

The results of the subject-specific spectro-spatial relevance patterns analysis prompted further exploration of the relationship between the calibration session relevance patterns and the rehabilitation session HO classification accuracy. From the subject-specific relevance patterns, it was observed that for subjects in whom the FBCNet

models learned to extract the class discriminative MI information from the motor region achieved very high HO classification accuracies and the FBCNet models focused in the frontal region achieved quite low accuracies. Therefore, a correlation analysis was conducted between the relevance from different brain regions and the rehabilitation session HO accuracy. In this analysis, as presented in Table 5.4, a significant positive correlation was observed between the motor region relevance and the HO accuracies. Also, HO accuracies were observed to be negatively correlated with the relevance from the frontal region of the brain. Furthermore, a high relevance in the non-motor region was observed to be associated with the poor HO accuracies and the motor - non-motor region relevance exhibited the strongest correlation with the HO accuracies. Lastly, there was no association between the occipital region relevance and the HO accuracies.

Result VI: Among the models trained with selected channels, the model trained using the data from motor region channels achieved the best classification accuracies in the HO analysis

The previous correlation analysis between HO accuracies and brain region relevance indicated that model providing higher relevance to the motor regions was more generalizable on the rehabilitation sessions' data. Although this analysis provided information about the relationship between HO accuracies and trained models relevance patterns, because the extracted relevance patterns are still dependent on the specific model's capabilities of learning relevant patterns, it did not provide any indication about the true class discriminative information present in the particular brain regions. Therefore, to analyze the true discriminative information present in the particular brain regions, a selected channel HO analysis was conducted. In this analysis, considering the previously identified significant role of the motor and the frontal region, the HO classification accuracies were calculated only using the EEG data from the motor and frontal region channels and the results of this analysis are presented in Table 5.5. From the table it can be observed that the best average classification accuracies were achieved by the data from the motor region and the difference between the motor and the frontal region classification accuracies was statistically significant in Group-II intervention ($p < 0.001$), marginally significant in Group-III intervention ($p = 0.06$) and insignificant in Group-I intervention ($p > 0.05$). Furthermore, in Group-II, the HO accuracies with data from only the motor region were even higher than the all channel classification accuracies.

TABLE 5.4: Relationship between rehabilitation session HO accuracy and calibration session relevance.

Subject	HO Acc.	Calibration Session Relevance					
		Motor	Non-Motor	Frontal	Non-Frontal	Occipital	(Motor)-(Non-Motor)
I-1	58.21	10.96	11.26	11.26	10.96	8.27	−0.31
I-2	62.31	9.59	10.80	9.89	10.11	9.89	−1.21
I-3	72.56	11.36	11.00	9.09	11.68	11.00	0.36
I-4	51.84	9.92	10.02	9.43	10.13	9.90	−0.10
I-5	52.05	14.50	14.96	14.96	14.58	10.61	−0.46
I-6	58.72	10.23	11.49	11.49	10.23	6.93	−1.26
I-7	74.36	11.51	10.49	10.25	11.62	8.52	1.03
I-8	74.62	13.03	12.04	11.11	13.71	10.10	0.99
I-9	53.59	9.02	10.73	10.22	10.32	10.32	−1.71
II-1	81.61	11.46	12.61	11.48	11.90	10.72	−1.15
II-2	71.28	9.56	9.48	9.48	9.56	8.36	0.08
II-3	77.18	8.49	12.81	11.99	10.44	10.44	−4.32
II-4	50.51	9.07	9.15	8.90	9.25	8.92	−0.08
II-5	89.49	14.77	11.48	11.48	14.77	8.87	3.29
II-6	67.44	8.58	12.34	12.34	8.58	7.40	−3.76
II-7	49.49	8.61	21.49	21.49	8.92	7.91	−12.88
II-8	63.08	9.51	12.30	12.30	9.51	9.12	−2.79
II-9	73.08	13.98	10.44	10.44	13.98	6.59	3.55
II-10	70.77	9.99	9.56	9.56	9.99	7.79	0.43
III-1	75.83	12.42	9.55	9.55	12.42	7.71	2.87
III-2	65.81	9.04	10.81	10.74	10.02	9.35	−1.77
III-3	68.09	11.91	13.19	8.42	14.57	13.19	−1.28
III-4	68.83	10.11	11.16	10.76	10.66	9.94	−1.04
III-5	53.30	11.46	14.05	14.05	12.41	8.73	−2.59
III-6	87.32	14.01	9.87	8.40	14.09	9.87	4.15
Correlation with HO Acc.	ρ	**0.463***	-0.342	**-0.398***	**0.454***	0.075	**0.533****
	p	0.020	0.094	0.049	0.023	0.720	0.006

The last column, "(Motor)-(Non-Motor)" presents the difference between the relevance of Motor (column 3) and Non-Motor (column 4) region.

Result VII: The brain region with maximum class discriminative information varied significantly across subjects

Following the selected channel HO accuracy analysis in a subject-averaged manner, the subject-specific difference in the classification accuracies was investigated and the results of this analysis are presented in Table 5.6. Here, as high as 25% difference in HO classification accuracy was observed between the motor and the frontal region analysis. Also, some subjects achieved very high classification accuracies with the information from the frontal region as compared to the motor

TABLE 5.5: HO classification accuracies by using the EEG data from the channels in a particular brain region.

Channels	Group-I	Group-II	Group-III
All	62.03	69.39	69.86
Frontal	59.91	64.68	63.80
Motor	**60.48**	**72.44**	**66.57**

TABLE 5.6: The HO classification accuracies with selected channels.

Subject	ΔFMA	HO Acc. with Different Channels				Subject Type		
		All	Motor	Frontal	(Motor)-(Frontal)	High Motor	High Frontal	Equal
III-2	3	65.81	50.85	66.10	−15.24		×	
I-4	3	51.84	48.29	57.56	−9.27		×	
I-7	0	74.36	63.59	70.77	−7.18		×	
II-3	4	77.18	73.59	80.00	−6.41		×	
III-6	8	87.32	76.78	82.05	−5.27		×	
I-5	-1	52.05	49.49	52.56	−3.08		×	
II-2	13	71.28	63.59	66.15	−2.56			×
I-9	3	53.59	51.54	53.85	−2.31			×
III-1	7	75.83	68.71	70.32	−1.60			×
I-8	4	74.62	71.54	72.82	−1.28			×
II-10	0	70.77	71.03	71.03	0.00			×
II-6	0	67.44	68.97	66.92	2.05			×
II-8	4	63.08	67.44	63.59	3.85	×		
I-1	12	58.21	60.64	56.03	4.62	×		
I-6	9	58.72	57.69	53.08	4.62	×		
II-9	10	73.08	74.10	69.23	4.87	×		
I-2	3	62.31	66.15	60.77	5.38	×		
III-4	10	68.83	70.98	63.43	7.55	×		
II-4	5	50.51	61.28	52.05	9.23	×		
III-3	10	68.09	67.09	53.99	13.11	×		
I-3	16	72.56	75.38	61.79	13.59	×		
II-5	7	89.49	93.33	76.15	17.18	×		
III-5	11	53.30	65.00	46.91	18.09	×		
II-7	7	49.49	72.31	48.46	23.85	×		
II-1	0	81.61	78.78	53.17	25.61	×		

region. Overall, the brain region with maximum class discriminative information was largely variable across the stroke patients.

5.3.5 Relationship between Interpretability, Classification Accuracy and Clinical Improvements

Result VIII: Marginally better clinical improvements were observed in subjects with maximum class discriminative information in the motor region

Considering the large difference in the motor and frontal region HO accuracies, the effect of this difference on the clinical improvement was investigated. For

TABLE 5.7: Clinical Improvements for different subject groups

Subject Groups	Average ΔFMA	N
High Motor Acc.	8.00	13
High Frontal Acc.	2.83	6
Equal Motor, Frontal Acc.	4.50	6

this analysis, based on their motor and frontal region HO accuracies, the patients were grouped in three categories; the high motor accuracy (acc.) subjects, the high frontal acc. subjects, and the equal motor and frontal acc. subjects. The subjects were classified as the high motor or frontal acc. subjects if the difference in their motor and frontal region classification accuracies was more than 5% of their all channel HO accuracy, otherwise, they were grouped as the equal motor and frontal acc. subjects. The results of this segregation are presented in Table 5.6. Based on the above-mentioned criterion, there were 13 patients with higher motor region accuracy, 6 subjects with higher frontal region accuracy and 6 subjects with equal accuracy in both the motor and frontal region. Also, the average FMA improvements were observed to be 8.00 for the high motor group, 2.83 for the high frontal group, and 4.50 for equal motor, frontal group (Table 5.7). Also, this observed FMA difference between the motor, the frontal, and the equal group subjects, was statistically significant (single-factor ANOVA, $F = 3.537$, $p = 0.046$).

5.4 Discussion

Continuing the analysis of traditional machine learning methods, deep learning architecture and the previously proposed architecture of FBCNet, this chapter presented the performance analysis of these algorithms in classifying the multi-session EEG data collected during three different BCI-based upper extremity motor rehabilitative interventions. The classification analysis was followed by an interpretability analysis which was aimed to understand the class discriminative signatures of MI that were extracted by the FBCNet architecture. Based on the observations from the interpretability analysis, the relationship between the relevance of different brain regions in MI decoding and rehabilitation session MI decoding accuracy was explored. Lastly, the extent of true class discriminative information present in

different brain regions was estimated with the help of selected channel HO classification accuracies and the relationship between the brain region with the most generalizable class discriminative information and the associated rehabilitation gains was investigated. Overall, the results indicated that the deep learning architectures, particularly, the proposed architecture of FBCNet can achieve the best MI classification accuracies in BCI-mediated stroke rehabilitation trials. Also, from the interpretability analysis, it was observed that the most robust signature of MI are observed in the motor regions of the brain and the models that learn to focus on this information can achieve higher classification accuracies during multi-session rehabilitation trials.

5.4.1 Clinical Improvements

Although classification accuracy was the focus of this retrospective analysis, the clinical results of the rehabilitation trials were also briefly presented in this work. The three BCI-mediated rehabilitative interventions discussed in this work resulted in significant clinical improvements at the end of the intervention. This result provides further evidence that BCI-based therapies can be successfully employed for post-stroke motor function restoration. Moreover, in line with the literature, high heterogeneity in the patients' clinical outcomes was observed in this study as well [80, 227], and it indicated a necessity of patient stratification strategy [38] which was explored in the latter part of this study.

5.4.2 CV and HO Classification Accuracies

The classification performance of the traditional machine learning methods, deep learning architecture and the previously proposed architecture of FBCNet was the primary objective of this work. In this regards, first, the performance of these methods was tested in an HO manner, wherein the classification algorithms were trained using the calibration session data and then trained models were tested to classify all the rehabilitation session data. In this analysis, the classification algorithms were postulated to suffer from the high inter-session variability in the EEG data leading to poor classification accuracies [262]. Due to this, the model that can learn to extract more robust class discriminative information from the calibration

session data was thought to achieve the highest classification accuracies. In this analysis, all the three baseline methods achieved similar classification accuracies and the classification accuracies achieved by the previously proposed algorithm of FBCNet were significantly better than all the baseline methods in all the intervention groups. It can be inferred from these results that the novel deep learning architectures like FBCNet can learn highly robust class discriminative features from the EEG data which remain valid even during multi-session rehabilitation trials and achieve significantly better classification accuracies than the traditional machine learning approaches. Despite the best results, the classification accuracies achieved by the FBCNet were in the range of 65% which was still quite low.

The low classification accuracies during the HO analysis could be hypothesized to result from two confounding factors, the first factor is the extent of true class discriminative information present in any session's data, and the second factor is the inter-session difference in the data distributions between the calibration and the test session data. Therefore, poor HO classification accuracy for any subject could either imply that there is a lack of enough class discriminative information in the data or there is a high mismatch between the data from calibration and rehabilitation sessions. Hence, to identify the contribution of each of these factors, a cross validation analysis on all sessions data was conducted. In this analysis as well, the FBCNet outperformed all the baseline methods and the improvements achieved by it over baseline methods were statistically significant. More importantly, the CV classification accuracies were 6%, 10%, and 15% higher than the respective intervention group's HO classification accuracies. These significant differences between the CV and HO accuracies indicate that owing to the intersession variability, there is a strong mismatch between the calibration and rehabilitation session data and special model adaptation approaches could improve the HO rehabilitation session accuracies by a significant margin [18].

5.4.3 Interpretability Analysis

With a wide range of 50% to 90%, the subject-specific HO classification accuracies were observed to have high heterogeneity. These high differences in the HO classification accuracies prompted an interpretability investigation. The interpretability analysis was aimed to identify the reasons behind the observed heterogeneity in

HO classification accuracies and to explore the possibility of interpretability feature, extracted from the calibration session data, that can be predictive of the rehabilitation session classification accuracies. The preliminary visual analysis of the spectro-spatial relevance patterns encoded by the individual subject's FBCNet model indicated that the trained models with high relevance in the motor region and low relevance in the frontal region of the brain achieved higher HO classification accuracies. This observation was then tested for statistical significance with a correlation analysis using Pearson's Correlation Test. The results of this analysis revealed the HO session accuracies to be positively correlated with motor region relevance and, negatively correlated with frontal region relevance and these correlations were statistically significant. Furthermore, the motor minus non-motor region relevance was observed to be the best predictor of the HO session accuracies, indicating that class discriminative information extracted from the motor regions of the brain can form the most robust signatures of the MI and the models that can learn this information may achieve a higher multi-session classification accuracy.

Although interpretability features were observed to provide strong predictive capabilities, these features were still dependent on the individual classification algorithm's capabilities of extracting robust discriminative features from the training data and hence they can not be considered to be a representative of the actual class discriminative information present in the training or test data. Therefore, to understand the extent of the actual class discriminative information present in particular regions of the brain, a selected channel HO analysis was conducted. The aim of this analysis was to explore whether the high frontal relevance extracted by the FBCNet for some subjects was a result of poor training of FBCNet or the true class discriminative information was actually present in the frontal region. In this analysis, the FBCNet models trained and tested only using the data from frontal region channels were observed to achieve higher classification accuracies than the motor region channels in few subjects. In some of these subjects, this difference in classification accuracies was as high as 15%. These results indicate that, for some subjects, the true class discriminative information might be present in the frontal region of the brain. These observations of MI related information in the frontal region cannot be clearly explained on neurophysiological grounds. However, one possible explanation can be that, owing to the stroke disrupted motor networks, in some patients, the class discriminative information associated with the kinesthetic MI could have been diminished and better discriminative information could

be extracted from other cognitive processes like attention or focus, to generate the brain activation patterns which are distinct from the rest state. This explains the higher involvement of frontal region in the model relevance and better classification accuracies with the EEG data from frontal region channels. However, more investigation in this direction is necessary to confirm this hypothesis.

The above hypothesis that in some patients neurological processes other than MI could have played greater role in the control of the BCI system also promoted an investigation about if this phenomenon results in any difference in clinical outcomes. For this purpose, the subjects were grouped into three categories; subjects with higher motor region accuracy, subjects with higher frontal region accuracy, and subjects with equal motor and frontal region accuracy. Here, it was observed that the patients from these three groups achieved FMA improvements of 8.0, 2.8, and 4.5 points respectively, indicating that the patients for whom the most MI related information is concentrated in the motor region can achieve significantly better clinical recovery. Furthermore, even the subjects with more discriminative information present in the frontal region also achieved some clinical improvements. This indicates that, even the neurological processes other than MI, could lead to marginal motor function improvements. Overall, in this analysis, we observed that along with the individual factors such as age [78], volume and location of initial infraction [269], extent of injury to corticospinal tract [46, 225, 270], presence of motor evoked potential [30, 46, 227], and other functional and structural neuroimaging factors [24, 38] which are associated with the neuro-clinical profile of the patient, the spatial location of MI related discriminative patterns can provide additional prognostic information.

5.5 Summary

The inter-session classification of the EEG data is a challenging problem which is unavoidable in the BCI-based rehabilitation trials. Considering that no previous work had analyzed the performance on various classification algorithms on the multi-session stroke rehabilitation data, this work presented an extensive retrospective analysis of the EEG data from 25 stroke patients undergoing three different BCI-mediated upper extremity motor rehabilitation interventions from the MI classification perspective. The classification results indicated that the deep learning

architectures, particularly, the proposed architecture of FBCNet can achieve the best MI classification accuracies in BCI-mediated stroke rehabilitation trials. Furthermore, from the interpretability analysis, it was observed that the most robust signatures of MI are observed in the motor regions of the brain and the models that learn to focus on this information can achieve higher classification accuracies during multi-session rehabilitation trials.

Chapter 6

Prognostication and Monitoring of Post-Stroke Motor Recovery

6.1 Introduction

All the previous works in this thesis were focused on achieving better post-stroke motor rehabilitation by improving the technology of BCI systems. In particular, these works attempted to enhance the MI decoding accuracy of BCI systems used in post-stroke motor rehabilitation settings. However, apart from the technological aspect of BCI, personalized rehabilitation is another domain that holds vast potential for improving the clinical outcomes of post-stroke rehabilitative interventions.

The work presented in this chapter has been published as:

1. Ravikiran Mane, et al., EEG Predictors for Upper Limb Motor Recovery of Stroke Patients Undergoing BCI and tDCS Rehabilitation. 7th International BCI Meeting. 21-25 May, 2018.
2. Ravikiran Mane, et al., Quantitative EEG as Biomarkers for the Monitoring of Post-Stroke Motor Recovery in BCI and tDCS Rehabilitation. Proceedings of 40nd Annual International Conference of the IEEE Engineering in Medicine and Biology Society (EMBC). 17-21 July, 2018. **(Top-10 EMBS Student Paper Competition Finalist)**
3. Ravikiran Mane, et al., Prognostic and Monitory EEG-Biomarkers for BCI Upper-Limb Stroke Rehabilitation. IEEE Transactions on Neural Systems and Rehabilitation Engineering. 27(8), 1654–1664, 2019.

As reviewed in Chapter 2, considering the global burden of stroke, many rehabilitative interventions have been developed for the purpose of post-stroke motor function restoration [9, 17, 24, 28, 80, 82, 271]. Although numerous studies have validated the group level clinical benefits of these interventions [10, 272, 273], at individual level, the extent to which patient respond to them is highly subject-specific [80, 227]. Therefore, it is necessary to identify the most suitable rehabilitative intervention for a patient and to predict the corresponding recovery. In literature, the heterogeneity in the rehabilitation gains has been primarily attributed to the unique neuro-clinical profile of the patient[9, 24, 38, 40, 46, 48, 270, 274]. Studies have identified that individual factors such as age [78], volume and location of initial infraction [269], extent of injury to corticospinal tract [46, 225, 270], presence of motor evoked potential [30, 46, 227], and other functional and structural neuroimaging factors [24, 38] affect the patient's response to the intervention and the overall potential of recovery. However, while determining patients' response, along with the neuro-clinical profile, the type of intervention in itself is another crucial factor, which is often ignored. Many studies have highlighted that different rehabilitative interventions facilitate the recovery of the damaged brain in a unique manner [28, 36, 42, 49, 144, 175, 192]. A direct consequence of these intervention-specific recovery mechanisms is that patients respond differently to interventions [40]. Hence, the process of rehabilitation should be treated as an interaction between the patient and the given intervention.

The previous approach of prognostication, which is solely based on the neuro-clinical profile of the patient, does not account for this interaction effect. Therefore, considering rehabilitation from an interaction viewpoint, this work proposes the existence of intervention-specific prognostic biomarkers. Here, it is hypothesized that these biomarkers can encapsulate the interactions between the intervention and the patient, and can uniquely predict the clinical efficacy of the given intervention. More importantly, identification of these prognostic biomarkers can be further pursued to distinctly predict the expected response of a patient to all available interventions. The intervention with the highest predicted gains may then be recommended to the patient, thereby enabling a highly personalized rehabilitation regime. Furthermore, since the mechanisms of neuronal recovery elicited by different interventions are not identical, it is hypothesized that these mechanisms can be encapsulated using intervention-specific monitory biomarkers. The change in these biomarkers can then be used to monitor the evolution of neuronal recovery

providing a finer scale to monitor patients' progress. To test these hypotheses, and to explore the possibility of personalized rehabilitation, this study investigates between-intervention differences in prognostic and monitory biomarkers of post-stroke recovery. For this purpose, this study analyses the previously mentioned (Section 5.2.1) data of chronic stroke patients undergoing upper extremity (UE) motor rehabilitation using a BCI controlled robotic paradigm (BCI group) and tDCS coupled BCI paradigm (tDCS-BCI group).

To quantify the neuronal changes induced by the tDCS-BCI and BCI interventions, and to predict clinical gains, this study uses Quantitative Electroencephalography (Q-EEG) features. As stated previously, compared to other neuroimaging modalities, EEG is a low cost and versatile technique which provides information about electrodynamic activations of the brain with high temporal resolution. EEG is also highly sensitive to the changes in the Cerebral Blood Flow (CBF) that occur in acute stage of the stroke [213]. Consequently, many acute stroke studies have demonstrated the usefulness of QEEG features. The features based on the power spectrum analysis of resting state EEG have been found to be particularly effective for monitoring of stroke progression as well as for prediction of sub-acute motor status[51, 53, 54, 54, 55, 208, 209, 214, 215]. Specifically, the relative power in classical EEG frequency bands [53, 55, 213], the ratio of power in slow v/s fast frequency bands (Power Ratio Index: PRI) [51, 54, 215] and delta to alpha power ratio (Delta Alpha Ratio: DAR) [51, 54, 215] have been observed to be informative in acute stage. In these studies, high relative power in slower frequencies and consequently high values of PRI and DAR have been normally associated with bad motor status and poor prognosis. Furthermore, since stroke most frequently results in inter-hemispheric imbalance of activations, features quantifying this inter-hemispheric brain asymmetry (Brain Symmetry Index: BSI) namely Revised BSI (rBSI), and Pairwise Derived BSI (pdBSI) have also shown the predictive and monitory capabilities in motor rehabilitation [57, 219, 220]. Despite their effectiveness in acute and sub-acute stages, very few chronic stroke rehabilitation studies have evaluated the prognostic and the monitory value of these QEEG features [49, 144, 275–277] and no other study has explored the effectiveness of QEEG features as biomarkers of recovery prediction and treatment evolution during BCI and tDCS-BCI motor rehabilitation.

To address this gap, this study investigates the prognostic and monitory capability

of resting state QEEG features for the same intervention. Moreover, the MI task state activations can be presumed to be more relevant, especially in the field of motor rehabilitation and hence they can provide unique information absent in rest state [36]. Therefore, this study also provides comparative insights about the efficacy of using rest and task state QEEG for prediction and monitoring of BCI and tDCS-BCI rehabilitation. Importantly, we investigate the between-intervention differences in the prognostic and the monitory capabilities of QEEG features with an aim to identify intervention-specific signature biomarkers which can open the possibilities of personalized rehabilitation.

6.2 Methods and Materials

6.2.1 Patients

As mentioned briefly before in Section 5.2.1, this clinical trial was designed as a participant and outcomes assessor blinded (double blinded), Randomized Controlled Trial (RCT) with parallel assignment and was conducted from January 2011 to January 2014 at National University Hospital, Singapore. The trial is registered with U.S. National Institutes of Health and detailed protocol is available at clinicaltrials.gov with Clinical Trial Registration Unique Identifier: NCT01897025 (date of registration: July 8, 2013). The sample size was determined by our preliminary results and other studies that used similar endpoints. The study targeted patients with moderate to severe unilateral UE motor impairments who had fewer other therapeutic options available owing to their greater difficulty in movement execution. The pre-intervention degree of impairments was assessed with UE motor part of Fugl-Meyer assessment (FMA) [104], and patients aged between 21 and 70 who had their first ever-stroke unilateral at least 9 months before enrollment with FMA score between 11 and 45 were considered for the study. 42 patients showed interest in this RCT and were assessed with the inclusion criteria and BCI performance criteria [119]. 16 patients were excluded because they did not meet the criteria and another 7 declined to participate. The remaining 19 eligible patients provided written informed consent and participated in the intervention. Trial design was not changed after the commencement of the trial. All the participants successfully completed the trial without any adverse effects and were considered in the analysis.

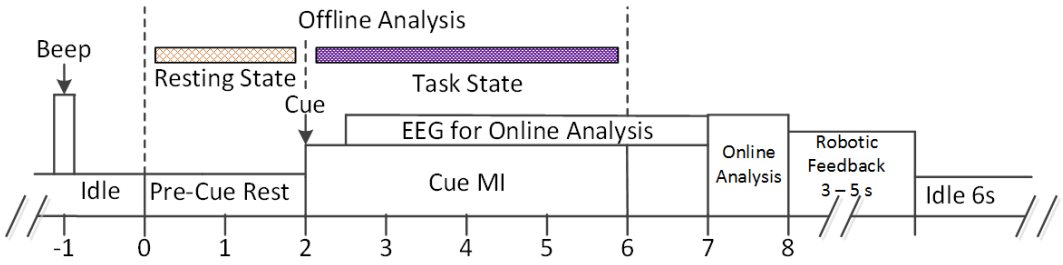

FIGURE 6.1: Rehabilitation protocol. Every run started with preparation cue. The MI cue was presented 2s after the preparation cue and following MI cue patients performed MI for 4s. The EEG data collected during 0.5 to 4.5 seconds from the MI cue was processed online to detect MI. In this offline study, the 0s to 2s pre-cue resting state data and 2s to 6s MI task state data have been analyzed.

6.2.2 tDCS-BCI and BCI Intervention

The recruited 19 patients were randomly assigned to the tDCS-BCI (n=10) or BCI (n=9) interventions. As mentioned in Section 5.2.1, all the recruited patients received BCI rehabilitation for two weeks, which consisted of ten sessions lasting one hour each. The BCI rehabilitation involved BCI triggered robotic movement of the paretic hand upon the detection of motor imagery (MI). In a trial-based setting, patients performed MI of the reaching task with the paretic hand; which was identified online using EEG and successful detection of MI was rewarded by immediate passive movement of the paretic hand using the Inmotion MIT-Manus robot. Each rehabilitation session involved four therapy runs with 40 such trials in each run constituting, in total, 160 repetitions. The design of the trial is presented in Fig. 6.1. In addition to the BCI rehabilitation, the patients in tDCS-BCI group received 20 minutes of 1 mA bi-hemispheric tDCS (the anode over the ipsilesional M1 and the cathode over the contralesional M1) before the start of every session. The M1 positions for tDCS electrodes were approximately determined as locations of the C3 and C4 electrodes in the international 10-20 EEG montage. To ensure the randomized blinding, the BCI group also received a similar but sham-tDCS where the current was applied only for the first 30s.

6.2.3 Clinical Evaluation

The UE motor part of FMA (range 0-66) was used to assess the clinical recovery of the motor functions, and it was conducted at three time points: 1. Pre-intervention (FMA_{T0}), 2. Post-intervention: immediately after the intervention (FMA_{T2}), and 3: Follow-up: at a two weeks follow-up after the intervention (FMA_{T4}). The intervention gain $\Delta FMA(0,2)$ was calculated as the difference between pre-intervention and post-intervention FMA (FMA_{T2} - FMA_{T0}). Also, 'intervention + follow-up' gain $\Delta FMA(0,4)$ was calculated as the difference between pre-intervention and follow-up FMA (FMA_{T4} - FMA_{T0}).

6.2.4 EEG Data Acquisition, Preprocessing and Feature Extraction

During all the rehabilitation sessions, BCI system continuously captured the brain activity using the Neuroscan Nuamps EEG amplifier with 27 unipolar channels with a sampling frequency of 250Hz [119]. With impedance kept below 5kΩ, the electrodes were positioned according to the international 10/20 system and were referenced to the ear electrode. For the offline analysis, the continuous EEG data was cleaned for the line noise and zero-phase FIR filtering with hamming window function was performed to bandpass filter the data between 0.5 - 45Hz. The first six seconds of single trial data was extracted from this filtered data and an expert user discarded noisy trials and channels (along with their homologous channels) with the help of PREP [278] and FASTER [279] toolbox. Following this, the common average referencing was performed and eye blink and muscle-related artefacts were removed using Independent Component Analysis (ICA). Expert user removed artefactual components with the help of SASICA [135] toolbox. Finally, from this clean data, a 2s pre-cue resting state EEG and 4s post-cue task state MI data were separately extracted from each trial for the analysis.

From the above data, the single trial Power Spectral Density (PSD) was computed using Welch's periodogram for every channel. This single trial PSD was averaged over all the trials and was summed across 1.0-4.0 Hz, 4.0-7.5 Hz, 7.5-12.5 Hz, and 12.5-30.0 Hz bands to obtain absolute band power in delta (δ), theta (θ), alpha (α), and beta (β) power bands respectively. Moreover, the relative band power

was calculated by dividing the absolute band power in each band with the total power in 1-30Hz. This relative power at each channel was then averaged over the scalp to obtain global relative power features: $r\delta$, $r\theta$, $r\alpha$, and $r\beta$. The absolute band power at all the channels was also averaged over the scalp to obtain a global absolute band power in δ, θ, α, and β power bands and it was used to calculate the five global power ratio based features:

$$\text{Power Ratio Index, PRI} = \frac{\delta+\theta}{\alpha+\beta} \tag{6.1}$$

$$\text{Delta Alpha Ratio, DAR} = \frac{\delta}{\alpha} \tag{6.2}$$

$$\text{Theta Beta Ratio, TBR} = \frac{\theta}{\beta} \tag{6.3}$$

$$\text{Theta Alpha Ratio, TAR} = \frac{\theta}{\alpha} \tag{6.4}$$

$$\text{Theta Beta Alpha Ratio, TBAR} = \frac{\theta}{\alpha+\beta} \tag{6.5}$$

Finally, the trial averaged absolute PSD at all channels was used to compute pdBSI [57] and rBSI [50]. Using the averaged activations over two hemispheres, rBSI encapsulates the global inter-hemispheric asymmetry whereas pdBSI is a more localized measure of asymmetry and quantifies the activation imbalance between the homologous channels pairs (left v/s right). As done in the previous study [49], the rBSI and pdBSI between 1-25Hz were calculated as:

$$rBSI = \frac{1}{N}\sum_{i=1}^{N}\left|\frac{R_i - L_i}{R_i + L_i}\right| \quad , \quad R_i = \frac{1}{M}\sum_{j=1}^{M} r_{ij} \tag{6.6}$$

$$pdBSI = \frac{1}{MN}\sum_{j=1}^{M}\sum_{i=1}^{N}\left|\frac{r_{ij} - l_{ij}}{r_{ij} + l_{ij}}\right| \tag{6.7}$$

Here, r_{ij} and l_{ij} represent the trial averaged PSD from right and left homologous channel pairs (at channel pairs *j= 1,2,...,M)* at frequency *i= 1,2,...,N*. R_i and L_i (similarly calculated) are the average power over all the channels on the right and left hemispheres at frequency i.

Considering these two brain symmetry features and nine band power features, in total eleven QEEG features were extracted for each subject from the first (pre-intervention: EEG_{T0}) and the last (post-intervention: EEG_{T2}) rehabilitation session from both the rest and task state EEG data.

6.2.5 Group-level Correlation Analysis and Statistical Tests

The usefulness of the above-mentioned EEG features as rehabilitation biomarkers was investigated by examining their correlation with the FMA scores. Owing to the non-normal distribution of the data, a non-parametric statistical analysis was performed, and hence the relationship between EEG features and the clinical outcome was assessed using Spearman's rank correlation. The correlation was computed for the following combination of time points.

- Prognostication:

  Pre-intervention values of biomarkers (EEG_{T0}) vs. two- and four-week change in the FMA score (EEG_{T0} vs. ΔFMA(0,2), EEG_{T0} vs. ΔFMA(0,4)). These correlations indicate whether the EEG-features can predict the functional outcomes and aid in intervention prognosis.

- Monitoring:

  FMA score vs. values of biomarkers at pre and post-intervention time points (EEG_{T0} vs. FMA_{T0}, EEG_{T2} vs. FMA_{T2}), as well as intervention-induced change in biomarkers vs. change in FMA ($\Delta EEG(0,2)$ vs. ΔFMA(0,2)). These regressions represent the utility of biomarkers for evaluation of recovery and may aid in monitoring the patients' progress.

The small sample size of the study and performing multiple correlations simultaneously increases the likelihood of overestimation of statistical significance and chance of false discoveries. Hence, for the proper estimation of statistical significance of correlations, as done in the previous studies [36], the method of non-parametric permutation testing was employed [280]. Permutation testing involves repeated shuffling of labels across subjects and recalculation of correlation coefficient (ρ) for each arrangement. Random shuffling destroys any relation between two variables, and hence these calculated ρ values represent a distribution of the null hypothesis that there is no relationship between the two variables. The distribution can be approximated to the normal distribution and using it, the statistical significance of the original observed correlation is calculated by two-tailed z-test, testing the hypothesis that the observed ρ lies at extreme tails of this distribution [280]. In this analysis, clinical parameters in the correlation (FMA_{T0}/ FMA_{T2}/

$\Delta FMA(0,2)$/ $\Delta FMA(0,4)$) were randomly shuffled 5000 times to obtain null distribution. This procedure provides a robust estimation of statistical significance, reducing the Type-I errors, and at the same time preserves the power of the study, limiting Type-II errors. Finally, assuming Spearman's rank correlation coefficient of 0.6, the sample size of the study was just enough (n≥9) to achieve a statistical power of 80% with a significance level of $\alpha = 0.05$.

To investigate the possibility of intervention-specific biomarkers, the inter-intervention difference in the strength of relation between any EEG biomarker and FMA feature was examined by statistical comparison of their correlation coefficients (CC) using Fisher Z-transformation [281]. This method allows statistical testing of whether a particular EEG feature has a rather strong relationship with the clinical features in one particular group and no/weak relationship with the other group, making that feature an intervention-specific biomarker of recovery. In addition, the differences in the relationship of pre-intervention EEG features with two vs. four week clinical gains were analyzed using Dunn's z-test [282]. This analysis was performed to understand the effect of prediction duration on the prognostic capabilities of EEG features. Moreover, to encapsulate the mechanism of recovery, the change in EEG features during the intervention was assessed using Wilcoxon signed-rank test. Finally, the inter-intervention differences in the features were tested using Wilcoxon rank sum test.

6.3 Results

6.3.1 Clinical Outcomes

The demographic and clinical details of the patients are listed in Table 6.1. No significant difference was observed between tDCS-BCI and BCI group in terms of age (p = 0.508), post-stroke time (p = 0.720), and baseline FMA (p = 0.6475). Both the groups showed improvements in the FMA scores immediately after the training (tDCS group: 0.9±3, BCI group: 2.8±4) as well as at follow-up assessment (tDCS group: 5±4.4, BCI group: 5.4±5.7) and these results are presented in Figure 6.2. However, only the improvement till the follow-up assessment was statistically significant (tDCS-BCI group: p = 0.006, BCI group: p = 0.021). Importantly, no significant inter-intervention difference was observed in the clinical

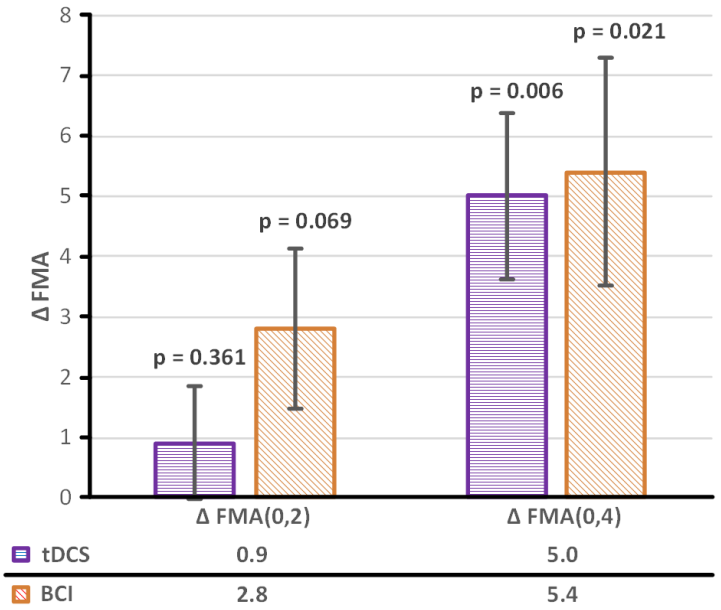

FIGURE 6.2: Functional Improvements following the tDCS-BCI and BCI based motor rehabilitation.

improvements at any time-point (T2: p = 0.250, T4: p = 0.793). Furthermore, both in the tDCS-BCI and BCI group, the 2 and 4 week clinical improvements did not display any significant correlation with the pre-intervention FMA, age, and post-stroke time (all p>0.4). Therefore, demographic variables did not present any prognostic value. Finally, the correlation between $\Delta FMA(0,2)$ and $\Delta FMA(0,4)$ was significant in BCI group (p = 0.018) but was not significant in tDCS-BCI group (p = 0.059) indicating better sustenance of recovery in the BCI group.

6.3.2 BCI Training Parameters

The subject-specific FBCSP model used for the BCI training may have a potential influence on patients' clinical and neurological evolution. Therefore, inter-group differences in spectral and spatial features selected by the FBCSP algorithm were investigated. Spectral analysis indicated that there was no significant difference in the selected filter bands between the two groups (Fisher's exact test, p = 0.523). Moreover, qualitative analysis of selected CSP filters displayed no between-group difference in the spatial features. MI detection accuracy during rehabilitation runs

TABLE 6.1: Clinical and Demographic Details of the Patients. (mean ± std)

Patient	Sex	Age	Lesion side	Type	Nature	Post stroke time (months)	FMA Score		
							FMA_{T0}	FMA_{T2}	FMA_{T4}
tDCS-BCI group									
P1	M	29	R	I	SC	45.2	51	50	51
P2	M	54	L	I	SC	23.3	29	34	42
P3	F	38	R	H	SC	24.3	38	41	42
P4	F	60	R	H	SC	50.1	26	22	31
P5	F	48	L	H	SC	49.1	39	42	46
P6	M	59	L	I	SC	16.0	31	28	31
P7	M	65	L	I	SC	29.5	41	45	48
P8	F	57	L	H	SC	12.9	40	40	44
P9	M	47	R	I	C	11.0	30	31	40
P10	M	64	R	I	SC	89.6	28	29	28
	6M/4F	52.1±11.6	5R/5L	4H/6I	1C/9SC	35.1±24.1	35.3±7.8	36.2±8.8	40.3±7.8
BCI group									
P12	M	51	R	I	SC	41.9	33	42	45
P13	M	39	L	I	SC	22.7	36	42	39
P14	M	59	R	H	SC	51.8	41	46	57
P15	F	70	R	I	SC	19.6	23	25	26
P16	M	59	R	I	SC	51.8	29	24	28
P17	M	58	L	I	SC	30.7	28	32	37
P18	M	47	L	I	SC	10.4	40	40	40
P19	M	58	R	H	SC	27.0	20	22	24
P20	M	66	R	I	SC	50.6	43	45	46
	8M/1F	56.3±9.5	6L/3L	2H/7I	9SC	34±15.5	32.6±8.1	35.3±9.6	38±10.7

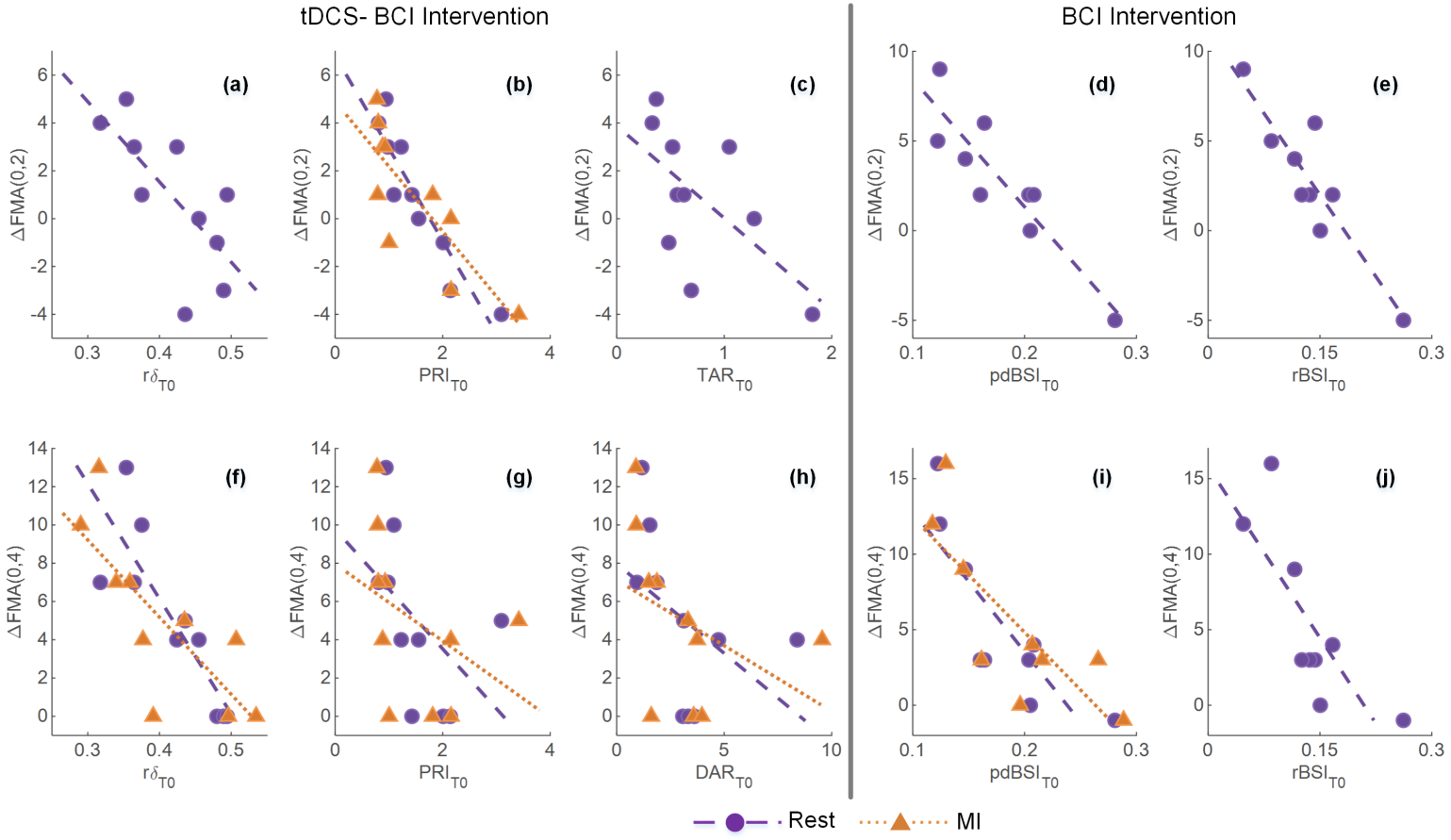

FIGURE 6.3: Statistically significant relationships for the prediction of intervention gains. Significant correlation between pre-intervention EEG features and two-week FMA gains for the tDCS-BCI group are presented in panels (a)-(c), whereas panels (d)-(e) represent the same relationship for the BCI group. Similarly, significant association between four-week FMA gains and pre-intervention EEG features is displayed in panels (f)-(h) for the tDCS-BCI group and panels (i)-(j) for the BCI group.

TABLE 6.2: Correlation analysis: pre-intervention EEG features (EEG_{T0}) and clinical improvement (ΔFMA(0,2), ΔFMA(0,4)) for tDCS-BCI group

EEG Features	ΔFMA(0,2)		ΔFMA(0,4)	
	Rest	Task	Rest	Task
$r\delta_{T0}$	***-0.74**	-0.62	****-0.90**	****-0.84**
$r\theta_{T0}$	-0.11	-0.32	0.49	0.29
$r\alpha_{T0}$	0.42	0.42	0.49	0.63
$r\beta_{T0}$	0.42	0.49	0.06	0.13
PRI_{T0}	****-0.96**	****-0.86**	***-0.70**	***-0.70**
DAR_{T0}	-0.54	-0.43	***-0.70**	***-0.71**
TBR_{T0}	-0.51	-0.55	0.02	0.03
TAR_{T0}	***-0.66**	-0.59	-0.39	-0.41
$TBAR_{T0}$	-0.58	-0.60	-0.10	-0.04
$pdBSI_{T0}$	-0.35	0.03	-0.20	0.03
$rBSI_{T0}$	0.07	0.24	0.30	0.49

correlation coefficients, * implies $p < 0.05$ and ** implies $p < 0.01$

was also not different between the two groups (tDCS-BCI = 83.7%, BCI = 86.3%, p = 0.523).

6.3.3 Prognostication

Many pre-intervention rest and task state QEEG features presented significant prognostic capabilities and Table 6.2 and Table 6.3 present these results. In the tDCS-BCI group, the two weeks FMA gains ($\Delta FMA(0,2)$) showed significant negative correlation with relative delta power ($r\delta_{T0}$, p = 0.028), PRI (PRI_{T0}, p = 0.004), and TAR (TAR_{T0}, p = 0.049) in the resting state. The task state relative delta power ($r\delta_{T0}$, p = 0.063) as well as TAR (TAR_{T0}, p = 0.077) also displayed similar correlations but only the negative correlation of $\Delta FMA(0,2)$ with task state PRI (PRI_{T0}, p = 0.001) was significant. In a similar manner, significant negative correlation was found between four weeks FMA gains ($\Delta FMA(0,4)$) and relative delta power ($r\delta_{T0}$, $p_{rest} = 0.007$, $p_{task} = 0.011$), PRI (PRI_{T0} $p_{rest} = 0.038$, $p_{task} = 0.039$), and DAR (DAR_{T0}, $p_{rest} = 0.036$, $p_{task} = 0.035$) in both resting and task state data. These relationships are illustrated in Figure 6.3. Importantly, the strength of relationship between many QEEG features and $\Delta FMA(0,2)$ vs $\Delta FMA(0,4)$ was very different and Dunn's z-test revealed that this difference was statistically significant for resting state PRI_{T0} (p = 0.019). Finally, both resting

TABLE 6.3: Correlation analysis: pre-intervention EEG features (EEG_{T0}) and clinical improvement (ΔFMA(0,2), ΔFMA(0,4)) for BCI group

EEG Features	ΔFMA(0,2)		ΔFMA(0,4)	
	Rest	Task	Rest	Task
$r\delta_{T0}$	-0.22	0.12	-0.25	-0.08
$r\theta_{T0}$	-0.22	-0.49	-0.02	-0.25
$r\alpha_{T0}$	0.27	-0.05	0.37	0.20
$r\beta_{T0}$	0.68	0.42	0.46	0.10
PRI_{T0}	-0.59	-0.24	-0.47	-0.46
DAR_{T0}	-0.22	0.15	-0.41	-0.24
TBR_{T0}	-0.46	-0.46	-0.2	-0.20
TAR_{T0}	-0.44	-0.24	-0.36	-0.29
$TBAR_{T0}$	-0.51	-0.51	-0.25	-0.25
$pdBSI_{T0}$	***-0.80**	-0.56	***-0.81**	***-0.80**
$rBSI_{T0}$	***-0.76**	-0.39	***-0.80**	-0.64

correlation coefficients, * implies $p < 0.05$ and ** implies $p < 0.01$

and task state EEG features demonstrated very similar correlations with functional improvements in the tDCS-BCI group.

In the BCI group, the pdBSI ($pdBSI_{T0}$, $p = 0.024$) and rBSI ($rBSI_{T0}$, $p = 0.028$) calculated from the resting state EEG were significantly correlated with the two weeks FMA gains. The same two features were also correlated with the four weeks motor gains ($pdBSI_{T0}$, $p = 0.022$; $rBSI_{T0}$, $p = 0.024$). On the other hand, in the task state features, only the significant correlation was observed between the $\Delta FMA(0,4)$ and pdBSI ($pdBSI_{T0}$, $p = 0.025$). These significant relationships are illustrated in Fig. 6.3. Noticeably, no significant correlation was observed between intervention gains and any EEG power ratio features in the BCI group.

From Table 6.2 and Table 6.3, it can be noted that the EEG features showing prognostic capabilities in tDCS-BCI and BCI groups are different. The outcomes of tDCS-BCI rehabilitation are strongly correlated with power ratio features whereas brain asymmetry features display strong relation with the clinical gains in the BCI rehabilitation. Statistical comparison confirmed these evident differences and it was observed that inter-intervention differences in the predictive capabilities of resting state PRI_{T0} ($p = 0.014$), $r\delta_{T0}$ ($p = 0.016$), $pdBSI_{T0}$ ($p = 0.047$), and $rBSI_{T0}$ ($p = 0.006$) features are statistically significant. This comparison supports the observation that resting state PRI_{T0}, $r\delta_{T0}$ are significantly better predictors

of recovery following the tDCS-BCI intervention, whereas resting state $pdBSI_{T0}$, $rBSI_{T0}$ have stronger relationship with the intervention gains following the BCI intervention. The differences in task state features did not reach statistical significance. Also, in both the groups, the difference in the prognostic capabilities of any QEEG features during rest and task state was not significant.

6.3.4 Monitoring

To assess the ability of EEG features in characterization of intervention-induced gains and for monitoring of recovery evolution, a three-fold analysis was performed. First, the association between pre-intervention motor status and pre-intervention EEG features was investigated. Next, the relationship between the intervention-induced changes in the EEG features and motor improvements was explored. Finally, the correlation between post-intervention EEG features and post-intervention motor status was studied. The entire analysis was performed on the FMA_{T0}, and FMA_{T2} features and the FMA_{T4} was not considered due to unavailability of week-4 EEG data.

Correlation between pre-intervention EEG features and pre-intervention FMA

Initially, a separate group analysis of the correlation between pre-intervention EEG features (EEG_{T0}) and FMA_{T0} was performed and it resulted in significant negative correlation of FMA_{T0} with rest and task state TBR (TBR_{T0}, $p_{rest} = 0.033$, $p_{task} = 0.034$) and significant positive correlation with task state relative beta power ($r\beta_{T0}$, $p = 0.033$), for the BCI group. In the tDCS-BCI group, only task state features, specifically, relative theta power ($r\theta_{T0}$, $p = 0.040$), TBR (TBR_{T0}, $p = 0.042$), and TBAR ($TBAR_{T0}$, $p = 0.019$) displayed significant correlations with the FMA_{T0}. The inter-intervention comparison of correlation coefficients was performed to investigate the possibility of inter-intervention difference in the monitory capabilities of any EEG_{T0} feature. No such statistically significant differences in the correlation as well as in the values of EEG features were observed (all $p>0.17$) and hence, a combined group analysis (all subjects) was performed. This correlation analysis considering all the patients revealed significant relationship of FMA_{T0} with task and rest state relative theta power ($r\theta_{T0}$, $p_{rest} = 0.008$, p_{task}

TABLE 6.4: Correlation between pre-intervention EEG features (EEG_{T0}) and pre-intervention FMA scores (FMA_{T0}).

EEG Features	tDCS-BCI		BCI		All	
	Rest	Task	Rest	Task	Rest	Task
$r\delta_{T0}$	-0.16	-0.10	0.13	-0.02	0.07	-0.13
$r\theta_{T0}$	-0.59	***-0.68**	-0.68	-0.57	****-0.61**	***-0.59**
$r\alpha_{T0}$	0.24	0.03	-0.25	-0.18	-0.02	0.01
$r\beta_{T0}$	0.22	0.60	0.55	***0.77**	0.34	****0.64**
PRI_{T0}	-0.21	-0.15	-0.40	-0.55	-0.18	-0.36
DAR_{T0}	-0.04	-0.03	0.12	0.05	0.06	-0.12
TBR_{T0}	-0.27	***-0.68**	***-0.75**	***-0.75**	***-0.48**	****-0.70**
TAR_{T0}	-0.39	-0.39	-0.50	-0.53	-0.33	-0.38
$TBAR_{T0}$	-0.56	***-0.78**	-0.60	-0.60	***-0.50**	****-0.64**
$pdBSI_{T0}$	-0.20	0.39	-0.45	-0.33	-0.38	-0.04
$rBSI_{T0}$	-0.50	-0.19	-0.33	-0.20	***-0.46**	-0.18

correlation coefficients, * implies p ¡ 0.05 and ** implies p ¡0.01

= 0.012), TBR (TBR_{T0}, p_{rest} = 0.043, p_{task} = 0.003), TBAR ($TBAR_{T0}$, p_{rest} = 0.033, p_{task} = 0.006), rest state rBSI ($rBSI_{T0}$, p = 0.046), and task state relative beta power ($r\beta_{T0}$, p = 0.007). The complete list of correlation coefficient values is presented in Table 6.4.

Post-intervention changes in the EEG features and their correlation with the functional improvement

The statistical analysis of pre and post-intervention EEG feature values revealed that there was a significant intervention-induced change in the relative theta band power (p=0.039) in the BCI group during rest state. Also, although not significant, BCI group displayed a marginal change in resting state TAR (p = 0.054) and TBAR (p = 0.074). No significant intervention-induced change was observed in task state EEG features in the BCI group. In the tDCS-BCI group, resting state pdBSI (p=0.019) and task state rBSI (p = 0.037) changed significantly during the intervention. Although the EEG features displaying significant changes in the tDCS and BCI group were mutually exclusive, no statistically significant between-intervention difference in change of EEG features was observed.

Following the identification of the EEG variables that changed significantly, it was

TABLE 6.5: Correlation between clinical improvement ($\Delta FMA(0,2)$) and intervention induced change in the EEG features (ΔEEG)

EEG Features	tDCS		BCI	
	Rest	Task	Rest	Task
$\Delta r\delta$	0.01	0.09	-0.02	0.15
$\Delta r\theta$	-0.16	0.09	***-0.76**	-0.61
$\Delta r\alpha$	0.24	0.37	0.37	0.46
$\Delta r\beta$	-0.64	-0.54	0.12	0.19
ΔPRI	0.12	0.10	0.08	-0.17
ΔDAR	0.13	0.10	0.05	0.14
ΔTBR	0.05	0.19	-0.59	-0.54
ΔTAR	-0.07	-0.31	***-0.70**	***-0.73**
$\Delta TBAR$	-0.06	-0.10	***-0.70**	-0.58
$\Delta pdBSI$	0.27	0.25	-0.63	-0.66
$\Delta rBSI$	-0.34	0.02	-0.54	-0.56

correlation coefficients, * implies p $<$ 0.05 and ** implies p $<$0.01

investigated if this change correlated with clinical improvements. The correlation analysis between ΔEEG and $\Delta FMA(0,2)$ revealed that there was a significant negative correlation between $\Delta FMA(0,2)$ and resting state $\Delta r\theta$ (p = 0.032), ΔTAR (p = 0.048), and $\Delta TBAR$ (p = 0.049) in the BCI group. Coherent with the resting state features, the task state $\Delta r\theta$ (p = 0.086), and $\Delta TBAR$ (p = 0.102) also demonstrated relationship with $\Delta FMA(0,2)$ in the BCI group but only correlation with ΔTAR (p = 0.038) was statistically significant. Despite the significant change, resting state $\Delta pdBSI$ and task state $\Delta rBSI$ did not show any significant correlation with $\Delta FMA(0,2)$ in the tDCS-BCI group. Moreover, right-tailed Fisher z-test revealed that the correlation between $\Delta FMA(0,2)$ and resting state $\Delta r\theta$, ΔTAR, and $\Delta TBAR$ was marginally stronger in the BCI group than in the tDCS-BCI group (p = 0.064, 0.076, 0.079). In the analysis of task state features, this trend was only observed for $\Delta r\theta$ (p = 0.076). Table.6.5 reports the correlation between all the ΔEEG features and $\Delta FMA(0,2)$. Also, the significant correlations are presented in figure 6.4.

Correlation between post-intervention EEG features and post-intervention FMA

The analysis of relation between post-intervention clinical score (FMA_{T2}) and post-intervention EEG features (EEG_{T2}) revealed that, in the BCI group, FMA_{T2} has statistically significant negative correlation with both task and resting state

TABLE 6.6: Correlation between post-intervention FMA score (FMA_{T2}) and post-intervention EEG features (EEG_{T2}).

EEG Features	tDCS		BCI	
	Rest	Task	Rest	Task
$r\delta_{T2}$	-0.22	-0.38	-0.25	-0.37
$r\theta_{T2}$	-0.26	-0.33	-0.61	-0.64
$r\alpha_{T2}$	0.31	0.43	0.21	0.23
$r\beta_{T2}$	0.04	0.43	***0.82**	****0.94**
PRI_{T2}	-0.44	***-0.67**	-0.55	-0.44
DAR_{T2}	-0.16	-0.35	-0.25	-0.16
TBR_{T2}	0.07	-0.41	***-0.76**	***-0.83**
TAR_{T2}	-0.52	-0.65	***-0.71**	***-0.71**
$TBAR_{T2}$	-0.39	-0.53	-0.66	***-0.69**
$pdBSI_{T2}$	-0.05	0.09	-0.51	-0.55
$rBSI_{T2}$	-0.27	-0.01	-0.59	-0.54

correlation coefficients, * implies p $<$ 0.05 and ** implies p $<$0.01

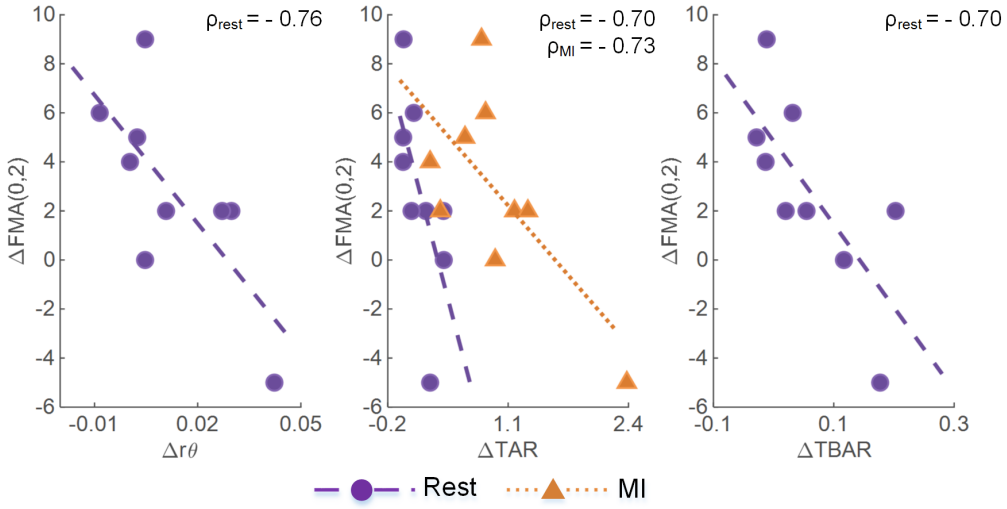

FIGURE 6.4: Statistically significant relationships for monitoring the evolution of intervention gains. All the panels represent the significant association observed between two-week intervention gains and intervention-induced changes in the EEG features in BCI group. No significant relationships where observed in the tDCS-BCI group.

TBR_{T2} ($p_{rest} = 0.030$, $p_{task} = 0.018$), and TAR_{T2} ($p_{rest} = 0.041$, $p_{task} = 0.046$) and a marginal negative trend with $r\theta_{T2}$ ($p_{rest} = 0.078$, $p_{task} = 0.072$), and $TBAR_{T2}$ ($p_{rest} = 0.061$, $p_{task} = 0.048$). Also, a strong positive correlation was observed between $r\beta_{T2}$ and FMA_{T2} ($p_{rest} = 0.020$, $p_{task} = 0.008$) in the BCI group. In tDCS-BCI group, only task state PRI_{T2} was significantly correlated with EEG_{T2} ($p = 0.038$). Complete correlation results are presented in Table.6.6.

6.4 Discussion

Previous studies have demonstrated the utility of QEEG features for post-stroke clinical prognosis and monitoring in acute/sub-acute stages [52]. This study demonstrated that QEEG features are informative in the chronic stage as well, pointing their potential use as rehabilitation biomarkers. In the BCI group, significant intervention-induced changes in resting state relative theta power, and marginally significant change in TAR, and TBAR were observed and these changes were negatively correlated with clinical gains. The task state features also resulted in similar negative correlations. These negative correlations signify that improvement in motor functions is associated with the reduction in power of low-frequency oscillations, which is in accordance with the previous literature [49, 52]. All these features have major involvement of theta band power and in acute stroke; theta band has been associated with the ischemic penumbra, a region with intact but deactivated neurons[215]. Moreover, pre and post- intervention FMA scores displayed positive correlation with the task state beta power in the BCI group and it indicates that presence of higher power in high frequency oscillations is associative of better motor status which is also reported in the stroke literature [49]. Hence, motor recovery in the BCI group can be inferred to be facilitated by training-induced reactivation of dysfunctional neuronal population. This inference is also supported by a recent report of CBF analysis performed on a subset cohort [192]. The restoration of CBF by perfusion of ischemic penumbra is associated with the reactivation of neuronal tissues, and a widespread change in CBF and its positive correlation with FMA change has been reported for the subset group, representing coherent conclusions from both EEG and CBF analysis [192]. Very different from the BCI group, significant changes in resting and task state inter-hemispheric brain asymmetry were characteristic to tDCS-BCI intervention. This indicates that tDCS indeed resulted in modification of hemispheric activations. Although, the observations are in accordance with the significant change in inter-hemispheric CBF asymmetry observed in the tDCS-BCI group alone[192], the changes were not correlated with the observed motor gains. Therefore, it is difficult to establish any direct relationship between brain asymmetry and functional motor gains, and more investigation is necessary to understand the exact mechanism of recovery following tDCS-BCI intervention.

Notably, both the tDCS-BCI and BCI groups resulted in similar clinical gains and despite the absence of any inter-group differences in pre-treatment conditions and

BCI training parameters, the QEEG features which changed significantly during these interventions were mutually exclusive. This indicates that similar clinical recovery may be achieved by different interventions through distinct mechanisms of neuronal repair. This justifies the rationale behind intervention-specific monitory biomarkers and their presence was validated in this study. Also, in the BCI group, the pre and post-intervention TBR showed significant correlation with the pre and post-intervention motor status, respectively. The post-intervention correlation was found to be specific to the BCI group, which indicates that TBR changed only following the BCI intervention and the final value of TBR was related to the final motor status. Biomarkers of this type can be used to assess patients' progress on a neurological scale when they are undergoing an intervention and can aid in recommending the appropriateness of an intervention.

The unique mechanisms of recovery facilitated by rehabilitative intervention also suggest the presence of a distinct set of intervention-specific prognostic biomarkers. In this study, for the tDCS-BCI group, a strong negative correlation of pre-intervention relative delta power, and PRI with two-week motor gains was observed, which implies that the presence of large value of slow oscillations is representative of poor expected recovery. Furthermore, the prediction of four-week gains in tDCS-BCI group also resulted in similar observations with relative delta power, DAR and PRI displaying significant negative correlations. These observations are consistent with the previous literature, where a high value of relative delta power, DAR and PRI has been associated with the poor prognosis in acute/sub-acute stages [55, 215, 219, 275, 283] and less intervention-induced motor recovery in the chronic stage [49]. Since the presence of large delta oscillations has been associated with severe ischemia and hypo-perfused neuronal population in the acute stage [53, 54, 213], it can be inferred that observed correlations may dictate the direct relationship between the extent of affected neuronal population and expected motor recovery. Distinct from the tDCS-BCI group, the prognostic information in the BCI group was entirely quantified using brain asymmetry features. A significant negative correlation was observed between two, four weeks clinical gains and pre-intervention pdBSI, rBSI; indicating that symmetrical pre-intervention brain activation favors motor recovery. This observation has been reported in the sub-acute state [219, 283], and this study confirmed the same relationship in the chronic stage as well. Importantly, a mutual exclusiveness in the significant prognostic features between two interventions was observed and the difference in the

strength of prognostic correlation was statistically significant for resting state PRI, relative delta power, pdBSI, and rBSI. These observations depict the existence of intervention-specific prognostic biomarkers which distinctly predict the clinical gains from a given intervention. These intervention-specific biomarkers quantify the expected interaction between the intervention and the patient, thereby uniquely predicting the rehabilitation gains following the given intervention. Following this approach, the clinical gains from all available interventions can be predicted and clinicians may then recommend the intervention with the highest predicted gains to the patient, thereby achieving maximum clinical recovery, better patient stratification and optimal allocation of resources. Although a vast number of studies have been conducted to investigate prognostic biomarkers of intervention-induced post-stroke motor recovery [24, 28, 30, 38], the lack of studies exploring same neurological features as a predictor for different interventions and common practice of reporting only positive results has made the task of identifying intervention-specific biomarkers difficult. Hence, more investigation in this direction is necessary, and a systematic review of prognostic biomarkers with a stratification based on rehabilitative interventions may shed some light on this topic.

Next, for both the interventions, we observed a very similar relationship of clinical features with both task and rest state QEEG features. There was no statistically significant difference in the strength of prognostic and monitory correlations between task and rest state data, which indicates that both types of features provide coherent results. However, only pdBSI and rBSI displayed considerable difference in the relationship of clinical features with task vs. rest state features. This difference can be mainly attributed to contralateral activation patterns associated the hand MI during the task state [284]. In our investigation, only resting state EEG features qualified as intervention-specific prognostic biomarkers on the statistical grounds. Yet, taking into account the absence of significant differences between task vs. rest state relationships, both task and rest features should be considered equally informative and further studies with a higher sample size may provide some conclusive remarks.

Finally, there are few limitations to this study. The main limitation is the small sample size from the statistical viewpoint which was restricted by the complexity and length of the rehabilitation protocol but it is at par with the other studies in this field [10]. Despite this, remarkably coherent results from both task and resting state

data are observed, and these results are consistent with the neuroimaging findings reported on the subset cohort [192], indicating the soundness of the results. Still, a confirmatory study with a higher sample size will be useful for verification of results of this study. Also, the primary motivation of this study was to demonstrate the possibility of intervention-specific prognostic and monitory biomarkers, and QEEG features were selected for this purpose because of their simplicity in calculations and interpretations. As the selected QEEG features lacked spatial resolution, further complementary EEG features, such as those derived from the signal and source space connectivity analysis may provide more comprehensive insights into the brain dynamics during motor recovery. Moreover, correlation analysis when accompanied with causal inferencing may provide more robust neurological interpretations of the observed results. Nonetheless, alone the capabilities of QEEG features to uniquely predict and monitor the intervention induced recovery and the envisioning of personalized rehabilitation, as done in this chapter, is highly relevant to clinical decision making.

6.5 Summary

In this study, it was found that the QEEG features can act as prognostic and monitory biomarkers in the chronic state post-stroke motor recovery following tDCS-BCI and BCI rehabilitation. Despite similar clinical recovery, the mechanism of neuronal recovery facilitated by these interventions were very different. The relative theta power was observed to be the signature monitory biomarker for BCI intervention whereas the tDCS group was characterized by a change in brain symmetry index. Also, pre-intervention relative delta power and power ratio index were the best predictors of clinical gains following tDCS-BCI intervention, whereas, the clinical gains following BCI intervention were best predicted using brain symmetry index. Consequently, prognostic and monitory biomarkers of motor recovery were observed to be significantly different between the two groups suggesting the possibility of intervention-specific biomarkers. This approach can be pursued to uniquely predict the expected response of a patient to an intervention and the intervention with the highest predicted gains may then be recommended to the patient, thereby enabling a highly personalized motor rehabilitation.

Chapter 7

Conclusions and Future Work

7.1 Conclusions

The objectives laid earlier in this thesis were aimed at improving the clinical outcomes of BCI-based post-stroke motor rehabilitation, firstly, by developing more accurate BCI systems and secondly, by providing guidelines for personalized rehabilitation. Therefore, the initial works presented in this thesis were focused on development of novel deep learning based methods for robust and accurate classification of motor imagery from EEG data for use in post-stroke motor rehabilitation. In the later part of the thesis, the emphasis was provided on identification of EEG based biomarkers for prognostication and monitoring of BCI-based motor rehabilitation to achieve better clinical outcomes by highly personalized rehabilitation.

To improve the classification accuracies of the BCI systems, first, a neurophysiologically motivated end-to-end CNN architecture named FBCNet was proposed in Chapter 3. Designed for subject-specific MI classification, FBCNet was targeted to learn generalizable discriminative features even in the presence of limited data and produce better classification accuracies. This aim was achieved by proposing a hybrid approach to MI classification, wherein, the complex feature learning capabilities of deep learning methods were leveraged and their sensitivity to small datasets was mitigated by incorporating the neurophysiological priors of MI in the architecture design. With this design philosophy, the proposed approach of FBCNet achieved significantly better classification accuracies than the state-of-the-art methods across 4 motor imagery datasets. Among them, since stroke patients were

the targeted population, the two large EEG datasets were collected from stroke patients. Moreover, with interpretability analysis, it was demonstrated that improved performance by FBCNet was driven by the effective learning of neurophysiologically relevant EEG feature. Furthermore, it was showed that there are differences in the MI data between healthy subjects and stroke patients and FBCNet can perform well on both healthy and patient data. Overall, the results of this work indicate that inclusion of neurophysiological priors while designing deep learning architectures, as done in FBCNet, will result in an architecture that is constrained enough that it can effectively focus on neurophysiological signatures even in the absence of large training datasets while being complex enough to effectively utilize a higher amount of training data when it is available and such an approach may lead to better classification results in the field of MI-BCI.

Following the better results, the FBCNet architecture was further modified to extract high level temporal information. To achieve this goal, in Chapter 4, two extensions of the FBCNet architecture were proposed. For this purpose, first, an architecture of FBCNet with High Level Temporal Information (FBCNet with HLTI) was presented. The FBCNet with HLTI architecture extended the temporal feature extraction capabilities of FBCNet with the use of a windowed Variance layer. Furthermore, to encapsulate the temporal dependence between the features from different time windows, the FBCNet with HLTI was expanded with an LSTM block to construct FBCNet+LSTM architecture. The classification performance of both of these architectures was evaluated using four diverse MI datasets. By achieving the best classification accuracies in most datasets, the FBCNet with HLTI architecture was observed to be able to successfully extract an additional temporal information while avoiding model overfitting. The FBCNet+LSTM resulted in best classification accuracies in one dataset and the results indicated that the FBCNet+LSTM may achieve better classification accuracies with a higher amount of training data. Collectively, the results presented in this work indicate that constrained extraction of EEG time domain information, as done in FBCNet with HLTI, may lead to improved classification accuracies in the EEG-BCI domain.

After validating the performance of the proposed architectures in single session MI classification, an inter-session classification, which is the general setting in stroke rehabilitation trials, was attempted. For this purpose, in Chapter 5, an extensive retrospective analysis of the EEG data from 25 stroke patients undergoing three

different BCI-mediated upper extremity motor rehabilitation interventions was presented from the MI classification perspective. Particularly, the performance on various classification algorithms on the multi-session stroke rehabilitation data was analyzed. The classification results indicated that the deep learning architectures, in particular, the previously proposed architecture of FBCNet, can achieve the best MI classification accuracies in BCI-mediated stroke rehabilitation trials. Furthermore, from the interpretability analysis, it was observed that the most robust signature of MI are observed in the motor regions of the brain and the models that learn to focus on this information can achieve higher classification accuracies during multi-session rehabilitation trials. Lastly, based on the spacial localization of the MI associated discriminative information, a stratification of the stroke patients was attempted. However, the differences between the different patient groups were observed to be statistically insignificant.

Finally, in Chapter 6, in an attempt to achieve personalized rehabilitation, a relationship between BCI-induced clinical improvements and pre-rehabilitation QEEG features was explored. In this work, it was found that the QEEG features can act as prognostic and monitory biomarkers in the chronic state post-stroke motor recovery following tDCS-BCI and BCI rehabilitation. Despite similar clinical recovery, the mechanisms of neuronal recovery facilitated by these interventions were observed to be very different. The relative theta power was observed to be the signature monitory biomarker for BCI intervention whereas the tDCS group was characterized by a change in brain symmetry index. Also, pre-intervention relative delta power and power ratio index were the best predictors of clinical gains following tDCS-BCI intervention, whereas, the clinical gains following BCI intervention were best predicted using brain symmetry index. Consequently, prognostic and monitory biomarkers of motor recovery were observed to be significantly different between the two groups suggesting the possibility of intervention-specific biomarkers. This approach can be pursued to uniquely predict the expected response of a patient to an intervention and the intervention with the highest predicted gains may then be recommended to the patient, which can enable a highly personalized motor rehabilitation.

Collectively, the research presented in this thesis indicated that EEG-based BCI systems can be used to characterize and promote recovery of stroke impaired motor

functions in a personalized manner and neurophysiologically inspired CNN architectures can significantly advance the technology of MI detection in rehabilitative BCI systems.

7.2 Future Research Directions

The work presented in this thesis has left some questions unanswered and they represent the opportunities for possible future works.

7.2.1 Subject-Independent BCI Systems

The classification algorithms presented in this thesis were all targeted towards the case of subject-specific classification analysis. In subject-specific classification, a separate BCI model is trained for each subject using that subject's labelled data. Although this approach has been known to achieve the best classification accuracies, particularly with the traditional machine learning algorithms, it is not the most user-friendly approach. In subject-specific BCI systems, the user first needs to participate in a calibration session and the data from this session is then used to build the classification model. Unlike subject-specific systems, the subject-independent systems, which do not need any training for the use on a new subject, are much more desirable. In subject-independent systems, the classification algorithms are trained with a data from a pool of multiple subjects and this trained model is then used for any new subject's brain state classification. This subject-independent approach of BCI classification offers two advantages. First, since these systems are trained using the data from multiple subjects, they offer an opportunity to create big training datasets by pooling the labelled data from large number of subjects and can solve the classical problem of small datasets in the BCI domain. Second, since these systems need not be calibrated for any particular subject, they offer a possibility of out-of the box use. Therefore, considering these two highly desirable advantages, many studies have explored the possibility of subject-independent BCI systems [23, 285–288]. However, owing to the inter-subject variability in the EEG data, these systems, particularly the traditional machine learning systems, have mostly been observed to be less accurate than their subject-specific counterparts. Although, the problem of inter-subject

variability can not be completely avoided, its effects can be partially mitigated by the use of deep learning models with very high complexity which are trained using the data from diverse subject groups. Such model may offer a possibility to encode all the probable signatures of any mental tasks. Pursuing this direction, with the availability of enough training data, more complex deep learning models can be used in the BCI domain, leading to higher classification accuracies.

Furthermore, more advanced transfer learning based algorithms can be explored to reduce the effect of inter-subject variability on the classification performance. In particular, the techniques of transductive transfer learning like sample selection bias, co-variate shift, and domain adaptation may provide more effective ways for accumulating the knowledge from a large pool of subjects [289, 290]. Also, the BCI data differs from the traditional transfer learning setting because, in BCI, the source domain data does not come from a single source, but it is an aggregation of multiple heterogeneously distributed distributions. Therefore, although the above-mentioned techniques of transfer learning may prove to be beneficial, special attention also needs to be paid to the intricacies of the BCI data.

7.2.2 Fine Movement Decoding with Deep learning

Rehabilitation of impaired fine motor movements, like precise movements of various finger joints is one of the most challenging problems in the post-stroke rehabilitation domain. Moreover, impaired fine motor movements result in high extent of disabilities and greater effect on activities-of-daily-living. Therefore, following the rehabilitation of major joint movements, the restoration of fine movements is the next overarching objective of any rehabilitative interventions. In this regards, the deployment of BCI systems for fine movements restoration necessitates an exploration of fine movement decoding from the EEG signals. For this purpose, a few studies have explored the decoding of hand movements in different directions from the EEG data [140]. Furthermore, one study has explored the possibility of decoding different finger movements using EEG data [291]. So, although these preliminary works indicate the feasibility of fine movement decoding, more exploration in this direction, particularly with deep learning architectures, is essential.

7.2.3 Source Space Connectivity Analysis for the Characterization of Post-Stroke Motor Recovery

Following the classification analysis, in the present work, it was observed that the QEEG features like EEG power in different frequency bands can successfully quantify the post-stroke brain-dynamics. However, these features do not provide any information about functional interactions between neural systems operating in each frequency band. Since it is well accepted in scientific community that stroke affects these neuronal communications, the quantification of these functional interactions in different brain areas using coherence between the EEG signal recorded at different electrodes may provide the prognostic and monitory utility in the post-stroke motor recovery. This analysis has been observed to be effective in predicting the motor gains during different rehabilitative interventions [292] and similar analysis can be performed for BCI-based interventions.

Since the signal space EEG recorded at any electrode is a linear combination of activations produced by multiple cortical sources, the coherence analysis in the signal space suffers from an inherent drawback of limited neurological interpretations [293]. One way to circumvent this problem is to calculate the underlying cortical activations using the observed EEG activity and this is the principle of EEG source imaging (ESI). ESI provides the activations of the underlaying cortical sources using signal space EEG and has direct neurological interpretations. Despite some debates about the validity of ESI, few studies have reported its utility in the stroke research as well. Therefore, this analysis may provide better understanding of neuro-physiological events post-stroke.

Along with the coherence analysis, which provides the information about the interactions between any two signal pairs, the analysis of post-stroke modulations of the entire brain network can be performed using connectivity measures. Cortical connectivity measures give an idea of the statistical dependencies between the time-series data of different brain regions (Functional Connectivity (FC)) and the causal interactions between them (Effective Connectivity (EC)) [140]. This analysis of FC and EC has been performed in some post-stroke EEG studies [36, 48, 235] and has been observed to effectively quantify the post-stoke motor recovery during standard therapy. Therefore, the changes in FC and EC can be investigated to quantify the neuronal changes during BCI-mediated rehabilitation [294].

Appendix A

Additional Information for FBCNet

A.1 Role of Variance Layer in FBCNet Training

FBCNet proposes a novel Variance layer for effective extraction of temporally discriminative information. Variance layer characterizes a time series by computing its variance. So, in the forward pass, for any time varying signal, $x(t)$, the output of the Variance layer is given by,

$$v = Var(x(t)) = \frac{1}{T}\sum_{t=1}^{T}(x_t - \mu)^2 \tag{A.1}$$

where, T is total number of time-points and μ is the mean of $x(t)$.

The Variance layer doesn't contain any learnable parameters but it affects the network training by redistribution of the incoming loss during backpropagation phase. In the backpropagation phase, the learnable parameters of the network are updated based on the gradient of the loss function. So, for any network, if $L_v = \frac{\partial L}{\partial v}$ is the incoming loss at the variance layer then the backpropagated loss from this layer with respect to the input $x(t)$, L_{x_t}, is given by,

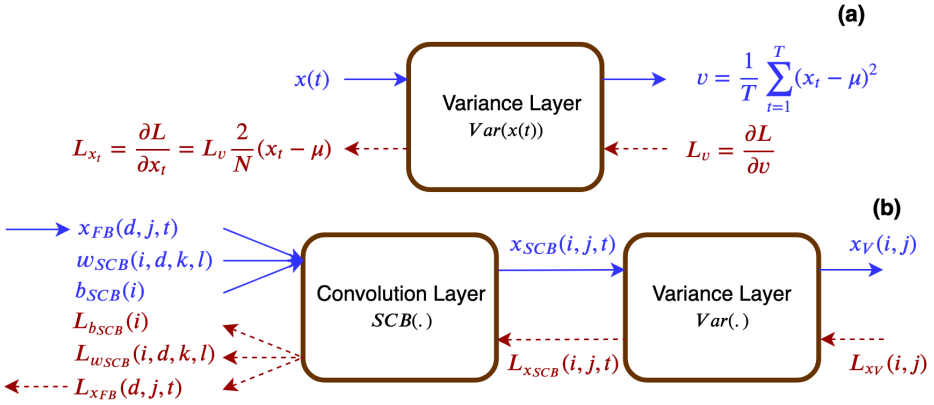

FIGURE A.1: The role of Variance Layer. Part (a) presents the forward and backward pass operations by the proposed Variance layer. In the forward pass, this layer computes the variance of the input time series. whereas, in the backward pass it redistributes the incoming loss proportional to the deviation of input time-series from its mean. Part (b) presents how the redistribution of loss by Variance layer affects the downstream learning of convolution layer in FBCNet.

$$L_{x_t} = \frac{\partial L}{\partial x_t} = \frac{\partial L}{\partial v} \cdot \frac{\partial v}{\partial x_t} = L_v \frac{2}{T}(x_t - \mu) \tag{A.2}$$
$$\therefore \quad L_{x_t} \propto (x_t - \mu)$$

Therefore, as it can be observed from (A.2), the Variance layer redistributes the incoming loss proportional to the deviation of x_t from the mean of the signal.

The effect of loss redistribution by Variance layer on FBCNet learning can be understood by backpropagating the loss from variance layer to the Convolution layer in Spatial Convolution Block (SCB) which is the first and the only layer with learnable parameters prior to the Variance layer. For simplicity of understanding, let us assume that SCB is only composed of Depthwise Convolution layer with kernel weights $w_{SCB}(i,d,k,l) \in \mathbb{R}^{(m\times N_b)\times 1\times C\times 1}$ and bias units $b_{SCB}(i) \in \mathbb{R}^{(m\times N_b)}$. Then the output of SCB, $x_{SCB_{i,j,t}}$ is given as,

$$x_{SCB_{i,j,t}} = \sum_k \sum_l w_{i,d,k,l} \cdot x_{FB_{d,j+k-1,t+l-1}} + b_i \tag{A.3}$$

Here, owing to the Depthwise Convolution layer, each CNN filter w only receives the input from one depth channel d from $x_{FB_{d,j,t}}$.

Assuming that $L_{x_{v_{i,j}}} = \frac{\partial L}{\partial x_{V_{i,j}}}$ is a loss backpropagated at the output of variance layer, following (A.2), the loss at the output of SCB, $L_{x_{SCB_{i,j,t}}}$, will be given by,

$$L_{x_{SCB_{i,j,t}}} = \frac{\partial L}{\partial x_{SCB_{i,j,t}}} = L_{x_{v_{i,j}}} \cdot \frac{2}{T}(x_{SCB_{i,j,t}} - \mu_{i,j}) \tag{A.4}$$

And backpropagation of loss to the w_{SCB} and b_{SCB} will be,

$$\begin{aligned} L_{w_{SCB_{i,d,k,l}}} &= \frac{\partial L}{\partial w_{SCB_{i,d,k,l}}} \\ &= \sum_j \sum_t L_{x_{SCB_{i,j,t}}} \cdot x_{FB_{d,j+k-1,t+l-1}} \\ &= \sum_j \sum_t L_{x_{v_{i,j}}} \frac{2}{T}(x_{SCB_{i,j,t}} - \mu_{i,j}) \cdot x_{FB_{d,j+k-1,t+l-1}} \end{aligned} \tag{A.5}$$

$$\begin{aligned} L_{b_{SCB_i}} &= \frac{\partial L}{\partial b_{SCB_i}} \\ &= \sum_j \sum_t L_{x_{SCB_{i,j,t}}} \\ &= \sum_j \sum_t L_{x_{v_{i,j}}} \frac{2}{T}(x_{SCB_{i,j,t}} - \mu_{i,j}) \end{aligned} \tag{A.6}$$

The $L_{w_{SCB}}$ and $L_{b_{SCB}}$ will then be used to update the w_{SCB} and b_{SCB} according to the optimization algorithm. Therefore, from (A.5) and (A.6), due to the introduction of Variance layer, the contribution of every time-point from x_{SCB} in the update of w_{SCB} and b_{SCB} will be proportional to its deviation from the mean of x_{SCB}. In this manner, in the presence of Variance layer, the downstream convolutional filters will be trained to maximize the class-discriminative variance at the output.

A.2 Details of Evaluation Datasets

The performance of FBCNet was tested on following four diverse datasets:

1. *BCIC-IV-2A Data*: A 4 class MI data from BCI Competition IV Dataset 2A [250].

2. *Korea Uni. Data*: A 2 class MI data from Korea University EEG dataset [251].

3. *Stroke Data: A*: A 2 class MI vs rest dataset [119].

4. *Stroke Data: B*: A 2 class MI vs rest dataset [88].

Further details of these datasets are as follows:

A.2.1 BCIC-IV-2A Data

The BCIC-IV-2A Data consists of EEG data from 9 subjects collected over 2 sessions. The data contains 4 classes; MI of left, and right hands, feet, and tongue. The EEG data has been recorded using 22 electrodes with a sampling frequency of 250 Hz. There are 72 trials of every class in each session and every trial is of 4s duration. In this analysis, all 22 channels data was used. The classification performance was primarily evaluated using the entire 4 seconds data. Also, for the purpose of matching the previously reported accuracies on baseline architectures and to validate our implementation of these architectures, the classification accuracies on a data epoched at [0.5, 2.5] seconds post-cue onset were also evaluated.

A.2.2 Korea Uni. Data

Korea Uni. Data contains 2 sessions of 2-class EEG-MI data from 54 healthy subjects [251]. The MI of left and right hand are the two classes in the data and there are in total 100 trials of each class per session and each trial is 4s in length. The EEG data has been originally recorded at 1000Hz using 62 electrodes. In this analysis, as it is done in the original work [251], the selected 20 channels in the motor region were used for the classification task (FC-5/3/1/2/4/6, C-5/3/1/z/2/4/6, and CP-5/3/1/z/2/4/6). Moreover, one of the baseline architectures, the Deep ConvNet is designed for the EEG data sampled at 250 Hz. Therefore, to maintain the compatibility and fairness of comparison, the data was down-sampled by a factor of 4 to have a sampling frequency of 250 Hz. Moreover, this analysis setting results in approximately similar EEG trial dimensions ($channels \times time$) across all the datasets.

A.2.3 Stroke Data: A

Stroke Data: A is part of post-stroke BCI motor rehabilitation trial wherein 37 stroke patients are screened for their ability to control MI-BCI [119]. The MI of stroke-paralyzed hand and rest are the two classes in the data and there are in total 80 trials of each class for every patient. Every trial is of 4 seconds duration and the EEG data is collected using 27 channels sampled at 250Hz with a hardware bandpass filtering from 0.5 -40Hz. In the present analysis, the entire 27 channel, 4s data was used for classification. Also, some of the important demographic information for this dataset is presented in Table A.1.

TABLE A.1: Demographic information of stroke patients from Stroke Data: A

Subject No.	1	2	3	4	5	6	7	8	9	10
Gender	M	F	M	M	M	F	M	M	M	F
Affected Hand	L	R	L	R	R	L	L	R	R	L
Subject No.	11	12	13	14	15	16	17	18	19	20
Gender	M	M	M	F	F	M	M	F	M	M
Affected Hand	L	L	L	L	R	R	L	L	L	L
Subject No.	21	22	23	24	25	26	27	28	29	30
Gender	M	M	F	M	M	M	M	M	F	M
Affected Hand	R	R	L	R	R	L	R	R	R	L
Subject No.	31	32	33	34	35	36	37			
Gender	M	M	M	F	M	M	M			
Affected Hand	R	L	R	L	L	R	L			

A.2.4 Stroke Data: B

Stroke Data: B is also a part of post-stroke BCI motor rehabilitation trial and similar to Stroke Data: A, contains a 2-class data with MI of stroke-paralyzed hand being one class and rest being the other class [88]. This dataset comprises of data from 34 stroke patients with 160 trials per patient. The data collection protocol is the same as that of the Stroke Data: A with the 4s of EEG data collected per trial using 27 channels sampled at 250 Hz. For this dataset as well, the entire 27 channel, 4s data was used for classification. Also, some of the important demographic information for this dataset is presented in Table A.2.

TABLE A.2: Demographic information of stroke patients from Stroke Data: B

Subject No.	1	2	3	4	5	6	7	8	9	10
Gender	F	M	F	M	M	M	M	M	M	M
Affected Hand	R	L	R	R	L	R	R	L	R	L
Subject No.	11	12	13	14	15	16	17	18	19	20
Gender	M	F	F	M	M	M	N	M	M	M
Affected Hand	L	L	L	L	R	L	N	R	L	L
Subject No.	21	22	23	24	25	26	27	28	29	30
Gender	M	M	F	F	M	M	M	F	F	M
Affected Hand	L	R	L	L	R	R	R	L	L	L
Subject No.	31	32	33	34						
Gender	M	M	F	M						
Affected Hand	L	L	R	R						

A.3 Implementation of Baseline Classification Methods

A.3.1 The Traditional Approach: FBCSP-SVM

The FBCSP-SVM algorithm was implemented as per its authors' recommendations in [142]. As done in the original work [142], the raw EEG data was decomposed using 9 narrow-band bandpass Chebyshev Type II filters, each of 4Hz bandwidth, spanning from 4 to 40 Hz (4-8, 8-12, ..., 36-40 Hz) with transition bandwidth of 2Hz and stopband ripple of 30dB. The narrow-band EEG was then spatially filtered using CSP algorithm and 4 most discriminative CSP filters from each band were extracted. The log-variance of the EEG data filtered using CSP filters was extracted as a feature. From these 36 features (9 frequency bands $\times$ 4 features per band) best 8 features were selected using the MIBIFPW algorithm [245]. An SVM classifier was then trained using the selected features to classify the trial into one of the two classes. An epsilon - support vector regression with a radial basis function kernel flavour of SVM was used for the classification [295].

The CSP algorithm is designed for a binary classification problem. Therefore, to classify the 4 class BCIC-IV-2A Data, a One-Verses-Rest (OVR) strategy was used. In this strategy, 4 binary classifiers were trained to classify one class from the remaining 3 classes. Then each trial was assigned to the class for which it received

the maximum SVR score among all 4 classifiers. Due to this approach, for BCIC-IV-2A Data, in total 16 CSP filters were extracted for each band (4 OVR-models $\times$ 4 filters per model).

Lastly, since both the FBCSP and FBCNet use the multi-view filtered EEG representation, the same filter bank was used in both of these algorithms for fairness in comparison.

A.3.2 Existing CNN Architectures : Deep ConvNet and EEGNet

The Deep ConvNet [20] and EEGNet-8,2 [22] were implemented following the descriptions found in the respective papers. One major modification was done to the EEGNet-8,2 architecture due to the difference in the sampling frequencies of the data. The original EEGNet was proposed for the data with 128 Hz sampling frequency. However, all 4 datasets in this work have a sampling frequency of 250Hz. Therefore, from the original architecture, the lengths of temporal kernels and temporal pooling layers were multiplied by 2 to correspond approximately to the sampling rate in this analysis. Deep ConvNet and EEGNet-8,2 were trained in the exact same manner as that of the FBCNet. The exact implementations of these architectures, as used in this work, are available at `https://github.com/ravikiran-mane/FBCNet`.

A.4 Single Subject Classification Accuracies

The detailed results of classification accuracies achieved by baseline methods and FBCNet along with the statistical significance are provided in Table A.3. Moreover, for the purpose of reproducibility and future comparisons, the single subject MI classification accuracies for all analyses are presented in Table A.4, Table A.5, and Table A.6.

TABLE A.3: Subject-specific classification accuracy: All analyses (mean±std)

Dataset	Analysis	FBCSP-SVM^{+}	Deep Convnet*	EEGNet-8,2$^{\times}$	FBCNet†
BCIC-IV-2A Data	CV	**75.89±13.87**	72.20±12.12	73.13±8.52	75.28±14.31
Korea Uni. Data	CV	64.61±17.07$^{\times\dagger}$	68.33±12.34$^{\times\dagger}$	70.89±13.01^{+*}	**73.36±14.20**$^{+*}$
Stroke Data: A	CV	71.37±14.52†	68.81±12.02†	69.15±12.94†	**75.49±14.17**$^{+*\times}$
Stroke Data: B	CV	74.14±14.35†	71.11±8.79$^{\times\dagger}$	73.48±8.05*	**77.39±13.99**$^{+*}$
BCIC-IV-2A Data	HO	68.06±14.11†	72.22±14.35	73.15±9.29	**74.11±13.40**$^{+}$
Korea Uni. Data	HO	60.36±14.97†	60.77±11.42$^{\times\dagger}$	63.63±11.08*	**65.75±13.07**$^{+*}$

The best performing method for each analysis is highlighted in boldface. To indicate statistically significant difference ($p < 0.05$) between any two methods, every method (column) is marked with a call-sign ($^{+}$, *, $^{\times}$, †, ‡). The presence of any method's call-sign in any other method's column represents a statistically significant difference in classification accuracies between those two methods. CV: 10-fold cross validation, HO: Hold out analysis with separate test session.

TABLE A.4: Classification accuracies for each subject in BCIC-IV-2A Dataset.

Subject No.	10-fold cross validation				Hold Out			
	FBCSP-SVM	Deep Convnet	EEGNet-8,2	FBCNet	FBCSP-SVM	Deep Convnet	EEGNet-8,2	FBCNet
1	85.31	71.03	72.86	83.75	77.78	78.13	79.51	84.38
2	64.51	52.05	56.25	60.18	55.56	45.14	61.11	53.47
3	90.00	82.41	83.39	89.73	79.51	85.42	88.54	85.76
4	64.02	58.93	67.54	61.43	63.19	67.01	71.53	71.53
5	73.66	73.57	76.38	77.10	53.47	77.43	71.18	61.81
6	52.72	62.50	67.05	53.62	46.88	53.13	59.03	57.29
7	92.10	79.33	73.53	94.06	86.81	86.46	71.53	87.85
8	88.62	82.41	80.27	85.45	81.25	78.13	80.56	81.94
9	72.10	87.59	80.94	72.19	68.06	79.17	75.35	82.99
Avg	**75.89**	72.20	73.13	75.28	68.06	72.22	73.15	**74.11**
Std	13.87	12.12	8.52	14.31	14.11	14.35	9.29	13.40

TABLE A.5: Classification accuracies for each subject in Korea Uni. Dataset.

Subject No.	10-fold cross validation				Hold out			
	FBCSP-SVM	Deep Convnet	EEGNet-8,2	FBCNet	FBCSP-SVM	Deep Convnet	EEGNet-8,2	FBCNet
1	64.00	53.00	56.00	68.00	69.50	56.50	56.00	74.00
2	99.00	73.50	73.00	98.00	63.00	62.50	70.50	71.00
3	91.00	65.50	78.50	91.00	92.00	65.00	75.00	89.00
4	52.50	79.50	78.00	74.50	46.50	65.50	72.50	57.00
5	90.50	78.50	79.00	87.50	69.00	54.00	61.50	61.50
6	68.00	89.00	89.00	88.50	68.50	92.00	91.50	84.00
7	63.00	78.00	84.00	71.50	56.50	49.50	61.50	65.00
8	56.50	81.50	83.00	77.00	51.50	63.00	66.50	60.50
9	52.00	51.50	49.00	69.00	48.00	53.00	49.50	66.50
10	51.00	55.50	56.50	58.50	52.00	53.50	53.00	64.00
11	53.50	57.00	65.50	46.00	52.00	56.50	50.00	55.50
12	62.50	81.50	81.50	76.50	52.00	58.50	62.50	58.00
13	67.00	71.00	68.50	66.50	47.50	54.50	55.50	50.50
14	48.00	63.00	64.00	59.00	50.50	57.00	58.50	58.50
15	52.50	91.50	97.00	89.50	48.00	68.50	67.00	58.00
16	59.00	62.00	71.50	67.50	52.00	76.00	86.00	66.50
17	54.50	59.50	64.00	68.50	49.50	52.50	56.00	65.50
18	89.00	49.50	55.50	91.00	76.50	45.00	57.00	80.00
19	80.00	61.00	69.00	81.50	64.50	53.00	66.50	63.00
20	41.50	62.00	60.50	56.50	43.50	56.50	60.00	62.00
21	93.50	56.00	69.50	94.50	92.00	52.00	65.00	86.00
22	80.00	58.50	52.50	84.00	57.50	55.50	53.00	68.50
23	54.00	55.00	46.50	56.50	61.50	46.50	48.00	56.00
24	49.00	50.00	53.50	48.00	56.00	46.50	50.50	47.50
25	50.00	67.00	70.50	52.50	53.50	85.00	81.00	57.00
26	50.00	79.50	78.50	69.00	52.50	72.50	77.00	69.50
27	50.00	77.50	80.50	64.00	54.00	73.50	76.50	57.50
28	97.00	95.50	95.00	96.50	90.50	60.50	67.50	83.00
29	89.50	83.50	81.50	86.00	97.00	93.50	66.50	96.50
30	73.00	72.50	74.00	74.50	60.50	58.00	59.00	61.00
31	57.00	83.00	84.00	72.00	51.50	71.50	71.00	60.00
32	72.50	58.50	57.50	71.50	69.50	54.50	56.00	67.00
33	87.50	75.50	75.50	91.00	72.00	65.50	61.50	83.00
34	49.00	63.00	64.00	56.50	45.50	58.50	58.00	55.50
35	63.00	100.00	100.00	98.50	54.50	87.00	90.00	66.00
36	97.50	73.00	95.50	98.50	97.50	77.00	90.00	96.50
37	89.50	43.00	47.00	93.00	89.00	50.00	49.50	92.00
38	57.50	66.50	67.50	59.50	50.50	52.00	72.00	49.00
39	57.00	68.50	69.50	70.50	49.50	53.00	62.00	57.50
40	46.50	61.50	62.00	59.50	51.00	70.00	64.00	57.00
41	57.00	59.00	57.00	61.50	49.00	48.50	53.50	57.00
42	50.50	66.50	69.00	60.00	52.00	68.00	68.00	62.50
43	80.50	81.00	86.50	81.50	68.50	51.50	50.50	50.00
44	92.50	75.50	83.00	91.00	94.50	59.50	78.00	95.50
45	84.50	63.00	65.00	82.00	70.50	50.00	55.50	77.50
46	47.50	69.00	70.50	66.50	54.00	66.00	58.00	81.00
47	49.50	66.00	73.00	70.00	49.00	69.00	71.00	59.50
48	48.00	85.00	83.50	81.50	45.00	55.50	59.50	56.50
49	58.00	63.00	66.00	68.00	49.00	50.50	49.00	59.50
50	47.50	57.00	55.50	61.50	55.00	54.50	53.00	50.50
51	53.00	70.00	74.00	65.50	51.50	59.50	61.50	55.50
52	63.00	63.00	75.50	77.00	61.50	67.00	68.00	63.00
53	45.00	61.50	66.50	58.00	52.00	58.50	63.00	58.00
54	54.50	59.50	55.50	55.50	50.00	48.50	53.00	48.50
Avg	64.61	68.33	70.89	**73.36**	60.36	60.77	63.63	**65.75**
Std	17.07	12.34	13.01	14.20	14.97	11.42	11.08	13.07

TABLE A.6: Classification accuracies for stroke patients from both stroke datasets.

Subject No.	Stroke Data: A				Stroke Data: B			
	FBCSP-SVM	Deep Convnet	EEGNet-8,2	FBCNet	FBCSP-SVM	Deep Convnet	EEGNet-8,2	FBCNet
1	74.23	68.65	73.82	75.60	73.75	66.88	68.66	73.57
2	51.70	49.11	45.54	50.27	78.54	65.79	71.42	77.83
3	96.79	95.36	94.73	98.75	59.55	68.93	71.79	71.88
4	49.55	47.95	43.75	48.93	46.21	61.42	65.79	57.54
5	77.41	77.68	78.48	79.91	84.79	73.92	80.29	80.46
6	96.88	80.64	80.73	93.75	82.14	90.98	88.48	92.14
7	67.32	73.04	70.80	74.46	82.29	77.79	79.67	82.25
8	90.45	83.13	87.59	88.39	55.08	50.00	56.46	65.25
9	77.14	56.16	58.57	75.27	82.95	77.23	81.61	88.04
10	78.75	71.79	79.55	80.71	53.04	72.83	65.79	53.79
11	86.43	76.70	70.18	92.95	73.66	69.02	69.55	78.66
12	56.07	60.63	59.29	65.71	86.08	67.79	72.25	85.46
13	53.52	58.17	48.09	55.66	91.16	78.66	76.70	92.23
14	61.95	60.21	64.58	68.91	53.92	73.50	74.67	50.67
15	96.13	81.42	83.92	96.71	80.63	65.45	68.93	86.52
16	62.75	60.13	61.01	69.71	65.79	65.08	70.71	60.83
17	43.76	57.05	51.12	54.42	53.83	72.75	70.79	56.33
18	64.14	67.85	69.36	74.40	73.21	61.88	67.59	77.14
19	79.84	75.26	77.48	83.50	90.00	70.00	73.39	90.00
20	60.88	78.38	77.04	63.38	72.05	67.86	65.89	76.70
21	71.14	63.15	59.80	74.48	57.14	62.32	67.95	53.21
22	77.46	86.63	84.75	87.88	86.67	72.75	77.17	82.88
23	73.54	67.21	72.33	78.75	78.42	68.92	72.21	78.92
24	62.23	80.18	74.29	73.13	81.34	72.23	81.88	82.77
25	71.46	72.18	81.76	80.55	53.13	67.08	70.96	73.38
26	67.68	62.68	61.61	72.23	91.96	78.30	79.91	94.73
27	91.61	87.78	87.07	94.91	83.75	72.77	67.86	86.88
28	56.88	53.30	56.34	56.43	87.95	71.70	74.11	91.70
29	79.57	74.48	69.94	84.83	66.92	66.92	72.00	68.92
30	92.95	79.89	84.52	94.82	81.52	67.14	61.43	80.89
31	81.25	78.04	78.66	89.29	97.50	81.13	82.25	99.38
32	60.98	61.61	61.52	72.41	50.08	58.13	66.25	53.13
33	60.67	58.38	54.88	51.96	75.98	94.46	94.64	88.39
34	71.84	47.32	53.02	77.77	89.64	85.98	89.20	98.66
35	67.96	62.29	67.92	79.71				
36	46.07	56.25	59.20	51.07				
37	81.71	75.47	75.51	81.58				
Avg	71.37	68.81	69.15	**75.49**	74.14	71.11	73.48	**77.39**
Std	14.52	12.02	12.94	14.17	14.35	8.79	8.05	13.99

A.5 Classification accuracies in ablation study

A.5.1 Role of the Variance layer

To understand the role of Variance layer in improved accuracy achieved by FBC-Net, an ablation analysis was performed. In this analysis, the temporal feature extraction was performed using various alternatives of Variance layer. The detailed results of this analysis are presented in Table A.7.

TABLE A.7: Subject-specific classification accuracy using FBCNet with different temporal feature extraction layers

Dataset	Analysis	Max^{+}	Average*	Variance$^{\times}$	Log-Variance†	Standard Deviation‡
BCIC-IV-2A Data	CV	62.77±14.12$^{*\times\dagger\ddagger}$	69.52±14.03$^{+\times\dagger\ddagger}$	**75.28±14.31**$^{+*\ddagger}$	72.99±13.88^{+*}	72.43±14.72$^{+*\times}$
Korea Uni. Data	CV	63.31±12.73$^{*\times\dagger\ddagger}$	68.09±12.11$^{+\times\dagger\ddagger}$	**73.36±14.20**$^{+*\dagger\ddagger}$	70.49±13.52$^{+*\times}$	69.99±14.11$^{+*\times}$
Stroke Data: A	CV	70.13±12.54$^{*\times\dagger\ddagger}$	63.07±11.76$^{+\times\dagger\ddagger}$	**75.49±14.17**$^{+*\ddagger}$	74.93±13.89$^{+*\ddagger}$	73.52±13.97$^{+*\times\dagger}$
Stroke Data: B	CV	70.55±14.13$^{*\times\dagger\ddagger}$	65.24±10.73$^{+\times\dagger\ddagger}$	**77.39±13.99**$^{+*\ddagger}$	76.44±13.51^{+*}	75.66±13.27$^{+*\times}$
BCIC-IV-2A Data	HO	58.87±12.54$^{*\times\dagger\ddagger}$	67.79±13.20$^{+\times}$	**74.11±13.40**$^{+*\dagger\ddagger}$	68.90±10.93$^{+\times}$	69.79±14.73$^{+\times}$
Korea Uni. Data	HO	56.59±8.52$^{\times\dagger\ddagger}$	58.83±10.03$^{\times\dagger\ddagger}$	**65.75±13.07**$^{+*\dagger\ddagger}$	62.59±11.90$^{+*\times}$	63.24±12.26$^{+*\times}$

The best performing method for each analysis is highlighted in boldface. To indicate statistically significant difference ($p < 0.05$) between any two methods, every method (column) is marked with a call-sign ($^{+}$, *, $^{\times}$, †, ‡). The presence of any method's call-sign in any other method's column represents a statistically significant difference in classification accuracies between those two methods. CV: 10-fold cross validation, HO: Hold out analysis with separate test session.

A.5.2 Role of Number of Convolutional Filters per Frequency Band

The classification accuracies using FBCNet with different number of convolutional filters per frequency band (m) are presented in Table A.8.

TABLE A.8: Subject-specific classification accuracy using FBCNet with different number of convolutional filters per frequency band (m)

Dataset	Analysis	m = 2^{+}	m = 4*	m = 8$^{\times}$	m = 16†	m = 32‡
BCIC-IV-2A Data	CV	69.29±14.10$^{\times\dagger\ddagger}$	72.83±14.87$^{\times\dagger\ddagger}$	74.58±15.00^{+*}	75.28±14.31^{+*}	**75.54±14.54**$^{+*}$
Korea Uni. Data	CV	72.52±14.57†‡	73.36±14.20†	73.25±14.80†	**74.28±14.26**$^{+*\times}$	73.84±14.56^{+}
Stroke Data: A	CV	74.61±14.42$^{\times\dagger\ddagger}$	75.49±14.17‡	76.13±14.12$^{+\ddagger}$	76.29±14.68^{+}	**76.86±13.59**$^{+*\times}$
Stroke Data: B	CV	76.56±13.80$^{\times\dagger\ddagger}$	77.39±13.99‡	77.97±13.69^{+}	78.41±13.51^{+}	**78.47±13.07**$^{+*}$
BCIC-IV-2A Data	HO	64.81±14.03$^{*\times\dagger\ddagger}$	69.87±13.51$^{+\dagger}$	71.22±14.40$^{+\dagger}$	**74.11±13.40**$^{+*\times}$	71.87±15.91^{+}
Korea Uni. Data	HO	65.30±13.60	65.75±13.07	65.74±13.24	**66.42±13.25**	66.31±13.41

The best performing method for each analysis is highlighted in boldface. To indicate statistically significant difference ($p < 0.05$) between any two methods, every method (column) is marked with a call-sign ($^{+}$, *, $^{\times}$, †, ‡). The presence of any method's call-sign in any other method's column represents a statistically significant difference in classification accuracies between those two methods. CV: 10-fold cross validation, HO: Hold out analysis with separate test session.

Appendix B

Additional Information for with High Level Temporal Information

B.1 Detailed Classification Accuracies

The detailed results of classification accuracies achieved by baseline methods, FBCNet with HLTI, and FBCNet+LSTM along with the statistical significance are provided in Table B.1.

Table B.1: Subject-specific classification accuracy: All analyses (mean)

Dataset	Analysis	FBCSP-SVM	Deep ConvNet	EEGNet-8,2	FBCNet	FBCNet with HLTI	FBCNet+ LSTM
BCIC-IV-2A Data	CV	75.89^{Δ}	72.20	73.13	75.54^{Δ}	$\mathbf{77.89}^{\Delta}$	$68.22^{+\dagger\ddagger}$
Korea Uni. Data	CV	$64.61^{\times\dagger\ddagger\Delta}$	$68.33^{\times\dagger\ddagger\Delta}$	70.89^{+*}	73.84^{+*}	73.69^{+*}	$\mathbf{74.07}^{+*}$
Stroke Data: A	CV	$71.37^{\dagger\ddagger\Delta}$	$68.81^{\dagger\ddagger\Delta}$	$69.15^{\dagger\ddagger\Delta}$	$76.86^{+*\times}$	$\mathbf{77.99}^{+*\times\Delta}$	$76.30^{+*\times\ddagger}$
Stroke Data: B	CV	$74.14^{\dagger\ddagger\Delta}$	$71.11^{\times\dagger\ddagger\Delta}$	$73.48^{*\dagger\ddagger\Delta}$	$78.47^{+*\times\ddagger}$	$\mathbf{81.47}^{+*\times\dagger\Delta}$	$79.09^{+*\times\ddagger}$
BCIC-IV-2A Data	HO	$68.06^{\ddagger}$	72.22^{Δ}	73.15^{Δ}	71.87^{Δ}	$\mathbf{74.31}^{+\Delta}$	$64.20^{*\times\dagger\ddagger}$
Korea Uni. Data	HO	$60.36^{\dagger\ddagger\Delta}$	$60.77^{\times\dagger\ddagger\Delta}$	$63.63^{*\ddagger\Delta}$	$66.31^{+*\ddagger\Delta}$	$68.62^{+*\times\dagger}$	$\mathbf{69.19}^{+*\times\dagger}$

The best performing method for each analysis is highlighted in boldface. To indicate statistically significant difference ($p < 0.05$) between any two methods, every method (column) is marked with a call-sign ($^{+}$, *, $^{\times}$, †, ‡, $^{\Delta}$). The presence of any method's call-sign in any other method's column represents a statistically significant difference in classification accuracies between those two methods. CV: 10-fold cross validation, HO: Hold out analysis with separate test session.

B.2 Effect of m, and w on Classification Accuracies of FBCNet with HLTI

The Effect of number of spatial filters per frequency band (m) and temporal window size (w) on classification accuracies of FBCNet with temporal localization, for different analyses are presented in Figure B.1, B.2, and B.3.

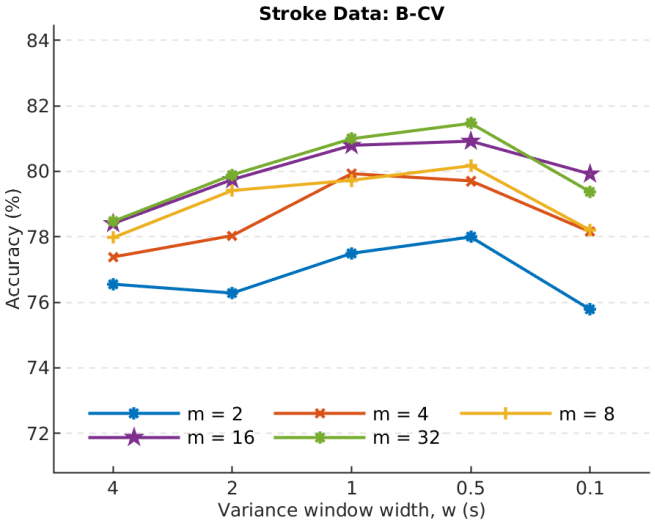

FIGURE B.1: FBCNet with HLTI's cross validation classification accuracies with different number of spatial filters per frequency band (m) and different temporal window sizes (w) for Stroke Data: B dataset.

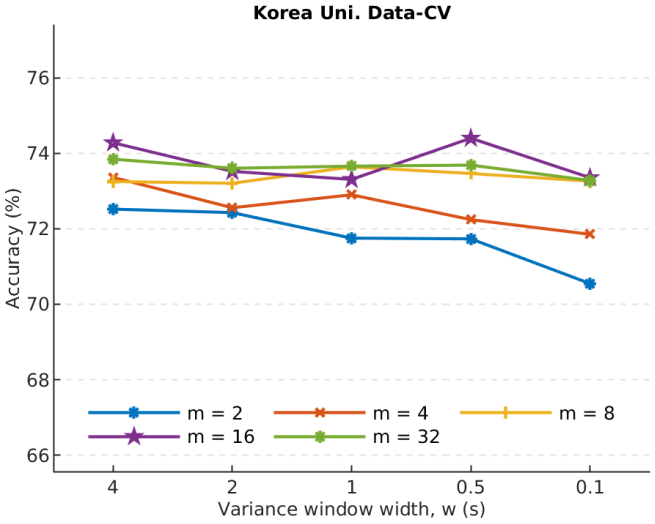

FIGURE B.2: FBCNet with HLTI's cross validation classification accuracies with different number of spatial filters per frequency band (m) and different temporal window sizes (w) for Korea Uni. Data.

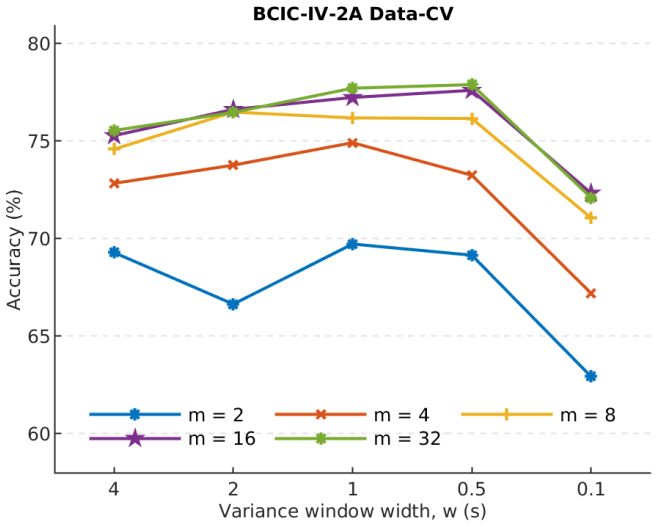

FIGURE B.3: FBCNet with HLTI's cross validation classification accuracies with different number of spatial filters per frequency band (m) and different temporal window sizes (w) for BCIC-IV-2A Data.

Appendix C

Additional Information for Deep Learning based MI Decoding for Post-Stroke Motor Rehabilitation

C.1 Detailed classification results

The detailed results of classification accuracies achieved by baseline methods and FBCNet, across all rehabilitation sessions, for Group-I and Group-III intervention are provided in Figure C.1, C.2 and Figure C.3, C.4 respectively.

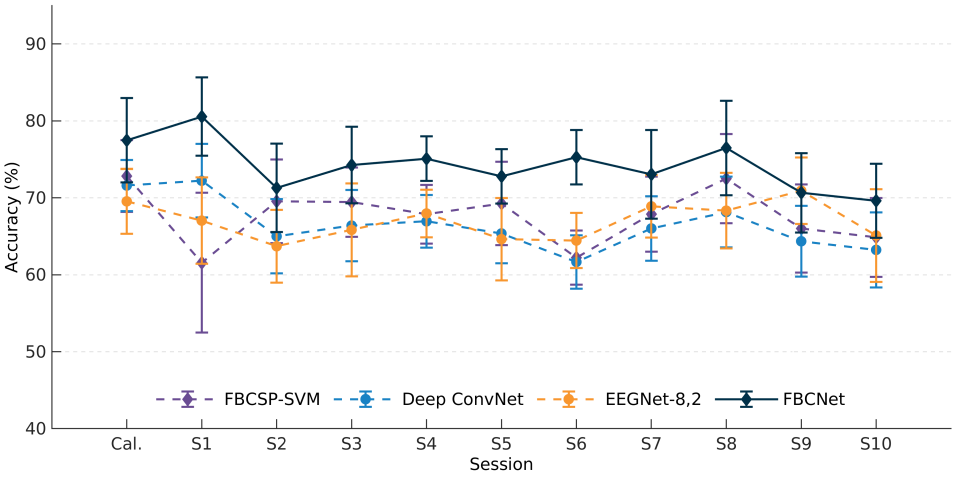

FIGURE C.1: Classification accuracy during every rehabilitation session for Group-I intervention in 10-fold cross-validation settings.

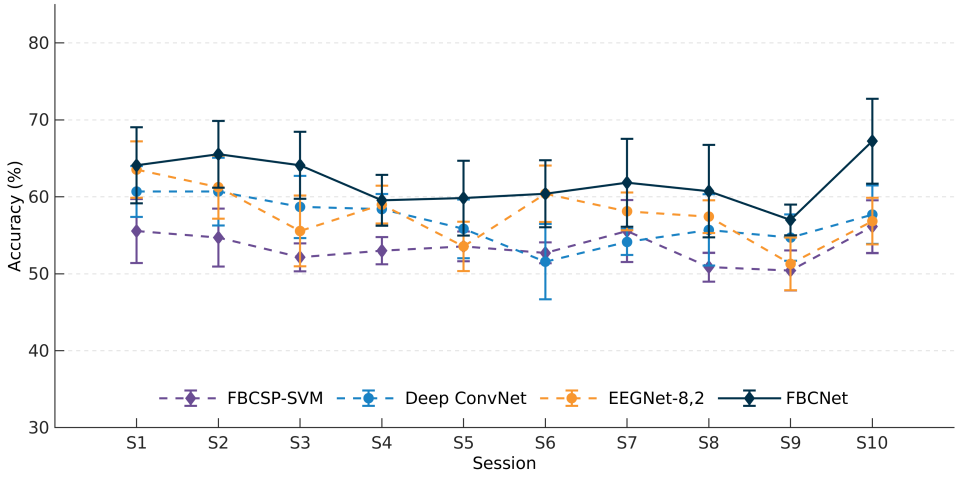

FIGURE C.2: Classification accuracy during every rehabilitation session for Group-I intervention in hold out settings.

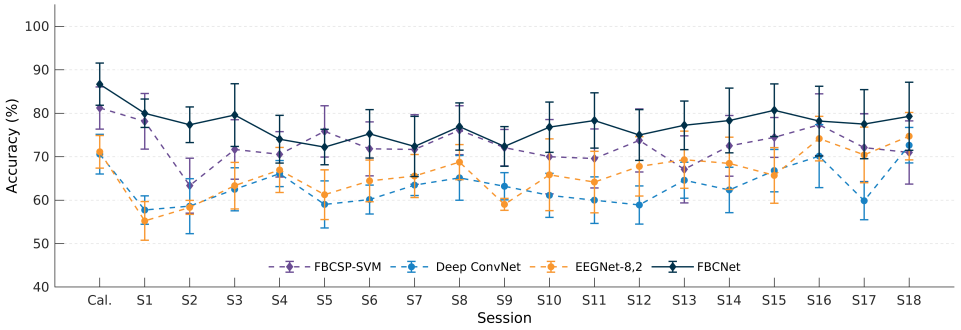

FIGURE C.3: Classification accuracy during every rehabilitation session for Group-III intervention in 10-fold cross-validation settings.

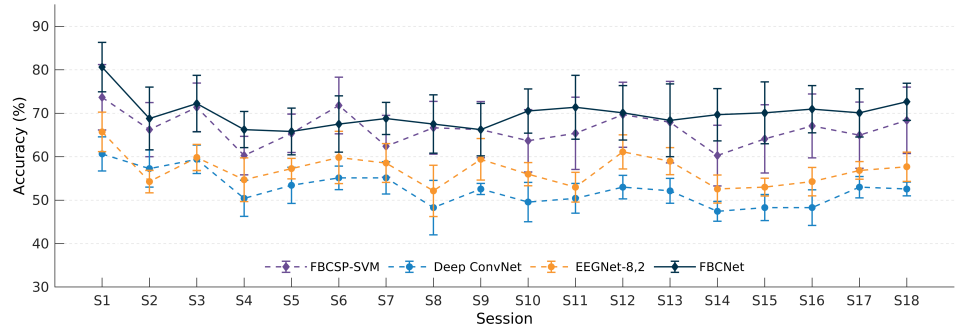

FIGURE C.4: Classification accuracy during every rehabilitation session for Group-III intervention in hold out settings.

Bibliography

[1] Rajesh P N Rao. *Brain-Computer Interfacing: An Introduction*. Cambridge University Press, 2013. xxiii, 4, 29, 32, 62

[2] Emelia J Benjamin, Paul Muntner, and Márcio Sommer Bittencourt. Heart disease and stroke statistics-2019 update: a report from the American Heart Association. *Circulation*, 139(10):56–528, 2019. 1

[3] Antonio Di Carlo. Human and economic burden of stroke. *Age and Ageing*, 38(1):4–5, 2009. ISSN 00020729. 1

[4] Xiang-Ming Xu, Emma Vestesson, Lizz Paley, et al. The economic burden of stroke care in England, Wales and Northern Ireland: Using a national stroke register to estimate and report patient-level health economic outcomes in stroke. *Eur. Stroke J.*, 3(1): 239698731774651, 2017. ISSN 2396-9873.

[5] World Health Organization. *Neurological disorders: public health challenges*. 2006. 1

[6] Vladimir Hachinski, Geoffrey A. Donnan, Philip B. Gorelick, et al. Stroke: Working Toward a Prioritized World Agenda. *Stroke*, 41(6):1084–1099, June 2010. 1, 15

[7] Jonathan R Wolpaw, Niels Birbaumer, Dennis J McFarland, et al. Brain-computer interfaces for communication and control. *Clinical Neurophysiology*, 113(6):767–791, 2002. 1, 15, 30

[8] Alexander Remsik, Brittany Young, Rebecca Vermilyea, et al. A review of the progression and future implications of brain-computer interface therapies for restoration of distal upper extremity motor function after stroke. *Expert Review of Medical Devices*, 13(5):445–454, 2016. 2, 16, 45, 46, 125

[9] Jessica M Cassidy and Steven C Cramer. Spontaneous and Therapeutic-Induced Mechanisms of Functional Recovery After Stroke. *Translational Stroke Research*, 8(1):33–46, February 2017. 2, 19, 44, 152

[10] María A. Cervera, Surjo R. Soekadar, Junichi Ushiba, et al. Brain-computer interfaces for post-stroke motor rehabilitation: a meta-analysis. *Annals of Clinical and Translational Neurology*, 5(5):651–663, 2018. 2, 16, 48, 51, 152, 171

[11] David T. Bundy, Lauren Souders, Kelly Baranyai, et al. Contralesional Brain-Computer Interface Control of a Powered Exoskeleton for Motor Recovery in Chronic Stroke Survivors. *Stroke*, 48(7):1908–1915, 2017. 2, 49, 50

[12] Alexander A Frolov, Olesya Mokienko, Roman Lyukmanov, et al. Post-stroke rehabilitation training with a motor-imagery-based brain-computer interface (BCI)-controlled hand exoskeleton: A randomized controlled multicenter trial. *Frontiers in Neuroscience*, 11(JUL), 2017. 43, 48

[13] Anirban Chowdhury, Yogesh Kumar Meena, Haider Raza, et al. Active Physical Practice Followed by Mental Practice Using BCI-Driven Hand Exoskeleton: A Pilot Trial for Clinical Effectiveness and Usability. *IEEE Journal of Biomedical and Health Informatics*, 22(6): 1786–1795, November 2018. 45, 46

[14] A Biasiucci, R Leeb, I Iturrate, et al. Brain-actuated functional electrical stimulation elicits lasting arm motor recovery after stroke. *Nature Communications*, 9(1):2421, 2018. 48, 50

[15] Kai Keng Ang, Cuntai Guan, Karen Sui Geok Chua, et al. A Large Clinical Study on the Ability of Stroke Patients to Use an EEG-Based Motor Imagery Brain-Computer Interface. *Clinical EEG and Neuroscience*, 42(4):253–258, October 2011. 5, 37, 63, 125

[16] Kai Keng Ang and Cuntai Guan. EEG-Based Strategies to Detect Motor Imagery for Control and Rehabilitation. *IEEE Transactions on Neural Systems and Rehabilitation Engineering*, 25:392–401, April 2017. 2, 50

[17] Steven C. Cramer. Repairing the human brain after stroke. II. Restorative therapies. *Annals of Neurology*, 63(5):549–560, 2008. ISSN 03645134. 3, 6, 22, 44, 46, 152

[18] Fabien Lotte, Laurent Bougrain, Andrzej Cichocki, et al. A review of classification algorithms for EEG-based brain–computer interfaces: a 10 year update. *Journal of neural engineering*, 15(3):31005, 2018. 4, 38, 62, 65, 124, 147

[19] Yannick Roy, Hubert Banville, Isabela Albuquerque, et al. Deep learning-based electroencephalography analysis: a systematic review. *Journal of neural engineering*, January 2019. 4, 40, 41, 62, 63

[20] Robin Tibor Schirrmeister, Jost Tobias Springenberg, Lukas Dominique Josef Fiederer, et al. Deep learning with convolutional neural networks for EEG decoding and visualization. *Human Brain Mapping*, 38(11):5391–5420, 2017. 4, 41, 42, 62, 63, 65, 69, 75, 95, 97, 133, 185

[21] Siavash Sakhavi, Cuntai Guan, and Shuicheng Yan. Learning Temporal Information for Brain-Computer Interface Using Convolutional Neural Networks. *IEEE Transactions on Neural Networks and Learning Systems*, 29(11):5619–5629, November 2018. 42

[22] Vernon J. Lawhern, Amelia J. Solon, Nicholas R. Waytowich, et al. EEGNet: A compact convolutional neural network for EEG-based brain-computer interfaces. *Journal of Neural Engineering*, 15(5):1–30, 2018. 41, 42, 65, 69, 75, 81, 95, 97, 133, 185

[23] O-yeon Kwon, Min-Ho Lee, Cuntai Guan, and Seong-whan Lee. Subject-Independent Brain-Computer Interfaces Based on Deep Convolutional Neural Networks. *IEEE Transactions on Neural Networks and Learning Systems*, XX(X):1–14, 2019. ISSN 2162-237X. 4, 40, 41, 62, 63, 65, 176

[24] Lara A Boyd, Kathryn S Hayward, Nick S Ward, et al. Biomarkers of stroke recovery: Consensus-based core recommendations from the Stroke Recovery and Rehabilitation Roundtable. *International Journal of Stroke*, 12(5):480–493, July 2017. 5, 6, 45, 46, 63, 149, 152, 171

[25] R Mane, E Chew, K S Phua, et al. Prognostic and Monitory EEG-Biomarkers for BCI Upper-Limb Stroke Rehabilitation. *IEEE Transactions on Neural Systems and Rehabilitation Engineering*, 27(8):1654–1664, August 2019. 5, 63

[26] N S Ward. Mechanisms underlying recovery of motor function after stroke. *Postgrad.Med J.*, 81(958):510–514, 2005. ISSN 0032-5473. 5

[27] Steven C Cramer. Brain repair after stroke. *New England Journal of Medicine*, 362(19): 1827–1829, 2010. ISSN 1074-7931. 5

[28] Naoyuki Takeuchi and Shin-Ichi Izumi. Rehabilitation with Poststroke Motor Recovery: A Review with a Focus on Neural Plasticity. *Stroke Research and Treatment*, 2013:1–13, 2013. ISSN 2090-8105. 5, 6, 152, 171

[29] Erin Burke Quinlan, Lucy Dodakian, L Otr, et al. Neural function, injury, and stroke subtype predict treatment gains after stroke. *Annals of Neurology*, 77(1):132–145, 2015. 5

[30] Cathy M Stinear. Prediction of motor recovery after stroke: advances in biomarkers. *Lancet Neurology*, 16(10):826–836, 2017. ISSN 14744465. 6, 149, 152, 171

[31] G Ntaios, M Faouzi, J Ferrari, et al. An integer-based score to predict functional outcome in acute ischemic stroke. *Neurology*, 78(24):1916 LP —- 1922, June 2012. 6

[32] Gustavo Saposnik, Moira K Kapral, Ying Liu, et al. IScore: A risk score to predict death early after hospitalization for an acute ischemic stroke. *Circulation*, 123(7):739–749, 2011. ISSN 00097322.

[33] Shoichiro Sato, Candice Delcourt, Emma Heeley, et al. Significance of Cerebral Small-Vessel Disease in Acute Intracerebral Hemorrhage. *Stroke*, 47(3):701–707, 2016. ISSN 15244628. 6

[34] Timea Hodics, Leonardo G Cohen, and Steven C Cramer. Functional Imaging of Intervention Effects in Stroke Motor Rehabilitation. *Archives of Physical Medicine and Rehabilitation*, 87(12 SUPPL.):36–42, 2006. ISSN 00039993. 6, 58

[35] Adrian D Wood, Nicholas D Gollop, Joao H Bettencourt-Silva, et al. A 6-point TACS score predicts in-hospital mortality following total anterior circulation stroke. *J. Clin. Neurol.*, 12(4):407–413, 2016. ISSN 20055013. 6

[36] Gavin R Philips, Janis J Daly, and José C Príncipe. Topographical measures of functional connectivity as biomarkers for post-stroke motor recovery. *Journal of NeuroEngineering and Rehabilitation*, 14(1):9–22, 2017. ISSN 17430003. 6, 58, 152, 154, 158, 178

[37] Steven C Cramer, Todd B Parrish, Robert M Levy, et al. Predicting functional gains in a stroke trial. *Stroke*, 38(7):2108–2114, 2007. ISSN 00392499. 6

[38] Bokkyu Kim and Carolee Winstein. Can Neurological Biomarkers of Brain Impairment Be Used to Predict Poststroke Motor Recovery? A Systematic Review. *Neurorehabilitation and Neural Repair*, 31(1):3–24, 2017. 6, 45, 46, 146, 149, 152, 171

[39] Giovanni Di Pino, Giovanni Pellegrino, Giovanni Assenza, et al. Modulation of brain plasticity in stroke: a novel model for neurorehabilitation. *Nature Reviews Neurology*, 10 (10):597–608, October 2014. 6, 22, 49, 50

[40] Steven C Cramer. Repairing the human brain after stroke: I. Mechanisms of spontaneous recovery. *Annals of Neurology*, 63(3):272–287, March 2008. 6, 19, 44, 46, 50, 99, 152

[41] Tyler Rickards, Edward Taub, Chelsey Sterling, et al. Brain parenchymal fraction predicts motor improvement following intensive task-oriented motor rehabilitation for chronic stroke. *Restor. Neurol. Neurosci.*, 30(5):355–361, 2012. ISSN 09226028. 6

[42] Bálint Várkuti, Cuntai Guan, Yaozhang Pan, et al. Resting state changes in functional connectivity correlate with movement recovery for BCI and robot-assisted upper-extremity training after stroke. *Neurorehabilitation and Neural Repair*, 27(1):53–62, 2013. 6, 46, 59, 152

[43] Judith D Schaechter, Eduard Kraft, Timothy S Hilliard, et al. Motor Recovery and Cortical Reorganization after Constraint-Induced Movement Therapy in Stroke Patients: A Preliminary Study. *Neurorehabilitation and Neural Repair*, 16(4):326–338, 2002. ISSN 1545-9683. 6, 58

[44] Kotaro Takeda, Yukihiro Gomi, and Hiroyuki Kato. Near-Infrared Spectroscopy and Motor Lateralization after Stroke: A Case Series Study. *International Journal of Physical Medicine and Rehabilitation*, 02(03), 2014. ISSN 23299096. 6

[45] Masahito Mihara, Noriaki Hattori, Megumi Hatakenaka, et al. Near-infrared spectroscopy-mediated neurofeedback enhances efficacy of motor imagery-based training in poststroke victims: A pilot study. *Stroke*, 44(4):1091–1098, 2013. 6, 48

[46] Cathy M Stinear, P Alan Barber, Peter R Smale, et al. Functional potential in chronic stroke patients depends on corticospinal tract integrity. *Brain*, 130(1):170–180, 2007. ISSN 00068950. 6, 19, 54, 58, 59, 149, 152

[47] Ethan Buch, Cornelia Weber, Leonardo G. Cohen, et al. Think to move: A neuromagnetic brain-computer interface (BCI) system for chronic stroke. *Stroke*, 39(3):910–917, 2008. 6, 31, 35, 43, 45, 47, 125

[48] Chun-Chuan Chen, Si-Huei Lee, Wei-Jen Wang, Yu-Chen Lin, and Mu-Chun Su. EEG-based motor network biomarkers for identifying target patients with stroke for upper limb rehabilitation and its construct validity. *PLOS ONE*, 12(6):e0178822, June 2017. ISSN 1932-6203. 6, 57, 152, 178

[49] Paula Trujillo, Alfonso Mastropietro, Alessandro Scano, et al. Quantitative EEG for Predicting Upper-limb Motor Recovery in Chronic Stroke Robot-assisted Rehabilitation. *IEEE Transactions on Neural Systems and Rehabilitation Engineering*, 4320(c):1, 2017. ISSN 1534-4320. 7, 59, 152, 153, 157, 169, 170

[50] Michel J.A.M. van Putten. The revised brain symmetry index. *Clinical Neurophysiology*, 118(11):2362–2367, November 2007. ISSN 13882457. 7, 157

[51] Simon Finnigan, Andrew Wong, and Stephen Read. Defining abnormal slow EEG activity in acute ischaemic stroke: Delta/alpha ratio as an optimal QEEG index. *Clinical Neurophysiology*, 127(2):1452–1459, February 2016. ISSN 13882457. 6, 54, 153

[52] S Finnigan and M.J.A.M. van Putten. EEG in ischaemic stroke: Quantitative EEG can uniquely inform (sub-)acute prognoses and clinical management. *Clinical Neurophysiology*, 124(1):10–19, 2013. 7, 54, 169

[53] Simon P Finnigan, Stephen E Rose, Michael Walsh, et al. Correlation of Quantitative EEG in Acute Ischemic Stroke with 30-Day NIHSS Score: Comparison with Diffusion and Perfusion MRI. *Stroke*, 35(4):899–903, 2004. ISSN 00392499. 55, 153, 170

[54] Simon P. Finnigan, Stephen E. Rose, and Jonathan B. Chalk. Rapid EEG changes indicate reperfusion after tissue plasminogen activator injection in acute ischaemic stroke. *Clinical Neurophysiology*, 117(10):2338–2339, October 2006. ISSN 13882457. 53, 54, 153, 170

[55] Simon P Finnigan, Michael Walsh, Stephen E Rose, and Jonathan B Chalk. Quantitative EEG indices of sub-acute ischaemic stroke correlate with clinical outcomes. *Clinical Neurophysiology*, 118(11):2525–2532, November 2007. ISSN 13882457. 53, 55, 153, 170

[56] S P Finnigan, Stephen E Rose, and Jonathan B Chalk. Contralateral hemisphere delta EEG in acute stroke precedes worsening of symptoms and death. *Clinical Neurophysiology*, 119(7):1690–1694, 2008. ISSN 13882457.

[57] Rishi V A Sheorajpanday, Guy Nagels, Arie J T M Weeren, Michel J A M van Putten, and Peter P De Deyn. Reproducibility and clinical relevance of quantitative EEG parameters in cerebral ischemia: A basic approach. *Clinical Neurophysiology*, 120(5):845–855, 2009. ISSN 13882457. 7, 55, 153, 157

[58] Ujwal Chaudhary, Niels Birbaumer, and Ander Ramos-murguialday. Brain – computer interfaces for communication and rehabilitation. *Nat. Rev.*, 12(9):513–525, 2016. 15

[59] Fabien Lotte. Study of Electroencephalographic Signal Processing and Classification Techniques towards the use of Brain-Computer Interfaces in Virtual Reality Applications. *Thesis*, page 236, 2008. 15

[60] Prabal Deb, Suash Sharma, and K M Hassan. Pathophysiologic mechanisms of acute ischemic stroke: An overview with emphasis on therapeutic significance beyond thrombolysis. *Pathophysiology*, 17(3):197–218, 2010. ISSN 09284680. 16

[61] Jian Wang. Preclinical and clinical research on inflammation after intracerebral hemorrhage. *Progn. Neurobiol.*, 92(4):463–477, 2010. 16, 17

[62] Jinbiao Liu, Yixuan Sheng, and Honghai Liu. Corticomuscular coherence and its applications: A review. *Frontiers in Human Neuroscience*, 13, 03 2019. doi: 10.3389/fnhum.2019.00100. 18

[63] Gert Kwakkel, Boudewijn J Kollen, Jeroen Van Der Grond, and Arie J H Prevo. Probability of Regaining Dexterity in the Flaccid Upper Limb. *Stroke*, 2003. 18, 19

[64] T K Tatemichi, D W Desmond, Y Stern, et al. Cognitive impairment after stroke: Frequency, patterns, and relationship to functional abilities. *Journal of Neurology, Neurosurgery and Psychiatry*, 57(2):202–207, 1994. ISSN 00223050. 18

[65] R das Nair, H Cogger, E Worthington, and N B Lincoln. Cognitive rehabilitation for memory deficits following stroke. *Cochrane Database Syst. Rev.*, 9(9):CD002293, 2016. ISSN 1469493X.

[66] Ljiljana Čengić, Vladimira Vuletić, Mladen Karlić, Marinko Dikanović, and Vida Demarin. Motor and cognitive impairment after stroke. *Acta Clin. Croat.*, 50(4):463–467, 2011. ISSN 0353-9466. 18

[67] T P Cassidy, S Lewis, and C S Gray. Recovery from visuospatial neglect in stroke patients. *Journal of Neurology, Neurosurgery and Psychiatry*, 64(4):555–557, 1998. ISSN 0022-3050. 18

[68] Audrey Bowen, Christine Hazelton, Alex Pollock, and Nadina B Lincoln. Cognitive rehabilitation for spatial neglect following stroke. *Cochrane Database Syst. Rev.*, 7(7):CD003586, 2013. ISSN 00283932. 18

[69] Palle Moller Pedersen, Hirofumi Nakayama, and Hans Otto Raaschou. Aphasia in acute stroke: incidence, determinants, and recovery. *Annals of Neurology*, 38(1):659–666, 1995. ISSN 0364-5134 (Print). 18

[70] Cameron Sellars, Thomas Hughes, and Peter Langhorne. Speech and language therapy for dysarthria due to non-progressive brain damage. *Cochrane Database Syst. Rev.*, pages 61–68, 2005. ISSN 1469-493X. 18

[71] Nadia Bologninia, Cristina Russoa, and Dylan J Edwards. The sensory side of post-stroke motor rehabilitation. *Restor. Neurol. Neurosci.*, 34(4):571–586, 2016. ISSN 1527-5418. 18

[72] Giselle Carnaby, Graeme J Hankey, and Julia Pizzi. Behavioural intervention for dysphagia in acute stroke: A randomised controlled trial. *Lancet Neurology*, 5(1):31–37, 2006. ISSN 14744422. 18

[73] Justine J Overman and S Thomas Carmichael. Plasticity in the injured brain: More than molecules matter. *Neuroscientist*, 20(1):15–28, 2014. ISSN 10738584. 19

[74] G Kwakkel and B J Kollen. Predicting activities after stroke: What is clinically relevant? *Int. J. Stroke*, 8(1):25–32, 2013. 19

[75] Henrik S Jørgensen, Hirofumi Nakayama, Hans O Raaschou, and Tom S Olsen. Recovery of walking function in stroke patients: The copenhagen stroke study. *Archives of Physical Medicine and Rehabilitation*, 76(1):27–32, 1995. ISSN 00039993. 19

[76] Jeffrey A Kleim, Sheila Chan, Erin Pringle, et al. BDNF val66met polymorphism is associated with modified experience-dependent plasticity in human motor cortex. *Nature Neuroscience*, 9(6):735–737, 2006. ISSN 10976256. 19

[77] S. C. Cramer and V. Procaccio. Correlation between genetic polymorphisms and stroke recovery: Analysis of the GAIN Americas and GAIN International Studies. *European Journal of Neurology*, 19(5):718–724, 2012. ISSN 13515101. 19

[78] Eric Y. Chang, Enoch Chang, Samantha Cragg, and Steven C Cramer. Predictors of Gains During Inpatient Rehabilitation in Patients with Stroke: A Review. *Critical Reviews in Physical and Rehabilitation Medicine*, 25(3-4):203–221, 2013. ISSN 0896-2960. 19, 149, 152

[79] R Lindenberg, V Renga, L L Zhu, et al. Structural integrity of corticospinal motor fibers predicts motor impairment in chronic stroke. *Neurology*, 74(4):280–287, 2010. ISSN 00283878. 19

[80] Peter Langhorne, Julie Bernhardt, and Gert Kwakkel. Stroke rehabilitation. *Lancet*, 377 (9778):1693–1702, 2011. ISSN 01406736. 19, 20, 146, 152

[81] Preeti Raghavan. Upper Limb Motor Impairment Post Stroke. *Phys Med Rehabil Clin N Am . 2015 Novemb. ; 26(4) 599–610*, 26(4):599–610, 2016. 20

[82] Samar M Hatem, Geoffroy Saussez, Margaux della Faille, et al. Rehabilitation of Motor Function after Stroke: A Multiple Systematic Review Focused on Techniques to Stimulate Upper Extremity Recovery. *Frontiers in Human Neuroscience*, 10(September):1–22, 2016. ISSN 1662-5161. 21, 152

[83] RPS Van Peppen, G Kwakkel, S Wood-Dauphinee, and Occupational Therapy. The impact of physical therapy on functional outcomes after stroke : what ' s the evidence ? *Clinical Rehabiliitation*, 18(00):833–862, 2004. ISSN 0269-2155. 21

[84] Shruti Sonni, Vasileios-Arsenios Lioutas, and Magdy H Selim. New Avenues for Treatment of Intracranial Hemorrhage. *Curr. Treat. Options Cardiovasc. Med.*, 18(9):1199–1216, 2014. ISSN 1878-5832. 21

[85] Stefano Masiero, Mario Armani, and Giulio Rosati. Upper-limb robot-assisted therapy in rehabilitation of acute stroke patients: Focused review and results of new randomized controlled trial. *Journal of Rehabilitation Research and Development*, 48(4):355–366, 2011. ISSN 0748-7711. 21

[86] Won Hyuk Chang and Yun-Hee Kim. Robot-assisted Therapy in Stroke Rehabilitation. *Stroke*, 15(3):174, 2013. ISSN 2287-6391. 21

[87] Kai Keng Ang, Cuntai Guan, Karen Sui, et al. A clinical study of motor-imagery based brain-computer interfaces for upper limb robotic rehabilitation. In *IEEE EMBS*, pages 5981–5984, 2009. 22, 47

[88] Kai Keng Ang, Cuntai Guan, Kok Soon Phua, et al. Brain-computer interface-based robotic end effector system for wrist and hand rehabilitation: results of a three-armed randomized controlled trial for chronic stroke. *Frontiers in Neuroengineering*, 7(July):30, July 2014. 31, 37, 43, 45, 46, 48, 74, 108, 124, 125, 126, 127, 182, 183

[89] K K Ang and C T Guan. Brain-Computer Interface for Neurorehabilitation of Upper Limb After Stroke. *Proceedings of the IEEE*, 103:944–953, 2015. ISSN 0018-9219. 22

[90] Steven L Wolf, Carolee J Winstein, J Philip Miller, et al. Effect of constraint-induced movement therapy on upper extremity function 3 to 9 months after stroke: the EXCITE randomized clinical trial. *JAMA*, 296(17):2095–2104, 2006. ISSN 0098-7484. 22

[91] George F Wittenberg, Robert Chen, Kenji Ishii, et al. Constraint-induced therapy in stroke: magnetic-stimulation motor maps and cerebral activation. *Neurorehabilitation and Neural Repair*, 17(1):48–57, 2003. ISSN 1545-9683. 22

[92] Brian R Webster, Pablo A Celnik, and Leonardo G Cohen. Noninvasive brain stimulation in stroke rehabilitation. *Neurorx*, 3(4):474–481, 2006. ISSN 1545-5343. 22

[93] Felipe Fregni, Paulo S Boggio, Carlos G Mansur, et al. Transcranial direct current stimulation of the unaffected hemisphere in stroke patients. *Neuroreport*, 16(14):1551–1555, 2005. ISSN 0959-4965. 22

[94] Bradley W. Vines, Carlo Cerruti, and Gottfried Schlaug. Dual-hemisphere tDCS facilitates greater improvements for healthy subjects' non-dominant hand compared to uni-hemisphere stimulation. *BMC Neuroscience*, 9(1):103, 2008. ISSN 1471-2202. 22

[95] Bamidele Oyebamiji Adeyemo, Marcel Simis, Debora Macea, and Felipe Fregni. Systematic review of parameters of stimulation, clinical trial design characteristics, and motor outcomes in non-invasive brain stimulation in stroke. *Frontiers in Psychiatry*, 3:88, 2012. ISSN 1664-0640. 22

[96] Jean Pascal Lefaucheur, Andrea Antal, Samar S. Ayache, et al. Evidence-based guidelines on the therapeutic use of transcranial direct current stimulation (tDCS). *Clinical Neurophysiology*, 128(1):56–92, 2017. 22, 49, 50

[97] Sook Joung Lee and Min Ho Chun. Combination transcranial direct current stimulation and virtual reality therapy for upper extremity training in patients with subacute stroke. *Archives of Physical Medicine and Rehabilitation*, 95(3):431–438, 2014. ISSN 0003-9993. 22

[98] R T Viana, G E C Laurentino, R J P Souza, et al. Effects of the addition of transcranial direct current stimulation to virtual reality therapy after stroke: a pilot randomized controlled trial. *NeuroRehabilitation*, 34(3):437–446, 2014. ISSN 1053-8135. 22

[99] Dinesh G Nair, Vijay Renga, Robert Lindenberg, Lin Zhu, and Gottfried Schlaug. Optimizing recovery potential through simultaneous occupational therapy and non-invasive brain-stimulation using tDCS. *Restor. Neurol. Neurosci.*, 29(6):411–420, 2011. ISSN 0922-6028. 22

[100] Nadia Bolognini, Giuseppe Vallar, Carlotta Casati, et al. Neurophysiological and behavioral effects of tDCS combined with constraint-induced movement therapy in poststroke patients. *Neurorehabilitation and Neural Repair*, 25(9):819–829, 2011. ISSN 1545-9683. 22

[101] Mitsuhiro Ochi, Satoru Saeki, Taiji Oda, Yasuyuki Matsushima, and Kenji Hachisuka. Effects of anodal and cathodal transcranial direct current stimulation combined with robotic therapy on severely affected arms in chronic stroke patients. *Journal of Rehabilitation Medicine*, 45(2):137–140, 2013. ISSN 1650-1977. 22

[102] Jennifer K Harrison, Katherine S McArthur, and Terence J Quinn. Assessment scales in stroke: Clinimetric and clinical considerations. *Clin. Interv. Aging*, 8:201–211, 2013. ISSN 11769092. 23

[103] T Brott, H P Adams, C P Olinger, et al. Measurements of acute cerebral infarction: a clinical examination scale. *Stroke*, 20(7):864 LP —- 870, July 1989. 23

[104] Axel R Fugl-Meyer, L Jääskö, Ingegerd Leyman, Sigyn Olsson, and Solveig Steglind. The post-stroke hemiplegic patient. 1. a method for evaluation of physical performance. *Scandinavian journal of rehabilitation medicine*, 7(1):13–31, 1975. ISSN 0036-5505. 23, 127, 154

[105] Johanna H van der Lee, Heleen Beckerman, Gustaaf J Lankhorst, and Lex M Bouter. The responsiveness of the Action Research Arm test and the Fugl-Meyer Assessment scale in chronic stroke patients. *Journal of Rehabilitation Medicine*, 2001. ISSN 1650-1977. 24

[106] Julie Sanford, Julie Moreland, Laurie R Swanson, Paul W Stratford, and Carolyn Gowland. Reliability of the Fugl-Meyer assessment for testing motor performance in patients following stroke. *Physical Therapy*, 73(7):447–454, 1993. ISSN 0031-9023. 24

[107] F. I. Mahoney and D. W Barthel. Functional evaluation: The Barthel Index. *Meryland State Medical Journal*, 930:1, 1965. 24

[108] Tj Quinn, J Dawson, and M Walters. Dr John Rankin; His Life, Legacy and the 50th Anniversary of the Rankin Stroke Scale. *Scottish Medical Journal*, 53(1):44–47, February 2008. ISSN 0036-9330. 24

[109] M Ferraro, J H Demaio, J Krol, et al. Assessing the Motor Status Score: A Scale for the Evaluation of Upper Limb Motor Outcomes in Patients after Stroke. *Neurorehabilitation and Neural Repair*, 16(3):283–289, 2002. ISSN 1545-9683. 24

[110] Stroke Center. Stroke Assessment Scales Overview. URL `http://www.strokecenter.org/professionals/stroke-diagnosis/stroke-assessment-scales-overview/`. 24

[111] Eduardo Fernández, Bradley Greger, Paul A House, et al. Acute human brain responses to intracortical microelectrode arrays : challenges and future prospects. *Frontiers in Neuroengineering*, 7(July):1–6, 2014. 26

[112] Vasilios A Zerris, John D Donoghue, Leigh R Hochberg, Daniel Kevin O'Rourke, and Ennio Antonio Chiocca. Braingate: Turning Thought into Action—First Experience with a Human Neuromotor Prosthesis: 885. *Neurosurgery*, 57(2):425, 2005. ISSN 0148-396X. 26

[113] Niels Birbaumer, Thomas Elbert, Anthony G Canavan, and Brigitte Rockstroh. Slow potentials of the cerebral cortex and behavior. *Physiological reviews*, 70(1):1–41, 1990. 30

[114] N Birbaumer, T Hinterberger, A Kübler, and N Neumann. The thought-translation device (TTD): Neurobehavioral mechanisms and clinical outcome. *IEEE Transactions on Neural Systems and Rehabilitation Engineering*, 11(2):120–123, 2003. 30

[115] Zhichuan Tang, Shouqian Sun, Sanyuan Zhang, et al. A brain-machine interface based on erd/ers for an upper-limb exoskeleton control. *Sensors*, 16:2050, 12 2016. 30

[116] Janis J Daly, Roger Cheng, Jean Rogers, et al. Feasibility of a New Application of Noninvasive Brain Computer Interface (BCI): A Case Study of Training for Recovery of Volitional Motor Control After Stroke. *Journal of Neurologic Physical Therapy*, 33(4):203–211, 2009. 31, 35, 43

[117] Doris Broetz, Christoph Braun, Cornelia Weber, et al. Combination of brain-computer interface training and goal-directed physical therapy in chronic stroke: a case report. *Neurorehabilitation and Neural Repair*, 24(7):674–679, 2010. ISSN 1552-6844.

[118] Keiichiro Shindo, Kimiko Kawashima, Junichi Ushiba, et al. Effects of neurofeedback training with an electroencephalogram-based brain-computer interface for hand paralysis in patients with chronic stroke: A preliminary case series study. *Journal of Rehabilitation Medicine*, 43(10):951–957, 2011. 35, 38

[119] Kai Keng Ang, Cuntai Guan, Kok Soon Phua, et al. Facilitating effects of transcranial direct current stimulation on motor imagery brain-computer interface with robotic feedback for stroke rehabilitation. *Archives of Physical Medicine and Rehabilitation*, 96(3):S79–S87, 2015. 31, 37, 43, 45, 46, 50, 73, 74, 108, 124, 125, 126, 127, 154, 156, 182, 183

[120] David J. Wright, Paul S. Holmes, and Dave Smith. Using the movement-related cortical potential to study motor skill learning. *Journal of Motor Behavior*, 43(3):193–201, 2011. ISSN 00222895. 31

[121] Natalie Mrachacz-Kersting, Ning Jiang, Andrew James Thomas Stevenson, et al. Efficient neuroplasticity induction in chronic stroke patients by an associative brain-computer interface. *Journal of Neurophysiology*, 115(3):1410–1421, March 2016. 43, 49

[122] Jennifer L. Sullivan, Nikunj A. Bhagat, Nuray Yozbatiran, et al. Improving robotic stroke rehabilitation by incorporating neural intent detection: Preliminary results from a clinical trial. *IEEE International Conference on Rehabilitation Robotics*, (Nct 01948739):122–127, 2017. 31

[123] Martin Spuler and Christian Niethammer. Error-related potentials during continuous feedback: using EEG to detect errors of different type and severity. *Frontiers in Human Neuroscience*, 9(March):1–10, March 2015. ISSN 1662-5161. 31

[124] Wen Wen, Rin Minohara, Shunsuke Hamasaki, et al. The Readiness Potential Reflects the Reliability of Action Consequence. *Scientific Reports*, 8(1):11865, 2018. ISSN 2045-2322. 31

[125] E W Sellers, T M Vaughan, and J R Wolpaw. A brain-computer interface for long-term independent home use. *Amyotrophic Lateral Sclerosis*, 11(5):449–455, 2010. 31

[126] Christoph Guger, Shahab Daban, Eric Sellers, et al. How many people are able to control a P300-based brain-computer interface (BCI)? *Neuroscience Letters*, 462(1):94–98, 2009. ISSN 03043940. 31

[127] D Lesenfants, D Habbal, Z Lugo, et al. An independent SSVEP-based brain-computer interface in locked-in syndrome. *Journal of Neural Engineering*, 11(3), 2014. 32

[128] D Zhu, J Bieger, G Garcia Molina, and R M Aarts. A survey of stimulation methods used in SSVEP-based BCIs. *Computational Intelligence and Neuroscience*, 2010, 2010.

[129] Zafer Işcan and Vadim V. Nikulin. Steady state visual evoked potential (SSVEP) based brain-computer interface (BCI) performance under different perturbations. *PLOS ONE*, 13(1):1–17, 2018. ISSN 19326203.

[130] Setare Amiri, Ahmed Rabbi, Leila Azinfar, and Reza Fazel-Rezai. A Review of P300, SSVEP, and Hybrid P300/SSVEP Brain- Computer Interface Systems. In *Brain-Computer Interface Systems - Recent Progress and Future Prospects*, volume i, page 13. InTech, June 2013. 32

[131] Dennis J McFarland, Lynn M McCane, Stephen V David, and Jonathan R Wolpaw. Spatial filter selection for EEG-based communication. *Electroencephalography and Clinical Neurophysiology*, 103(3):386–394, 1997. ISSN 0013-4694. 34

[132] Aapo Hyvärinen, Juha Karhunen, and Erkki Oja. Independent Component Analysis. *Applied and Computational Harmonic Analysis*, 21(1):135–144, 2001. ISSN 10635203. 35

[133] Te-Won Lee, Mark Girolami, and Terrence J Sejnowski. Independent Component Analysis Using an Extended Infomax Algorithm for Mixed Subgaussian and Supergaussian Sources. *Neural Computation*, 11(2):417–441, 1999. ISSN 0899-7667. 35

[134] Jason A Palmer, Ken Kreutz-Delgado, and Scott Makeig. AMICA: An adaptive mixture of independent component analyzers with shared components. *Swartz Center for Computatonal Neursoscience, University of California San Diego, Tech. Rep*, 2012. 35

[135] Maximilien Chaumon, Dorothy V.M. Bishop, and Niko A Busch. A practical guide to the selection of independent components of the electroencephalogram for artifact correction. *Journal of Neuroscience Methods*, 250:47–63, July 2015. ISSN 01650270. 35, 156

[136] Andrea Mognon, Jorge Jovicich, Lorenzo Bruzzone, and Marco Buiatti. ADJUST: An automatic EEG artifact detector based on the joint use of spatial and temporal features. *Psychophysiology*, 48(2):229–240, 2011. ISSN 00485772. 35

[137] Tim R Mullen, Christian A E Kothe, Mike Chi, et al. Real-time Neuroimaging and Cognitive Monitoring Using Wearable Dry EEG. *IEEE Transactions on Biomedical Engineering*, 62(11):2553–2567, 2015. 35

[138] Jose Antonio Urigüen and Begoña Garcia-Zapirain. EEG artifact removal-state-of-the-art and guidelines. *Journal of Neural Engineering*, 12(3):31001, 2015. ISSN 1741-2552. 35

[139] Laurel J. Gabard-Durnam, Adriana S. Mendez Leal, Carol L. Wilkinson, and April R. Levin. The Harvard Automated Processing Pipeline for Electroencephalography (HAPPE): Standardized Processing Software for Developmental and High-Artifact Data. *Frontiers in Neuroscience*, 12(February):1–24, 2018. ISSN 1662-453X. 35

[140] Vikram Shenoy Handiru, A P Vinod, and Cuntai Guan. EEG Source Imaging of Movement Decoding. *IEEE Systems, Man, & Cybernetics Magazine*, pages 14–23, 2018. 36, 177, 178

[141] Fabien Lotte and Cuntai Guan. Regularizing common spatial patterns to improve BCI designs: Unified theory and new algorithms. *IEEE Transactions on Biomedical Engineering*, 58(2):355–362, 2011. ISSN 00189294. 36

[142] Kai Keng Ang, Zheng Yang Chin, Haihong Zhang, and Cuntai Guan. Filter Bank Common Spatial Pattern (FBCSP). *2008 Int. Jt. Conf. Neural Networks (IJCNN 2008)*, pages 2391–2398, 2008. 37, 62, 65, 68, 75, 133, 184

[143] Kai Keng Ang, Cuntai Guan, Kok Soon Phua, et al. Transcranial direct current stimulation and EEG-based motor imagery BCI for upper limb stroke rehabilitation. In *2012 Annual International Conference of the IEEE Engineering in Medicine and Biology Society*, pages 4128–4131. IEEE, August 2012. 37, 50

[144] Kai Keng Ang, Karen Sui Geok Chua, Kok Soon Phua, et al. A Randomized Controlled Trial of EEG-Based Motor Imagery Brain-Computer Interface Robotic Rehabilitation for Stroke. *Clinical EEG and Neuroscience*, 46:310–320, 2015. 37, 45, 46, 48, 59, 124, 125, 126, 152, 153

[145] Fabien Lotte, Marco Congedo, L Anatole, et al. A review of classification algorithms for EEG-based brain-computer interfaces. *Journal of Neural Engineering*, 4(2):R1–R13, 2007. ISSN 1741-2560. 37, 38

[146] Richard O Duda, Peter E Hart, and David G Stork. *Pattern classification*. John Wiley & Sons, 2012. ISBN 111858600X. 37, 38

[147] B Obermaier, C Guger, C Neuper, and G Pfurtscheller. Hidden Markov models for online classification of single trial EEG data. *Pattern Recognition Letters*, 22(12):1299–1309, 2001. ISSN 0167-8655. 37

[148] Peter Sykacek, Stephen J Roberts, and Maria Stokes. Adaptive BCI based on variational Bayesian Kalman filtering: an empirical evaluation. *IEEE Transactions on biomedical engineering*, 51(5):719–727, 2004. ISSN 0018-9294. 37

[149] Andrew Y Ng and Michael I Jordan. On discriminative vs. generative classifiers: A comparison of logistic regression and naive bayes. In *Advances in neural information processing systems*, pages 841–848, 2002. 38

[150] Y Dan Rubinstein and Trevor Hastie. Discriminative vs Informative Learning. In *KDD*, volume 5, pages 49–53, 1997. 38

[151] Gary N Garcia, Touradj Ebrahimi, and J-M Vesin. Support vector EEG classification in the Fourier and time-frequency correlation domains. In *First International IEEE EMBS Conference on Neural Engineering, 2003. Conference Proceedings.*, pages 591–594. IEEE, 2003. ISBN 0780375793. 38

[152] Christopher J C Burges. A tutorial on support vector machines for pattern recognition. *Data Min. Knowl. Discov.*, 2(2):121–167, 1998.

[153] Kristin P Bennett and Colin Campbell. Support vector machines: hype or hallelujah? *ACM SIGKDD Explor. Newsl.*, 2(2):1–13, 2000. ISSN 19310145.

[154] Xin Zhang, Ahmed M Elnady, Bubblepreet K Randhawa, Lara A Boyd, and Carlo Menon. Combining Mental Training and Physical Training With Goal-Oriented Protocols in Stroke Rehabilitation: A Feasibility Case Study. *Frontiers in Human Neuroscience*, 12(April): 1–12, April 2018. 38, 45, 46, 48

[155] Deon Garrett, David A Peterson, Charles W Anderson, and Michael H Thaut. Comparison of linear, nonlinear, and feature selection methods for EEG signal classification. *IEEE Transactions on neural systems and rehabilitation engineering*, 11(2):141–144, 2003. ISSN 1534-4320. 38

[156] Reinhold Scherer, G R Muller, Christa Neuper, Bernhard Graimann, and Gert Pfurtscheller. An asynchronously controlled EEG-based virtual keyboard: improvement of the spelling rate. *IEEE Transactions on Biomedical Engineering*, 51(6):979–984, 2004. ISSN 0018-9294. 38

[157] Fengyu Cong, Qiu-Hua Lin, Li-Dan Kuang, et al. Tensor decomposition of EEG signals: A brief review. *Journal of Neuroscience Methods*, 248:59–69, 2015. ISSN 0165-0270. 38

[158] Ramaswamy Palaniappan. Brain Computer Interface Design Using Band Powers Extracted During Mental Tasks. In *Conference Proceedings. 2nd International IEEE EMBS Conference on Neural Engineering, 2005.*, volume 2005, pages 321–324. IEEE, 2005. ISBN 0-7803-8710-4. 39

[159] Yann LeCun, Bernhard Boser, John S Denker, et al. Backpropagation applied to handwritten zip code recognition. *Neural computation*, 1(4):541–551, 1989. 39

[160] David E Rumelhart, Geoffrey E Hinton, and Ronald J Williams. Learning representations by back-propagating errors. *Nature*, 323(6088):533–536, 1986. 40

[161] Sepp Hochreiter and Jürgen Schmidhuber. Long short-term memory. *Neural computation*, 9(8):1735–1780, 1997. 40

[162] Kyunghyun Cho, Bart van Merrienboer, Dzmitry Bahdanau, and Yoshua Bengio. On the Properties of Neural Machine Translation: Encoder-Decoder Approaches. *arxiv*, 2014. 40

[163] Dalin Zhang, Lina Yao, Kaixuan Chen, and Jessica Monaghan. A Convolutional Recurrent Attention Model for Subject-Independent EEG Signal Analysis. *IEEE Signal Processing Letters*, 26(5):715–719, May 2019. ISSN 1070-9908. 40, 41, 42, 102

[164] Xiu An, Deping Kuang, Xiaojiao Guo, Yilu Zhao, and Lianghua He. A Deep Learning Method for Classification of EEG Data Based on Motor Imagery. In De-Shuang Huang, Kyungsook Han, and Michael Gromiha, editors, *Intelligent Computing in Bioinformatics*, pages 203–210. Springer International Publishing, 2014. ISBN 978-3-319-09330-7. 40, 42

[165] Siavash Sakhavi, Cuntai Guan, and Shuicheng Yan. Parallel convolutional-linear neural network for motor imagery classification. In *2015 23rd European Signal Processing Conference (EUSIPCO)*, pages 2736–2740. IEEE, August 2015. 41, 80, 81

[166] Mouad RIYAD, Mohammed KHALIL, and Abdellah ADIB. Mi-eegnet: A novel convolutional neural network for motor imagery classification. *Journal of Neuroscience Methods*, page 109037, 2020. ISSN 0165-0270. 42

[167] Guangyi Zhang and Ali Etemad. RFNet: Riemannian Fusion Network for EEG-based Brain-Computer Interfaces. *arXiv*, c:1–12, aug 2020. URL `http://arxiv.org/abs/2008.08633`. 42

[168] L J Trejo, R Rosipal, and B Matthews. Brain-computer interfaces for 1-D and 2-D cursor control: designs using volitional control of the EEG spectrum or steady-state visual evoked potentials. *IEEE Transactions on Neural Systems and Rehabilitation Engineering*, 14(2):225–229, 2006. ISSN 1534-4320 VO - 14. 43

[169] Jianjun Meng, Shuying Zhang, Angeliki Bekyo, et al. Noninvasive Electroencephalogram Based Control of a Robotic Arm for Reach and Grasp Tasks. *Scientific Reports*, 6(1):38565, 2016. ISSN 2045-2322. 43

[170] Jin-he Shi, Ji-zhong Shen, Yu Ji, and Feng-lei Du. A submatrix-based P300 brain-computer interface stimulus presentation paradigm. *Journal of Zhejiang University Science*, 13(6):452–459, 2012. ISSN 1869-196X. 43

[171] F Nijboer, A Furdea, I Gunst, et al. An auditory brain-computer interface (BCI). *Journal of Neuroscience Methods*, 167(1):43–50, 2008. 43

[172] Aya Rezeika, Mihaly Benda, Piotr Stawicki, et al. Brain–computer interface spellers: A review. *Brain sciences*, 8(4):57, 2018. 43

[173] Madiha Tariq, Pavel M Trivailo, and Milan Simic. EEG-Based BCI Control Schemes for Lower-Limb Assistive-Robots. *Frontiers in Human Neuroscience*, 12(August), 2018. 43

[174] Girijesh Prasad, Pawel Herman, Damien Coyle, Suzanne McDonough, and Jacqueline Crosbie. Applying a brain-computer interface to support motor imagery practice in people with stroke for upper limb recovery: a feasibility study. *Journal of NeuroEngineering and Rehabilitation*, 7(1):60, 2010. 43, 48

[175] Floriana Pichiorri, Giovanni Morone, Manuela Petti, et al. Brain-computer interface boosts motor imagery practice during stroke recovery. *Annals of Neurology*, 77(5):851–865, May 2015. 43, 48, 50, 51, 59, 152

[176] Andrea Caria, Cornelia Weber, Doris Brötz, et al. Chronic stroke recovery after combined BCI training and physiotherapy: A case report. *Psychophysiology*, 48(4):578–582, April 2011. 43, 47

[177] Ander Ramos-Murguialday, Doris Broetz, Massimiliano Rea, et al. Brain-machine interface in chronic stroke rehabilitation: A controlled study. *Annals of Neurology*, 74(1):100–108, July 2013. 43, 45, 46, 48, 50

[178] Fei Meng, Kai-yu Tong, Suk-tak Chan, et al. BCI-FES training system design and implementation for rehabilitation of stroke patients. *, 2008. Ijcnn 2008.*, pages 4103–4106, 2008. 43, 45

[179] Mingfen Li, Ye Liu, Yi Wu, et al. Neurophysiological substrates of stroke patients with motor imagery-based brain-computer interface training. *International Journal of Neuroscience*, 124(6):403–415, June 2014. 45, 46, 48

[180] Yun Young Jang, Tae Hoon Kim, and Byoung Hee Lee. Effects of Brain-Computer Interface-controlled Functional Electrical Stimulation Training on Shoulder Subluxation for Patients with Stroke: A Randomized Controlled Trial. *Occupational Therapy International*, 23(2): 175–185, 2016. 45, 48, 50, 125

[181] Taehoon Kim, Seongsik Kim, and Byounghee Lee. Effects of Action Observational Training Plus Brain-Computer Interface-Based Functional Electrical Stimulation on Paretic Arm Motor Recovery in Patient with Stroke: A Randomized Controlled Trial. *Occupational Therapy International*, 23(1):39–47, 2016. 43, 45, 48, 125

[182] Takashi Ono, Masahiko Mukaino, and Junichi Ushiba. Functional recovery in upper limb function in stroke survivors by using brain-computer interface A single case A-B-A-B design. *Proceedings of the Annual International Conference of the IEEE Engineering in Medicine and Biology Society, EMBS*, pages 265–268, 2013. 43, 48

[183] N N Johnson, J Carey, B J Edelman, et al. Combined rTMS and virtual reality brain–computer interface training for motor recovery after stroke. *Journal of Neural Engineering*, 15(1):016009, February 2018. 43, 50

[184] U. Chaudhary, N. Birbaumer, and M. R. Curado. Brain-Machine Interface (BMI) in paralysis. *Annals of Physical and Rehabilitation Medicine*, 58(1):9–13, 2015. ISSN 18770665. 44

[185] Kai Keng Ang and Cuntai Guan. Brain-computer interface in stroke rehabilitation. *Journal of Computing Science and Engineering*, 7(2):139–146, 2013. 44

[186] Anais Mottaz, Marco Solcà, Cécile Magnin, et al. Neurofeedback training of alpha-band coherence enhances motor performance. *Clinical Neurophysiology*, 126(9):1754–1760, 2015. 45, 48, 125

[187] Brittany M. Young, Julie M. Stamm, Jie Song, et al. Brain–Computer Interface Training after Stroke Affects Patterns of Brain–Behavior Relationships in Corticospinal Motor Fibers. *Frontiers in Human Neuroscience*, 10(September):1–13, 2016. 45, 125

[188] Burrhus Frederic Skinner. *The behavior of organisms: An experimental analysis*. BF Skinner Foundation, 1938. 45

[189] Colin M. McCrimmon, Christine E. King, Po T. Wang, et al. Brain-controlled functional electrical stimulation therapy for gait rehabilitation after stroke: a safety study. *Journal of NeuroEngineering and Rehabilitation*, 12(1):57, December 2015. 45

[190] Jie Song, Veena A. Nair, Brittany M. Young, et al. DTI measures track and predict motor function outcomes in stroke rehabilitation utilizing BCI technology. *Frontiers in Human Neuroscience*, 9(April):1–13, 2015.

[191] Alexander B. Remsik, Keith Dodd, Williams Leroy, et al. Behavioral outcomes following brain-computer interface intervention for upper extremity rehabilitation in stroke: A randomized controlled trial. *Frontiers in Neuroscience*, 12(NOV):1–16, 2018. 45

[192] Xin Hong, Zhong Kang Lu, Irvin Teh, et al. Brain plasticity following MI-BCI training combined with tDCS in a randomized trial in chronic subcortical stroke subjects: A preliminary study. *Scientific Reports*, 7(1):1–12, 2017. 46, 50, 60, 152, 169, 172

[193] Surjo R. Soekadar, Niels Birbaumer, Marc W. Slutzky, and Leonardo G. Cohen. Brain-machine interfaces in neurorehabilitation of stroke. *Neurobiology of Disease*, 83:172–179, 2015. 46

[194] Jaime Ibáñez, Esther Monge-Pereira, Francisco Molina-Rueda, et al. Low latency estimation of motor intentions to assist reaching movements along multiple sessions in chronic stroke patients: A feasibility study. *Frontiers in Neuroscience*, 11(MAR):1–12, 2017. 46

[195] Rong-Rong Lu, Mou-Xiong Zheng, Jie Li, et al. Motor imagery based brain-computer interface control of continuous passive motion for wrist extension recovery in chronic stroke patients. *Neuroscience Letters*, 718:134727, January 2020. 46

[196] S M Rayegani, S a Raeissadat, L Sedighipour, et al. Effect of neurofeedback and electromyographic-biofeedback therapy on improving hand function in stroke patients. *Top. Stroke Rehabil.*, 21(2):137–151, 2014. 48

[197] Kai Keng Ang, Cuntai Guan, Karen Sui Geok Chua, et al. A clinical evaluation of non-invasive motor imagery-based brain-computer interface in stroke. In *2008 30th Annual International Conference of the IEEE Engineering in Medicine and Biology Society*, pages 4178–4181. IEEE, August 2008. 48

[198] Chuanchu Wang, Kok Soon Phua, Kai Keng Ang, et al. A feasibility study of non-invasive motor-imagery BCI-based robotic rehabilitation for Stroke patients. In *2009 4th International IEEE/EMBS Conference on Neural Engineering*, pages 271–274. IEEE, April 2009.

[199] Kai Keng Ang, Cuntai Guan, Karen Sui Geok Chua, et al. Clinical study of neurorehabilitation in stroke using EEG-based motor imagery brain-computer interface with robotic feedback. In *2010 Annual International Conference of the IEEE Engineering in Medicine and Biology*, pages 5549–5552. IEEE, August 2010. 48

[200] Athanasios Vourvopoulos, Carolina Jorge, Rodolfo Abreu, et al. Efficacy and brain imaging correlates of an immersive motor imagery BCI-driven VR system for upper limb motor rehabilitation: A clinical case report. *Frontiers in Human Neuroscience*, 13(July):1–17, 2019. 48

[201] Athanasios Vourvopoulos, Octavio Marin Pardo, Stéphanie Lefebvre, et al. Effects of a brain-computer interface with virtual reality (VR) neurofeedback: A pilot study in chronic stroke patients. *Frontiers in Human Neuroscience*, 13(June):1–17, 2019. 48

[202] Maryam Alimardani, Shuichi Nishio, and Hiroshi Ishiguro. Brain-Computer Interface and Motor Imagery Training: The Role of Visual Feedback and Embodiment. In *Evolving BCI Therapy-Engaging Brain State Dynamics*. IntechOpen, 2018. 48

[203] Sam Darvishi, Michael C Ridding, Brenton Hordacre, Derek Abbott, and Mathias Baumert. Investigating the impact of feedback update interval on the efficacy of restorative brain–computer interfaces. *Royal Society Open Science*, 4(8):170660, August 2017. 49

[204] Brittany M. Young, Zack Nigogosyan, Léo M. Walton, et al. Dose-response relationships using brain–computer interface technology impact stroke rehabilitation. *Frontiers in Human Neuroscience*, 9(June):1–14, 2015. 49

[205] Charlotte J. Stagg, Andrea Antal, and Michael A. Nitsche. Physiology of Transcranial Direct Current Stimulation. *The Journal of ECT*, 34(3):1, June 2018. 49

[206] Yuko Kasashima-Shindo, Toshiyuki Fujiwara, Junichi Ushiba, et al. Brain-computer interface training combined with transcranial direct current stimulation in patients with chronic severe hemiparesis: Proof of concept study. *Journal of Rehabilitation Medicine*, 47(4):318–324, 2015. 50

[207] Brittany M Young, Zack Nigogosyan, LÃ©o M Walton, et al. Changes in functional brain organization and behavioral correlations after rehabilitative therapy using a brain-computer interface. *Frontiers in Neuroengineering*, 7(July):26, 2014. 50

[208] Kenneth G Jordan. Emergency EEG and continuous EEG monitoring in acute ischemic stroke. *Journal of clinical neurophysiology*, 21(5):341–52, 2004. ISSN 0736-0258. 53, 153

[209] B Foreman and J Claassen. Quantitative EEG for the detection of brain ischemia. *Critical Care*, 16(2), 2012. 153

[210] E Faught. Current role of electroencephalography in cerebral ischemia. *Stroke*, 24(4): 609–613, 1993.

[211] N M Branston, L Symon, H A Crockard, and E Pasztor. Relationship between the cortical evoked potential and local cortical blood flow following acute middle cerebral artery occlusion in the baboon. *Experimental Neurology*, 45(2):195–208, 1974.

[212] F W Sharbrough, J M Messick, and T M Sundt. Correlation of continuous electroencephalograms with cerebral blood flow measurements during carotid endarterectomy. *Stroke*, 4(4): 674–683, 1973. 53

[213] Gratianne Rabiller, Ji-Wei He, Yasuo Nishijima, Aaron Wong, and Jialing Liu. Perturbation of Brain Oscillations after Ischemic Stroke: A Potential Biomarker for Post-Stroke Function and Therapy. *International Journal of Molecular Sciences*, 16(10):25605–25640, October 2015. ISSN 1422-0067. 53, 153, 170

[214] Yanping Wang, Xiaoling Zhang, Junjun Huang, et al. Associations between EEG beta power abnormality and diagnosis in cognitive impairment post cerebral infarcts. *Journal of molecular neuroscience*, 49(3):632–8, March 2013. ISSN 1559-1166. 53, 153

[215] E. Cuspineda, C. Machado, L. Galán, et al. QEEG Prognostic Value in Acute Stroke. *Clinical EEG and Neuroscience*, 38(3):155–160, July 2007. ISSN 1550-0594. 54, 55, 153, 169, 170

[216] Antonello Baldassarre, Lenny Ramsey, Jennifer Rengachary, et al. Dissociated functional connectivity profiles for motor and attention deficits in acute right-hemisphere stroke. *Brain*, 139(7):2024–2038, 2016. ISSN 1460-2156. 54

[217] A. Feydy, R. Carlier, A. Roby-Brami, et al. Longitudinal study of motor recovery after stroke: Recruitment and focusing of brain activation. *Stroke*, 33(6):1610–1617, 2002. ISSN 00392499. 54

[218] Franca Tecchio, Patrizio Pasqualetti, Filippo Zappasodi, et al. Outcome prediction in acute monohemispheric stroke via magnetoencephalography. *Journal of Neurology*, 254(3): 296–305, March 2007. ISSN 0340-5354. 55

[219] Rishi V.A. Sheorajpanday, Guy Nagels, Arie J.T.M. Weeren, and Peter P De Deyn. Quantitative EEG in ischemic stroke: Correlation with infarct volume and functional status in posterior circulation and lacunar syndromes. *Clinical Neurophysiology*, 122(5):884–890, May 2011. ISSN 13882457. 55, 153, 170

[220] Rishi V.A. Sheorajpanday, Guy Nagels, Arie J.T.M. Weeren, Didier De Surgeloose, and Peter P De Deyn. Additional value of quantitative EEG in acute anterior circulation syndrome of presumed ischemic origin. *Clinical Neurophysiology*, 121(10):1719–1725, October 2010. ISSN 13882457. 55, 153

[221] Cathrin M Buetefisch. Role of the contralesional hemisphere in post-stroke recovery of upper extremity motor function. *Frontiers in Neurology*, 6(OCT):1–10, 2015. ISSN 16642295. 55

[222] Jennifer Wu, Ramesh Srinivasan, Erin Burke Quinlan, et al. Utility of EEG measures of brain function in patients with acute stroke. *Journal of Neurophysiology*, 115(5):2399–2405, 2016. ISSN 0022-3077. 56

[223] Charlotte Rosso and Yves Samson. The ischemic penumbra: the location rather than the volume of recovery determines outcome. *Current Opinion in Neurology*, 27(1):35–41, 2014. ISSN 1350-7540. 56

[224] Hongmei Wen, Mohamad J Alshikho, Yao Wang, et al. Correlation of fractional anisotropy with motor recovery in patients with stroke after postacute rehabilitation. *Archives of Physical Medicine and Rehabilitation*, 97(9):1487–1495, 2016. ISSN 0003-9993. 56

[225] W Feng, J Wang, P Y Chhatbar, et al. Corticospinal tract lesion load: An imaging biomarker for stroke motor outcomes. *Annals of Neurology*, 78(6):860–870, 2015. 56, 149, 152

[226] Katarzyna Bembenek Jan Paweł and Kurczych and Anna Karliński Michał and Członkowska. The prognostic value of motor-evoked potentials in motor recovery and functional outcome after stroke–a systematic review of the literature. *Functional Neurology*, 27(2):79, 2012. 56

[227] Cathy M Stinear, P Alan Barber, Matthew Petoe, Samir Anwar, and Winston D Byblow. The PREP algorithm predicts potential for upper limb recovery after stroke. *Brain*, 135 (8):2527–2535, August 2012. ISSN 0006-8950. 56, 146, 149, 152

[228] F E Buma, E Lindeman, N F Ramsey, and G Kwakkel. Functional neuroimaging studies of early upper limb recovery after stroke: A systematic review of the literature. *Neurorehabilitation and Neural Repair*, 24(7):589–608, 2010. 56

[229] I Favre, T A Zeffiro, O Detante, et al. Upper limb recovery after stroke is associated with ipsilesional primary motor cortical activity: A meta-analysis. *Stroke*, 45(4):1077–1083, 2014.

[230] C Grefkes and N S Ward. Cortical reorganization after stroke: How much and how functional? *Neuroscientist*, 20(1):56–70, 2014.

[231] A Thiel and S Vahdat. Structural and resting-state brain connectivity of motor networks after stroke. *Stroke*, 46(1):296–301, 2015.

[232] J Puig, G Blasco, J Daunis-I-Estadella, et al. Decreased corticospinal tract fractional anisotropy predicts long-term motor outcome after stroke. *Stroke*, 44(7):2016–2018, 2013.

[233] Sandra Hanneman. Design, analysis and interpretation of method-compariosn studies. *AACN Adv Crit Care.*, 19(2):223–234, 2010.

[234] A K Rehme, L J Volz, D.-L. Feis, et al. Individual prediction of chronic motor outcome in the acute post-stroke stage: Behavioral parameters versus functional imaging. *Human Brain Mapping*, 36(11):4553–4565, 2015. 56

[235] Jennifer Wu, Erin Burke Quinlan, Lucy Dodakian, et al. Connectivity measures are robust biomarkers of cortical function and plasticity after stroke. *Brain*, 138(8):2359–2369, 2015. ISSN 14602156. 58, 178

[236] T Platz, I.-H. Kim, U Engel, A Kieselbach, and K.-H. Mauritz. Brain activation pattern as assessed with multi-modal EEG analysis predict motor recovery among stroke patients with mild arm paresis who receive the Arm Ability Training. *Restor. Neurol. Neurosci.*, 20 (1-2):21–35, 2002. 58

[237] Y Dong, B H Dobkin, S Y Cen, A D Wu, and C J Winstein. Motor cortex activation during treatment may predict therapeutic gains in paretic hand function after stroke. *Stroke*, 37 (6):1552–1555, 2006. 58

[238] S L Fritz, K E Light, T S Patterson, A L Behrman, and S B Davis. Active finger extension predicts outcomes after constraint-induced movement therapy for individuals with hemiparesis after stroke. *Stroke*, 36(6):1172–1177, 2005.

[239] L Koski, T J Mernar, and B H Dobkin. Immediate and Long-Term Changes in Corticomotor Output in Response to Rehabilitation: Correlation with Functional Improvements in Chronic Stroke. *Neurorehabilitation and Neural Repair*, 18(4):230–249, 2004.

[240] S C Cramer, W J Koroshetz, and S P Finklestein. The case for modality-specific outcome measures in clinical trials of stroke recovery-promoting agents. *Stroke*, 38(4):1393–1395, 2007. 58

[241] P Sale, F Infarinato, C Del Percio, et al. Electroencephalographic markers of robot-aided therapy in stroke patients for the evaluation of upper limb rehabilitation. *International Journal of Rehabilitation Research*, 38(4):294–305, 2015. 59

[242] M Caimmi, A Chiavenna, A Scano, et al. Using robot fully assisted functional movements in upper-limb rehabilitation of chronic stroke patients: preliminary results. *Eur J Phys Rehabil Med*, (November), 2016. ISSN 19739095. 59

[243] G Pfurtscheller, C Brunner, A. Schlögl, and F.H. Lopes da Silva. Mu rhythm (de)synchronization and EEG single-trial classification of different motor imagery tasks. *Neuroimage*, 31(1):153–159, May 2006. 62, 68, 98, 102, 106, 121, 122

[244] Haider Raza, Anirban Chowdhury, and Saugat Bhattacharyya. Deep Learning based Prediction of EEG Motor Imagery of Stroke Patients ' for Neuro-Rehabilitation Application. In *International Joint Conference on Neural Networks (IJCNN 2020)*, Glasgow, 2020. 63, 95

[245] Kai Keng Ang, Zheng Yang Chin, Haihong Zhang, and Cuntai Guan. Mutual information-based selection of optimal spatial-temporal patterns for single-trial EEG-based BCIs. *Pattern Recognition*, 45(6):2137–2144, 2012. 65, 68, 184

[246] Neethu Robinson, Seong-whan Lee, and Cuntai Guan. EEG Representation in Deep Convolutional Neural Networks for Classification of Motor Imagery. In *2019 IEEE International Conference on Systems, Man and Cybernetics (SMC)*, pages 1322–1326. IEEE, October 2019. 65, 69

[247] K K Ang, Z Y Chin, C Wang, C Guan, and H Zhang. Filter bank common spatial pattern algorithm on BCI competition IV datasets 2a and 2b. *Frontiers in Neuroscience*, (MAR), 2012. 68

[248] Sergey Ioffe and Christian Szegedy. Batch Normalization: Accelerating Deep Network Training by Reducing Internal Covariate Shift. *32nd International Conference on Machine Learning, ICML 2015*, 1:448–456, February 2015. 68, 77, 105

[249] François Chollet. Xception: Deep Learning with Depthwise Separable Convolutions. *Proceedings - 30th IEEE Conference on Computer Vision and Pattern Recognition, CVPR 2017*, 2017-Janua:1800–1807, October 2016. 68

[250] Michael Tangermann, Klaus Robert Müller, Ad Aertsen, et al. Review of the BCI competition IV. *Frontiers in Neuroscience*, 6(JULY):1–31, 2012. 73, 74, 108, 181

[251] Min Ho Lee, O. Yeon Kwon, Yong Jeong Kim, et al. EEG dataset and OpenBMI toolbox for three BCI paradigms: An investigation into BCI illiteracy. *GigaScience*, 8(5):1–16, 2019. 73, 74, 79, 108, 125, 182

[252] Diederik P Kingma and Jimmy Ba. Adam: A method for stochastic optimization. *arXiv preprint arXiv:1412.6980*, 2014. 75, 108, 133

[253] Tim Salimans and Diederik P. Kingma. Weight normalization: A simple reparameterization to accelerate training of deep neural networks. *Advances in Neural Information Processing Systems*, pages 901–909, 2016. ISSN 10495258. 77

[254] Avanti Shrikumar, Peyton Greenside, and Anshul Kundaje. Learning important features through propagating activation differences. *34th International Conference on Machine Learning, ICML 2017*, 7:4844–4866, 2017. 79, 110, 135

[255] Narine Kokhlikyan, Vivek Miglani, Miguel Martin, et al. PyTorch Captum. https://github.com/pytorch/captum, 2019. URL `https://github.com/pytorch/captum`. 79, 110, 135

[256] Laurens Van Der Maaten and Geoffrey Hinton. Visualizing data using t-SNE. *Journal of Machine Learning Research*, 9:2579–2625, 2008. 79

[257] Xiaokang Shu, Shugeng Chen, Lin Yao, et al. Fast recognition of BCI-inefficient users using physiological features from EEG signals: A screening study of stroke patients. *Frontiers in neuroscience*, 12:93, 2018. 84

[258] Pouya Bashivan, Irina Rish, Mohammed Yeasin, and Noel Codella. Learning Representations from EEG with Deep Recurrent-Convolutional Neural Networks. *arxiv*, 2015. 102

[259] K. Chen, L. Yao, X. Wang, et al. Interpretable parallel recurrent neural networks with convolutional attentions for multi-modality activity modeling. In *2018 International Joint Conference on Neural Networks (IJCNN)*, pages 1–8, 2018.

[260] M. M. Hasib, T. Nayak, and Y. Huang. A hierarchical LSTM model with attention for modeling EEG non-stationarity for human decision prediction. In *2018 IEEE EMBS International Conference on Biomedical Health Informatics (BHI)*, pages 104–107, 2018.

[261] Jinwon An and Sungzoon Cho. Hand motion identification of grasp-and-lift task from electroencephalography recordings using recurrent neural networks. In *2016 International Conference on Big Data and Smart Computing (BigComp)*, pages 427–429, 2016. 102

[262] Simanto Saha and Mathias Baumert. Intra- and Inter-subject Variability in EEG-Based Sensorimotor Brain Computer Interface: A Review. *Frontiers in Computational Neuroscience*, 13:87, 2020. ISSN 1662-5188. 124, 125, 146

[263] Benjamin Blankertz, Claudia Sanelli, Sebastian Halder, et al. Predicting BCI performance to study BCI illiteracy. *BMC Neuroscience*, 10(Suppl 1):P84, 2009. 125

[264] Claudia Sannelli, Carmen Vidaurre, Klaus-Robert Müller, and Benjamin Blankertz. A large scale screening study with a SMR-based BCI: Categorization of BCI users and differences in their SMR activity. *PLOS ONE*, 14(1):e0207351, 2019. 125

[265] Camille Jeunet, Bernard N'Kaoua, Sriram Subramanian, Martin Hachet, and Fabien Lotte. Predicting mental imagery-based BCI performance from personality, cognitive profile and neurophysiological patterns. *PLOS ONE*, 10(12):e0143962, 2015. 125

[266] Femke Nijboer, Niels Birbaumer, and Andrea Kubler. The influence of psychological state and motivation on brain–computer interface performance in patients with amyotrophic lateral sclerosis–a longitudinal study. *Frontiers in neuroscience*, 4:55, 2010. 125

[267] Wojciech Samek, Duncan AJ Blythe, Gabriel Curio, et al. Multiscale temporal neural dynamics predict performance in a complex sensorimotor task. *Neuroimage*, 141:291–303, 2016. 125

[268] Kazumi Kasahara, Charles Sayo DaSalla, Manabu Honda, and Takashi Hanakawa. Neuroanatomical correlates of brain–computer interface performance. *Neuroimage*, 110:95–100, 2015. 125

[269] Jeff D Riley, Vu Le, Lucy Der-Yeghiaian, et al. Anatomy of Stroke Injury Predicts Gains From Therapy. *Stroke*, 42(2):421–426, February 2011. ISSN 0039-2499. 149, 152

[270] Erin Burke Quinlan, Lucy Dodakian, Jill See, et al. Neural function, injury, and stroke subtype predict treatment gains after stroke. *Annals of Neurology*, 77(1):132–145, January 2015. ISSN 03645134. 149, 152

[271] Peter Langhorne, Fiona Coupar, and Alex Pollock. Motor recovery after stroke: a systematic review. *Lancet Neurology*, 8(8):741–754, 2009. ISSN 14744422. 152

[272] J Mehrholz, M Pohl, T Platz, J Kugler, and B Elsner. Electromechanical and robot-assisted arm training for improving activities of daily living, arm function, and arm muscle strength after stroke. *Cochrane Database of Systematic Reviews*, (9), 2018. ISSN 1465-1858. 152

[273] Bernhard Elsner, Joachim Kugler, Marcus Pohl, and Jan Mehrholz. Transcranial direct current stimulation (tDCS) for improving activities of daily living, and physical and cognitive functioning, in people after stroke. *Cochrane Database of Systematic Reviews*, 2016 (3), 2016. ISSN 1469493X. 152

[274] Pai Chuan Huang, Yu Wei Hsieh, Chin Man Wang, et al. Predictors of motor, daily function, and quality-of-life improvements after upper-extremity robot-assisted rehabilitation in stroke. *American Journal of Occupational Therapy*, 68(3):325–333, 2014. ISSN 02729490. 152

[275] Jose Leon-Carrion, Juan Francisco Martin-Rodriguez, Jesus Damas-Lopez, Juan Manuel Barroso y Martin, and Maria Rosario Dominguez-Morales. Delta – alpha ratio correlates with level of recovery after neurorehabilitation in patients with acquired brain injury. *Clinical Neurophysiology*, 120(6):1039–1045, June 2009. ISSN 13882457. 153, 170

[276] Aurore Thibaut, Marcel Simis, Linamara Rizzo Battistella, et al. Using Brain Oscillations and Corticospinal Excitability to Understand and Predict Post-Stroke Motor Function. *Frontiers in Neurology*, 8(MAY):1–8, May 2017. ISSN 1664-2295.

[277] Donatella Mattia, Francesca Spanedda, Fabio Babiloni, Andrea Romigi, and Maria Grazia Marciani. Quantitative EEG patterns following unilateral stroke: a study in chronic stage. *The International journal of neuroscience*, 113(4):465–82, April 2003. ISSN 0020-7454. 153

[278] Nima Bigdely-Shamlo, Tim Mullen, Christian Kothe, Kyung-Min Su, and Kay A. Robbins. The PREP pipeline: standardized preprocessing for large-scale EEG analysis. *Frontiers in Neuroinformatics*, 9(June):1–20, June 2015. ISSN 1662-5196. 156

[279] H Nolan, R Whelan, and R.B. Reilly. FASTER: Fully Automated Statistical Thresholding for EEG artifact Rejection. *Journal of Neuroscience Methods*, 192(1):152–162, September 2010. ISSN 01650270. 156

[280] Thomas E Nichols and Andrew P Holmes. Nonparametric permutation tests for functional neuroimaging: A primer with examples. *Human Brain Mapping*, 15(1):1–25, January 2002. ISSN 1065-9471. 158

[281] R A Fisher. Statistical Methods for Research Workers. In Samuel Kotz and Norman L Johnson, editors, *Break. Stat. Methodol. Distrib.*, pages 66–70. Springer New York, New York, NY, 1992. ISBN 978-1-4612-4380-9. 159

[282] Birk Diedenhofen and Jochen Musch. Cocor: A comprehensive solution for the statistical comparison of correlations. *PLOS ONE*, 10(4):1–12, 2015. ISSN 19326203. 159

[283] Rishi V.A. Sheorajpanday, Guy Nagels, Arie J.T.M. Weeren, Michel J.A.M. van Putten, and Peter P. De Deyn. Quantitative EEG in ischemic stroke: Correlation with functional status after 6months. *Clinical Neurophysiology*, 122(5):874–883, May 2011. ISSN 13882457. 170

[284] Alyssa M. Batula, Jesse A. Mark, Youngmoo E. Kim, and Hasan Ayaz. Comparison of Brain Activation during Motor Imagery and Motor Movement Using fNIRS. *Computational Intelligence and Neuroscience*, pages 1–12, 2017. ISSN 1687-5265. 171

[285] Fabien Lotte, Cuntai Guan, and Kai Keng Ang. Comparison of designs towards a subject-independent brain-computer interface based on motor imagery. In *2009 Annual International Conference of the IEEE Engineering in Medicine and Biology Society*, pages 4543–4546. IEEE, 2009. 176

[286] Siamac Fazli, Florin Popescu, Márton Danóczy, et al. Subject-independent mental state classification in single trials. *Neural networks*, 22(9):1305–1312, 2009.

[287] Md AM Joadder, Siuly Siuly, E Kabir, Hua Wang, and Yanchun Zhang. A new design of mental state classification for subject independent BCI systems. *IRBM*, 40(5):297–305, 2019.

[288] Fatemeh Fahimi, Zhuo Zhang, Wooi Boon Goh, et al. Inter-subject transfer learning with an end-to-end deep convolutional neural network for EEG-based BCI. *Journal of neural engineering*, 16(2):026007, 2019. 176

[289] S. J. Pan and Q. Yang. A survey on transfer learning. *IEEE Transactions on Knowledge and Data Engineering*, 22(10):1345–1359, 2010. doi: 10.1109/TKDE.2009.191. 177

[290] Fuzhen Zhuang, Zhiyuan Qi, Keyu Duan, et al. A comprehensive survey on transfer learning. *arXiv*, pages 1–31, 2019. 177

[291] Ke Liao, Ran Xiao, Jania Gonzalez, and Lei Ding. Decoding individual finger movements from one hand using human eeg signals. *PloS one*, 9(1):e85192, 2014. 177

[292] C Gerloff, K Bushara, A Sailer, et al. Multimodal imaging of brain reorganization in motor areas of the contralesional hemisphere of well recovered patients after capsular stroke. *Brain*, 129(3):791–808, 2006. 178

[293] Ramesh Srinivasan, William R. Winter, Jian Ding, and Paul L. Nunez. EEG and MEG coherence: Measures of functional connectivity at distinct spatial scales of neocortical dynamics. *Journal of Neuroscience Methods*, 166(1):41–52, 2007. ISSN 01650270. 178

[294] Emanuela Formaggio, Silvia Francesca Storti, Roberto Cerini, Antonio Fiaschi, and Paolo Manganotti. Brain oscillatory activity during motor imagery in EEG-fMRI coregistration. *Magnetic Resonance Imaging*, 28(10):1403–1412, 2010. ISSN 0730725X. 178

[295] Chih-Chung Chang and Chih-Jen Lin. LIBSVM: A library for support vector machines. *ACM transactions on intelligent systems and technology (TIST)*, 2(3):1–27, 2011. 184